The University of Nottingham

Genetic Dissection of Auxin Regulated Root Development

AFAF ABDULLAH RASHED, MSc.

Thesis submitted for a degree of Doctor of Philosophy

September 2016

ABSTRACT

As plants are sessile organisms, their developmental plasticity is crucial for adapting to environmental signals. Plant roots play a key role foraging resources in the soil to facilitate uptake of water and nutrients. The plant hormone auxin is a critical regulator of root growth and development, controlling root hair, branching and root angle. This thesis investigates the function of several auxin-regulated genes that control different aspects of root growth and development.

It is important to maintain an appropriate auxin level in plant tissues by regulating auxin biosynthesis, transportation, conjugation and degradation pathways. In *Arabidopsis thaliana*, the *DIOXYGENASE FOR AUXIN OXIDATION 1* (*AtDAO1*) gene has recently been identified to have a major function in regulating the oxidation of IAA to oxIAA. Metabolic profiling data of *Atdao1* mutant lines identified that IAA level remains similar to wildtype in contrast to oxIAA and IAA congregates, revealing IAA degradation acts redundantly with the conjugate machinery. In addition, close examination of *dao1* loss of function lines revealed several auxin-related phenotypes including the lengths of primary roots and root hairs.

Auxin also plays a key role during lateral root branching. Bioinformatic analyses of a lateral root transcriptomic time course identified *LATERAL ROOT KINASE 1* and *2* (*LRK1* and *LRK2*, two putative LRR kinases) that exhibit the same expression dynamics during early stages of lateral root development as the auxin regulated transcription factor *GATA23* that controls lateral root founder cell priming. *lrk* mutant analysis revealed that *LRK1* and *LRK2* function to control

lateral root initiation. Reporter studies identified *LRK1* and *LRK2* are induced in root endodermal cells in the elongation zone, suggesting these genes regulate lateral root initiation indirectly.

Auxin also regulates root angle. Transcriptomic profiling of a gravitropic auxin mutant *arf7 arf19* identified 195differently expressed genes regulated by auxin and *ARF7 ARF19*. Reverse genetic studies characterised several candidates *AT2G25900* (Cys3His transcription factor, TF) and *AT5G47540* putative Mo25-like protein have been characterized to have function in root gravity response. Several experiments have been performed on several independent knock-out alleles to investigate the expression pattern of these two genes. The phenotyping results showed no significant differences in response to gravity stimulus, despite the original *MO25* allele (*mo25-2*) exhibiting a strong lateral root phenotype.

ACKNOWLEDGMENT

Dedicated to my parents ABDULLAH RASHED and ALAWEYAH SAMKARI,

You are my inspiration

I would like to express my gratitude to my supervisor Professor Malcolm Bennett who providing me the opportunity to be a member of his group. I greatly appreciate his guidance, valuable suggestions and continuous support throughout my PhD journey. It was a pleasure working with him.

I owe a deep sincere of thanks to Dr. Ranjan Swarup to be my co-supervisor and for giving me the right advice at the right time. I am hugely indebted to Dr. Ute Voβ for finding time for me and for her unwavering support, mentorship and motivations ideas over the four years.

I would like to extend my thankful to Rahule, Daniela, Kamal, Regina, Silvana, Hussein, Masoud and Effat for continues encouragement and support associated with kind words and helps, thank you all.

A heartfelt thanks to Wael who was there for me through the years. Words can never be enough to thank your kindness.

Finally, thanks should also due to all members of my Family. My brothers, my sisters and my uncle Hassan, Who put their faith in me, I won't be this stronger without you.

ABBREVIATIONS

AUX1	Auxin-Resistant 1
ARFs:	Auxin Response Factors
AREs:	Auxin-Responsive Elements
cDNA:	Complementary Deoxyribonucleic Acid
Col-0:	Columbia-0
DNA:	Deoxyribonucleic Acid
dNTPs:	Deoxyribonucleotide Triphosphate
GFP:	Green Fluorescence Protein
GUS:	β-glucuronidase
IAA:	Indole-3-Acetic Acid
KO:	Knock -Out
LB:	Left Border Primer
LP:	Forward Primer
LR	Lateral Root
LRI	Lateral Root Initiation
LRP	Lateral Root Primordium
mRNA:	Messenger Ribonucleic Acid
NASC:	Nottingham Arabidopsis Stock Centre
PCR:	Polymerase Chain Reaction
Bp:	Base Pair
RNA:	Ribonucleic Acid
RP:	Reverse Primer
RT-PCR:	Reverse Transcriptase-Polymerase Chain Reaction
T-DNA:	Transferred-Deoxyribonucleic Acid
UV:	UltraViolet
WT:	Wild Type

TABLE OF CONTENTS

ABSTRACT ..... *I*
ACKNOWLEDGMENT ..... *III*
ABBREVIATIONS ..... *IV*
TABLE OF CONTENTS ..... *V*
LIST OF TABLES ..... *VIII*
LIST OF FIGURES ..... *IX*
GENERAL INTRODUCTION *1*
1.1 GENERAL INTRODUCTION **2**
1.2 *ARABIDOPSIS THALIANA* AS A MODEL PLANT **2**
1.3 PLANT ROOT SYSTEM **5**
1.3.1 THE PRIMARY ROOT 5
1.3.2 ROOT HAIRS 7
1.3.3 LATERAL ROOT DEVELOPMENT 9
1.3.4 ENVIRONMENTAL CHANGES THAT AFFECT PLANT PROGRESS 12
1.4 PLANT GROWTH REGULATORS **13**
1.4.1 THE PLANT HORMONE: AUXIN 14
1.4.1.1 AUXIN SYNTHESIS 15
1.4.1.2 AUXIN TRANSPORT 17
1.4.1.3 AUXIN REGULATION OF GENE EXPRESSION 19
1.4.1.4 AUXIN DEGRADATION and CONJUGATION PATHWAYS 21
PROJECT AIMS AND OBJECTIVES *25*
GENERAL MATERIALS AND METHODS *26*
2.1 PLANT MATERIAL **27**
2.2 SEED STERILIZATION AND PLANT GROWTH CONDITIONS **27**
2.3 GENOTYPIC EXPERIMENTS **28**
2.3.1 GENOMIC DNA ISOLATION 28
2.3.2 PRIMERS DESIGN 29
2.3.3 POLYMERASE CHAIN REACTION 29
2.3.4 AGAROSE GEL ELECTROPHORESIS 31
2.4 GENE EXPRESSION ANALYSIS **31**
2.4.1 RNA EXTRACTION 31
2.4.2 COMPLEMENTARY DNA (cDNA SYNTHESIS) 31
2.4.3 REVERSE TRANSCRIPTASE POLYMERASE CHAIN REACTION 32
2.4.4 QUANTITATIVE REVERSE TRANSCRIPTASE POLYMERASE CHAIN REACTION 33
2.5 PLANT PHENOTYPIC ANALYSIS **34**
2.5.1 PRIMARY ROOT LENGTH (PRL) 34
2.5.2 LATERAL ROOT DENSITY (LRD) 34
2.5.3 GRAVISTIMULAUS OF PRIMARY ROOT 34
2.6 MICROSCOPY **35**
2.6.1 CONFOCAL MICROSCOPY 35
2.6.2 LIGHT MICROSCOPY 35
IDENTIFICATION OF THE ROLE OF AtDAO1 IN AUXIN HOMEOSTASIS IN ARABIDOPSIS *36*
3.1 INTRODUCTION **37**
3.2 MY CONTRIBUTION TO BOTH PAPERS INCLUDED **38**
3.3 MATERIALS AND METHODS **39**
3.3.1 *ARABIDOPSIS THALIANA* MUTANTS LINES 39
3.3.2 STERILIZATION AND GROWTH CONDITIONS 39

3.3.3 GENOTYPIC ANALYSIS OF T-DNA INSERTION LINES 40
3.3.4 RNA EXTRACTION, REVERSE TRANSCRIPTASE POLYMERASE CHAIN REACTION AND QUANTITATIVE REVERSE TRANSCRIPTASE POLYMERASE CHAIN REACTION 41
3.3.5 PHENOTYPIC ANALYSIS 42
3.3.5.1 PRIMARY ROOT LENGTH, LATERAL ROOT NUMBER AND LATERAL ROOT DENSITY 42
3.3.5.2 GRAVISTIMULATION ASSAY 42
3.3.5.3 ROOT HAIR NUMBER 43
3.4 COMPLEMENTARY RESULTS 44
3.4.1 GENOTYPING ANALYSIS OF T-DNA INSERTION LINES 44
3.4.2 RT-PCR and qRT-PCR 46
3.4.3 PHENOTYPIC ANALYSIS 48
3.4.3.1 PRIMARY ROOT LENGTH AND LATERAL ROOT DENSITY 48
3.4.3.2 GRAVITROPISUM ASSAY 50
3.4.3.3 ROOT HAIR (RH) PHENOTYPE 50
3.4.3.4 *DAO1* and *GH3.3* EXPRESSION LEVELS 52
3.4.3.5 IAA FEEDING EXPERIMENTS 53
3.5 DISCUSSION 54
3.6 DIOXYGENASE-ENCODING *AtDAO1* GENE CONTROLS IAA OXIDATION AND HOMEOSTASIS IN *ARABIDOPSIS* (Porco et al., 2016) 57
3.7 DYNAMIC REGULATION OF AUXIN OXIDASE AND CONJUGATING ENZYMES *AtDAO1* AND *GH3* MODULATES AUXIN HOMEOSTASIS (Mellor et al., 2016) 54
INVESTIGATION OF THE ROLE OF LATERAL ROOT KINASES (LRK1 AND LRK2) DURING LATERAL ROOT INITIATION AND DEVELOPMENT 66
4.1 ABSTRACT 67
4.2 INTRODUCTION 67
4.2.1 THE HIDDEN PART OF THE PLANT 67
4.2.2 *AT2G15300* AND *AT4G34220*: ENCODE PUTATIVE LEUCINE-RICH REPEAT KINASE-LIKE PROTEINS 69
4.3 MATERIALS AND METHODS 71
4.3.1 *ARABIDOPSIS THALIANA* MUTANT LINES 71
4.3.2 PLANT MATERIALS AND GROWTH CONDITIONS 71
4.3.3 GENOMIC DNA EXTRACTION FOR GENOTYPING 72
4.3.4 RNA EXTRACTION, cDNA SYNTHESIS AND REVERSE TRANSCRIPTASE POLYMERASE CHAIN REACTION 72
4.3.5 ROOT PHENOTYPING ANALYSIS: PRIMARY ROOT LENGTH, LATERAL ROOT NUMBER AND LATERAL ROOT DENSITY 73
4.3.6 ROOT GRAVITY RESPONSE ANALYSIS 74
4.3.7 TRANSCRIPTIONAL AND TRANSLATIONAL FUSION LINES OF *AT2G15300* AND *AT4G34220* 74
4.3.7.1 AMPLIFICATION OF GENES OF INTEREST 74
4.3.7.2 EXTRACTION AND PURIFICATION OF DNA FRAGMENTS FROM THE GEL 76
4.3.7.3 INTRODUCTION OF DNA FRAGMENT TO pENTR™-D-TOPO® ENTRY VECTOR 76
4.3.7.4 TRANSFORMATION OF ONE SHOT® COMPETENT *ESCHERICHIA COLI* 76
4.3.7.5 PLASMID PURIFICATION 77
4.3.7.6 LR REACTION 77
4.3.7.7 TRANSFORMATION OF AGROBACTERIUM TUMEFACIENS 78
4.3.7.8 TRANSFORMATION OF *ARABIDOPSIS* 78
4.4 RESULTS 80
4.4.1 GENOTYPIC ANALYSIS OF T-DNA INSERTION LINES 81
4.4.2 RT-PCR AND qRT-PCR 83
4.4.3 PHENOTYPIC ANALYSIS 86

4.4.3.1 PRIMARY ROOT LENGTH AND LATERAL ROOT NUMBER 86
4.4.3.2 GRAVITROPISUM ASSAY 87
4.4.4 TRANSCRIPTIONAL AND TRANSLATIONAL FUSION LINES 88
4.5 DISCUSSION 92
INVESTIGATING THE FUNCTION OF MO25 IN REGULATING PLANT GRAVITROPIC RESPONSE 95
5.1 ABSTRACT 96
5.2 INTRODUCTION 96
5.2.1 GRAVITY RESPONSE IN ROOT 96
5.2.1.1 GRAVITY PERCEPTION 98
5.2.1.2 GRAVITROPIC SIGNAL TRANSDUCTION 99
5.2.1.3 GRAVITROPIC RESPONSE 101
5.2.2 IDENTIFICATION OF REGULATORY GENE FOR PLANT GROWTH RESPONSES BY MICROARRAY TRANSCRIPTOME ANALYSIS 102
5.2.2.1 AT2G25900 (CYSTEINE- CYSTEINE- CYSTEINE-HISTAMINE TANDEM ZINC FINGER PROTEIN) OR CYS3HIS ZINC FINGER TRANSCRIPTION FACTOR 103
5.2.2.2 *AT5G47540*: PUTATIVE MO25-LIKE PROTEIN 104
5.3 MATERIALS AND METHODS 106
5.3.1 *ARABIDOPSIS THALIANA* MUTANTS LINES 106
5.3.2 STERILIZATION, GERMINATION AND GROWTH CONDITIONS 107
5.3.3 GENOTYPIC ANALYSIS 107
5.3.4 RNA EXTRACTION, *c*DNA SYNTHESIS, REVERSE TRNANSCRIPTASE-POLYMERASE CHAIN REACTION AND QUANTITATIVE REVERSE TRANSCRIPTASE-POLYMERASE CHAIN REACTION 108
5.3.5 PLANT PHENOTYPIC ANALYSIS 109
5.3.6 GRAVITISTIMULATION ASSAY 110
5.3.7 MERISTEM TISSUE SIZE 110
5.4 RESULTS 111
5.4.1 GENOTYPIC ANALYSIS OF T-DNA INSERTION LINES 111
5.4.2 RT-PCR 115
5.4.3 PHENOTYPIC ANALYSIS 119
5.4.3.1 PRIMARY ROOT GRAVITROPISM 119
5.4.3.2 PRIMARY ROOT LENGTH 121
5.4.3.3 MERISTEM SIZE 123
5.4.3.4 LATERAL ROOT NUMBER 125
5.4.3.5 LATERAL ROOT NUMBER AND PRIMORDIUM DENSITY 127
5.4.3.6 BACKCROSSING OF *mo25-2* 128
5.5 DISCUSSION 130
SUMMARY AND CONCLUSION 133
6.1 SUMMARY 134
6.1 CONCLUSIONS 138
REFERENCES 139

LIST OF TABLES

Table 2-1: T-DNA specific left border (LB) primer sequences. 29

Table 2-2: The PCR genotyping reaction mixture concentrations and volumes (in 20 µl). 30

Table 2-3: The PCR cycling for genotyping. 30

Table 2-4: RT-PCR reaction mixture concentrations and volumes (in 20 µl). 32

Table 2-5: qRT-PCR reaction mixture concentrations and volumes (in 20 µl). 33

Table 3-1: *Arabidopsis thaliana* T-DNA insertion lines. 39

Table 3-2: Gene specific primer sequences of T-DNA insertion lines. 40

Table-3-3: RT-PCR specific primer sequences. 41

Table 3-4: qRT-PCR specific primer sequences. 42

Table 4-1: *Arabidopsis thaliana* Knock-out (KO) lines. 71

Table 4-2: Gene specific primer sequences of T-DNA insertion lines. 72

Table 4-3: RT-PCR specific primer sequences. 73

Table 4-4: QRT-PCR specific primer sequences. 73

Table 4-5: PCR reaction (the reagents and volumes in 20 µl) to amplify the gene of interest.. 75

Table 4-6: PCR cycling for DNA fragments amplification. 75

Table 4-7: PCR primer sequences to amplify the gene of interest. 75

Table 5-5-1: *Arabidopsis thaliana* T-DNA insertion lines. 106

Table 5-5-2: Gene specific primer sequences for T-DNA insertion lines. 108

Table 5-3: RT-PCR specific primer sequences. 108

Table 5-4: qRT-PCR specific primer sequences. 109

LIST OF FIGURES

Figure 1-1: The flowering plant *Arabidopsis thaliana* (*Columbia*; *Col-0*). A) The plant life cycle from seeds to mature plant (about 8 weeks after germination) B) the flower; four petals, four sepals, six stamens (4 long and 2 short) and one pistil with two carpels. C) The pollen grain D) the silique (20-30 seeds/silique) (This figure is reproduced from Kramer (2015)). 4

Figure 1-2: The five developmental zones of the primary root. 1. Meristem zone (~350 µm), 2. Accelerating elongation (~900 µm), 3. Decelerating elongation (~1.2 mm), 4. Mature zone (~500 µm) and 5. Rest of root / Lateral root emergence zone (~2.5 cm) (This figure is reproduced from Ubeda-Tomas et al. (2012)). 6

Figure 1-3: The early stages of the development of *Arabidopsis* embryo (This figure is reproduced from Smit and Weijers (2015)). 7

Figure 1-4: A: Root hair zone along the *Arabidopsis thaliana* primary root. B: The H and N positions of the root hair within the epidermis layer (This figure is reproduced from Grierson et al. (2014)). 8

Figure 1-5: Pericycle cell start to initiat a new founder cell for lateral root primordia in response to auxin oscillation in the elongation zone at the root tip (This figure is reproduced fromScheres and Laskowski (2016). 10

Figure 1-6: Lateral root primordium initiation and development from the pericycle cell.(a) *Arabidopsis* root tissues. (b) The roman numbers shows the eight stages of primordium development. (c) Auxin signalling (pretended by DR5:GUS) during the LR development process. (d) Aniline-blue-stained roots for the LR stages, scale bar 20mm. (This figure is reproduced from Peret et al. (2009)). 11

Figure 1-7: Indole Acetic Acid (Auxin; IAA) structure. 14

Figure 1-8: Auxin biosynthesis pathways. Tryptophan synthetic pathway in chloroplast (Green arrows). The known genes and enzymes in Tryptophan dependent IAA biosynthetic pathway (Blue arrows). Indole alkaloid and serotonin biosynthetic pathway (Red arrows). Brassicaceae species- specific pathway (Yellow arrows). Unknown genes and enzymes (Black arrows and ? marks). (This figure is reproduced from Mano and Nemoto (2012)). 16

Figure 1-9: Auxin signalling. Under low IAA: Aux/IAA proteins (repressor) binds to ARFs (transcription factors) which leads to deactivation of auxin-responsive genes transcription. Under high IAA: auxin promotes the binding of Aux/IAA with the SCF ^{TIR1} complex, as a result of this interaction the Aux/IAA corepressor is ubiqutinated and degraded via the 26S proteasome pathway which leads to depress of downstream auxin responsive genes (This figure is reproduced from Ljung (2013)). 21

Figure 1-10: Auxin can be degraded and conjugated to different storage forms of IAA. IAA conjugates via a reversible process to IAA-Glc (by UGT84B1) or amino acids (by GH3) or via a irreversible process to IAA-Asp and IAA-Glu (by GH3). . IAA can be oxidised to oxIAA then to oxIAA-Glc by UGT74D1. (This figure is reproduced from Porco et al. (2016)). 22

Figure 2-1: Gravitropic stimulation. 6 days old seedlings were germinated under 12/12 light/dark conditions then turned 90º for gravity stimulation. 35

Figure 3-1: AT1G1430's map indicating the T-DNA insertion lines positions of *dao1-1* (SALK_097787), *dao1-3* (SALK_082522), *dao1-2D* (SAIL_349_D02) and *dao1-4D* (SALK_09593). 44

Figure 3-2: Genotypic analysis by PCR for *dao1-1* (SALK_097787), using two genomic primers (LP + RP: forward and reverse primers) Product size = 1161bp, and RP + left T-DNA border primer (LB) Product size= 889bp. WT: wild type (Columbia) and 4 SALK_097787 line seedlings. (1kB DNA ladder, *: Homozygous plants). 45

Figure 3-3: Genotypic analysis by PCR for *dao1-3* (SALK_082522), using two genomic primers (LP + RP: forward and reverse primers) Product size = 1075bp, and RP + left T-DNA border primer (LB) Product size= 484bp. WT: wild type (Columbia) and 3 SALK_082522 line seedlings. (1kB DNA ladder, *: Homozygous plants). 45

Figure 3-4: Genotypic analysis by PCR for *dao1-2D* (SAIL_349_D02), using two genomic primers (LP + RP: forward and reverse primers) Product size = 1021bp, and RP + left T-DNA border primer (LB) Product size= 505bp. WT: wildtype (Columbia) and 2 SAIL_349_D02 line seedlings. (1kB DNA ladder, *: Homozygous plants). 45

Figure 3-5: Genotypic PCR analysis for *dao1-4D* (SALK_09593), using two genomic primers (LP + RP: forward and reverse primers) Product size = 1167bp, and RP + left T-DNA border primer (LB) Product size= 740bp. WT: wildtype (Columbia) and 2 SALK_09593 line seedlings. (1kB DNA ladder, *: Homozygous plants). 46

Figure 3-6: RT-PCR expression analysis of the different mutants of AT1G14130 compared with WT (*Col-0*). A) Expression of a house-keeping gene using house-keeping primers (product size ~ 200bp). B) Expression analysis of AT1G14130 (*dao1-1*(SALK_097787), *dao1-3* (SALK_082522), *dao1-2D* (SAIL_349_D02) and *dao1-4D* (SALK_09593), using forward and reversed cDNA specific primers (Product size= 90 bp). 47

Figure 3-7: qRT-PCR expression quantification for *AT1G14130* of *dao1-1*(SALK_097787), *dao1-3* (SALK_082522), *dao1-2D* (SAIL_349_D02) and *dao1-4D* (SALK_09593) lines, normalized to WT (*Col-0*). * denotes significant difference compared to WT ($P < 0.05$)..... 47

Figure 3-8: Map of *AT1G14130* indicating RT-PCR (forward: FP + reverse: RP) and qRT-PCR (forward: FP + reverse: RP) primers. 48

Figure 3-9: The primary root length of 5, 10 and 15 day old seedlings for *AT1G14130* of *dao1-1*(SALK_097787), *dao1-3* (SALK_082522), *dao1-2D* (SAIL_349_D02) and *dao1-4D* (SALK_09593) lines, in compared to WT (*Col-0*). * denotes significant difference compared to WT (Mann-Whitney *U* test; $P < 0.05$). 48

Figure 3-10: The lateral root number of 10 and 15 day old seedlings for *AT1G14130* of *dao1-1*(SALK_097787), *dao1-3* (SALK_082522), *dao1-2D* (SAIL_349_D02) and *dao1-4D* (SALK_09593) lines, in compared to WT (*Col-0*). 49

Figure 3-11: Lateral root density (cm^{-1}) of 10 and 15 day old seedlings for *AT1G14130* of *dao1-1*(SALK_097787), *dao1-3* (SALK_082522), *dao1-2D* (SAIL_349_D02) and *dao1-4D* (SALK_09593) lines, in compared to WT (*Col-0*). * denotes significant difference compared to WT (Mann-Whitney *U* test; $P < 0.05$). 49

Figure 3-12: Responses of gravistimulated roots of 6 day old seedlings after turning through 90° for *AT1G14130* of *dao1-1*(SALK_097787), *dao1-3* (SALK_082522), *dao1-2D* (SAIL_349_D02) and *dao1-4D* (SALK_09593) lines, in compared to WT (*Col-0*). 50

Figure 3-13: The root hair measurements from 5 -10 day old seedlings for *AT1G14130* of *dao1-1*(SALK_097787), *dao1-3* (SALK_082522), *dao1-2D* (SAIL_349_D02) and *dao1-4D* (SALK_09593) lines, in compared to WT (*Col-0*). * denotes significant difference compared to WT (Mann-Whitney *U* test; P < 0.001). 51

Figure 3-14: Confocal images of 10 day old seedlings for *AT1G14130* of *dao1-1*(SALK_097787), *dao1-3* (SALK_082522), *dao1-2D* (SAIL_349_D02) and *dao1-4D* (SALK_09593) lines and WT (*Col-0*). (Scale bar: 120 µm)..... 51

Figure 3-15: qRT-PCR expression quantification for *RSL4* for *dao1-1*(SALK_097787), *dao1-3* (SALK_082522), *dao1-2D* (SAIL_349_D02) and *dao1-4D* (SALK_09593) lines, normalized to WT (*Col-0*). * denotes significant difference compared to WT (*P* < 0.05). 52

Figure 3-16: qRT-PCR expression quantification for *GH3.3* and *GH3.2* of *dao1-1*(SALK_097787) and *dao1-2D* (SAIL_349_D02) lines, normalized to WT (*Col-0*). 53

Figure 3-17: Effect of IAA on the expression of *DAO1* and *GH3.3* genes in 7 day old Col-0 seedlings..... 53

Figure 4-1: The molecular mechanism for auxin and several regulatory genes that have function in regulating lateral root initiation and emergence. (This figure is reproduced from De Rybel et al. (2010))..... 68

Figure 4-2: Lateral root development was synchronized using the gravistimulation for transcriptomic profiling (This figure is reproduced fromVoss et al. (2015)). 80

Figure 4-3: Log_2 expression data of *GATA23*; *LRK1*: AT2G15300 and *LRK2*: AT4G34220 (This figure is shows the transcriptomic data from Voss et al. (2015))..... 81

Figure 4-4: Genotypic PCR analysis for *lrk1-1* (SALK_097787), using: A) two genomic primers (LP + RP: forward and reverse primers) Product size = 1018bp; and B) RP + left T-DNA border primer (LB) Product size= 469bp. WT: wild type (Columbia) and 6 SALK_097787 lines seedlings. (1kB DNA ladder; *: Homozygous plants). 82

Figure 4-5: Genotyping PCR analysis for *lrk2-1* (SALK_112336C) using two genomic primers (LP + RP: left and right primers) Product size = 1137bp; and left T-DNA border primer (LB) Product size= 594bp. WT: wild type (Columbia) and 3 SALK__112336C lines seedlings. (1kB DNA ladder; *: Homozygous plants)..... 82

Figure 4-6: Genotyping PCR analysis for *lrk1-2/lrk2-2* (gk_2702) using: A) two genomic primers of *LRK1* (LP + RP: forward and reverse primers) Product size = 1110bp; and B) RP + left T-DNA border primer (LB) Product size= 595bp. WT: wild type (Columbia) and 6 individual seedlings. (1kB DNA ladder; *: Homozygous plants). 82

Figure 4-7: Genotyping PCR analysis for *lrk1-2/lrk2-2* (gk_2702) using: A) two genomic primers of *LRK2* (LP + RP forward and reverse primers) Product size = 1098bp, and B) RP + left T-DNA border primer (LB) Product size= 567bp. WT: wild type (Columbia) and 6 individual seedlings. (1kB DNA ladder; *: Homozygous plants). 83

Figure 4-8: RT-PCR expression analysis of the different knockout lines of AT2G15300, AT4G34220 and the double mutant line, in comparison to WT (*Col-0*). A) Expression of a house-keeping gene using house-keeping primers (product size ~ 200bp). B) Expression analysis of AT2G15300, *lrk1-1* (SALK_097787) and *lrk1-2/lrk2-2* (gk_2702) using forward and reverse *LRK1* cDNA specific primers (Product size = 162 bp). C) Expression analysis of AT4G34220, *lrk2-1* (SALK_112336C) and *lrk1-2/lrk2-2* (gk_2702) using forward and reverse *LRK2* cDNA specific primers. (Product size = 104 bp)..... 84

Figure 4-9: qRT-PCR expression quantification for *AT2G15300* and *AT4G34220* of *lrk1-1* (SALK_097787), *lrk2-1* (SALK_112336C) and the double mutant *lrk1-2/lrk2-2* (gk_2702) lines, normalized to WT (*Col-0*). * denotes significant difference compared to WT ($P < 0.05$)..... 85

Figure 4-10: Map of *AT2G15300* indicating the T-DNA insertion line position of *lrk1-1* (SALK_097787) with RT-PCR (forward: FP + reverse: RP) and qRT-PCR (forward: FP + reverse: RP) primers. 85

Figure 4-11: Map of *AT4G34220* indicating the T-DNA insertion line position of *lrk2-1* (SALK_112336C) with RT-PCR (forward: FP + reverse: RP) and qRT-PCR (forward: FP + reverse: RP) primers. 85

Figure 4-12: The primary root length of 5 and 10 day old seedlings for AT2G15300 *lrk1-1* (SALK_097787), AT4G34220 *lrk2-1* (SALK_112336C) and the double mutant *lrk1-2/lrk2-2* (gk_2702), in compared to WT (*Col-0*). 86

Figure 4-13: The lateral root number of 10 day old seedlings for AT2G15300 *lrk1-1* (SALK_097787), AT4G34220 *lrk2-1* (SALK_112336C) and the double mutant *lrk1-2/lrk2-2* (gk_2702), in comparison to WT (*Col-0*). * denotes significant difference compared to WT ($P < 0.05$). 87

Figure 4-14: Lateral root density (cm^{-1}) of 10 day old seedlings for AT2G15300 *lrk1-1* (SALK_097787), AT4G34220 *lrk2-1* (SALK_112336C) and the double mutant *lrk1-2/lrk2-2* (gk_2702), in comparison to WT (*Col-0*). * denotes significant difference compared to WT ($P < 0.05$). 87

Figure 4-15: Responses of gravistimulated roots of 6 day old seedlings after turning through 90° for AT2G15300 *lrk1-1* (SALK_097787), AT4G34220 *lrk2-1* (SALK_112336C) and the double mutant *lrk1-2/lrk2-2* (gk_2702), in comparison to WT (*Col-0*)..... 88

Figure 4-16: Expression pattern of GFP in the transgenic plants of *AT2G15300* (*LRK1*). *pLRK1*::GFP of 5 day old seedlings of *A. thaliana* root tip. GFP expression is present in the endodermis tissues beginning where the vascular tissue differentiating zone. 89

Figure 4-17: *AT2G15300* (*LRK1*) localization in the cytosol. Expression pattern of GFP in the transgenic plants of *pLRK1*::*LRK1*:GFP of 5 day old seedlings of *A. thaliana* root tip. GFP expression is present in the cytosol of the endodermis tissues beginning where the vascular tissue differentiating zone. 89

Figure 4-18: Expression pattern of GFP in the transgenic plants of *AT4G34220* (*LRK2*). *pLRK2*::GFP of 5 day old seedlings of *A. thaliana* root tip. GFP expression is present in the endodermis tissues beginning where the vascular tissue differentiating zone. 90

Figure 4-19: *AT4G34220* (*LRK2*) localization in the cytosol. Expression pattern of GFP in the transgenic plants of *pLRK2*::*LRK2*:GFP of 5 day old seedlings of *A. thaliana* root tip. GFP expression is present in the cytosol of the endodermis tissues beginning where the vascular tissue differentiating zone. 90

Figure 4-20: *LRK1* (AT2G15300) and *LRK2* (AT4G34220) genes expression patterns in different tissues of Arabidopsis roots ten Hove et al. (2011))..... 91

Figure 5-1: 3 day-day-old *Arabidopsis thaliana* root structure. a) Gravistimulated seedling. b) Root dissection zones; root cap (RC), distal elongation zone (DEZ), central elongation zone (CEZ) and differentiation zone (DZ). c) Stained root tip (with iodine-potassium iodide) showing the statoliths bodies in columella cells. d) Columella cell structure (A. starch bodies, ER

endoplasmic reticulum, V. vacuole and N. the nucleus. (This figure is reproduced from Morita (2010)). 99

Figure 5-2: Statoliths bodies have the ability to reposition on the lower side of collumella cells in the gravistimulated root tip within 5 minutes. (This figure is reproduced from Sato et al. (2014)). 99

Figure 5-3: Analytical view of the AT2G25900 (TF) subfamily of CCCH zinc-finger family. AT2G25900 contains two CCCH motifs with 35464.6 Da (This figure is reproduced from Wang et al. (2008a)). 104

Figure 5-4: Genotyping analysis by PCR for *tf_112* (SALK_112158), using A) two genomic primers (LP + RP: forward and reverse primers) Product size = 1147bp, and B) RP + left T-DNA border primer (LB) Product size= 764bp. WT: wild type (Columbia) and 6 SALK__112158 line seedlings. (1kB DNA ladder; *: Homozygous plants). 112

Figure 5-5: Genotyping analysis by PCR for *tf_14* (SALK_143721), using A) two genomic primers (LP + RP: forward and reverse primers) Product size = 1004bp, and B) RP + left T-DNA border primer (LB) Product size= 491bp. WT: wild type (Columbia) and 6 SALK_143721 line seedlings. (1kB DNA ladder; *: Homozygous plants). 112

Figure 5-6: Genotyping analysis by PCR for *gk_8* (GK-788F09.1), using two genomic primers (LP + RP: forward and reverse primers) Product size = 1091bp, and RP + left T-DNA border primer (LB) Product size= 481bp. WT: wild type (Columbia) and 6 GABI-Kat_788F09.1 line seedlings. (1kB DNA ladde; *: Homozygous plants). 112

Figure 5-7: Genotyping analysis by PCR for *tf_980* (SALK_139980), using two genomic primers (LP + RP: forward and reverse primers) Product size = 1232bp, and RP + left T-DNA border primer (LB) Product size= 578bp. WT: wild type (Columbia) and 6 SALK__139980 line seedlings. (1kB DNA ladder; *: Homozygous plants). 113

Figure 5-8: Genotyping analysis by PCR for *mo25-1* (SALK_000304), using two genomic primers (LP + RP: forward and reverse primers) Product size = 1295bp, and RP + left T-DNA border primer (LB) Product size= 598bp. WT: wild type (Columbia) and 9 SALK_000304 line seedlings. (1kB DNA ladder; *: Homozygous plants). 113

Figure 5-9: Genotyping analysis by PCR for *mo25-2* (SALK_076387), using two genomic primers (LP + RP: forward and reverse primers) Product size = 1024bp, and RP + left T-DNA border primer (LB) Product size= 490bp. WT: wild type (Columbia) and 6 SALK_076387 line seedlings. (1kB DNA ladder; *: Homozygous plants). 114

Figure 5-10: Genotyping analysis by PCR for *mo25-3* (SAIL_513_B05), using two genomic primers (LP + RP: forward and reverse primers) Product size = 1240bp, and RP + left T-DNA border primer (LB) Product size= 596bp. WT: wild type (Columbia) and 14 SAIL_513_B05 line seedlings. (1kB DNA ladder; *: Homozygous plants). 114

Figure 5-11: Genotyping analysis by PCR for *mo25-4* (SAIL_1227_H04), using two genomic primers (LP + RP: forward and reverse primers) Product size = 1024bp, and RP + left T-DNA border primer (LB) Product size= 492bp. WT: wild type (Columbia) and 6 SAIL_1227_H04 line seedlings. (1kB DNA ladder; *: Homozygous plants). 114

Figure 5-12: Genotyping analysis by PCR for *mo25-5* (SALK_066597), using two genomic primers (LP + RP: forward and reverse primers) Product size = 1090bp, and RP + left T-DNA border primer (LB) Product size= 431bp. WT: wild type (Columbia) and 6 SALK_066597 line seedlings. (1kB DNA ladder; *: Homozygous plants). 115

Figure 5-13: RT-PCR expression analysis of the different mutants of AT2G25900 compared with WT (*Col-0*). A) Expression of a house-keeping gene using house-keeping primers (product size ~ 200bp). B) Expression analysis of AT2G25900 *tf_112* (SALK_112158) and *tf_14* (SALK_143721). C) The expression analysis of AT2G25900 (*gk_8* (GK-788F09.1) and *tf_980* (SALK_139980) using forward and reversed cDNA specific primers (Product size= 614 bp). 116

Figure 5-14: RT-PCR expression analysis of the different mutants of AT5G47540 compared with WT (*Col-0*). A) Expression of a house-keeping gene using house-keeping primers (product size ~ 200bp). B) Expression analysis of AT5G47540 *mo25-1* (SALK_000304), *mo25-2* (SALK_076387), *mo25-3* (SAIL_513_B05), *mo25-4* (SAIL_1227_H04) and *mo25-5* (SALK_066597) using forward and reversed cDNA specific primers. (Product size= 440 bp). 116

Figure 5-15: The map of *AT2G25900* indicating the four different T-DNA insertion positions *tf_112* (SALK_112158), *tf_14* (SALK_143721), *gk_8* (GK-788F09.1) and *tf_980* (SALK_139980), with RT-PCR (forward; FP + reverse; RP) and QRT-PCR (forward; FP + reverse; RP) primers. 117

Figure 5-16: qRT-PCR expression quantification for *AT2G25900* of *tf_112* (SALK_112158), *tf_14* (SALK_143721), *gk_8* (GK-788F09.1) and *tf_980* (SALK_139980), normalized to WT (*Col-0*). * denotes significant difference compared to WT ($P < 0.05$)..... 118

Figure 5-17: The map of *AT5G47540* indicating the different T-DNA insertion positions of *mo25-1* (SALK_000304), *mo25-2* (SALK_076387) and *mo25-3* (SAIL_513_B05), *mo25-4* (SAIL_1227_H04) and *mo25-5* (SALK_066597), with RT-PCR (forward; FP + reverse; RP) and qRT-PCR (forward; FP + reverse; RP) primers. 118

Figure 5-18: qRT-PCR expression quantification for *AT5G47540* of *mo25-1* (SALK_000304), *mo25-2* (SALK_076387), *mo25-3* (SAIL_513_B05), *mo25-4* (SAIL_1227_H04) and *mo25-5* (SALK_066597), normalized to WT (*Col-0*). * denotes significant difference compared to WT ($P < 0.05$). 118

Figure 5-19: 6 day old homozygous seedlings were turned 90°, and then the primary root angle (α) in response to gravity was measured. 119

Figure 5-20: The response of the gravistimulated root of the 6 day old seedlings after turning 90° for AT2G25900 *tf_112* (SALK_112158), *tf_14* (SALK_143721), *gk_8* (GK-788F09.1) and *tf_980* (SALK_139980), Compared with WT (*Col-0*). 120

Figure 5-21: The response of the primary root to gravity after seedlings turned 90° for 8 hours. For AT5G47540 *mo25-1* (SALK_000304), *mo25-2* (SALK_076387), *mo25-3* (SAIL_513_B05), *mo25-4* (SAIL_1227_H04) and *mo25-5* (SALK_066597), compared with WT (*Col-0*) * denotes a significant difference from WT ($P < 0.05$). 121

Figure 5-22: The primary root length after 3, 5 and 7 days, for AT2G25900 *tf_112* (SALK_112158), *tf_14* (SALK_143721), *gk_8* (GK-788F09.1) and *tf_980* (SALK_139980)), compared with WT (*Col-0*). * denotes a significant difference from WT ($P < 0.05$). 122

Figure 5-23: The primary root length of 10 day old seedlings, For AT5G47540 *mo25-1* (SALK_000304), *mo25-2* (SALK_076387), *mo25-3* (SAIL_513_B05), *mo25-4* (SAIL_1227_H04) and *mo25-5* (SALK_066597), compared with WT (*Col-0*). * denotes a significant difference from WT ($P < 0.05$)..... 122

Figure 5-24: The number of the meristem cells of AT2G25900 *tf_14* (SALK_143721) and *gk_8* (GK-788F09.1), compared with WT (*Col-0*). 123

Figure 5-25: The meristem tissue cell length of AT2G25900 *tf_14* (SALK_143721) and *gk_8* (GK-788F09.1), compared with WT (*Col-0*). 124

Figure 5-26: Confocal image of the root tip cross sections of of AT2G25900 mutants and wildtype: A) *tf_14* (SALK_143721) and B) *gk_8* (GK-788F09.1), compared with WT (C, *Col-0*). The number of cortical cells were counted from the QC to the beginning of the elongation zone were the cortex cells start to elongate. 124

Figure 5-27: 10 day old seedlings of AT5G47540 mutants. A) WT (*Col-0*), B) *mo25-2* (SALK_076387), C) *mo25-3* (SAIL_513_B05), D) *mo25-4* (SAIL_1227_H04) and E) *mo25-5* (SALK_066597) and F) *mo25-1* (SALK_000304). The black marks used to follow seedlings growth. 125

Figure 5-28: The lateral root number of 10 day old seedlings for AT5G47540 mutants. *mo25-1* (SALK_000304), *mo25-2* (SALK_076387), *mo25-3* (SAIL_513_B05), *mo25-4* (SAIL_1227_H04) and *mo25-5* (SALK_066597) compared with WT (*Col-0*). * denotes significant difference from WT ($P < 0.05$). 126

Figure 5-29: The lateral root density (cm^{-1}) of 10 day old seedlings, for AT5G47540 *mo25-1* (SALK_000304), *mo25-2* (SALK_076387), *mo25-3* (SAIL_513_B05), *mo25-4* (SAIL_1227_H04) and *mo25-5* (SALK_066597), compared with WT (*Col-0*). * denotes significant difference from WT ($P < 0.05$). 126

Figure 5-30: The density of different stages of the primordium for AT5G47540 *mo25-2* (SALK_076387), compared with WT (*Col-0*). * denotes significant difference from WT ($P < 0.05$). 127

Figure 5-31: Total lateral root density of AT5G47540 *mo25-2* (SALK_076387), compared with WT (*Col-0*) * denotes significant difference from WT ($P < 0.05$). 128

Figure 5-32: The F1 generation of *Col-0* X *mo25-2* (SALK_076387). By using genotyping primers (LP + RP (Product size = 1024bp) + LB (Product size= 490bp), all seedlings were generated to be heterozygous lines (1kB DNA ladder; *: Hetrozygous plants). 129

Figure 5-33: The F2 generation of *Col-0* X *mo25-2* (SALK_076387). By using genotyping primers (LP + RP (Product size = 1024bp) + LB (Product size= 490bp), 7% of the seedlings (with strong phenotype) were homozygous lines for *Mo25*(*), and 2.5% of the seedlings (with strong phenotype) were WT for *Mo25* (*). 129

GENERAL INTRODUCTION

1.1 GENERAL INTRODUCTION

Plants are the basis of life; almost all terrestrial organisms depend directly or indirectly on plants. Plants play an important role in maintaining suitable levels of water, oxygen, carbon dioxide and nitrogen in the atmosphere.

In the current era of climate changes, much of the current research is focused on uncovering the mechanisms controlling plant growth and development. Such understanding will help develop crops better adapted to future climate conditions and contribute to ensuring global food security.

1.2 *ARABIDOPSIS THALIANA* AS A MODEL PLANT

Arabidopsis thaliana is a member of the taxonomic family Brassicaceae (the mustards). The oldest description of *Arabidopsis* first appeared in (the Harz Mountains of) Northern Germany by the physician Johannes Thal in 1577. *Arabidopsis* was the third multicellular organism to be sequenced after *Caenorhabditis elegans* and *Drosophila melanogaster* (Bevan and Walsh, 2006, Carneiro et al., 2015). It has a small genome of approximately 114.5 Mb/125 Mb, counting 25,500 genes in five chromosomes, which encode proteins from 11,000 families. This small flowering plant is widely used as a model organism for research in genetic, cellular and molecular plant biology (Page and Grossniklaus, 2002).

During the last decade, advanced development in scientific tools and techniques in molecular biology enabled the identification of a wide range of genes in the *Arabidopsis thaliana* genome as well as the determination of their functions (The

Arabidopsis Genome Initiative (2000). The consequent improvement in knowledge of *A. thaliana* genetics significantly advanced our understanding of plant development and responses (Koornneef and Meinke, 2010, Carneiro et al., 2015).

Arabidopsis has a short life cycle from germination to seed maturation (about 8 weeks, Fig. 1-1). The height of the mature plant ranges between 20 and 30 cm. It produces small white flowers and the length of its fruit is about 5-20 mm with 20-30 seeds in each silique (about 50,000 seeds can fit into one 1500 ml Eppendorf tube) (Komaki et al., 1988, Meinke et al., 1998, Ngara and Ndimba, 2014).

From the research point of view, *Arabidopsis thaliana* makes an ideal candidate for molecular and developmental research (http://www.arabidopsis.org), and this is attributed to two main reasons. First, DNA-transformation *of Arabidopsis thaliana* with *Agrobacterium tumefaciens* can be remarkably efficient using the simple technique of floral dipping (Bent, 2000). In addition, a vast number of T-DNA insertion lines of *Arabidopsis* have been made available for research purposes (http://signal.salk.edu/tdnaprimers.2.html).

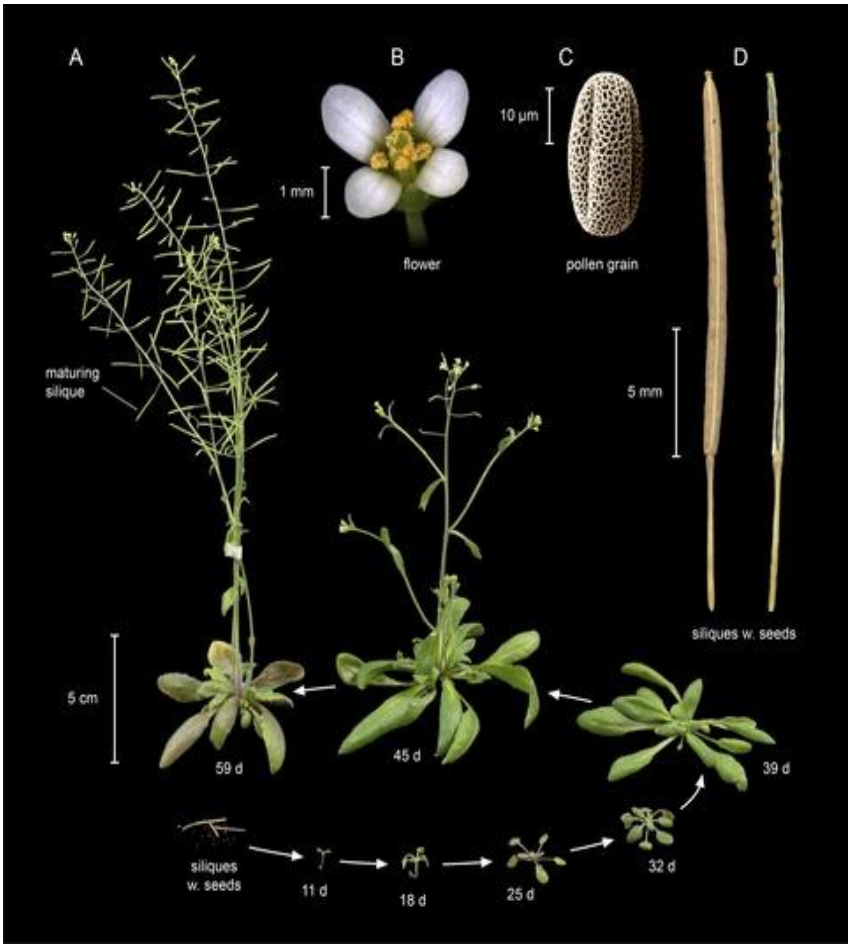

Figure 1-1: The flowering plant *Arabidopsis thaliana* (*Columbia*; *Col-0*). A) The plant life cycle from seeds to mature plant (about 8 weeks after germination) B) the flower; four petals, four sepals, six stamens (4 long and 2 short) and one pistil with two carpels. C) The pollen grain D) the silique (20-30 seeds/silique) (This figure is reproduced from Kramer (2015)).

1.3 PLANT ROOT SYSTEM

In vascular plants, the root system represents the hidden half of the plant that grows under the soil surface downward in the same direction of gravity. The primary root (radicle) is the first visible part that shows upon seed germination. (Malamy and Benfey, 1997). In the majority of higher plants species, the root system has central functions such as water absorption and mineral nutrient uptake, carbohydrate storage (such as in sweet potato and sugar beet) and anchorage for the aerial parts of the plant. In addition, it plays an important role in the adaptability of the plant to biotic and abiotic stress (Bareja, 2011). The primary root has the ability to change its growth direction according to the availability of water, as well as micro- and macronutrients (Tian et al., 2014a). Root growth and development are affected by physical and environmental variables such as soil temperature, bulk density of the soil, air- and water-filled pores, soil pH, biotic interactions and the concentration of nutrients (Dubrovsky et al., 2006, De Smet, 2012).

1.3.1 THE PRIMARY ROOT

All root tissues result from the activity of cell division and differentiation of the apical meristem of the primary root at the root tip (Tian et al., 2014a). The primary root is divided into five main anatomical areas: meristematic zone, accelerating elongation zone, decelerating elongation zone, differentiation and maturation zone, and the rest of the root including the lateral root emergence zone (see Fig. 1-2) (Ubeda-Tomas et al., 2012).

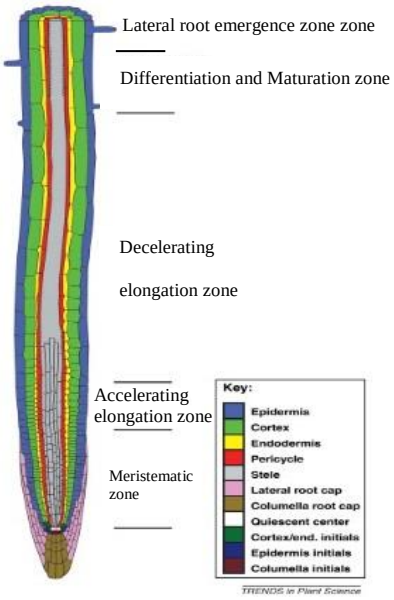

Figure 1-2: The five developmental zones of the primary root. 1. Meristem zone (~350 µm), 2. Accelerating elongation (~900 µm), 3. Decelerating elongation (~1.2 mm), 4. Mature zone (~500 µm) and 5. Rest of root / Lateral root emergence zone (~2.5 cm) (This figure is reproduced from Ubeda-Tomas et al. (2012)).

Polar auxin transport and signalling regulates the primary root patterning during early embryogenesis (Friml et al., 2003). After asymmetric cell division of the hypophysis (the embryonic suspensor cell), the primary root meristem is established from the globular embryo stage. Two cells types are generated from this division: a small apical cell give rise to the quiescent centre (QC, four central cells) and the columella stem cells (the large basal cell). All different primary root tissues files (stele, cortex, endodermis, epidermis, columella cells and lateral root cap) are initiated via several asymmetric cell divisions of the stem cells which are located around the QC (Fig. 1-3) (Dolan et al., 1993, De Smet et al., 2010).

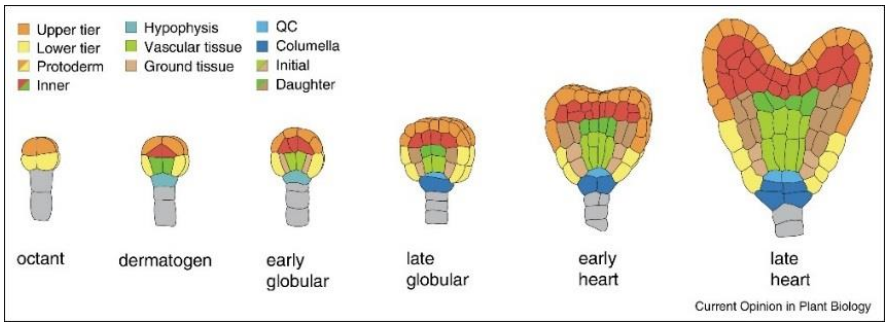

Figure 1-3: The early stages of the development of *Arabidopsis* embryo (This figure is reproduced from Smit and Weijers (2015)).

1.3.2 ROOT HAIRS

Root hairs are important for increasing the root-soil contact surface which allows the plant to obtain additional water and nutrients from the soil, root hairs expand from the primary root. Plant growth and development depend essentially on the amount of principal nutrients and water that are absorbed by the root system, and delivered to the rest of the plant body via the vascular tissues (Jones et al., 2006, Yi et al., 2010, Datta et al., 2011, Li et al., 2015, Salazar-Henao et al., 2016). Numerous studies have suggested a possible contribution of root hairs in anchoring the root tip in the soil, and in providing uprooting force and frictional force in *Arabidopsis* (Grierson et al., 2014, Bengough et al., 2016).

In *Arabidopsis* root hairs are the result of outgrowth from specific files of epidermal cells near the root tip. Hairs grow rapidly (1µm min^{-1}) after seedling germination, and can elongate up to 1mm or more with a diameter of up to 10µm (Keyes et al., 2013, Grierson et al., 2014). Many plant hormones regulate root hair initiation and development, such as auxin and ethylene (Sun et al., 2010,

Datta et al., 2011). Furthermore, genetic studies have determined groups of gene families that control the root hair epidermal cell specification, cell expansion, cell wall modification and whole root hair formation, such as the WD-bHLH-Myb transcriptional complex and *RHD6* bHLH gene family. Epidermal cells are separated into two cell types: root hair cells (trichoblasts) and non-hair cells (atrichoblasts). Each root hair cell is positioned such that is in contact with two underlying cortical cells, forming what is known as the H position. In contrast, the non-hair cells occupy what is known as the N position, whereby the root hair cell is located adjacent to single cortical cell (see Fig. 1-4) (Leitner et al., 2010, Yi et al., 2010, Grierson et al., 2014).

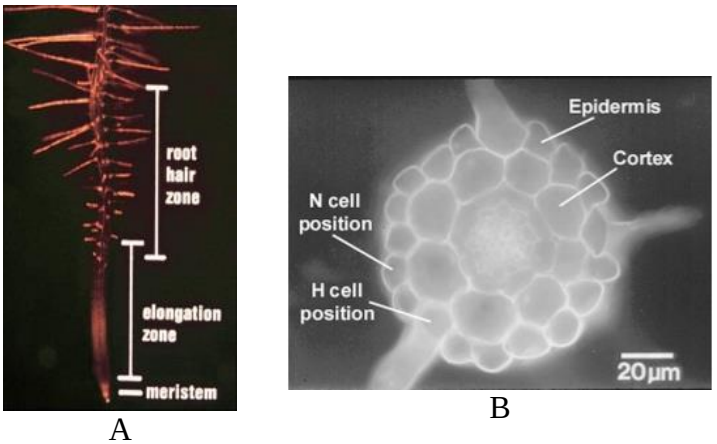

A B

Figure 1-4: A: Root hair zone along the *Arabidopsis thaliana* primary root. B: The H and N positions of the root hair within the epidermis layer (This figure is reproduced from Grierson et al. (2014)).

1.3.3 LATERAL ROOT DEVELOPMENT

The primary root has the ability to exploit a volume of soil through branching (Peret et al., 2009, Orman-Ligeza et al., 2013). Genetic studies in the model plant *Arabidopsis* have identified many genes that control LR initiation, emergence and development. The plant hormone auxin plays an important promotive role triggering LR initiation in root pericycle cells overlaying the xylem pole (Bhalerao et al., 2002, Dubrovsky et al., 2009, Overvoorde et al., 2010, Moreno-Risueno and Benfey, 2011). Lateral roots initiate in the basal meristem close to the root apical meristem (Malamy and Benfey, 1997). In *Arabidopsis thaliana*, oscillating gene expression determines where lateral root are positioned along the primary root. An initial series of stereotypical asymmetric cell divisions in the pericycle cell produce new LR primordia (LRP) (Moreno-Risueno et al., 2010, Moreno-Risueno and Benfey, 2011, De Smet et al., 2007).

LR development occurs in two different zones in the main root: the LR formation zone where young LRP develop near to the root apex, and the branching zone where LRs emerge (Dubrovsky and Forde, 2012). LR formation, LR founder cell specification, LR initiation, LR primordium (LRP) development and emergence are controlled by series of regulators modules composed of auxin response pathways components, such as ARFs (AUXIN RESPONSE FACTORS) and Aux/IAA proteins (Dubrovsky et al., 2009, Overvoorde et al., 2010, Lavenus et al., 2013).

Single or two pericycle founder cells (positioned opposite the xylem pole) divide several times anticlinally to generate the first layer of the LRP (stage I) that can

contain up to ten equal small size cells (Jansen et al., 2009). Which pericycle cells along the main root will become a LR founder cell is determined by the oscillation of the auxin response in the basal meristem (Fig. 1-5) (Moreno-Risueno et al., 2010).

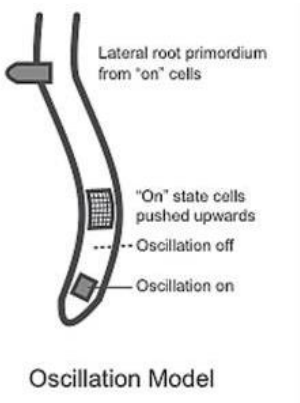

Figure 1-5: Pericycle cell start to initiat a new founder cell for lateral root primordia in response to auxin oscillation in the elongation zone at the root tip (This figure is reproduced fromScheres and Laskowski (2016).

An inner and outer layer results from a periclinally division of the first layer (stage II), followed by several anticlinal, periclinal and tangential divisions to generate stages III to VII of the primordium which form a dome shape (Lucas et al., 2013). This new organ has the ability to emerge through overlying tissues of the main root (endodermal, cortical and epidermal layers, respectively), from initiation to emergence (stage VIII) (Fig. 1-6) (Malamy and Benfey, 1997).

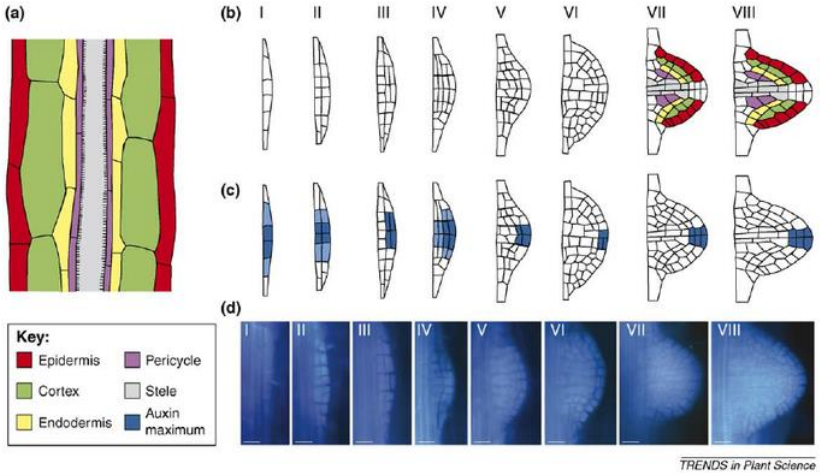

Figure 1-6: Lateral root primordium initiation and development from the pericycle cell.(a) *Arabidopsis* root tissues. (b) The roman numbers shows the eight stages of primordium development. (c) Auxin signalling (pretended by DR5:GUS) during the LR development process. (d) Aniline-blue-stained roots for the LR stages, scale bar 20mm. (This figure is reproduced from Peret et al. (2009)).

Many genes have been identified that have defined functions during lateral root development, such as *GATA23* a transcription factor that plays a critical role in lateral root founder cell specification, *ACR4* a receptor – like kinase that represses the divisions in the cells surrounding the founder cell and LAX3 the auxin influx carrier which controls the expression of cell wall remodelling enzymes (Peret et al., 2009).

A transcriptomic time course data set of lateral root development revealed several auxin-related components that regulate LR initiation and emergence (Voss et al., 2015). Two putative kinases *AT2G15300* and *AT4G34220* (LRR-TYPE RECEPTOR KINASE) were selected from this dataset as co-expressed with *GATA23* (Voss et al., 2015). Both genes were selected and analysed for their role in Lateral root Initiation and development. Investigation of the role of

AT2G15300 and *AT4G34220* in LR development are described in chapter four of this thesis

1.3.4 ENVIRONMENTAL CHANGES THAT AFFECT PLANT PROGRESS

Environmental signals such as water availability, nutrient availability, salinity and gravity play important roles in controlling root growth (Nakashima et al., 2012, Khraiwesh et al., 2012, Atkinson et al., 2014, Elda et al., 2012).

Higher plants respond to gravity positively or negatively, depending on the plant organs. The upper part of the plant (shoot system) grows to the opposite side of gravity, while the root system (the lower part of the plant) grows in the same direction as gravity (Blancaflor, 2013, Kazan, 2013, Hashiguchi et al., 2013).

The root tip region of the primary root performs gravitropism responses. These tissues have columella cells which contain starch bodies which undergo sedimentation, repositioning in response to gravity. However, the plant hormone (auxin) is a key regulator of the plant response to gravity (Aubry-Hivet et al., 2014, Herranz and Medina, 2014).

Chapter five of this thesis describes the plant gravity responses in more detail. In addition, the possible contributions of two candidate genes *AT2G25900* (Cys3His ZINC FINGER TRANSCRIPTION FACTOR) and *AT5G47540* (MO25- LIKE PROTEIN) from a previous study (Hijazi, 2013) have been investigated for their role in mediating gravitropism.

1.4 PLANT GROWTH REGULATORS

Phytohormones are small endogenous signalling chemical components that regulate plant growth and developmental processes. These (non-protein) molecules are structurally diverse, and have important effects on plant adaptive and responses to biotic and abiotic stress (Bari and Jones, 2009, Jaillais and Chory, 2010, Peleg and Blumwald, 2011, Yang et al., 2013).

Classically, five plant hormones have been described as developmental regulators: Gibberellins, Ethylene, Cytokinins, Abscisic acid and Auxin. Gibberellins (GA) are produced in the embryo, stem and root tips, young leaves and developing fruits. They control seed germination, plant height, leaf size and the initiation of the flowers and fruits (Gao et al., 2011, Iqbal et al., 2011, Porri et al., 2012). Ethylene (ET) is synthesized in response to wounding injury in flowers, fruits and leaves. This hormone regulates shoot and root growth and differentiation, germination, loss of chlorophyll, fruit ripening, cell aging and cell death (Camehl et al., 2010, Sun et al., 2010).

Cytokinins (CK) are produced in the plant roots and are important for plant adaptation to different environmental stresses, cell division, leaf expansion, growth stimulation, shoot initiation and bud formation (Ha et al., 2012, Choi et al., 2011, Nishiyama et al., 2011). Abscisic acid (ABA) regulates plant responses to drought, salinity and cold temperature, seed germination and maturation, cell division and elongation (Kanno et al., 2010, Sirichandra et al., 2010, Finkelstein, 2013).

In addition, many other classes of plant hormones exist that have important functions in plant growth and responses such as Jasmonic acid, Brassinosteroids, Salicylic acid, etc. These hormones have been the focus of a wealth of research in recent years in order to determine the mechanism and impact of the functions of each hormone during the plant life cycle (Zhang et al., 2009, Wang and Irving, 2011, Niu et al., 2011, Saini et al., 2015).

1.4.1 THE PLANT HORMONE: AUXIN

Indole-3-Acetic Acid (Auxin, IAA) is a weak organic acid. The chemical structure of auxin is shown in Fig. 1-7. Auxin (IAA, pKa = 4.75). It is a cyclic compound consisting of a side harbouring ring that is covalently linked to a carboxyl group (Webb and Hall, 1995, Vanneste and Friml, 2009, Tromas et al., 2010).

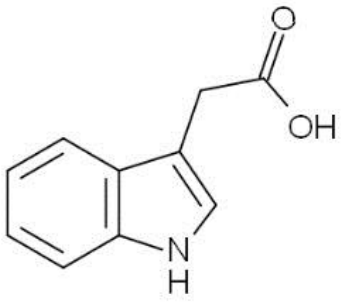

Figure 1-7: Indole Acetic Acid (Auxin; IAA) structure.

Historically, auxin is reported as the first plant hormone to have been discovered. Its scientific name was derived from the Greek word ‘αυξανω’ meaning ‘to grow’. In 1933, Kenneth Thimann and his group discovered and correctly identified the main form of IAA in higher plants. Since then, extensive research

has been conducted to understand the functions of auxin during the different plant growth stages (Teale et al., 2006).

Auxin regulates almost every aspect of plant growth and patterning processes throughout the plant's life cycle (Vanneste and Friml, 2009). Examples of auxin-controlled processes include cell division, embryonic and post-embryonic patterning, vascular differentiation, cell elongation, root and lateral root initiation and tropic responses (depending on light and gravity) (Paciorek and Friml, 2006, Teale et al., 2006).

1.4.1.1 AUXIN SYNTHESIS

Auxin biosynthesis mainly occurs in shoot apical meristematic tissues and young leaves. In addition, it can be also synthesised locally in the root or lateral root meristems. Auxin synthesis is regulated by developmental and environmental signals such as temperature (Woodward and Bartel, 2005, Mano and Nemoto, 2012, Franklin et al., 2011).

Two main pathways have been found for auxin biosynthesis in bacteria and plants; namely, the TRP-dependant and the TRP-independent pathways. The TRP-dependant pathway includes four different auxin biosynthesis routes: Indole-3-Pyruvic Acid (IPyA), Indole-3-Acetamide (lAM), Tryptamine (TAM) and Indole-3-Acetaldoxime (IAOx) (see Fig. 1-8) (Mashiguchi et al., 2011, Mano and Nemoto, 2012, Ljung, 2013, Larrieu, 2011). Recent discoveries have identified two enzymes that are required for IAA biosynthesis in plants: TRYPTOPHAN AMINOTRANSFERASE OF ARABIDOPSIS (TAA), found

to be responsible for producing Indole-3-Pyruvic Acid (IPA) from L-tryptophan (L-TRP); and YUCCA FLAVIN MONOOXYGENASE-LIKE proteins (YUC), which catalyses the conversion of IPA to IAA in *Arabidopsis*.

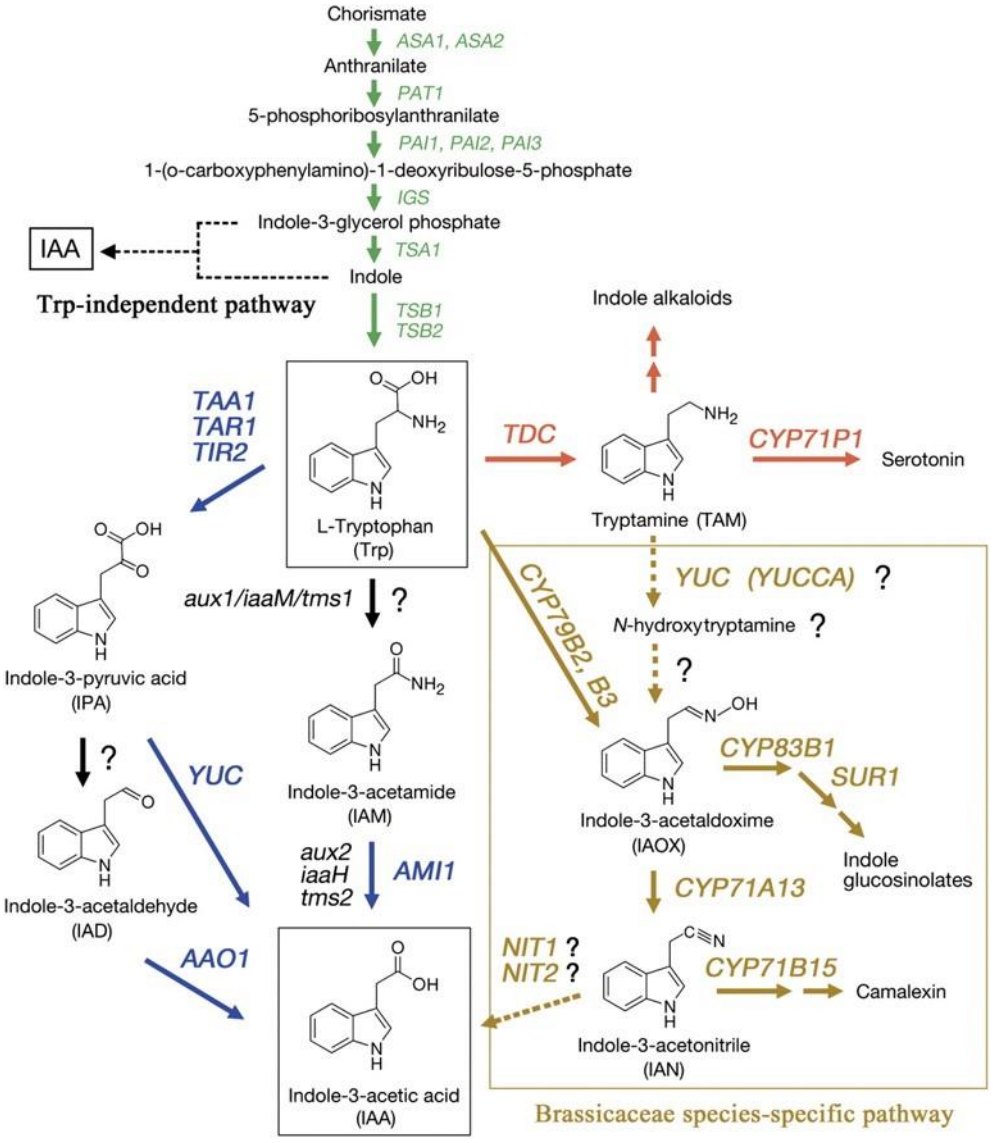

Figure 1-8: Auxin biosynthesis pathways. Tryptophan synthetic pathway in chloroplast (Green arrows). The known genes and enzymes in Tryptophan dependent IAA biosynthetic pathway (Blue arrows). Indole alkaloid and serotonin biosynthetic pathway (Red arrows). Brassicaceae species- specific pathway (Yellow arrows). Unknown genes and enzymes (Black arrows and ? marks). (This figure is reproduced from Mano and Nemoto (2012)).

1.4.1.2 AUXIN TRANSPORT

Auxin has the capability of polar movement from its sites of synthesis to target tissues. Auxin transport is mediated through two distinct routes. The first route consists of rapid transport across long distances via the phloem, e.g. when translocating auxin from biosynthesis sources (young shoot tissues) to sink tissues (roots) (Swarup et al., 2001, Marchant et al., 2002). For short distances intercellular (cell to cell) is mediated by influx and efflux carriers (Vanneste and Friml, 2009, Abel and Theologis, 2010). The efflux (such as PIN-FORMED (PIN) and PHOSPHO-GLYCOPROTEIN (PGPs) and influx (such as AUXIN-RESISTANT 1 (AUX1) and LIKE AUX 1 (LAX 1-3) carriers are membrane-localised transport proteins which control auxin movement (Bennett et al., 1996, Swarup and Peret, 2012, Peret et al., 2012, Viaene et al., 2013). These different classes of auxin carriers have the ability to relocalize on different faces of the cell, thus determining the direction and flux of auxin transport within tissues.

A recent system modelling study revealed that PIN carriers determine the direction of auxin transport but Aux/LAX carriers regulate in which tissues auxin accumulates (Band et al., 2014).

The PIN gene family contains eight members; five of which (*PIN1, 2, 3, 4* and *7*) are asymmetrically localized on the plasma membrane (PM), whereas *PIN5* and *PIN8* are localized in the endoplasmic reticulum membrane (ER), moreover *PIN6* is localized in both PM and ER (Ding et al., 2012, Simon et al., 2016). These PINs are important for tropism, root, lateral root (LR), embryogenesis and developmental processes of vascular tissues. Furthermore, they can regulate

auxin homeostasis and controls the direction of subcellular auxin movement. In addition, *pin* mutants have been shown to display defects in developmental processes which are regulated by auxin (Swarup and Peret, 2012, Dal Bosco et al., 2012, Habets and Offringa, 2014, Geisler et al., 2014).

Another major auxin transporter family is the P-Glycoproteins (PGPs; *PGP1*, *PGP4*, *PGP19* and *ABCB14/15*), which have been identified to be auxin efflux carriers (Kaneda et al., 2011) and are members of the ATP-BINDING CASSETTE PROTEIN subfamily B (ABCB). In addition, a group of seven members (PIN-LIKES; PILs) and a group of serine/threonine protein kinase (Ser/Thr; the *PINOID*) have been shown to function as PIN auxin efflux regulators in *Arabidopsis* (Barbez et al., 2012, Ueda et al., 2014, Lee and Cho, 2014, Band et al., 2014).

A group of four genes (*AUX1* (Bennett et al., 1996), *LAX1*, *LAX2* and *LAX3* (Swarup et al., 2008) function as auxin influx carriers (Swarup and Peret, 2012, Peret et al., 2012).

Classic studies have described how auxin transport through the plant cell membrane is dependent on an H^+ gradient. As a result of acidity in the apoplast region (pH 5.5), IAA becomes protonated (IAAH). In this form it is lipophilic, and as such can diffuse through the cell membrane. However, it is possible for IAAH to convert back to IAA^- (deprotonated; lipophobic) in the alkaline pH of the cytosol. This leads to the accumulation of IAA^- inside the cell which requires auxin efflux carriers to transport auxin outside the cell across the cell membrane (Li et al., 2004, Swarup and Peret, 2012, Ljung, 2013).

1.4.1.3 AUXIN REGULATION OF GENE EXPRESSION

Recent studies have elucidated several proteins that comprise auxin receptors in *Arabidopsis*. AUXIN RELATED F-BOX PROTEINS (AFBs; AFB1, AFB2 and AFB3) and TRANSPORT INHIBITOR RESPONSE 1 (TIR1) are F-box proteins located in the nucleus, which, in combination with SKP1-LIKE protein and CULLN1 (E3 upiquitin protein ligase complex; SCF) form the SCF^{TIR1} auxin receptor pathway (Teale et al., 2006, Orman-Ligeza et al., 2013).

Two families of auxin response complex genes were identified in the nucleus in *Arabidopsis*: the *Aux/IAAs*, a family of proteins containing a potent transcriptional repression domain (29 members), and the DNA-binding *AUXIN RESPONSE FACTORS* (*ARFs*; 23 members). The Aux/IAAs family negatively regulates auxin signalling, while members of the ARFs act as either repressors or as activators (associated with Aux/IAA and TPL proteins) for transcriptional processes (Dahlke et al., 2010, Brunoud et al., 2012). *Aux/IAA* and *ARFs* genes have four conserved domains. In Aux/IAA proteins, the amino-terminal (N-terminal) domain I is important for binding TOPLESS proteins (TPL; transcriptional corepressors). The carboxy-terminal (C-terminal) domains III in Aux/IAA and IV ARFs proteins are important in the dimerization between Aux/IAA with ARFs proteins. Lastly, domain II in Aux/IAA proteins represents the co-receptor binding sites for auxin TIR1/AFB F-box proteins, which facilitate Aux/IAA ubiquitination and degradation via the 26S proteasome. The N-terminal conserved domain in ARFs proteins binds with AuxREs (AUXIN RESPONSES ELEMENTS (TGTCTC) located in the promoter region of the

auxin responses genes, while the middle domain can be used to identify the *ARF* functions (up or down regulation of the gene expression) according to the type of the related amino acid (about 13 amino acid). For example *ARF7* and *ARF5* act as transcriptional activators whereas *ARF2* acts as transcription repressor (Teale et al., 2006, Havens et al., 2012, Pitaksaringkarn et al., 2014, Habets and Offringa, 2014). Additionally, *ARF8* plays a role in regulating lateral root architecture under nitrogen treatments (Gifford et al., 2008).

Figure 1-9 shows that, in the absence of auxin (a), Aux/IAA proteins (repressors of ARFs functions) bind to ARFs transcription factors (via C-terminal domains III & IV), which in turn bind to AuxRE (AUXIN RESPONSIVE ELEMENTS) located at the promoter region of the auxin-responsive genes, resulting in deactivation of auxin-responsive genes. However, under high auxin concentration (b), auxin promotes the binding of Aux/IAA with TIR1/AFBs (via domain, II), and as a result of this interaction the Aux/IAA corepressor is ubiqutinated and degraded via the 26S proteasome pathway (Paciorek and Friml, 2006). Free ARFs (which remain bound to AuxRE), then activate (as a single or in a pair with another ARFs protein) downstream auxin-responsive genes, such as LBD/ASL (LATERAL ORGAN BOUNDARIES domains/ ASYMMETRIC LEAVES- LIKE) transcription factors (Yadav et al., 2010, Demeulenaere and Beeckman, 2014).

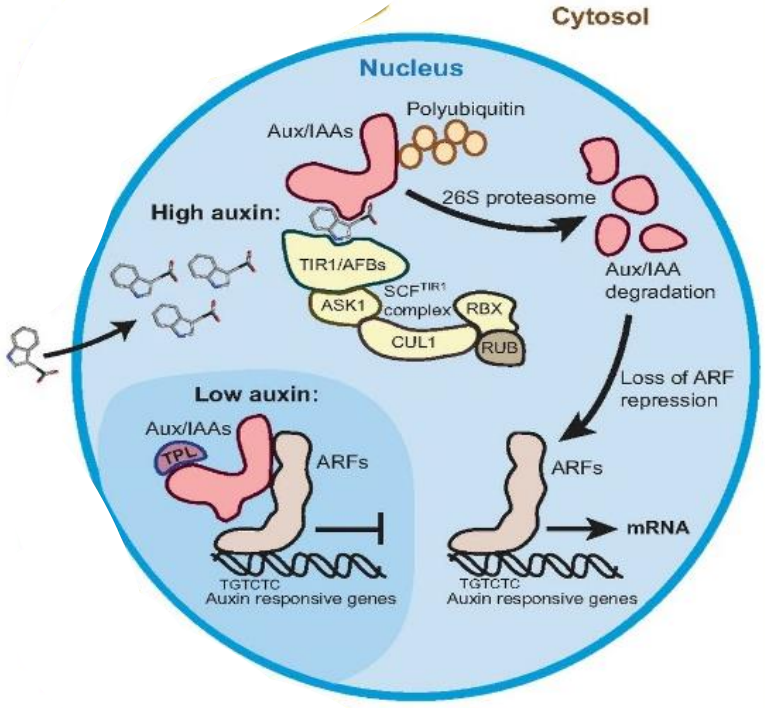

Figure 1-9: Auxin signalling. Under low IAA: Aux/IAA proteins (repressor) binds to ARFs (transcription factors) which leads to deactivation of auxin-responsive genes transcription. Under high IAA: auxin promotes the binding of Aux/IAA with the SCF ^{TIR1} complex, as a result of this interaction the Aux/IAA corepressor is ubiqutinated and degraded via the 26S proteasome pathway which leads to depress of downstream auxin responsive genes (This figure is reproduced from Ljung (2013)).

1.4.1.4 AUXIN DEGRADATION and CONJUGATION PATHWAYS

One of the mechanisms for a plant to maintain a suitable intercellular auxin level is to control auxin conjugation and degradation pathways (Zhao, 2010). In *Arabidopsis*, there are four main pathways (Fig. 1-10):

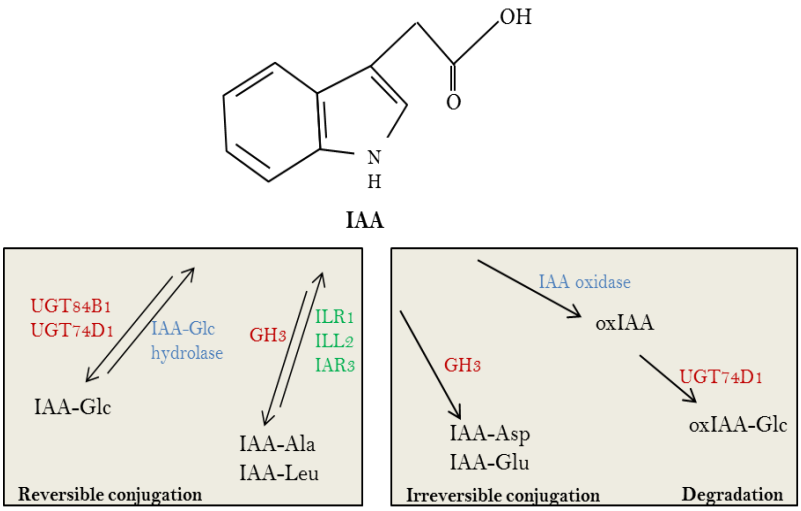

Figure 1-10: Auxin can be degraded and conjugated to different storage forms of IAA. IAA conjugates via a reversible process to IAA-Glc (by UGT84B1) or amino acids (by GH3) or via a irreversible process to IAA-Asp and IAA-Glu (by GH3). . IAA can be oxidised to oxIAA then to oxIAA-Glc by UGT74D1. (This figure is reproduced from Porco et al. (2016)).

1) Ester-linked conjugation with sugars, in which UDP-glucose transferase (UGT74D1 & UGT84B1) catalyses the glucosylation of IAA to IAA-Glucose (IAA-Glc) (reversible conjugation).

2) Amide-linked conjugation with amino acids. In this pathway, IAA amino acid conjugates (group of GRETCHEN HAGEN 3 Family; *GH3*) convert IAA to IAA-Alanine (IAA-Ala), IAA-Leucine (IAA-Leu), IAA-Phenylalanine (IAA-Phe), IAA-Aspartic (IAA-Asp) and IAA-Glutamine (IAA-Glu). The first three products can be hydrolysed back to free IAA via IAR3, ILL2 and ILR1 in a process known as reversible conjugation, whereas the last two products cannot be hydrolysed to active IAA (irreversible conjugation).

3) Amide-linked conjugates with peptides and proteins whereby IAA is converted to IAA-Tryptophan (IAA-Trp).

4) Another irreversible pathway is the oxidation of free IAA to 2-oxoindole-3 acetic acid (oxIAA), which is then converted to oxIAA-Glc via UGT74D1.

Despite being the major of auxin regulation, the latter auxin degradation route remains to be elucidated (Ludwig-Muller, 2011, Korasick et al., 2013, Ljung, 2013, Porco et al., 2016, Mellor et al., 2016).

It has been recently reported that in rice (*Oryza sativa*) the gene, DIOXYGENASE FOR AUXIN OXIDATION (*DAO*), which encodes a putative 2-oxoglutarate-dependent-Fe (II) dioxygenase, is responsible for catalysing the oxidation of IAA to oxIAA. There is one copy of this enzyme in rice and mutation in this gene confers male sterility, displaying high levels of free IAA in anthers and ovaries (Zhao et al., 2013). *Arabidopsis thaliana* has two copies of *DAO: AT1G14130* and *AT1G14120* (*DAO1* and *DAO2*, putative 2OG-Fe (II) oxygenases). There is strong evidence confirming that these two genes are active in converting IAA to oxIAA in *Arabidopsis* (Porco et al., 2016, Mellor et al., 2016).

The two gene products DIOXYGENASE FOR AUXIN OXIDATION 1 (*AtDAO1; AT1G14130*) and 2 *AtDAO2*; *AT1G14120*) are members of the 2-oxoglutarate-dependent-Fe (II) dioxygenase gene family. They share 76% of their amino acids, and are positioned in tandem on chromosome 1. In addition, they are also closely related to a sequence of genes descried in apple (*ARRO-1*;

Adventitious Rooting Related Oxygenase) and Rice (*DAO*; Dioxygenase for Auxin Oxidation) as well as to a gene family of GA2-oxidases which mediate Gibberellin inactivation (Butler and Gallagher, 2000, Zhao et al., 2013, Porco et al., 2016, Mellor et al., 2016). However, these two genes are regulated very differently, *AtDAO1* is an auxin inducible gene (Porco et al., 2016, Mellor et al., 2016), while *AtDAO2* expression is controlled by the circadian rhythm (Voss et al., 2015).

The characterisation of *AtDAO1* and interaction with auxin conjugation is described in chapter three of this thesis.

.

PROJECT AIMS AND OBJECTIVES

Understanding the molecular mechanisms that regulate the architecture of root systems is fundamental for generating improved crops. Identifying genes that control root architecture, root hair, branching and angle, using *Arabidopsis thaliana* as a model plant, this project had three main objectives.

1) The characterization of the *AtDAO1* gene that regulates auxin oxidation and homeostasis in roots, and controls root hair length.
2) Elucidation of the roles of two kinase genes (*LRK1* and *LRK2*) that control lateral root initiation and development.
3) The functional characterization of candidate genes (*TF* and *Mo25*) that regulate root angle.

GENERAL MATERIALS AND METHODS

2.1 PLANT MATERIAL

Arabidopsis thaliana (wildtype *Columbia* (*Col-0*) and *Arabidopsis thaliana* T-DNA insertion "knock-out (KO)" lines) seeds were obtained from the Nottingham *Arabidopsis* stock centre (NASC, http://www.arabidopsis.org/portals/education/aboutarabidopsis.jsp, University of Nottingham, Loughborough, UK. All seeds which were used in the experiments are available within the lab from previous research.

2.2 SEED STERILIZATION AND PLANT GROWTH CONDITIONS

Seeds were surface sterilized with 70% (v/v) ethanol (1 min) followed by 5% (v/v) hypochloric acid (HC1O, 5 min), then washed three times with 0.001% (v/v) triton X-100 (1 min), followed by two washes with sterile deionized water (ddH_2O). Sterilized seeds were plated on plastic square Petri dishes (Greiner Bio-One Ltd., 120x120x17 mm) containing 70 ml 0.5 × plant growth media MS salt (Murashige and Skoog; 1962 (Sigma), 2.15 g/L [pH 5.8]; solidified by adding 1% (w/v) Bacto-agar (Appleton Woods)). Seeds were stored at 4°C for 24h in the dark to synchronise germination. The plates were then incubated vertically in the growth room for germination. Conditions in the growth room were controlled at 23°C under continuous light and ~75 $\mu E^2/s/m^2$ white fluorescent light intensity.

After germination, seedlings (approx. 15 days old) were transferred to 9 cm plastic pots with Levington M3 compost supplemented with 0.2 g l^{-1} of intercept

(pesticide). Plants were grown in the glass house compartments under conditions of 20 ºC ± 2 ºC day and 16 ºC ± 2 ºC night temperatures with a 22 h under light intensity (111 $\mu E^2 s^{-1} m^{-2}$). Mature seeds were harvested from dry plants and then stored at room temperature.

2.3 GENOTYPIC EXPERIMENTS

2.3.1 GENOMIC DNA ISOLATION

In order to extract genomic DNA, young *Arabidopsis thaliana* leaves were collected from the plants and placed in Eppendorf tubes (1500 µL) and immediately frozen in liquid nitrogen. Leaf tissues were then ground to powder using a Qiagene Tissue Lyser II (Adapter set 2x24) with metal beads. To this 600 µl of DNA extraction buffer (1 M Tris-HCL [pH 7.5], 4 M NaCl, 0.5 M EDTA and 10% Sodium dodecyl sulfate (SDS)) was added and vortexed for 5 sec then centrifuged for 5 min at highest speed in a microcentrifuge. The supernatant (500 µl) was transferred to a new Eppendorf tube with 500 µl of isopropanol (1:1) added to precipitate the DNA. The mixture was incubated for 2-3 min at room temperature, centrifuged for 5 min at 13,000 rpm , and then the supernatant discarded without disrupting the pellet. The pellet was washed with 150 µl of 70% (v/v) ethanol (EtOH) which was then discarded immediately. The pellet was left to dry at room temperature overnight then 50 µl of distilled water was added to re-suspend the DNA. The extracted genomic DNA was stored at -20 °C for further use.

2.3.2 PRIMERS DESIGN

In order to identify homozygous lines for each allele (T-DNA insertion lines), two gene specific primers were designed: forward and reverse genomic primers (LP and RP respectively) using SIGnAL website, (http://signal.salk.edu/tdnaprimers.2.html). T-DNA specific Left border (LB) primer was used to determine the T-DNA insertion: LBb1.3 for SALK lines; LB1 for SAIL lines; and LBG for GABI Kat lines (Table 2-1).

Table 2-1: T-DNA specific left border (LB) primer sequences.

Primer Name	Sequence (5'>3')
LBb1.3 (SALK lines)	ATTTTGCCGATTTCGGAAC
LB1 (SAIL lines)	GCCTTTTCAGAAATGGATAAATAGCCTTGCTTCC
LBG (GABI KAT lines)	ATATTGACCATCATACTCATTGC

2.3.3 POLYMERASE CHAIN REACTION

Using the Gene Amp® Polymerase chain reaction (PCR) system 9700 (Applied Biosciences), genomic DNA was amplified by PCR (Table 2-2) in a total reaction volume of 20 µl over 35 cycles, Genomic DNA from T-DNA insertion lines (heterozygous and homozygous lines) in addition to genomic DNA from *Col*-0 (as a wildtype, positive control for gene specific primers and negative control for T-DNA insertion primers) was amplified for 35 cycles (see Table 2-3). Three PCR assays were performed for T-DNA insertion screening. A first assay used the two pairs of gene specific primers (LP & RP), the second used

the forward gene specific primer (LP) with T-DNA left border primer (LB), and the third used the reverse gene specific primer (RP) with LB.

Table 2-2: The PCR genotyping reaction mixture concentrations and volumes (in 20 µl).

REAGENTS	VOLUME (µl)
Template DNA (~100 ng/µl)	2-4
PCR Buffer (Sigma) with $MgCl_2$ (10×)	2.0
dNTPs (10 mM)	0.4
Forward primer; LP (10 µM)	1.0
Reverse primer; RP (10 µM)	1.0
Left border primer LB (10 µl)	1.0
Taq DNA Polymerase (Sigma)	0.2
Distilled water (ddH_2O)	x
Total volume	20.0

Table 2-3: The PCR cycling for genotyping.

Step	Temperature °C	Time	No. Cycle
Initial Denaturation	94	5:00	1
Denaturation	94	0:30	35
Annealing	58	0:30	
Extension	72	2:00	
Final Extension	72	7:00	1
	4	∞	

2.3.4 AGAROSE GEL ELECTROPHORESIS

PCR products were checked for size by gel electrophoresis on a 1% Agarose gel (1 g Agarose with 100 ml Buffer (Tris (0.445M)/Borate (0.445M)/EDTA (0.01M), TBE) stained with 5 µl of ethidium bromide. 4 µL of 1 kb DNA ladder was used as a marker to determine the size of DNA fragments under 100 V for about 1 h, which were visualized under UV light.

2.4 GENE EXPRESSION ANALYSIS

2.4.1 RNA EXTRACTION

Total RNA was extracted from *Arabidopsis thaliana* the total root system of 7 day old seedlings using RNase Mini kit (Qiagen) according to manufacturer's instructions.. RNA quantity was measured by using Nanodrop™ spectorophotometer (Thermo Scientific).

2.4.2 COMPLEMENTARY DNA (cDNA SYNTHESIS)

Superscript II Reverse Transcriptase (Invitrogen; 2.4 µl (0.4 µl Oligo-(dT) primer and 2 µl of deoxy nucleotide triphosphates (dNTPs= 10 mM each dATP, dGTP, dCTP and dTTP)) was added to each RNA sample. Samples were vortexed and incubated at 65 ˚C for 5 min, then chilled in ice for 1 min. A reaction mixture (13 µl) comprising SuperScript II, (SSII; 1 µl), 0.1 M dithiothreitol (DTT; 4 µl) and 5X First-Strand Buffer (8 µl) were added to each RNA sample then vortexed and incubated at 42 ˚C for 50 min. The reaction temperature was increased to 70 ˚C for 5 min to inactive the reaction, then the

mixture was chilled on ice for 1 min. The quantity of single stranded of cDNA was measured by using Nanodrop^{TM} spectorophotometer (Thermo Scientific). cDNA extract was stored at -80 °C until required.

2.4.3 REVERSE TRANSCRIPTASE POLYMERASE CHAIN REACTION

Complementary DNA (cDNA) samples were amplified by reverse transcriptase polymerase chain reaction (RT-PCR) (Table 2-4). By using the Gene Amp® PCR system 9700 (Applied Biosciences) with forward and reverse cDNA primers with At1G04850 (FP: 5'-CTCGGGTAGCACGAGCTT-'3, RP: AGTGGAGAGGCTGCAGAA-'3) primers as a positive control, at a total volume of 20 µl per PCR tube, to confirm there was no expression in all knock out lines for homozygous lines and to detect any RNA contamination. For each T-DNA insertion line, two gene specific primers were designed using a cDNA sequence (forward: FP and reverse: RP primers).

Table 2-4: RT-PCR reaction mixture concentrations and volumes (in 20 µl).

REAGENTS	VOLUME (µl)
cDNA (50 – 100 ng/ µl)	2-4
PCR Buffer (Sigma) with $MgCl_2$ (10×)	2.0
dNTPs (10 mM)	0.4
Forward primer; FP (10µM)	1.0
Reverse primer; RP (10µM)	1.0
Taq DNA Polymerase (Sigma)	0.2
Distilled water (ddH_2O)	x
Total volume	20

2.4.4 QUANTITATIVE REVERSE TRANSCRIPTASE POLYMERASE CHAIN REACTION

Quantitative reverse transcriptase polymerase chain reaction (qRT-PCR) technique was used to quantify cDNA sequences and confirm whether T-DNA insertion lines showed either over expression or no expression, as this approach provides a very accurate analysis to identify any gene expression at very low levels. By using the Universal Probe Library Assay Design Centre (http://lifescience.roche.com/shop/CategoryDisplay?catalogId) qRT-PCR specific primers pairs were designed, and (*At1G04850* primer (house-keeping primers (FP: 5' AGTGGAGAGGCTGCAGAA'3; RP: 5' CTCGGGTAGCACGAGCTT'3, in order to normalize the gene expression results) were used as a positive control to examine the cDNA quality. Gene expression was tested in 1% of cDNA samples using 6 µl of a fluorescent dye SYBR® Green Master Mixes (Bioline) for each standard reaction (Table 2-5). The LightCycler®480 System (Roche, USA) was used for gene expression analysis and The LightCycler®480 software, Version 1.5 with Microsoft Excel 2010 were used to analyse the data.

Table 2-5: qRT-PCR reaction mixture concentrations and volumes (in 20 µl).

REAGENTS	VOLUME (µl)
fluorescent dye SYBR® Green	6.0
Forward primer; FP (10µM)	0.1
Reverse primer; RP (10µM)	0.1
cDNA	5
ddH_2O	x
Total	12

2.5 PLANT PHENOTYPIC ANALYSIS

2.5.1 PRIMARY ROOT LENGTH (PRL)

20 seeds were germinated on plastic square Petri dishes (Greiner Bio-One Ltd., 120x120x17 mm) containing 70 ml of half strength plant growth media (MS). The seeds were stored at 4 °C for 24 h then transferred to germinate in the light in a growth room under controlled conditions for 24 h. The length of the primary root was measured after 5, 7, 9 and 10 days using Canon digital camera and Fiji software (an updated version of Image J software, or Image J 1.44b).

2.5.2 LATERAL ROOT DENSITY (LRD)

The number of lateral roots was counted for each seedling (10 days old) germinated on MS plant growth media using a binocular microscope. The lateral root density (cm^{-1}) was calculated by dividing the number of lateral roots by the primary root length.

2.5.3 GRAVISTIMULAUS OF PRIMARY ROOT

Twenty seedlings were grown vertically on MS plants growth media under 12h/12h light/dark conditions. Six day old seedlings were subjected to 90° gravistimulation (Fig. 2-1), and the angles of the deviation of the roots were measured every 60 minutes using an automated image acquisition system (Wells et al., 2012) and Fiji software (an updated version of Image J software, or Image J 1.44b).

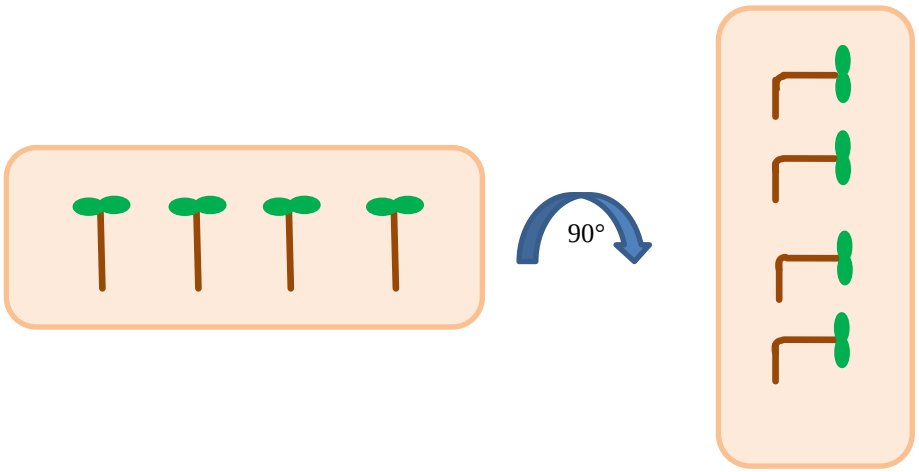

Figure 2-1: Gravitropic stimulation. 6 days old seedlings were germinated under 12/12 light/dark conditions then turned 90º for gravity stimulation.

2.6 MICROSCOPY

2.6.1 CONFOCAL MICROSCOPY

Propidium iodide (5 µg ml^{-1} H_2O) (Sigma) was used for localised staining. The images were taken by Leica SP5 laser scanning confocal microscope (Leica Microsystems) and analysed by Fiji software (an updated version of Image J software, or Image J 1.44b).

2.6.2 LIGHT MICROSCOPY

Roots were cleared using an Ethanol series and clear roots were then loaded on 50% glycerol and observed under a Leica light microscope.

IDENTIFICATION OF THE ROLE OF *AtDAO1* IN AUXIN HOMEOSTASIS IN *ARABIDOPSIS*

3.1 INTRODUCTION

Auxin (Indole-3-acetic acid, IAA) is phytohormone which plays roles in the control of almost every aspect of plant growth and developmental processes, such as in cell division, elongation, differentiation, lateral root initiation and development and tropism responses (Vanneste and Friml, 2009, De Rybel et al., 2010, Abel and Theologis, 2010). Due to the importance of auxin in plants, this gives cause to investigate its biosynthesis within tissues, transportation through cells, signalling mechanism, so as to define how auxin regulate plant processes (Zhao, 2010). It is very important to maintain a suitable auxin concentration in plant cells; this can be achieved by regulating auxin synthesis, conjugation (to sugar or amino acids) and degradation. Despite the progress which has been made to understand auxin biosynthetic pathways in plants, auxin degradation and conjugation pathways are still being elucidated due to a lack of molecular tools which would enable understanding of auxin perception at subcellular levels remains to be clarified (Ljung, 2013).

An important element of the IAA degradation machinery is the oxidation (irreversible step) of IAA to 2-oxindole-3-acetic acid (oxIAA) (Pěnčík et al., 2013). In *Arabidopsis thaliana* root tissues, two copies of IAA oxidases genes have been revealed (*DIOXYGENASE FOR AUXIN OXIDATION 1 (AtDAO1*, *At1g14130*) and 2 (*AtDAO2*, *At1g14120*)) to have functions in IAA oxidation.

The role of the dioxygenase-encoding *AtDAO1* gene in regulating auxin homeostasis in *Arabidopsis thaliana* has been identified and characterised. This work has been published in the Proceedings of the National Academy of

Sciences of the United States of America (PNAS) back to back with a mathematical model of auxin metabolism work to confirm the importance of *AtDAO1* in IAA oxidation pathway (Porco et al., 2016, Mellor et al., 2016).

3.2 MY CONTRIBUTION TO BOTH PAPERS INCLUDED

- Isolating and characterizing *dao1* mutant alleles (Porco et al., 2016).
- Identifying the root hair defect in *dao1-1* (Porco et al., 2016).
- Working closely with Nathan Mellor to test his mathematical model predictions using qRT-PCR (Mellor et al., 2016).

3.3 MATERIALS AND METHODS

3.3.1 *ARABIDOPSIS THALIANA* MUTANTS LINES

Four *dao1* alleles in addition to the wildtype (*Col-0*) were obtained from the Nottingham *Arabidopsis* stock centre (NASC). The exact position of each T-DNA insert was identified by using TAIR website (https://www.arabidopsis.org/) (Table 3-1).

Table 3-1: *Arabidopsis thaliana* T-DNA insertion lines**.**

Gene ID	Mutants	NASC ID	CODE	INSERT POSITION
AT1G14130 (*AtDAO1*)	*dao1-1*	N593162	SALK_093162	Exon 1
	dao1-3	N582522	SALK_082522	Upstream the start codon of *AtDAO1*
	dao1-2D	N816250	SAIL_349_D02	Upstream the start codon of *AtDAO2*
	dao1-4D	N595931	SALK_09593	Upstream the start codon of *AtDAO1*

3.3.2 STERILIZATION AND GROWTH CONDITIONS

Surface sterilisation of seeds was performed in a sterile laminar flow cabinet, and consisted of one wash in 70% (v/v) ethanol (1 min), one wash in 5% (v/v) of hypochloric acid (5 min), three washes in 0.1% (v/v), and finally two washes in sterile ddH_2O. Sterile seeds were grown on half MS medium (Sigma) (pH 5.8) and stored at 4^0C for 24h in order to synchronise the germination before being

transferred to a controlled growth room (see section 2.2 for more details of growth conditions).

3.3.3 GENOTYPIC ANALYSIS OF T-DNA INSERTION LINES

In order to identify homozygous lines for *AtDAO1*, Genomic DNA (gDNA) was extracted from two cotyledons (following the DNA extraction protocol, section 2.3.1). Extracted gDNA was used as template in Polymerase Chain Reaction reactions (PCR) assays (see section 2.3.3), either by using gene specific primers (forward and reverse primers; LP and RP) or by using the gene specific primer reverse (RP) with the T-DNA LB primer. To design the primers (LP and RP), the SIGnAL website (http://signal.salk.edu/tdnaprimers.2.html) used (Table 3-2).

Table 3-2: Gene specific primer sequences of T-DNA insertion lines.

T-DNA insertion mutant line		Forward Primer	Reverse Primer
AT1G14130 (*AtDAO1*)	*dao1-1* (SALK_093162)	TTCCCCACGGAATTAAGGTAC	CTATGGGGAAAAAGGTTCCTG
	*dao1-3 (*SALK_082522)	ATAAATTTGGGCCCAAAAGTG	TGAAACATCCCCATCTCTCAC
	*dao1-2D (*SAIL_349_D02)	TTGGTGGACTTGAAGCTATGG	GCGGTTTGAGATACATGTGG
	*dao1-4D (*SALK_09593)	TCGTGTTTTGGGTCTCCTATG	TCCGTTTAGTTCCCCCATATC

3.3.4 RNA EXTRACTION, REVERSE TRANSCRIPTASE POLYMERASE CHAIN REACTION AND QUANTITATIVE REVERSE TRANSCRIPTASE POLYMERASE CHAIN REACTION

Whole roots of 7 day old seedlings were used for RNA extraction. The extraction was performed using Trizol Reagent (Invitrogen) following the RNase Mini Kit protocol (Qiagen) (section 2.4.1). The Superscript II Reverse Transcriptase' protocol (Invitrogen, section 2.4.2) was carried out using 1 µg of RNA to synthesize cDNA. Reverse transcriptase polymerase chain reaction (RT-PCR) reaction was performed to qualify the gene expression level in all mutant lines compared with the gene expression in *Col-0* (Table 3-3 shows the RT-PCR specific primer sequences).

Table-3-3: RT-PCR specific primer sequences.

Line	Forward Primer	Reverse Primer
AT1g14130 (*AtDAO1*)	CTATTAGTCACGAAGGGGTACG	CTAGTCCTGCATGGGTTATAAG

Quantitative reverse transcriptase PCR (qRT-PCR) was performed to quantify the gene expression level of *AtDAO1* by using LightCycler® 480 system (Roche, USA) with the fluorescent dye SYBR® Green Master Mixes (Bioline). The data was normalized withAt1G04850 and Microsoft Excel 2010 (Microsoft Corporation, Redmond, USA) was used to analyse the data. Specific qRT-PCR primers were designed by the Universal Probe Library Assay Design Centre (Table 3-4 shows qRT-PCR primers sequences).

Table 3-4: qRT-PCR specific primer sequences.

Line	Forward Primer	Reverse Primer
AT1g14130 (*AtDAO1*)	TCGAAGCTTCTGCAGATCAA	TTTCCTCGCTAAATCCGTTG

3.3.5 PHENOTYPIC ANALYSIS

3.3.5.1 PRIMARY ROOT LENGTH, LATERAL ROOT NUMBER AND LATERAL ROOT DENSITY

Sterilized seeds of mutant lines were grown vertically on half MS under controlled conditions (section 2.2). The lengths of primary roots were measured for 5, 10 and 15 day old seedlings using Fiji software. To determine the number of emerged lateral roots along the primary root samples were examined with a binocular microscope. The lateral root density was calculated (cm^{-1}) for individual T-DNA insertion lines.

3.3.5.2 GRAVISTIMULATION ASSAY

Under a controlled environment, approximately 20 seeds were grown with a 12 h photoperiod. Six day old seedlings were turned 90^0 during the dark period. The angle of each primary root was measured over 8 h by automated image acquisition system (Wells et al., 2012). All data were analysed using Fiji software.

3.3.5.3 ROOT HAIR NUMBER

Leica Light Microsystems was used to count the number of the root hairs for 5, 10 and 15 day old seedlings within a 100 µm section of the root length starting at, the first root hair bud in the root tip which extended up the root towards the aerial parts of the seedling. The lengths of root hairs were measured by Fiji software (an updated version of Image J software).

3.4 COMPLEMENTARY RESULTS

Four T-DNA insertion lines (*dao1-1* (SALK_097787), *dao1-3* (SALK_082522), *dao1-2D* (SAIL_349_D02) and *dao1-4D* (SALK_09593)) were selected for genotyping analysis in order to find knock out lines (Fig. 3-5). PCR was performed using three primers (forward and reverse gene specific primers (LP & RP) and the left T-DNA border primer (LB). Two cotyledons were used to extract genomic DNA from knock out lines and wild type (WT, Columbia *Col-0*).

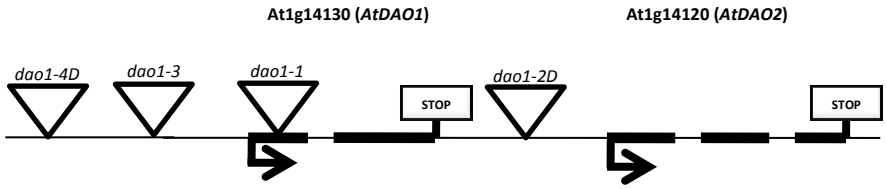

Figure 3-1: AT1G1430's map indicating the T-DNA insertion lines positions of *dao1-1* (SALK_097787), *dao1-3* (SALK_082522), *dao1-2D* (SAIL_349_D02) and *dao1-4D* (SALK_09593).

3.4.1 GENOTYPING ANALYSIS OF T-DNA INSERTION LINES

Following visualisation of PCR products separated out on agarose gel it was observed that all mutant lines of AT1G14130 (*dao1-1*(SALK_097787), *dao1-3* (SALK_082522), *dao1-2D* (SAIL_349_D02) and *dao1-4D* (SALK_09593)) are homozygous for *AtDAO1* compared with WT (Columbia, *Col-0*) (Figs.3-2 - 3-5).

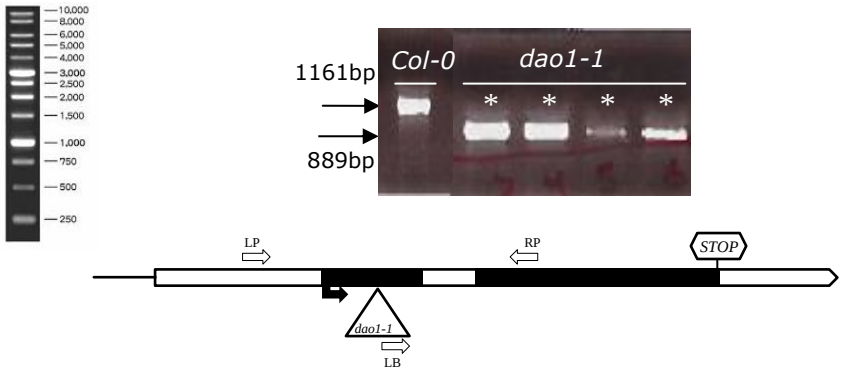

Figure 3-2: Genotypic analysis by PCR for *dao1-1* (SALK_097787), using two genomic primers (LP + RP: forward and reverse primers) Product size = 1161bp, and RP + left T-DNA border primer (LB) Product size= 889bp. WT: wild type (Columbia) and 4 SALK_097787 line seedlings. (1kB DNA ladder, *: Homozygous plants).

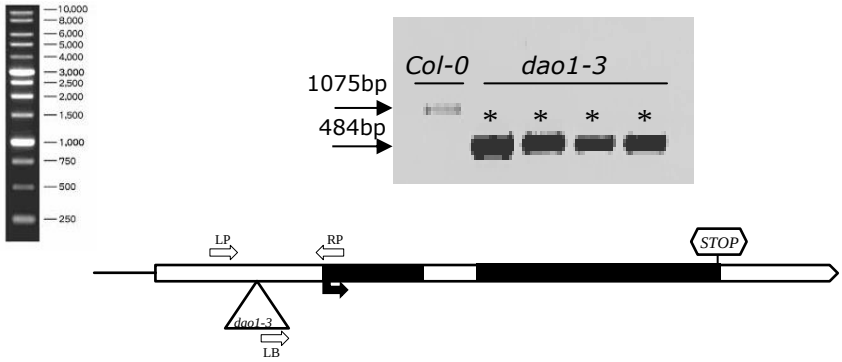

Figure 3-3: Genotypic analysis by PCR for *dao1-3* (SALK_082522), using two genomic primers (LP + RP: forward and reverse primers) Product size = 1075bp, and RP + left T-DNA border primer (LB) Product size= 484bp. WT: wild type (Columbia) and 3 SALK_082522 line seedlings. (1kB DNA ladder, *: Homozygous plants).

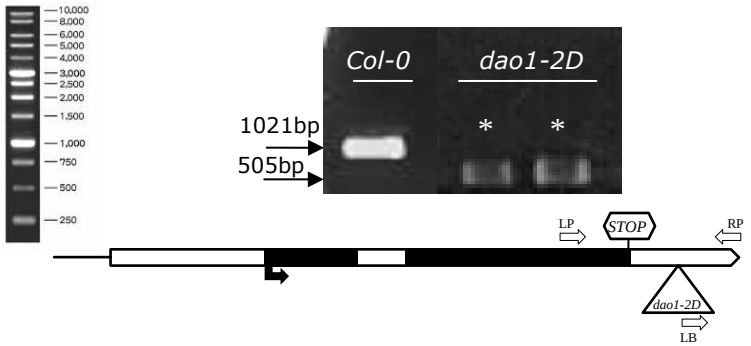

Figure 3-4: Genotypic analysis by PCR for *dao1-2D* (SAIL_349_D02), using two genomic primers (LP + RP: forward and reverse primers) Product size = 1021bp, and RP + left T-DNA border primer (LB) Product size= 505bp. WT: wildtype (Columbia) and 2 SAIL_349_D02 line seedlings. (1kB DNA ladder, *: Homozygous plants).

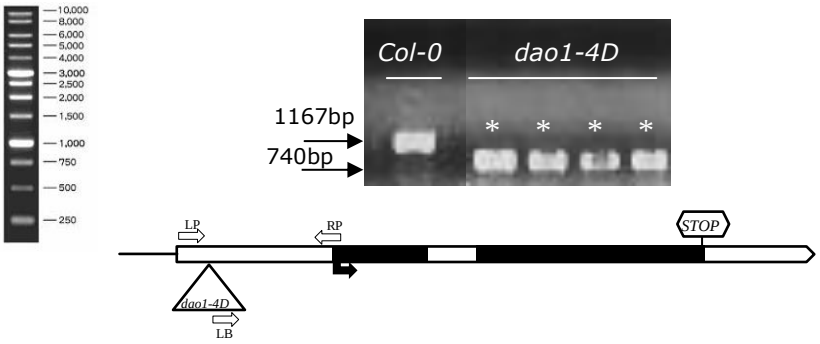

Figure 3-5: Genotypic PCR analysis for *dao1-4D* (SALK_09593), using two genomic primers (LP + RP: forward and reverse primers) Product size = 1167bp, and RP + left T-DNA border primer (LB) Product size= 740bp. WT: wildtype (Columbia) and 2 SALK_09593 line seedlings. (1kB DNA ladder, *: Homozygous plants).

3.4.2 RT-PCR and qRT-PCR

Complementary DNA (cDNA) was synthesised from RNA samples (extracted from the whole root system of 7 day-old seedlings). Samples of cDNA were used to measure the transcript level of the gene of interest; by performing RT-PCR assays using forward (FP) and reverse (RP) primes. In addition, assays using *CTRL1* (*At1G04850*) primers were used to check the quality of cDNA (Fig. 3-6A).

Visualisation of RT-PCR products run on agarose gel showed there was no expression of *AtDAO1* in the *dao1-1* mutant line, whereas there was a faint band in *dao1-3* T-DNA insertion line. However, expressions of *AtDAO1* occurred in both *dao1-2D* and *dao1-4D* mutant lines, suggesting these are not full knock-out lines for *AtDAO1* (Fig. 3-6B).

qRT-PCR data showed that the abundance of *DAO1* mRNA was significantly reduced in both homozygous lines *dao1-1* and *dao1-3*, indicating that these two

lines are full knock-out lines for *AtDAO1*. On the other hand, the level of gene expression was 4-and 2.4-fold higher in *dao1-2D* and *dao1-4D*, respectively, compared to *Col-0*, suggesting that they are overexpression lines for *AtDAO1* (Fig. 3-7 and Fig. 3-8).

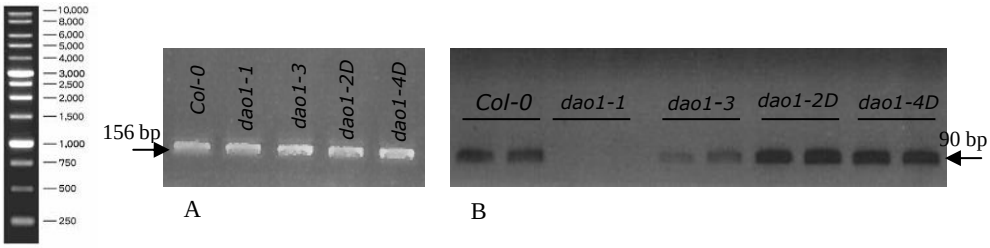

Figure 3-6: RT-PCR expression analysis of the different mutants of AT1G14130 compared with WT (*Col-0*). A) Expression of a house-keeping gene using house-keeping primers (product size ~ 200bp). B) Expression analysis of AT1G14130 (*dao1-1*(SALK_097787), *dao1-3* (SALK_082522), *dao1-2D* (SAIL_349_D02) and *dao1-4D* (SALK_09593), using forward and reversed cDNA specific primers (Product size= 90 bp).

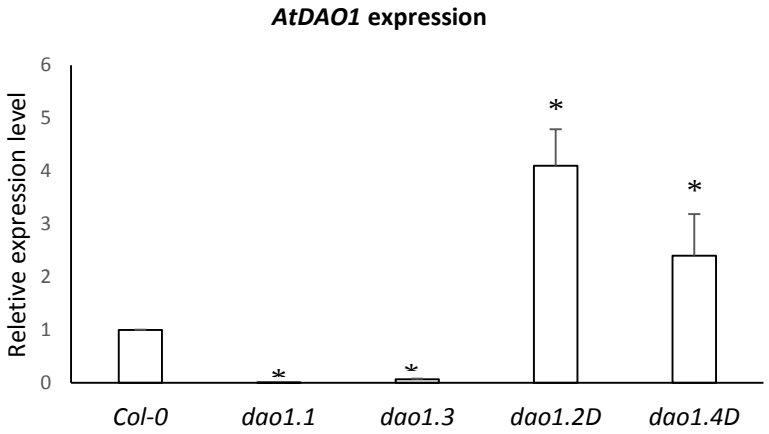

Figure 3-7: qRT-PCR expression quantification for *AT1G14130* of *dao1-1*(SALK_097787), *dao1-3* (SALK_082522), *dao1-2D* (SAIL_349_D02) and *dao1-4D* (SALK_09593) lines, normalized to WT (*Col-0*). * denotes significant difference compared to WT ($P < 0.05$).

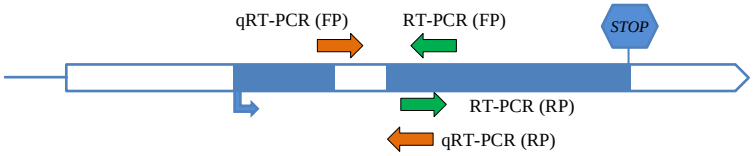

Figure 3-8: Map of *AT1G14130* indicating RT-PCR (forward: FP + reverse: RP) and qRT-PCR (forward: FP + reverse: RP) primers.

3.4.3 PHENOTYPIC ANALYSIS

The phenotypes of the four mutants of *dao1* were characterised to determine any changes in the plants appearance.

3.4.3.1 PRIMARY ROOT LENGTH AND LATERAL ROOT DENSITY

The length of the primary root was measured for 5, 10 and 15 day old seedlings. There were no significant changes in the primary root length for all *dao1* mutants lines (Fig. 3-9). *AtDAo1* mutants exhibit an increase in the lateral root density compared to WT (Fig. 3-10 and 3-11).

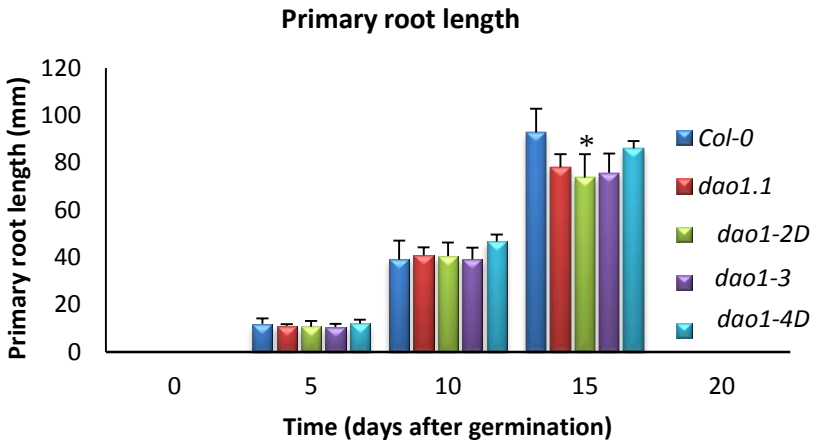

Figure 3-9: The primary root length of 5, 10 and 15 day old seedlings for *AT1G14130* of *dao1-1*(SALK_097787), *dao1-3* (SALK_082522), *dao1-2D* (SAIL_349_D02) and *dao1-4D* (SALK_09593) lines, in compared to WT (*Col-0*). * denotes significant difference compared to WT (Mann-Whitney *U* test; $P < 0.05$).

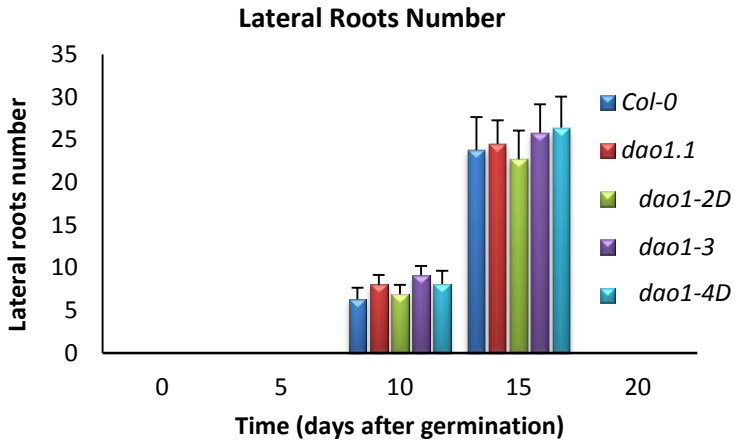

Figure 3-10: The lateral root number of 10 and 15 day old seedlings for *AT1G14130* of *dao1-1*(SALK_097787), *dao1-3* (SALK_082522), *dao1-2D* (SAIL_349_D02) and *dao1-4D* (SALK_09593) lines, in compared to WT (*Col-0*).

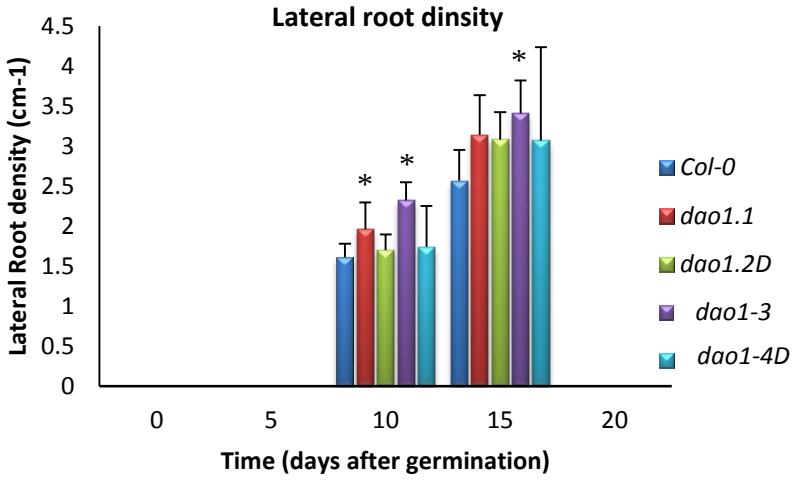

Figure 3-11: Lateral root density (cm^{-1}) of 10 and 15 day old seedlings for *AT1G14130* of *dao1-1*(SALK_097787), *dao1-3* (SALK_082522), *dao1-2D* (SAIL_349_D02) and *dao1-4D* (SALK_09593) lines, in compared to WT (*Col-0*). * denotes significant difference compared to WT (Mann-Whitney *U* test; $P < 0.05$).

3.4.3.2 GRAVITROPISUM ASSAY

Compared with WT roots, *dao1-1* and *dao1-3* less of function mutant lines shows a slower response to gravity factor. While the overexpression lines (*dao1-2D and dao1-4D*) were similar to WT (Fig. 3-12).

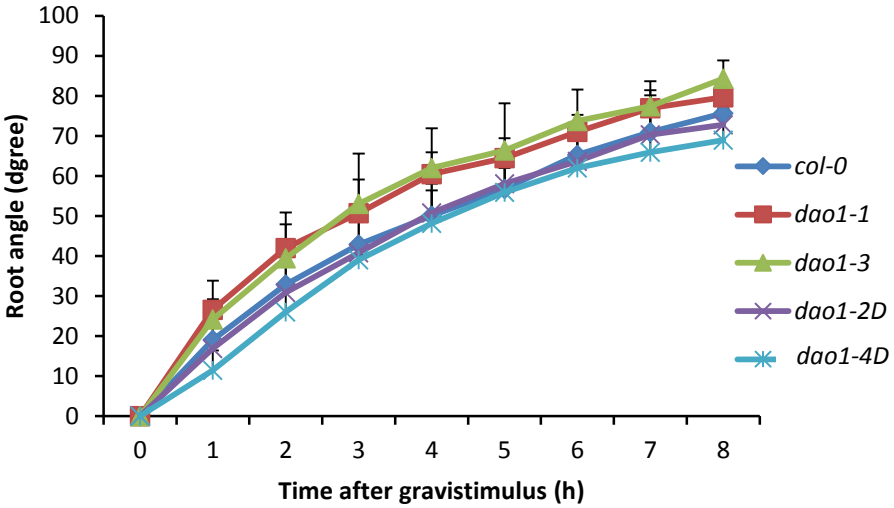

Figure 3-12: Responses of gravistimulated roots of 6 day old seedlings after turning through 90° for *AT1G14130* of *dao1-1*(SALK_097787), *dao1-3* (SALK_082522), *dao1-2D* (SAIL_349_D02) and *dao1-4D* (SALK_09593) lines, in compared to WT (*Col-0*).

3.4.3.3 ROOT HAIR (RH) PHENOTYPE

Root hair length from 5 and 10 day old Col-0 and *dao1* mutant seedlings increased by ~80% in loss of function *dao1-1* and *dao1-3* mutants compared with WT. The RH length measurements of the gain of function lines (*dao1-2D* and *dao1-4D*) revealed shorter root hairs compared to WT (Fig. 3-13). Confocal images showing the RH length differences in 10 day old seedlings of Col-0 and *dao1* alleles (Fig. 3-14).

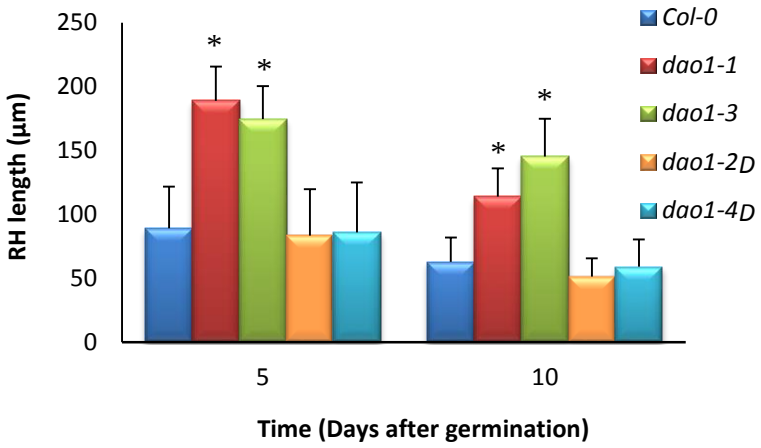

Figure 3-13: The root hair measurements from 5 -10 day old seedlings for *AT1G14130* of *dao1-1*(SALK_097787), *dao1-3* (SALK_082522), *dao1-2D* (SAIL_349_D02) and *dao1-4D* (SALK_09593) lines, in compared to WT (*Col-0*). * denotes significant difference compared to WT (Mann-Whitney *U* test; $P < 0.001$).

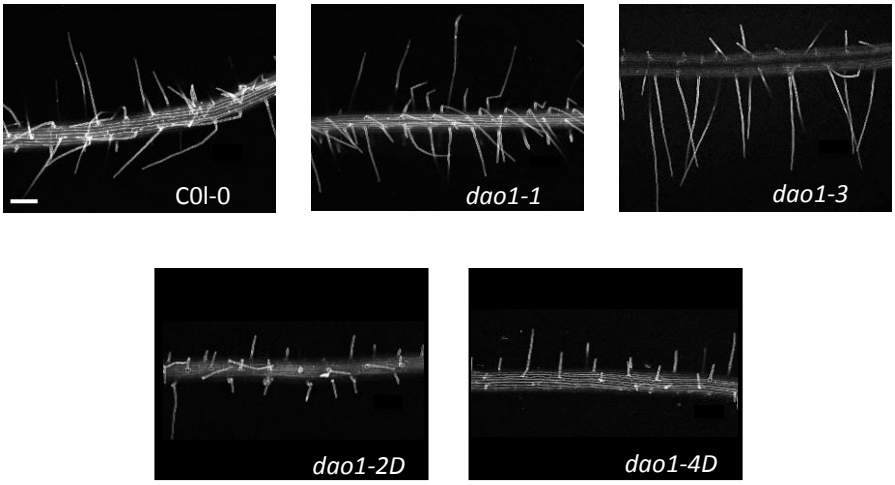

Figure 3-14: Confocal images of 10 day old seedlings for *AT1G14130* of *dao1-1*(SALK_097787), *dao1-3* (SALK_082522), *dao1-2D* (SAIL_349_D02) and *dao1-4D* (SALK_09593) lines and WT (*Col-0*). (Scale bar: 120 µm).

Quantitative RT-PCR was performed to measure the mRNA abundance of (ROOT HAIR DEFECTIVE 6-LIKE 4) which promotes the root hair cell elongation in *Arabidopsis*. The data revealed that the loss of function lines *dao1-1* and *dao1-3* have ~80% mRNA of *RSL4* comparing with WT. which help in explain the longer root hairs in the knock-out *dao1* mutants (Fig. 3-15).

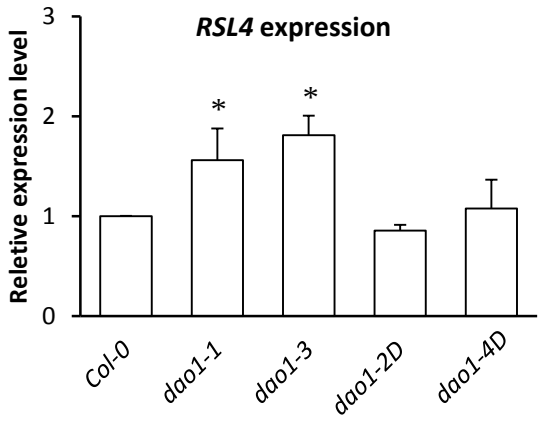

Figure 3-15: qRT-PCR expression quantification for *RSL4* for *dao1-1*(SALK_097787), *dao1-3* (SALK_082522), *dao1-2D* (SAIL_349_D02) and *dao1-4D* (SALK_09593) lines, normalized to WT (*Col-0*). * denotes significant difference compared to WT ($P < 0.05$).

3.4.3.4 *DAO1* and *GH3.3* EXPRESSION LEVELS

IAA metabolite profiling data reveals that *AtDAO1* promotes the oxidation of IAA to oxIAA in *Arabidobsis* ((Porco et al., 2016). IAA metabolite profiling of the loss of function line (*dao1-1*) shown that the level of oxIAA similar to WT, while there was an up-regulation of the IAA amino acid conjugation pathway (regulated by *GH3* genes) to maintain a suitable level of IAA. qRT-PCR was performed to measure *GH3.3* (auxin inducible) expression level. The data shows up-regulation in *GH3.3* expression level compared to WT (Fig. 3-16).

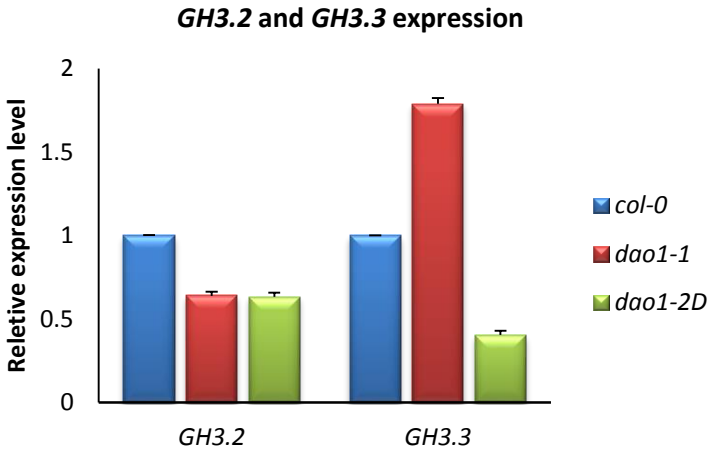

Figure 3-16: qRT-PCR expression quantification for *GH3.3* and *GH3.2* of *dao1-1*(SALK_097787) and *dao1-2D* (SAIL_349_D02) lines, normalized to WT (*Col-0*).

3.4.3.5 IAA FEEDING EXPERIMENTS

7 day old Col-0 seedlings incubated for 4 h in different IAA concentrations. The mRNA abundance of *AtDAO1* and *GH3.3* have been quantified. The analysed data revealed that *DAO1* and *GH3.3* expression levels increases with the concentration of IAA increases (Fig. 3-17) (Mellor et al., 2016).

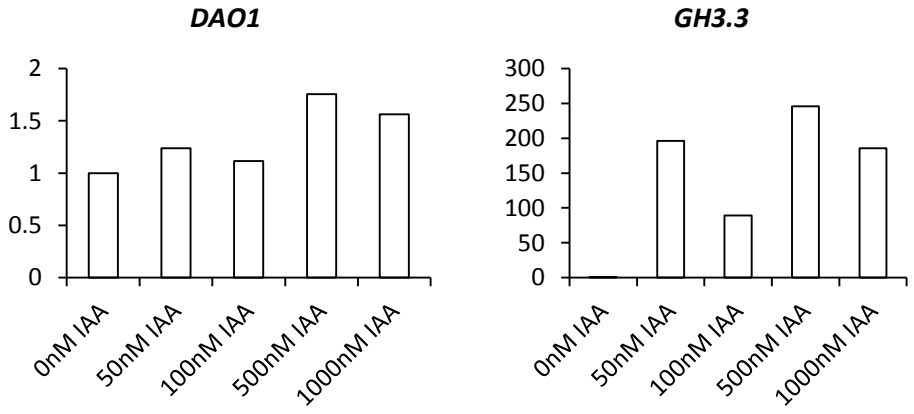

Figure 3-17: Effect of IAA on the expression of *DAO1* and *GH3.3* genes in 7 day old Col-0 seedlings.

3.5 DISCUSSION

The plant hormone auxin is a key morphogenetic regulator for almost all aspects of plant growth and development (Nanao et al., 2014, Zhao, 2010). Several mechanisms control auxin homeostasis including biosynthesis, transport, conjugation and degradation pathways (Ljung, 2013, Mashiguchi et al., 2011).

Very recently two genes have been identified to function in oxidation the major form of auxin in plants IAA to oxIAA in *Arabidopsis thaliana* (Porco et al., 2016, Mellor et al., 2016, Zhang et al., 2016). *DIOXYGENASE FOR AUXIN OXIDATION 1 (AtDAO1, At1g14130*) and 2 (*AtDAO2, At1g14120*). They are also related to genes discribed in apple (*ARRO1*) and rice (*DAO*) (Butler and Gallagher, 2000, Zhao et al., 2013).

AtDAO1 and *AtDAO2* sequences are arranged in tandem making it difficult to generate double mutant lines in both genes. However, new developments in gene editing using CRISPR/Cas (Clustered regularly interspaced short palindromic repeats) (Bortesi and Fischer, 2015) would help generate loss of function lines in both *AtDAO1* and *AtDAO2* sequences in order to study the combined function of those genes.

GUS reporter activity (*pDAO1:GUS*) and GFP-expression of the *AtDAO1* transgenic plants (*pDAO1::DAO1-GFP*) were observed in the root tip and vascular tissues, plus epidermal cells in the maturation zone incloding root hairs cells but not in the lateral root primordia. The *pDAO1::DAO1-GFP* translational

reporter line also revealed that *AtDAO1* is localized cytoplasmically (Porco et al., 2016).

Several T-DNA insertion lines have been isolated to study the role of *AtDAO1* during *Arabidopsis* root growth and development (Fig. 3-1) (Porco et al., 2016). Loss of function lines (*dao1-1* and *dao1-3*) exhibited longer root hairs (~80%), faster response to gravity, slight reduction in primary root length and increase in lateral root density in comparison with in WT and gain of function lines.

Metabolic profiling studies have indicated that IAA levels in the loss of function mutant of *dao1* (*dao1-1*) is similar to WT (Porco et al., 2016), but significant reduction in oxIAA and oxIAA-Glc levels (Porco et al., 2016, Mellor et al., 2016). This similarity in IAA level in WT and *dao1-1* could help in explain the weak auxin-related phenotype. However, we cannot rule out whether there are differences at a cell scale. Auxin response markers such as DR5 and DII (reporter systems, function in monitoring auxin response in different plant tissues) would help reveal cell scale change in auxin concentrations.

Consistent with elevated auxin levels in epidermal cells *RSL4* (transcription factor control RH length) mRNA abundance was significantly higher in both *dao1-1* and *dao1-3* consistent with Mellor et al. (2016) prediction. Generating double mutant lines in both *DAO1* and *RSL4* may display a stronger RHs phenotype (in progress).

Metabolic profiling also revealed that the level of IAA conjugates IAA-Asp and IAA-Glu were significantly higher in the *dao1-1* mutant (>100 fold) suggesting

that the amino acid conjugate pathway can compensate for the lack IAA oxidation indeed. *GH3* (auxin inducible) expression level was higher in *dao1-1*, supporting this suggestion as *GH3* converts IAA to IAA amino acids.

Mathematical modelling was employed to probe the homeostat mechanisms operating, revealing that conjugation and synthesis pathways needed to be upregulated to cause the observed changes in metabolitc abundance. Double mutant lines in *GH3* and *DAO1* would help to test whether they exhibit stronger phenotype and disrupt IAA homeostasis.

3.6 DIOXYGENASE-ENCODING *AtDAO1* GENE CONTROLS IAA OXIDATION AND HOMEOSTASIS IN *ARABIDOPSIS* (Porco et al., 2016)

PNAS

Dioxygenase-encoding *AtDAO1* gene controls IAA oxidation and homeostasis in *Arabidopsis*

Silvana Porco[a,1,2], Aleš Pěnčík[b,c,d,1], Afaf Rashed[a,1], Ute Voß[a,1], Rubén Casanova-Sáez[b,1], Anthony Bishopp[a], Agata Golebiowska[a,e], Rahul Bhosale[a], Ranjan Swarup[a], Kamal Swarup[a], Pavlína Peňáková[c,d], Ondřej Novák[b,c,d], Paul Staswick[f], Peter Hedden[g], Andrew L. Phillips[g], Kris Vissenberg[e], Malcolm J. Bennett[a,3,4], and Karin Ljung[b,3,4]

[a]Centre for Plant Integrative Biology, Plant and Crop Science Division, School of Biosciences, University of Nottingham, Loughborough LE12 5RD, United Kingdom; [b]Umeå Plant Science Centre, Department of Forest Genetics and Plant Physiology, Swedish University of Agricultural Sciences, SE-901 83 Umea, Sweden; [c]Laboratory of Growth Regulators, Centre of the Region Haná for Biotechnological and Agricultural Research, Institute of Experimental Botany Academy of Sciences of the Czech Republic (AS CR), CZ-78371 Olomouc, Czech Republic; [d]Faculty of Science, Palacký University, CZ-78371 Olomouc, Czech Republic; [e]Integrated Molecular Plant Physiology Research, Biology Department, Antwerp University, 2020 Antwerp, Belgium; [f]Department of Agronomy and Horticulture, University of Nebraska, Lincoln, NE 68583-0915; and [g]Department of Plant Biology and Crop Science, Rothamsted Research, Hertfordshire AL5 2JQ, United Kingdom

Edited by Mark Estelle, University of California at San Diego, La Jolla, CA, and approved July 26, 2016 (received for review March 22, 2016)

Auxin represents a key signal in plants, regulating almost every aspect of their growth and development. Major breakthroughs have been made dissecting the molecular basis of auxin transport, perception, and response. In contrast, how plants control the metabolism and homeostasis of the major form of auxin in plants, indole-3-acetic acid (IAA), remains unclear. In this paper, we initially describe the function of the *Arabidopsis thaliana* gene *DIOXYGENASE FOR AUXIN OXIDATION 1* (*AtDAO1*). Transcriptional and translational reporter lines revealed that *AtDAO1* encodes a highly root-expressed, cytoplasmically localized IAA oxidase. Stable isotope-labeled IAA feeding studies of loss and gain of function *AtDAO1* lines showed that this oxidase represents the major regulator of auxin degradation to 2-oxoindole-3-acetic acid (oxIAA) in *Arabidopsis*. Surprisingly, *AtDAO1* loss and gain of function lines exhibited relatively subtle auxin-related phenotypes, such as altered root hair length. Metabolite profiling of mutant lines revealed that disrupting *AtDAO1* regulation resulted in major changes in steady-state levels of oxIAA and IAA conjugates but not IAA. Hence, IAA conjugation and catabolism seem to regulate auxin levels in *Arabidopsis* in a highly redundant manner. We observed that transcripts of *AtDOA1* IAA oxidase and *GH3* IAA-conjugating enzymes are auxin-inducible, providing a molecular basis for their observed functional redundancy. We conclude that the *AtDAO1* gene plays a key role regulating auxin homeostasis in *Arabidopsis*, acting in concert with *GH3* genes, to maintain auxin concentration at optimal levels for plant growth and development.

Arabidopsis thaliana | IAA degradation | oxidase | dioxygenase | root hair elongation

Distinct indole-3-acetic acid (IAA) conjugation and degradation pathways operate to maintain optimal auxin concentrations for plant growth and developmental processes. There are three major forms of auxin conjugates identified in diverse plants: ester-linked IAA-sugar conjugates, amide-linked IAA-amino acid conjugates, and amide-linked IAA peptide and protein conjugates (reviewed in ref. 1). In *Arabidopsis thaliana*, Group II of the Gretchen Hagen3 (GH3) family of auxin-inducible acyl amido synthetases converts IAA to IAA-amino acids (2, 3). Most amino acid IAA conjugates are believed to be inactive; however, there are enzymes that can hydrolyze some of the IAA-amino acid conjugates to free IAA (reviewed in ref. 1). Some of the IAA-amino acid conjugates, such as indole-3-acetic acid aspartic acid (IAA-Asp) and indole-3-acetic acid glutamic acid (IAA-Glu), can also be further metabolized (4–6). The conversion of IAA to indole-3-acetic acid glucose (IAA-glc) is catalyzed by the UDP glucosyltransferase UGT84B1 (7).

The major IAA catabolite in *Arabidopsis* is 2-oxoindole-3-acetic acid (oxIAA), the oxidized form of IAA (4, 6, 8). oxIAA can be further metabolized by conjugation to glucose (4, 5), and it was recently shown that the UDP glucosyltransferase UGT74D1 is able to catalyze the glucosylation of oxIAA to 2-oxoindole-3-acetic acid glucose (oxIAA-glc) (9). IAA catabolism has been shown to be an irreversible step (4, 10), and the oxIAA product has very little biological activity and is not transported via the polar auxin transport system (6, 8).

Although many metabolites in the conjugation and catabolic pathways have been identified in *Arabidopsis* (4–7, 9–11), it has proved difficult to identify and characterize the genes and enzymes involved. We have now identified two closely related components of the IAA degradation machinery in *Arabidopsis*, *DIOXYGENASE FOR AUXIN OXIDATION 1* (*AtDAO1*; *At1g14130*) and *AtDAO2* (*At1g14120*), which are closely related to genes described in apple [*Adventitious Rooting Related Oxygenase 1* (12)] and rice [*DAO* (13)]. The *AtDAO1* and *AtDAO2* genes belong to a distinct clade of the 2-oxoglutarate–dependent dioxygenase gene family and are related to enzymes involved in gibberellin biosynthesis and inactivation. We report that the *AtDAO1* gene plays a key role regulating auxin homeostasis in *Arabidopsis*, acting in concert with *GH3* genes to maintain auxin concentration at optimal levels for plant growth and development. As a result, plants lacking *AtDAO1* activity led to

Significance

Understanding how hormones like auxin control plant growth and development has fascinated scientists since Darwin. The past two decades have seen breakthroughs in elucidating the molecular basis of auxin transport, perception, and response, but little is known about how auxin is metabolized or its homeostasis is controlled. We report that the *DIOXYGENASE FOR AUXIN OXIDATION 1* (*AtDAO1*) enzyme represents the major pathway for auxin oxidation in *Arabidopsis*. Disrupting *AtDAO1* function elevates levels of auxin conjugates between ∼50- and 280-fold, but auxin levels remain close to the WT, helping explain why mutant phenotypes are relatively weak. We conclude that *AtDAO1* and auxin conjugation pathways play highly redundant roles and reveal a level of regulation of auxin abundance in plants.

Author contributions: S.P., A.P., A.R., U.V., R.C.-S., O.N., M.J.B., and K.L. designed research; S.P., A.P., A.R., U.V., R.C.-S., A.B., A.G., R.B., R.S., K.S., P.P., and O.N. performed research; P.S. contributed new reagents/analytic tools; S.P., A.P., A.R., U.V., R.C.-S., A.B., A.G., R.B., R.S., K.S., P.P., O.N., P.H., A.L.P., and K.V. analyzed data; and M.J.B. and K.L. wrote the paper.

The authors declare no conflict of interest.

This article is a PNAS Direct Submission.

Freely available online through the PNAS open access option.

[1]S.P., A.P., A.R., U.V., and R.C.-S. contributed equally to this work.

[2]Present address: Department of Cell and Molecular Biology, The Scripps Research Institute, La Jolla, CA 92037.

[3]M.J.B. and K.L. contributed equally to this work.

[4]To whom correspondence may be addressed. Email: malcolm.bennett@nottingham.ac.uk or karin.ljung@slu.se.

This article contains supporting information online at www.pnas.org/lookup/suppl/doi:10.1073/pnas.1604375113/-/DCSupplemental.

major changes in conjugated forms of the hormone, but auxin level remains within a normal range, helping explain why the mutant exhibited subtle phenotypic changes. We conclude that IAA catabolism and conjugation regulate auxin homeostasis in *Arabidopsis* in a highly redundant manner.

Results

IAA Oxidation in *Arabidopsis* Is Controlled by the Dioxygenase Gene *AtDAO1*. To study the in vivo formation of IAA metabolites, a feeding experiment was performed using [$^{13}C_6$]IAA with WT *Arabidopsis* seedlings. We observed rapid labeling of the pools of the major IAA conjugates IAA-Asp, IAA-Glu, and IAA-glc as well as the catabolites oxIAA and oxIAA-glc within 3 h after treatment began, revealing that IAA is rapidly turned over in *Arabidopsis* seedlings (Fig. 1*A*).

A rice *DAO1* gene that encodes a 2-oxoglutarate–dependent Fe (II) dioxygenase-like enzyme has recently been reported to mediate IAA oxidation (13). Phylogenetic analyses revealed that the *Arabidopsis* genome contains two genes related to *OsDAO1* termed *At1g14130* (*AtDAO1*) and *At1g14120* (*AtDAO2*). *AtDAO1* and *AtDAO2* belong to the 2-oxoglutarate–dependent Fe (II) dioxygenase gene family, and their sequences are related to enzymes involved in gibberellin biosynthesis and inactivation (Fig. S1*A*). A BLAST search of the sequenced plant genomes at Phytozome (https://phytozome.jgi.doe.gov/pz/portal.html) identified sequences closely related to *AtDAO1* and *AtDAO2* in a range of species, with amino acid identities ranging from 47 to 93% (Fig. S1*B*).

To address the putative IAA oxidative role of *AtDAO1* in *Arabidopsis*, we identified several Transfer-DNA (T-DNA) insertion lines (Fig. 1*B*). The T-DNA for the Salk_093162 line (*dao1-1*) is inserted in the first exon of At1g14130 311 bp downstream of the start codon. Sail line 349_D02 (*dao1-2D*) has a T-DNA insertion in the intergenic region between the *AtDAO1* and *AtDAO2* genomic sequences 542 bp upstream of the *AtDAO2* start codon. T-DNA insertions in Salk_082522 (*dao1-3*) and Salk_095931 (*dao1-4D*) lines are positioned upstream of the start codon of *AtDAO1* (591 and 789 bp, respectively). Quantitative RT-PCR (qRT-PCR) was performed to measure transcript levels of *DAO1* and *DAO2* in the T-DNA lines (Fig. S2*A*). *DAO1* mRNA was strongly reduced in *dao1-1* and *dao1-3* lines, suggesting that they represent loss of function lines. In contrast, for *dao1-2D* and *dao1-4D* lines, *AtDAO1* mRNA abundances were 4- and 2.4-fold higher than the WT, respectively, suggesting that they represent *AtDAO1* overexpressing lines. No significant changes were detected in the expression level of *DAO2* in any of these lines compared with in the WT (Fig. S2*A*).

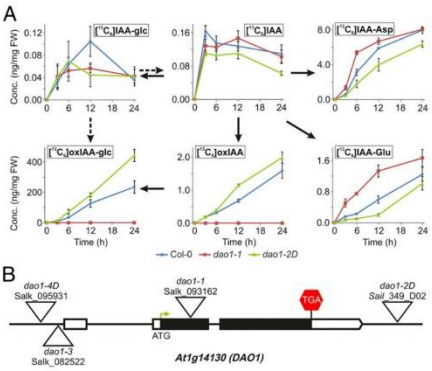

Fig. 1. IAA oxidation in *Arabidopsis* is regulated by the dioxygenase gene family member *At1g14130* (*AtDAO1*). (*A*) IAA feeding experiment. Formation of labeled IAA conjugates and catabolites after incubation of 7-d-old *Arabidopsis* Col-0, *dao1-1*, and *dao1-2D* seedlings with [$^{13}C_6$]IAA. Samples were analyzed in three independent biological replicates. Error bars represent SD. FW, fresh weight. (*B*) Structure of the *Arabidopsis DAO1* gene with indication of the position of the T-DNA insertions (triangles) in the different *dao1* alleles studied.

The [$^{13}C_6$]IAA feeding experiments were also performed using seedlings from *dao1-1* (*AtDAO1* mutant) and *dao1-2D* (*AtDAO1* overexpressing) lines, revealing that (unlike the WT and *dao1-2D*) *dao1-1* seedlings failed to oxidize [$^{13}C_6$]IAA to [$^{13}C_6$]oxIAA (Fig. 1*A*). Formation of [$^{13}C_6$]oxIAA-glc was also abolished in the *dao1-1* mutant line. Instead, ^{13}C-labeled IAA was converted to IAA conjugates ([$^{13}C_6$]IAA-Asp and [$^{13}C_6$]IAA-Glu) at a higher rate than in WT seedlings. Conversely, the *dao1-2D* line oxidized [$^{13}C_6$]IAA to [$^{13}C_6$]oxIAA and [$^{13}C_6$]oxIAA-glc more rapidly than the WT, and the [$^{13}C_6$]IAA conjugate levels were diminished in this line. Labeling of IAA-glc is similar in all lines, suggesting that the formation of this conjugate is not altered in *AtDAO1* mutant and overexpressing lines (Fig. 1*A*). Hence, our [$^{13}C_6$]IAA feeding experiments revealed that *AtDAO1* plays an essential role regulating IAA oxidation in *Arabidopsis* seedlings.

Mutants Disrupting *AtDAO1* Activity Exhibit Subtle Changes in Shoot and Root Phenotypes. We next characterized the phenotypes of the *dao1* mutants (Fig. 2). Given the apparent importance of *AtDAO1* mediating IAA oxidation in *Arabidopsis* seedlings (Fig. 1*A*), we expected mutant and overexpressing plants to exhibit multiple IAA-related developmental defects. Surprisingly, *AtDAO1* mutant and overexpressing lines exhibited only mild defects in plant growth and development (Fig. 2). Compared with WT seedlings, *AtDAO1* mutant lines exhibit a slight reduction in primary root length and increase in lateral root density (Fig. 2*A* and Fig. S3 *A* and *B*). The root gravitropic response was faster in loss of function *dao1-1* and *dao1-3* mutants compared with in *dao1-2D* and *dao1-4D*, with response that was similar to that in the WT (Fig. S3*C*). In shoot tissues, increased branching and shorter siliques were observed in *dao1-1*, whereas *dao1-2D* adult plants exhibited a growth phenotype closer to the WT (Fig. 2 *B* and *C*).

Our root hair (RH) measurements revealed that their length increased ~80% in *dao1-1* and *dao1-3* seedlings compared with the WT (Fig. 2 *D* and *E*). RH determination and elongation in *Arabidopsis* is controlled (in part) by a small family of basic Helix-Loop-Helix transcription factors that includes the auxin-inducible gene member *RSL4* (14–16). Datta et al. (17) have recently shown that RH length is proportional to *RSL4* mRNA abundance. Significantly, qRT-PCR analysis revealed that *dao1-1* and *dao1-3* seedlings contained an ~80% increase in *RSL4* transcript levels (Fig. 2*F*), which is directly proportional to their altered RH length. Interestingly, multicellular root modeling predicts an accumulation of IAA in epidermal tissues in the *dao1-1* mutant (18), and the RH phenotype in *dao1-1* and *dao1-3* (Fig. 2 *D* and *E*) supports the model. We conclude that, despite the importance of *AtDAO1* controlling auxin oxidation (Fig. 1*A*), loss and gain of function lines exhibit surprisingly weak auxin-related phenotypic alterations (Fig. 2). Nevertheless, *dao1-1* primary root length, lateral root density, and lateral root length were all more sensitive to external IAA treatments than the WT or *dao1-2D* (Fig. S3 *D*–*F*), consistent with the *dao1-1* mutant having a reduced ability to break down auxin.

***AtDAO1* Encodes a Root-Expressed Cytoplasmically Localized IAA Oxidase.** To determine whether the mild *dao1* RH phenotype (Fig. 2 *D*–*F*) could be caused by an RH-specific expression

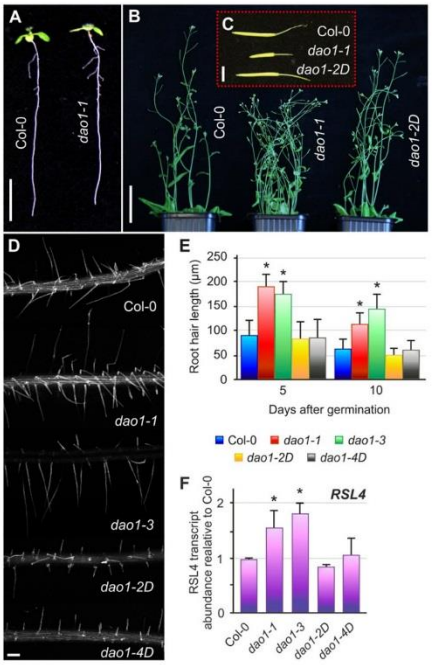

Fig. 2. Developmental phenotypes of *dao1* mutants. (*A*) Seedlings from Col-0 and the *dao1-1* mutant 10 d after germination. (*B*) Adult Col-0, *dao1-1*, and *dao1-2D* plants. (*C*) Mature siliques from plants in *B*. (*D*) Confocal images showing propidium iodide-stained mature RHs from the root tip of 10-d-old Col-0 and *dao1* alleles. (*E*) RH length from 5- and 10-d-old Col-0 and *dao1* alleles. *Values significantly different from those in Col-0 (Mann–Whitney *U* test; $P < 0.001$; $n = 10$). (*F*) qRT-PCR analysis of the expression of the *RSL4* gene in roots from Col-0 and *dao1* alleles harvested 7 d after germination. Error bars indicate SDs from three biological replicates. *Expression values significantly different from those in Col-0 (Student's *t* test; $P < 0.05$). (Scale bars: *A*, 1 cm; *B*, 5 cm; *C*, 5 mm; *D*, 120 μm.)

pattern, we created a transcriptional fusion of At1g14130 (*AtDAO1*) with the β-glucuronidase (GUS) reporter (*pDAO1:GUS*) (Fig. S4). Histochemical staining of transgenic *pDAO1:GUS* seedlings revealed reporter activity in the root tip and vascular (stele) tissues (Fig. S4 *A*, *C*, and *G*). In addition, GUS was detected in epidermal cells in the mature part of the root differentiation zone (Fig. S4*D*), including RHs (Fig. S4 *E* and *F*). In contrast, no GUS expression was observed in lateral root (LR) primordia (Fig. S4*D*) or aerial tissues (Fig. S4*B*).

To investigate whether DAO1 stability is subject to posttranslational regulation, transgenic *Arabidopsis* plants expressing a GFP translational fusion to the At1g14130 genomic sequence (p*DAO1::DAO1-GFP*) were engineered. Confocal microscopy revealed that the DAO1-GFP fusion protein was detected throughout root apical (Fig. 3*A*) and mature tissues, including RHs (Fig. 3 *B* and *E*). The spatial expression pattern of *DAO1* is similar in a transcriptional reporter (*pDAO1:GUS*) (Fig. S4) as it is in a translational fusion (*pDAO1:DAO1-GFP*) (Fig. 3), suggesting that the pattern is largely controlled at the transcriptional level. Higher-magnification confocal images of the p*DAO1::DAO1-GFP* expressing root cells revealed that the IAA oxidase is localized in the cytoplasm and probably excluded from nuclei and central vacuole compartments (Fig. 3 *C*–*E*).

IAA Metabolite Profiling Reveals That *AtDAO1* Regulates oxIAA Levels in *Arabidopsis*. To study the effect of the *AtDAO1* gene on auxin homeostasis, we performed IAA metabolite profiling of *dao1-1* mutant and *dao1-2D* overexpressing lines. Using liquid chromatography–tandem MS (LC-MS/MS) analysis (11), we quantified free IAA and the major IAA precursors, catabolites, and conjugates in 7-d-old seedlings of WT Columbia-0 (Col-0), *dao1-1*, and *dao1-2D*.

In *dao1-1* and *dao1-2D*, the concentrations of IAA and the IAA precursors tryptophan (TRP), anthranilate, and indole-3-acetaldoxime were not significantly affected (Fig. S5). However, the IAA precursors indole-3-acetamide, indole-3-pyruvic acid, and indole-3-acetonitrile were significantly reduced in these lines compared with in the WT (Fig. S5). We also quantified IAA conjugates and catabolites in *dao1-1* and *dao1-2D* seedlings and observed a significant reduction of oxIAA and oxIAA-glc levels in *dao1-1* as well as a significant increase in oxIAA and oxIAA-glc levels in *dao1-2D*, confirming that *dao1-1* and *dao1-2D* behave as KO and overexpressing lines, respectively (Fig. 4). In contrast, the levels of IAA-glc were not changed in these lines. In a second experiment, we performed IAA metabolite profiling of

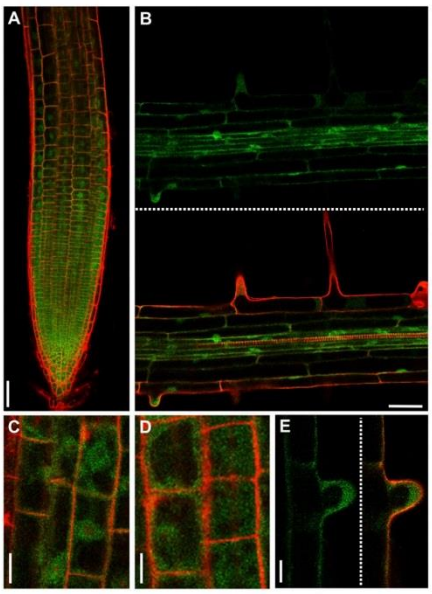

Fig. 3. Cellular localization of DAO1-GFP in roots. Confocal images of root cells from 5-d-old transgenic p*DAO1::DAO1-GFP* plants, showing (*A*) root tip epidermal cells, (*B*) section of the root vasculature in the mature root region, (*C* and *D*) magnification of cells from *A*, and (*E*) magnification of a trichoblast from *B*. Green and red signals correspond to GFP and propidium iodide, respectively. (Scale bars: *A* and *B*, 50 μm; *C* and *D*, 10 μm; *E*, 25 μm.)

PLANT BIOLOGY

all *DAO1* mutant and overexpressing lines compared with the Col-0 WT. The profiles were very similar between the two mutant (*dao1-1* and *dao1-3*) as well as between the two overexpressing (*dao1-2D* and *dao1-4D*) lines (Fig. S2*B*).

Strikingly, a major up-regulation of the IAA amino acid conjugates IAA-Asp and IAA-Glu was observed in *dao1-1* compared with the WT (around ~280- and 46-fold, respectively) (Fig. 4). In contrast, the oxidase overexpressing line *dao1-2D* exhibited significantly reduced levels of IAA-Glu and IAA-Asp (Fig. 4). This discovery prompted us to quantify IAA metabolites in a mutant line disrupting IAA amino acid conjugation. The *GH3* sextuple mutant *gh3.1,2,3,4,5,6*, which comprises six of eight IAA-amino acid–conjugating enzyme genes, exhibited a significant increase in IAA and its precursor TRP (Fig. S5). However, levels of oxIAA, oxIAA-glc, and IAA-glc were not affected compared with Col-0, but the levels of IAA-Asp were below the detection limit, whereas the IAA-Glu levels were significantly elevated (Fig. 4). This increase is most likely caused by the IAA-conjugating activity of GH3.17, which prefers Glu over other amino acids, whereas GH3 1–6 exhibits activity with Asp (2, 3). The *gh3.1,2,3,4,5,6* mutant line also has a stronger auxin overproduction phenotype compared with the mild auxin overproduction phenotype in *dao1-1*, with increased lateral root formation and elongated petioles (Fig. S6).

IAA metabolite profiling different tissues of 10-d-old seedlings revealed similar changes in metabolite distribution in every WT and *dao1-1* tissue analyzed (Fig. S7). We conclude that disrupting *AtDAO1* caused major changes in steady-state levels of oxIAA, oxIAA-Glc, and IAA conjugates but only minor changes in IAA levels (Fig. 4 and Figs. S2*B* and S7).

IAA Conjugation and Catabolism Redundantly Regulate IAA Homeostasis. To monitor the rates of de novo synthesis of these metabolites, a feeding experiment was performed using [$^{15}N_1$]indole as IAA precursor. IAA as well as IAA conjugates and catabolites were rapidly labeled after incubation (Fig. S8). The *gh3.1,2,3,4,5,6* line exhibited the most rapid labeling of IAA, consistent with a higher IAA synthesis rate and/or lower turnover via conjugation. Labeling of oxIAA and oxIAA-glc was highest in *dao1-2D* and lowest in *dao1-1* as expected in IAA oxidase overexpressing and IAA oxidase mutant lines, respectively. In contrast, extremely rapid labeling of IAA-Asp and IAA-Glu was observed in *dao1-1*, indicating that the high endogenous IAA conjugate levels observed (Fig. 4 and Figs. S2*B* and S7) originate from de novo synthesis.

We also quantified IAA metabolites in two *35S:DAO1* lines (Fig. S9). In these constitutive IAA oxidase overexpressing lines, we could not observe any significant changes in IAA and oxIAA levels compared with in the WT. However, a significant up-regulation of both oxIAA-glc and IAA-glc was detected in one of the *35S:DAO1* lines, suggesting that glucosylation pathways were active, whereas the levels of IAA-Asp and IAA-Glu were strongly down-regulated in both *35S:DAO1* lines (Fig. S9). Hence, IAA metabolite profiling has revealed that IAA conjugation and catabolism regulate IAA homeostasis redundantly in *Arabidopsis* seedlings.

Previously described components of the IAA homeostasis machinery, such as *GH3* genes, have been described to be rapidly auxin inducible (1). Transcript profiling of auxin-treated root apical tissues revealed that, like *GH3* genes, *AtDAO1* was auxin inducible, albeit with a lower level of induction and on a longer timescale >4 h (18).

IAA metabolite profiling of *AtDAO1* and *GH3* mutant lines has revealed that IAA conjugation and catabolism regulate auxin homeostasis redundantly (Fig. 4). Given that IAA-Asp and IAA-Glu were present at high levels in the *dao1-1* mutant, we measured the expression of *GH3.2* and *GH3.3* genes in the *dao1-1* and *dao1-2D* mutant backgrounds (Fig. S10). A 1.8-fold increase in gene expression was detected for *GH3.3* in the *dao1-1* mutant compared with in the WT. In contrast, *GH3.3* expression was down-regulated in the *dao1-2D* overexpressor line (Fig. S10). We conclude that auxin-inducible expression of both *AtDOA1* and *GH3* genes could provide a molecular mechanism to explain the observed functional redundancy in IAA catabolism and conjugation that regulates auxin homeostasis.

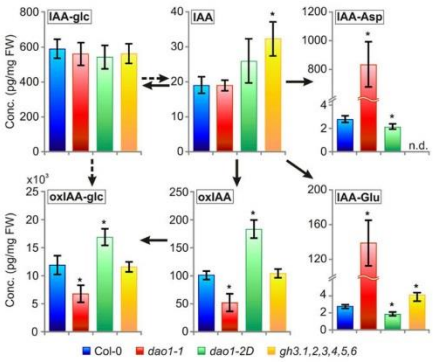

Fig. 4. Levels of IAA metabolites in IAA oxidase and *GH3* sextuple mutant lines. IAA and the metabolites oxIAA, oxIAA-glc, IAA-glc, IAA-Asp, and IAA-Glu were quantified in 7-d-old seedlings of Col-0, *dao1-1*, *dao1-2D*, and the *gh3* sextuple mutant line *gh3.1,2,3,4,5,6*. The concentrations for all metabolites except oxIAA-glc [nanograms per milligram fresh weight (FW)] are given in picograms per milligram FW. Samples were analyzed in five independent biological replicates, and error bars represent the SD. *Statistically significant differences from Col-0 ($P < 0.05$; Student's t test).

Discussion

Maintaining auxin homeostasis is critical for growth and developmental processes in plants. Several mechanisms have been proposed to control auxin homeostasis, including IAA metabolism (biosynthesis, degradation, and conjugation), transport, and compartmentation (reviewed in ref. 19). In this paper, we initially describe the key gene regulating IAA oxidation in *Arabidopsis*, *AtDAO1*. In parallel, Zhang et al. (20) have shown that the recombinant *AtDAO1* protein (and the closely related *AtDAO2* sequence) has IAA oxidase activity in vitro. Confocal imaging of GFP-tagged AtDAO1-expressing transgenic plants suggests that the IAA oxidase is localized cytoplasmically (Fig. 3) and based on subcellular fractionation studies (20), behaves as a soluble protein.

In planta stable isotope-labeled auxin feeding studies have revealed the critical importance of AtDAO1 converting IAA to oxIAA in *Arabidopsis* seedlings (Fig. 1). In contrast, the in planta role of *AtDAO2* is currently less clear given that oxidation of [$^{13}C_6$]IAA to [$^{13}C_6$]oxIAA and [$^{13}C_6$]oxIAA-glc was completely blocked in the *dao1-1* loss of function mutant (Fig. 1*A*). A clue comes from transcript profiling results by Zhang et al. (20), which reported that *AtDAO1* is widely expressed in root and shoot tissues at much higher levels than *AtDAO2*. In addition, transcriptomic profiling revealed that *AtDAO1* and *AtDAO2* exhibit auxin and circadian regulated patterns of expression, respectively (18,21). Hence, the *Arabidopsis AtDAO* sequences seem to have subfunctionalized since their tandem duplication event, with *AtDAO1* functioning as the major IAA oxidase at the seedling stage of development.

Given how widely the IAA oxidase *AtDAO1* is expressed across root and shoot tissues, loss of function *dao1* mutant alleles exhibit surprisingly subtle auxin-related developmental defects (Fig. 2 and Fig. S3) (20). This observation can be explained in part, following metabolite profiling and modeling studies (Fig. 4)

(18), by IAA oxidation and conjugation pathways regulating auxin homeostasis in a redundant manner. For example, loss of *AtDAO1* expression leads to up-regulation of *GH3* genes (such as *GH3.3*) (Fig. S10), increasing concentrations of IAA conjugates IAA-Asp and IAA-Glu (Fig. 4) that maintain IAA homeostasis (Fig. 5). Nevertheless, *dao1-1* mutant plants exhibit subtle but clear phenotypes (Fig. 2) (20). These data indicate that, although homeostatic mechanisms regulating IAA levels in *Arabidopsis* act redundantly, they cannot fully compensate for the loss of *AtDAO1* (or *GH3*) expression, resulting in auxin-related mutant phenotypes (Fig. 2 and Figs. S3 and S6) (20).

Materials and Methods

Growth Conditions. Seeds were surface sterilized with 50% (vol/vol) hypochlorous acid for 5 min and then, washed three times with sterile deionized water. For IAA metabolite profiling experiments, plant seeds were plated in Murashige and Skoog medium (4.4 g salts per 1 L), including 1% sucrose and 0.5 g/L MES monohydrate, at pH 5.7 and solidified with 0.8% Plant Agar (Duchefa). Seeds were stratified at 4 °C for 72 h in the dark to synchronize germination and then, incubated vertically in a culture room under long-day (LD) conditions (16 h light at 22 °C and 8 h dark at 18 °C; 150 μmol m^{-2} s^{-1}) and at a relative humidity of 67%. For the rest of the experiments, seeds were plated on 1/2 Murashige and Skoog medium (2.17 g salts per 1 L) without sucrose, stratified at 4 °C for 2–3 d, and then, incubated vertically in a culture room at 22 °C under continuous light (120–150 μmol m^{-2} s^{-1}).

Plant Material. The *Arabidopsis* ecotype Columbia was used as the WT in all experiments. The *dao1* T-DNA insertion mutants were obtained from Nottingham *Arabidopsis* Stock Centre, and the insertion was confirmed by PCR using forward and reverse primers in combination with LBb1.3 (for *dao1-1*, *dao1-3*, and *dao1-4D*) or LB1 (for *dao1-2D*) (Table S1). The *gh3* sextuple mutant (*gh3.1,2,3,4,5,6*) was assembled by repeated rounds of crossing between the single-gene insertion mutants or their double- or triple-mutant derivatives. Mutants *gh3.1* and *gh3.2* are in the Landsberg *erecta* background, and primers for their genotyping were previously described (2). All other mutants were in the Col-0 background; *gh3.5* was described previously as *wes1* (22), and *gh3.4* and *gh3.6* are T-DNA insertion lines (Salk_102549 and Salk_013458, respectively), whereas *gh3.3* is a transposon line (SM.37350). Genotyping of *gh3* insertions was done with forward and reverse primers along with Lba1 (for *gh3.4*, *gh3.5*, and *gh3.6*) or 3′dSpm (for *gh3.3*) (Table S1). Each single mutant was verified to be essentially a complete KO by Northern blot hybridizations.

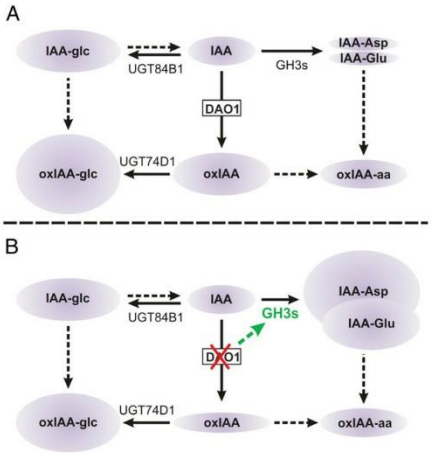

Fig. 5. IAA degradation and conjugation regulate IAA homeostasis in *Arabidopsis*. (*A*) In WT plants, IAA is irreversibly oxidized to oxIAA by DAO1 and subsequently conjugated with glucose by the UGT74D1 enzyme to produce oxIAA-glc (9). IAA can also be conjugated to either glucose (IAA-glc) or amino acids by UGT84B1 (7) and members of the GH3 family (2), respectively. IAA-Glu and IAA-Asp are the most abundant IAA-amino acid conjugates in *Arabidopsis* (5, 10, 11) and believed to be irreversible conjugates that cannot be hydrolyzed to form free IAA (4, 10). (*B*) In the *dao1-1* mutant, *GH3* genes are up-regulated to drain accumulating IAA by irreversible conjugation to form IAA-Asp and IAA-Glu, whereas IAA-glc levels are unaltered. Solid arrows indicate steps in which the indicated enzyme is known to catalyze the reaction. Dashed arrows indicate steps that are not well-defined. oxIAA-aa, 2-oxoindole-3-acetic acid amino acid.

Root Phenotyping. The number of lateral roots per seedling was counted using a stereo microscope, and digital images were taken. For RH measurements, seedlings were imaged with a camera mounted to a Leica stereomicroscope. The digital images were used for RH and primary root length measurement with FIJI software. RHs ~3 mm from the root tip were measured (10 RHs per seedling). For hormone treatment, the indicated concentration of IAA was added to 1/2 Murashige and Skoog medium before it solidified. For gravitropic response assays, plates containing 6-d-old seedlings grown on a 12-h/12-h light/dark period were turned 90°, and the root angle was imaged every 60 min for 8 h using an automated image acquisition system (23) and quantified using FIJI software.

Cloning of At1g14130 and *Arabidopsis* Transformation. The transcriptional and translational fusions as the overexpression lines of At1g14130 were generated in gateway-compatible vectors. Genomic DNA from Col-0 was used to amplify 847 bp upstream of the At1g14130 translational start codon by using the At1g14130pro forward and reverse primers (Table S1). The PCR product was cloned into pENTR-D-Topo entry vector (Invitrogen) and recombined by LR reaction into the pGWB3 destination binary vector to create a transcriptional GUS fusion. For the translational fusion, a fragment of 1,846 bp, containing the At1g14130 promoter and coding sequence region without the stop codon, was amplified with At1g14130gfp primers (Table S1). The PCR product was cloned into pENTR-D-Topo entry vector (Invitrogen) and recombined by LR reaction into the pGWB4 (24) destination binary vector to create a translational GFP fusion. To create an overexpression line, the coding sequence of At1g14130 was amplified using the At1g14130cds primers (Table S1). The PCR product was cloned into pENTR-D-Topo entry vector (Invitrogen) and recombined by LR reaction into the pK2GW7 (24) destination binary vector. The authenticity of all constructs was verified by sequencing before transformation. *A. thaliana* (ecotype Columbia) plants were transformed with *Arabidopsis tumefaciens* (strain GV3101) using the floral dipping method (25). Screening of T3 seeds for 100% antibiotic resistance identified homozygous plants for the transgene.

IAA Metabolite Profiling. *A. thaliana* WT Col-0 as well as *gh3.1,2,3,4,5,6* and *dao1* mutant lines were grown under LD conditions for 7 or 10 d. Whole seedlings or dissected tissues were collected in five replicates (20 mg tissue per sample). Sample purification and quantification of IAA metabolites were performed as described in ref. 11.

Feeding Experiments with Labeled IAA and Indole. Seven-day-old *Arabidopsis* seedlings (Col-0, *gh3.1,2,3,4,5,6*, and *dao1* mutant lines) were incubated with liquid medium containing 0.5 μM [$^{13}C_6$]IAA or 10 μM [$^{15}N_1$]indole for 0, 3, 6, 12, and 24 h under gentle shaking and in darkness. For each time point, 20 mg whole seedlings were collected in three replicates. The samples were extracted and purified by solid-phase extraction as described in ref. 11. Incorporation of the label into IAA metabolites was measured using LC-MS/MS, with the Multiple Reaction Monitoring transitions corresponding to endogenous and labeled compounds. De novo synthesis of IAA metabolites was expressed as the concentration of labeled metabolites at individual time points after correction for natural isotope abundances (26).

Microscopy. Confocal microscopy was performed using a Leica SP5 Confocal Laser-Scanning Microscope (Leica Microsystems). Cell walls were stained using propidium iodide (10 μg/mL; Sigma). Scanning settings used for one experiment were optimized and kept unchanged throughout the experiment. Images were processed using the Leica SP5 Image Analysis software. Images for Fig. 2 were processed with Adobe Photoshop only for adjustment of brightness and contrast.

Histochemical Analysis. The GUS gene activity was revealed by incubating seedlings at 37° for 1 h in a phosphate buffer (500 mM; pH 7) containing

0.5 mM potassium ferricyanide, 0.5 mM potassium ferrocyanide, 1 mM EDTA (pH 8), 0.5% (vol/vol) Triton X-100, and 1 mM 5-bromo-4-chloro-3-indolyl β-D-glucuronide (X-Gluc; Sigma). The X-Gluc was initially dissolved in dimethylformamide to reach a final concentration of 0.5%. After GUS staining, seedlings were cleared and mounted in 50% (wt/vol) glycerol.

qRT-PCR. Real-time qRT-PCR reactions were performed on a LightCycler 480 apparatus (Roche) using SYBR Green Master Mix (Bioline). A standard reaction mixture (12 μL) contained 5 μL cDNA template, 6 μL 2× SYBR Green I Master Mix (Roche), 0.1 μL 100 μM forward and reverse primers, and 0.8 μL H_2O. All of the specific primer pairs (Table S1) were designed with the Universal Probe Library Assay Design Center (Roche; lifescience.roche.com/shop/home) and used to quantify the gene expression levels. *Arabidopsis ACT2* gene (At3g18780) was used as a constitutive internal standard, which showed no clear changes in *Cycle threshold* values, to normalize the obtained gene expression results. All individual reactions were done in triplicates.

ACKNOWLEDGMENTS. We thank the Swedish Metabolomics Centre for the use of instrumentation. S.P. and M.J.B. acknowledge PhD scholarship support from the University of Nottingham. This work was funded by Ministry of Education, Youth and Sport of the Czech Republic National Program for Sustainability I Grant LO1204 and Internal Grant Agency of Palacky University Grant IGA_PrF_2016_011 (to A.P., P.P., and O.N.). A.R. and M.J.B. acknowledge support of the Saudi Arabian Ministry of Higher Education. U.V., A.B., R.S. and M.J.B. acknowledge support of the Biological and Biotechnology Science Research Council Responsive Mode and CISB awards to the Centre for Integrated Structural Biology. R.C.-S., A.P., O.N., and K.L. acknowledge support from the Swedish Foundation for Strategic Research, the Swedish Research Council, Carl Tryggers Stiftelse för Vetenskaplig Forskning, and Kempestiftelserna. A.G. and K.V. were supported by Research Foundation Flanders Grants G009412N, G.0.602.11.N.10, and 1.5.091.11.N.00 and University of Antwerp Grant BOF-DOCPRO4. K.S. and M.J.B. acknowledge support of the European Research Council FUTUREROOTS Project. P.H. and A.L.P. are funded by the 20:20 Wheat Institute Strategic Programme Grant from the Biotechnology and Biological Sciences Research Council of the United Kingdom.

1. Ludwig-Müller J (2011) Auxin conjugates: Their role for plant development and in the evolution of land plants. *J Exp Bot* 62(6):1757–1773.
2. Staswick PE, et al. (2005) Characterization of an Arabidopsis enzyme family that conjugates amino acids to indole-3-acetic acid. *Plant Cell* 17(2):616–627.
3. Westfall CS, Herrmann J, Chen Q, Wang S, Jez JM (2010) Modulating plant hormones by enzyme action: The GH3 family of acyl acid amido synthetases. *Plant Signal Behav* 5(12):1607–1612.
4. Östin A, Kowalyczk M, Bhalerao RP, Sandberg G (1998) Metabolism of indole-3-acetic acid in Arabidopsis. *Plant Physiol* 118(1):285–296.
5. Kai K, Horita J, Wakasa K, Miyagawa H (2007) Three oxidative metabolites of indole-3-acetic acid from *Arabidopsis thaliana*. *Phytochemistry* 68(12):1651–1663.
6. Pencík A, et al. (2013) Regulation of auxin homeostasis and gradients in Arabidopsis roots through the formation of the indole-3-acetic acid catabolite 2-oxindole-3-acetic acid. *Plant Cell* 25(10):3858–3870.
7. Jackson RG, et al. (2001) Identification and biochemical characterization of an Arabidopsis indole-3-acetic acid glucosyltransferase. *J Biol Chem* 276(6):4350–4356.
8. Peer WA, Cheng Y, Murphy AS (2013) Evidence of oxidative attenuation of auxin signalling. *J Exp Bot* 64(9):2629–2639.
9. Tanaka K, et al. (2014) UGT74D1 catalyzes the glucosylation of 2-oxindole-3-acetic acid in the auxin metabolic pathway in Arabidopsis. *Plant Cell Physiol* 55(1):218–228.
10. Kowalczyk M, Sandberg G (2001) Quantitative analysis of indole-3-acetic acid metabolites in Arabidopsis. *Plant Physiol* 127(4):1845–1853.
11. Novák O, et al. (2012) Tissue-specific profiling of the *Arabidopsis thaliana* auxin metabolome. *Plant J* 72(3):523–536.
12. Butler ED, Gallagher TF (2000) Characterization of auxin-induced ARRO-1 expression in the primary root of Malus domestica. *J Exp Bot* 51(351):1765–1766.
13. Zhao Z, et al. (2013) A role for a dioxygenase in auxin metabolism and reproductive development in rice. *Dev Cell* 27(1):113–122.
14. Yi K, Menand B, Bell E, Dolan L (2010) A basic helix-loop-helix transcription factor controls cell growth and size in root hairs. *Nat Genet* 42(3):264–267.
15. Balcerowicz D, Schoenaers S, Vissenberg K (2015) Cell fate determination and the switch from diffuse growth to planar polarity in Arabidopsis root epidermal cells. *Front Plant Sci* 6:1163.
16. Velasquez SM, Barbez E, Kleine-Vehn J, Estevez JM (2016) Auxin and Cellular Elongation. *Plant Physiol* 170(3):1206–1215.
17. Datta S, Prescott H, Dolan L (2015) Intensity of a pulse of RSL4 transcription factor synthesis determines Arabidopsis root hair cell size. *Nat Plants* 1(10):15138.
18. Mellor N, et al. (2016) Dynamic regulation of auxin oxidase and conjugating enzymes *AtDAO1* and *GH3* modulates auxin homeostasis. *Proc Natl Acad Sci USA*, 10.1073/pnas.1604458113.
19. Ljung K (2013) Auxin metabolism and homeostasis during plant development. *Development* 140(5):943–950.
20. Zhang J, et al. (2016) DAO1 catalyzes temporal and tissue-specific oxidative inactivation of auxin in *Arabidopsis thaliana*. *Proc Natl Acad Sci USA*, 10.1073/pnas.1604769113.
21. Voß U, et al. (2015) The circadian clock rephases during lateral root organ initiation in *Arabidopsis thaliana*. *Nat Commun* 6:7641.
22. Park JE, et al. (2007) GH3-mediated auxin homeostasis links growth regulation with stress adaptation response in Arabidopsis. *J Biol Chem* 282(13):10036–10046.
23. Wells DM, et al. (2012) Recovering the dynamics of root growth and development using novel image acquisition and analysis methods. *Philos Trans R Soc Lond B Biol Sci* 367(1595):1517–1524.
24. Nakagawa T, et al. (2007) Development of series of gateway binary vectors, pGWBs, for realizing efficient construction of fusion genes for plant transformation. *J Biosci Bioeng* 104(1):34–41.
25. Clough SJ, Bent AF (1998) Floral dip: A simplified method for Agrobacterium-mediated transformation of *Arabidopsis thaliana*. *Plant J* 16(6):735–743.
26. Cobelli C, Toffolo G, Foster DM (1992) Tracer-to-tracee ratio for analysis of stable isotope tracer data: Link with radioactive kinetic formalism. *Am J Physiol* 262(6 Pt 1): E968–E975.

Supporting Information

Porco et al. 10.1073/pnas.1604375113

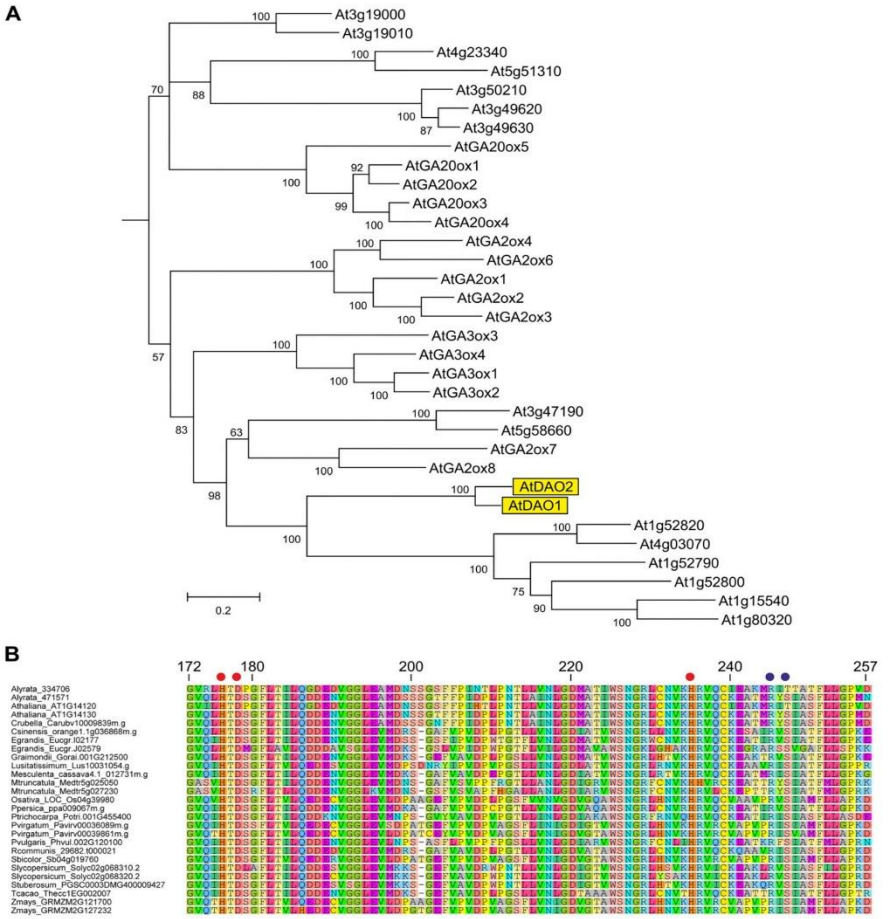

Fig. S1. Phylogenetic relationships between AtDAOs and related proteins. (*A*) Phylogenetic tree of the AtDAO1 and AtDAO2 and related *Arabidopsis* proteins. *Arabidopsis* 2-ODD sequences were aligned using MUSCLE within Geneious and trimmed to remove unaligned residues. Phylogenetic analysis was carried out using PhyML and MrBayes within ToPALI (www.topali.org/). A section of the MrBayes tree was selected and displayed in MEGA6. Numbers show branch support values; the scale bar shows substitutions per site. (*B*) Sequence alignment of the active site region of AtDAOs and related proteins from various plant species identified at https://phytozome.jgi.doe.gov/pz/portal.html. Sequences were aligned using MUSCLE. The Fe binding residues are indicated with red dots, and the 2-oxoglutarate binding residues are indicated with blue dots. Residue numbering is from the AtDAO1 (At1g14130) sequence.

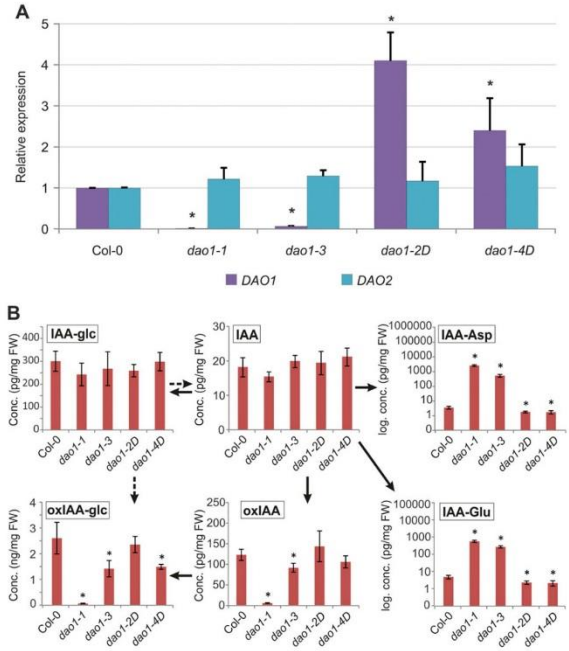

Fig. S2. (*A*) *AtDAO1* and *AtDAO2* transcript abundance in the different *dao1* alleles studied in this work relative to Col-0. qRT-PCR analysis was performed using cDNA from 7-d-old roots. Fold change was calculated by comparative *Cycle threshold* (*Ct*) method, and values were normalized with the expression of the *ACT2* gene. Error bars indicate SDs from three biological replicates. *Expression values significantly different from those in Col-0 (Student's *t* test; $P < 0.05$). (*B*) Levels of IAA metabolites in the different *dao1* alleles. IAA and the metabolites oxIAA, oxIAA-glc, IAA-glc, IAA-Asp, and IAA-Glu were quantified in 7-d-old seedlings of Col-0, *dao1-1*, *dao1-3*, *dao1-2D*, and *dao1-4D*. The concentrations for all metabolites except oxIAA-glc [nanograms per milligram fresh weight (FW)] are given in picograms per milligram FW. Samples were analyzed in five independent biological replicates, and error bars represent the SDs. *Statistically significant differences from Col-0 ($P < 0.05$; Student's *t* test).

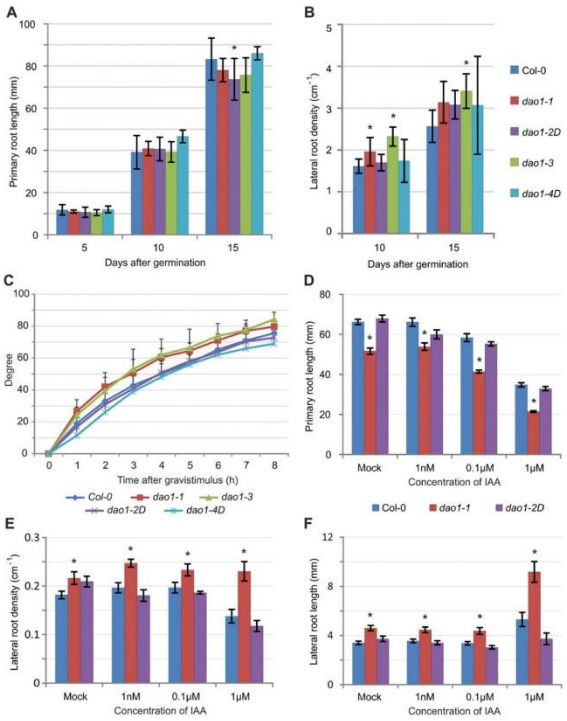

Fig. S3. Root phenotypes of the *dao1* mutant alleles. (*A*) Primary root length and (*B*) lateral root density of *dao1* mutants over the vegetative phase. *Values significantly different from those in Col-0 (Mann–Whitney *U* test; $P < 0.05$; $n = 10$). (*C*) Gravitropic response of the *dao1* mutants measured from 6-d-old seedlings ($n = 20$). (*D–F*) Effect of IAA on (*D*) primary root length, (*E*) lateral root density, and (*F*) lateral root length in 10-d-old *dao1-1* and *dao1-2D* mutants. Error bars indicate SD. *Values significantly different from those in Col-0 (Student's *t* test; $P < 0.05$; $n > 12$).

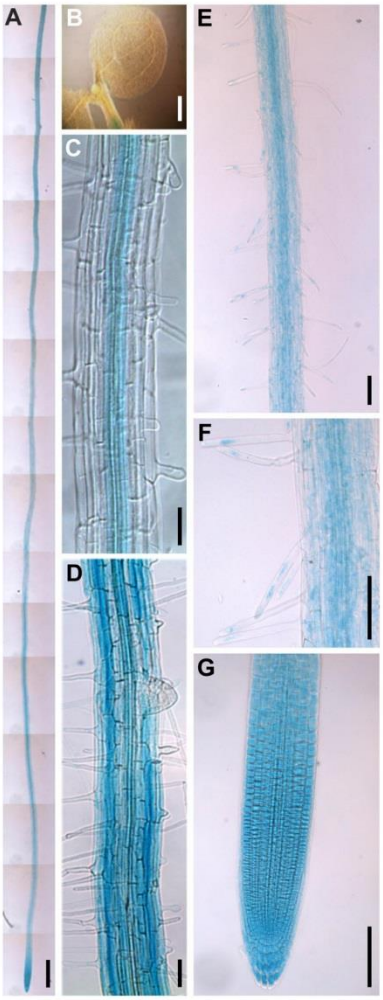

Fig. S4. DAO1 promoter is mainly active in roots. Visualization of *pDAO1:GUS* activity in (*A*) the root, (*B*) the aerial portion, (*C*) the stele, (*D*) epidermal cells in the mature part of the root, (*E* and *F*) RHs, and (*G*) the root tip. Pictures were taken from (*A* and *E*–*G*) 7-, (*B*) 4-, and (*C* and *D*) 5-d-old seedlings. (Scale bars: *A*, 500 μm; *B* and *E*–*G*, 100 μm; *C* and *D*, 50 μm.)

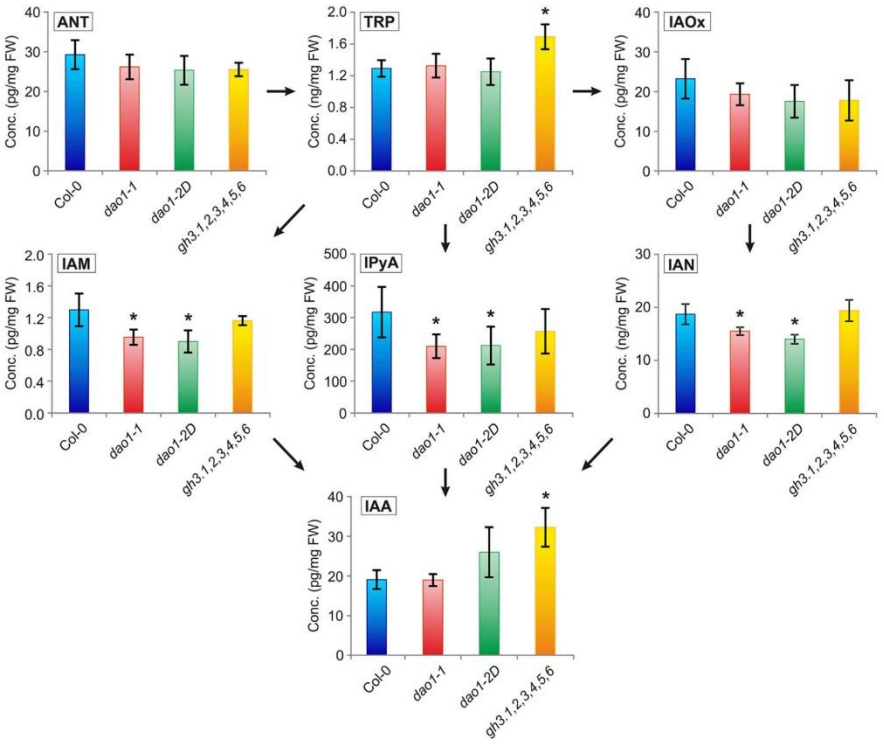

Fig. S5. Levels of IAA precursors in IAA oxidase and GH3 mutant backgrounds. IAA and the IAA precursors [anthranilate (ANT), indole-3-acetaldoxime (IAOx), indole-3-acetamide (IAM), indole-3-pyruvic acid (IPyA), and indole-3-acetonitrile (IAN)] were quantified in 7-d-old seedlings of Col-0, *dao1-1*, *dao1-2D*, and the *gh3* sextuple mutant line *gh3.1,2,3,4,5,6*. The concentration is given in picograms per milligram fresh weight (FW), except for TRP and IAN (nanograms per milligram FW). Samples were analyzed in five independent biological replicates, and error bars represent SDs. *Statistically significant differences from Col-0 ($P < 0.05$; Student's *t* test).



Fig. S6. Seedlings from the Col-0 WT and the *dao1-1* and *gh3.1,2,3,4,5,6* mutant lines. Pictures were taken 7 and 14 d after germination (dag). (Scale bars: 5 mm.)

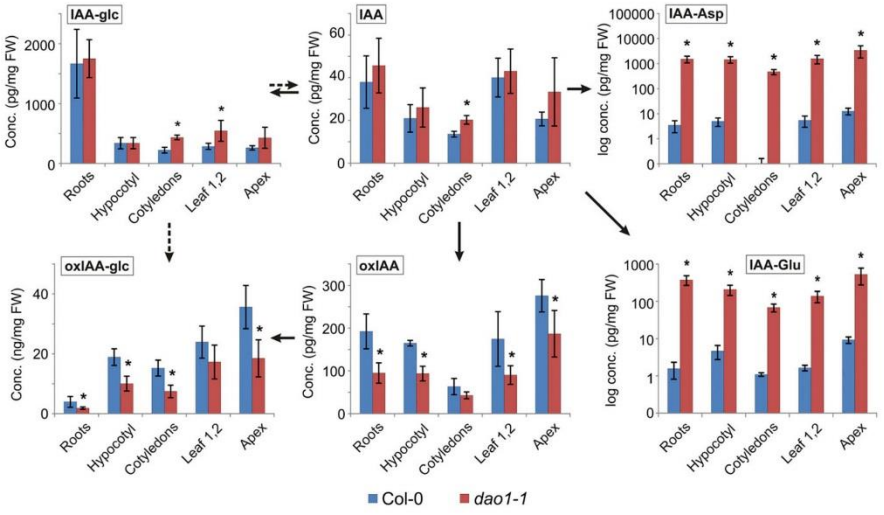

Fig. S7. Levels of IAA metabolites in different tissues of WT Col-0 and *dao1-1* seedlings. IAA and the IAA metabolites oxIAA, oxIAA-glc, IAA-glc, IAA-Asp, and IAA-Glu were quantified in root, hypocotyl, cotyledons, leaves 1 and 2, and shoot apex tissues from 10-d-old Col-0 (blue) and *dao1-1* mutant (red) seedlings. The concentrations for all metabolites are given in picograms per milligram fresh weight (FW) or nanograms per milligram FW (IAA-Asp and IAA-Glu are given in log scale). Samples were analyzed in five independent biological replicates, and error bars represent SDs. *Statistically significant differences from Col-0 ($P < 0.05$; Student's t test).

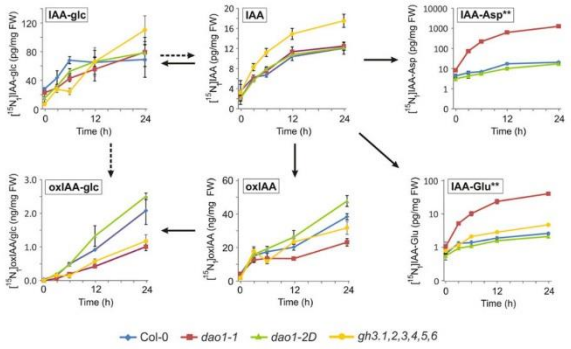

Fig. S8. In vivo labeling of IAA and IAA metabolites after feeding with [$^{15}N_1$]indole. Seven-day-old Col-0, *dao1-1*, *dao1-2D*, and *gh3.1,2,3,4,5,6* seedlings were incubated with [$^{15}N_1$]indole, and the levels of IAA and IAA metabolites were quantified after different times of incubation. The level of [$^{15}N_1$]IAA-Asp in the *gh3.1,2,3,4,5,6* mutant line was under the detection limit of the used LC-MS/MS method. The levels of de novo synthesized metabolites are given in picograms per milligram fresh weight (FW) or nanograms per milligram FW; $n = 3$. Error bars indicate SD. **Concentrations are given in log scale.

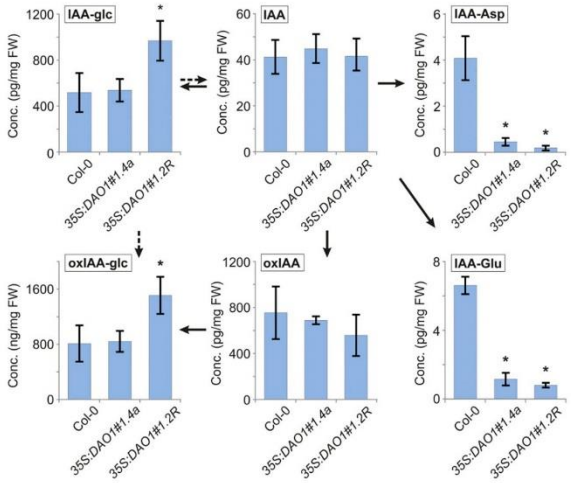

Fig. S9. Levels of IAA metabolites in IAA oxidase overproducing lines. IAA and the metabolites oxIAA, oxIAA-glc, IAA-glc, IAA-Asp, and IAA-Glu were quantified in 7-d-old seedlings of Col-0 and two independent *35S:DAO1* lines (*35S:DAO1#1.4a* and *35S:DAO1#1.2R*). The concentrations for all metabolites except oxIAA-glc [nanograms per milligram fresh weight (FW)] are given in picograms per milligram FW. Samples were analyzed in five independent biological replicates, and error bars represent the SDs. *Statistically significant differences from Col-0 ($P < 0.05$; Student's *t* test).

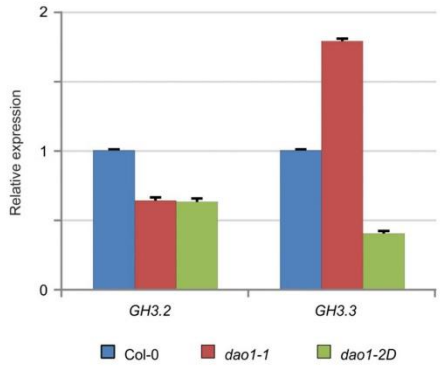

Fig. S10. *GH3* transcript abundance in the *dao1-1* and *dao1-2D* mutants relative to Col-0. qRT-PCR analysis was performed using cDNA from 7-d-old roots. Fold change was calculated by comparative *Ct* method, and values were normalized with the expression of the *ACT2* gene. Error bars indicate SDs.

Table S1. Primers used in this work

Purpose and primer name	Primer sequence (5′→3′) Forward primer	Reverse primer
Genotyping of insertion lines		
dao1-1	TTCCCCACGGAATTAAG GTAC	CTATGGGGAAAAAGGTTCC TG
dao1-2D	AGCGGTTTGAG ATAC ATGTGG	TTGGTGGACTTG AAGC TATGG
dao1-3	TGAAACATCCCC ATC TCTC AC	ATAAATTTG GGCCC AAAAGTG
dao1-4D	TCCGTTTAGTTCCCCC ATATC	TCGTGTTTTGGG TCTC CTATG
Gh3.3	GTGACAGGCAG AG TCACAAG C	TTTTAACGTATTAATC TTGGC ACG
Gh3.4	CAATGACGGGATTTTGATC AC	TGTGGAGCGGAATTATG AAAC
Gh3.5	AGGCCAGTGTTG TTGTC TTTG	TGGTCTTGAGCATAG ATTCCG
Gh3.6	GCAAAAACAGC ACC AAC ACG A	CGCAGCTTTGGAG GTTTC TG A
LBb3.1	ATTTTGCCGATTTC GG AAC	
LB1	GCCTTTTCAGAAATGG ATAAATAG CCTT GCTTCC	
Lba1	TGGTTCACGTAG TG GGCC ATCG	
3′dSpm	TACGAATAAGAGCG TCC ATTTTAG AGT	
Cloning		
At1g14130pro	CACCTTCCATAGAAATGTATATG TG	ATCTTCAATGG AG AG GTTAAC
At1g14130gfp	CACCTTCCATAGAAATGTATATG TG	TTTATCTAGTCC TGC ATGG G
At1g14130cds	CACCATGGGGGAACTAAACG G	TCATTTATCTAGTC CTG CATG
qRT-PCR		
qDAO1	TCGAAGCTTCTGC AG ATCAA	TTTCCTCGCTAAATCC GTTG
qDAO2	CCAGTGGATAG AG ATCTTG AAGC	GGCTTGTATAG TCGC GG ATG
qGH3.2	GTTTGCTTCCGGTC TCCTC	CACGAGCAAGTTCCTTCC A
qGH3.3	CATCACAGAGTTCCTC AC AAGC	GTCGGTCCATGTCTTC ATC A
qRSL4	TCTCTTGGGGATGTTCAAC TTT	AGGCCAAGCAAC TCG TCTC
qACT2	CCGCTCTTTCTTTCCAAGC	CCGGTACCATTGTC AC AC AC

3.7 DYNAMIC REGULATION OF AUXIN OXIDASE AND CONJUGATING ENZYMES *AtDAO1* AND *GH3* MODULATES AUXIN HOMEOSTASIS (Mellor et al., 2016)

PNAS

Dynamic regulation of auxin oxidase and conjugating enzymes *AtDAO1* and *GH3* modulates auxin homeostasis

Nathan Mellor[a,b], Leah R. Band[a,b], Aleš Pěnčík[c], Ondřej Novák[c], Afaf Rashed[a], Tara Holman[a], Michael H. Wilson[a,d], Ute Voß[a], Anthony Bishopp[a], John R. King[a,b], Karin Ljung[c], Malcolm J. Bennett[a,b,1], and Markus R. Owen[a,b,1]

[a]Centre for Plant Integrative Biology, Division of Plant and Crop Sciences, School of Biosciences, University of Nottingham, Loughborough LE12 5RD, United Kingdom; [b]Centre for Mathematical Medicine and Biology, School of Mathematical Sciences, University of Nottingham, Nottingham NG7 2RD, United Kingdom; [c]Umeå Plant Science Centre, Department of Forest Genetics and Plant Physiology, Swedish University of Agricultural Sciences, SE-901 83 Umea, Sweden; and [d]Centre for Plant Sciences, School of Biology, Faculty of Biological Sciences, University of Leeds, Leeds LS2 9JT, United Kingdom

Edited by Mark Estelle, University of California at San Diego, La Jolla, CA, and approved July 26, 2016 (received for review March 22, 2016)

The hormone auxin is a key regulator of plant growth and development, and great progress has been made understanding auxin transport and signaling. Here, we show that auxin metabolism and homeostasis are also regulated in a complex manner. The principal auxin degradation pathways in *Arabidopsis* include oxidation by *Arabidopsis thaliana* gene *DIOXYGENASE FOR AUXIN OXIDATION 1/2* (AtDAO1/2) and conjugation by Gretchen Hagen3s (GH3s). Metabolic profiling of *dao1-1* root tissues revealed a 50% decrease in the oxidation product 2-oxoindole-3-acetic acid (oxIAA) and increases in the conjugated forms indole-3-acetic acid aspartic acid (IAA-Asp) and indole-3-acetic acid glutamic acid (IAA-Glu) of 438- and 240-fold, respectively, whereas auxin remains close to the WT. By fitting parameter values to a mathematical model of these metabolic pathways, we show that, in addition to reduced oxidation, both auxin biosynthesis and conjugation are increased in *dao1-1*. Transcripts of *AtDAO1* and *GH3* genes increase in response to auxin over different timescales and concentration ranges. Including this regulation of *AtDAO1* and *GH3* in an extended model reveals that auxin oxidation is more important for auxin homoeostasis at lower hormone concentrations, whereas auxin conjugation is most significant at high auxin levels. Finally, embedding our homeostasis model in a multicellular simulation to assess the spatial effect of the *dao1-1* mutant shows that auxin increases in outer root tissues in agreement with the *dao1-1* mutant root hair phenotype. We conclude that auxin homeostasis is dependent on *AtDAO1*, acting in concert with *GH3*, to maintain auxin at optimal levels for plant growth and development.

hormone regulation | auxin | metabolism | homeostasis | *Arabidopsis thaliana*

The plant hormone auxin regulates a myriad of processes in plant growth and development (1). Although significant progress has been made in understanding the molecular basis of auxin transport, perception, and response, the control of auxin metabolism and homeostasis via conjugation and degradation remains less well-studied.

Several forms of auxin conjugates have been identified in plants, including ester-linked indole-3-acetic acid (IAA)-sugar conjugates and amide-linked IAA-amino acid conjugates (2). In *Arabidopsis thaliana*, the Gretchen Hagen3 (*GH3*) family of auxin-inducible acyl amido synthetases has been shown to convert IAA to IAA-amino acids (3). Most amino acid IAA conjugates are believed to be inactive, and some, such as indole-3-acetic acid aspartic acid (IAA-Asp) and indole-3-acetic acid glutamic acid (IAA-Glu), can also be further metabolized (4–6). The conversion of IAA to indole-3-acetic acid glucose (IAA-glc) is catalyzed by the uridine diphosphate glucosyltransferase UGT84B1 (UGT) (7). The oxidized form of IAA, 2-oxindole-3-acetic acid (oxIAA), has been identified as a major IAA catabolite in *Arabidopsis* (4, 6, 8) and can be further metabolized by conjugation to glucose (9). oxIAA has been shown to be an irreversible IAA catabolite that has very little biological activity compared with IAA and is not transported via the polar auxin transport system (6, 8). Although these metabolites and pathways have been identified, it has been difficult to identify the genes and enzymes involved. Two closely related components of the IAA degradation machinery have recently been identified in *Arabidopsis*, *DIOXYGENASE FOR AUXIN OXIDATION 1* (*AtDAO1*; *At1g14130*) and *AtDAO2* (*At1g14120*) (10–12). *AtDAO1* and *AtDAO2* are closely related to genes described in apple [*Adventitious Rooting Related Oxygenase 1* (13)] and rice [*DAO* (14)] and a family of gibberellin 2 (GA2) oxidases that mediates degradation of GAs (15). Radiolabeled IAA feeding studies of loss and gain of function *AtDAO1* lines have shown that this oxidase represents the major regulator of auxin degradation to oxIAA in *Arabidopsis* (11). Metabolite profiling of mutant lines revealed that disrupting *AtDAO1* regulation resulted in major changes in steady-state levels of oxIAA and IAA conjugates but not IAA. Hence, IAA conjugation and catabolism seem to regulate auxin levels in *Arabidopsis* in a highly redundant manner.

In this paper, we describe a systems biology approach to understanding the highly nonlinear regulation of auxin homeostasis in *Arabidopsis*. We initially use a mathematical model of auxin metabolism to reveal the importance in *dao1-1* mutant plants of not only a reduction in IAA oxidation rate but a more than

Significance

Auxin is a key hormone regulating plant growth and development. We combine experiments and mathematical modeling to reveal how auxin levels are maintained via feedback regulation of genes encoding key metabolic enzymes. We describe how regulation of auxin oxidation via transcriptional control of *Arabidopsis thaliana* gene *DIOXYGENASE FOR AUXIN OXIDATION 1* (*AtDAO1*) expression is important at low to normal auxin concentrations. In contrast, higher auxin levels lead to increased Gretchen Hagen3 expression and auxin conjugation. Integrating this understanding into a multicellular model of root auxin dynamics successfully predicts that the *dao1-1* mutant has an auxin-dependent longer root hair phenotype. Our findings reveal the importance of auxin homeostasis to maintain this hormone at optimal levels for plant growth and development.

Author contributions: N.M., J.R.K., K.L., M.J.B., and M.R.O. designed research; N.M., L.R.B., A.P., O.N., A.R., T.H., U.V., and M.R.O. performed research; N.M., L.R.B., M.H.W., A.B., K.L., M.J.B., and M.R.O. analyzed data; and N.M., L.R.B., U.V., J.R.K., K.L., M.J.B., and M.R.O. wrote the paper.

The authors declare no conflict of interest.

This article is a PNAS Direct Submission.

[1]To whom correspondence may be addressed. Email: malcolm.bennett@nottingham.ac.uk or Markus.Owen@nottingham.ac.uk.

This article contains supporting information online at www.pnas.org/lookup/suppl/doi:10.1073/pnas.1604458113/-/DCSupplemental.

200-fold increase in the rate of irreversible GH3 conjugation coupled with an increase in the rate of IAA biosynthesis. Our transcriptomic data show that there are feedbacks on the auxin degradation pathway, namely the IAA induction of *AtDAO1* and members of the *GH3* family. To investigate the effect of these feedbacks on auxin homeostasis, we add them to an extended model, revealing that the AtDAO1 degradation pathway is much more effective when IAA is at physiological levels, whereas the GH3 degradation pathway is dominant after high levels of IAA input. Finally, we embed our homeostasis model in a multicellular context that predicts that one spatial effect of the *dao1-1* mutant is to increase IAA in outer root tissues, consistent with the auxin-dependent elongated root hair phenotype described for the *dao1-1* mutant (11).

Results

A Mathematical Model of Auxin Metabolism Predicts That the *dao1-1* Mutant Has Altered Rates of Auxin Oxidation, Conjugation, and Synthesis. The principal degradation pathways in *Arabidopsis* include irreversible conjugation by GH3s and oxidation by AtDAO1/2 (Fig. 1*A*). In the roots of *dao1-1* KO seedlings, oxidized IAA (oxIAA) levels are halved, and the conjugated forms IAA-Asp and IAA-Glu are increased by 438- and 240-fold, respectively, whereas the level of IAA is only increased by 20% (statistically insignificant) (Fig. 1*B*). These root data are consistent with metabolite profiling from whole seedlings and different tissues (11).

To investigate whether the conceptual model of the main IAA degradation pathways summarized in Fig. 1*A* is consistent with the metabolite data given in Fig. 1*B*, a linear ordinary differential equation (ODE) model was formulated (*Materials and Methods* and *SI Text*). The model simulates the biosynthesis of IAA and its subsequent conversion to IAA-glc via UGT, IAA-Asp and IAA-Glu via GH3, and oxIAA via AtDAO1/2. IAA-glc and oxIAA can both be conjugated further to form 2-oxoindole-3-acetic acid glucose (oxIAA-glc), and oxIAA-glc and the conjugates IAA-Asp and IAA-Glu are then degraded at fixed rates. We calculated steady-state levels of the model variables in the WT (wild type), modeled the mutant by setting the rate of AtDAO1-mediated IAA oxidation in *dao1-1* to zero ($d_1^* = 0$, where the * notation indicates a parameter value in the *dao1-1* mutant), and estimated model parameters to best fit the data in Fig. 1*B* (see Table S1, set 1 for parameter values). The model is able to reproduce the observed reductions in $[oxIAA]$ and $[oxIAA-glc]$ while maintaining levels of $[IAA]$ and $[IAA-glc]$ but yields only an 8% increase in the levels of conjugated auxin ($[IAA-Asp]/[IAA-Glu]$), far less than the experimentally observed changes of greater than 200-fold (Fig. 1*C* and Fig. S1). Thus, our mathematical modeling predicts that a decrease in oxidation rate alone is not sufficient to account for the massive increase in conjugation products and IAA homeostasis in *dao1-1*.

To explore whether increased GH3 conjugation rates in *dao1-1* can explain the data, we increased those rates 10-fold in our model, so that $g_a^* = 10g_a$ and $g_g^* = 10g_g$. Using these parameters in the *dao1-1* simulation surprisingly results in only a 13% increase in the level of $[IAA-Asp]$ and $[IAA-Glu]$ conjugates and decreases in all other metabolites (Fig. 1*D*). We conclude that altering GH3 conjugation rates is insufficient in isolation to explain the metabolic data. We, therefore, tested in our model whether increasing the auxin biosynthesis rate in *dao1-1* ($\lambda^* = 10\lambda$) as well as GH3-mediated conjugation rates could capture the experimentally observed behavior of the *dao1-1* mutant compared with the WT. Fig. 1*E* shows that increasing both IAA biosynthesis and GH3 conjugation rates in the *dao1-1* simulation can qualitatively match metabolomic data. Hence, auxin homeostasis seems to be maintained in the IAA oxidase mutant *dao1-1* by adjusting conjugation and synthesis rates.

Systems Analysis Reveals That, in Addition to Reduced Oxidation, both IAA Biosynthesis and Conjugation Are Increased in *dao1-1*. Next, we sought experimental evidence for changes in conjugation and synthesis rates before attempting more precise fitting of our model to the data. Quantitative RT-PCR (qRT-PCR) shows that the mRNA expression level of *GH3.3* is 2.7 times higher in *dao1-1* than in the WT (Fig. 2*A*), and additional metabolite profiling in whole seedlings shows that the levels of three IAA precursors indole-3-acetamide (IAM), indole-3-pyruvic acid (IPyA), and indole-3-acetonitrile (IAN) all drop significantly in the *dao1-1* mutant relative to the WT (Fig. 2*B*), indicating a higher IAA biosynthetic rate in *dao1-1*.

To further establish the plausibility of increased IAA biosynthesis and GH3 conjugation in the *dao1-1* mutant, model parameters were fitted to the steady-state metabolite data for $[IAA]$, $[oxIAA]$, $[IAA-Asp]$, $[IAA-Glu]$, $[IAA-glc]$, and $[oxIAA-glc]$ in both the WT and *dao1-1*. To fix the IAA synthesis rate in *dao1-1* (λ^*), we assume that IAM, IPyA, and IAN have constant production rates (which do not vary between the WT and *dao1-1*) and that each is converted to IAA at a rate that is different in *dao1-1* compared with in the WT. It follows that λ^* is inversely proportional to the corresponding drop in auxin precursor concentrations (0.74 averaged across IAM, IPyA, and IAN), giving $\lambda^* = 1.36$. We then allowed the remaining parameters, including g_a, g_a^* and g_g, g_g^* (the respective rates, in the WT and *dao1-1*, of GH3-mediated conjugation to $[IAA-Asp]$ and $[IAA-Glu]$), to take any values within a wide range of fixed bounds. The parameter fitting used a hybrid genetic algorithm plus local minimum search, which sought to minimize the squared difference between model steady-state and metabolite data, for both the WT and *dao1-1*. We found that, with conjugation rates free to vary in *dao1-1*, a wide range of parameter sets can fit the quantitative data. (Fig. 2*C*). Running the parameter fitting algorithm a number of times, we generated 100 different parameter sets, which all result in good agreement of the model with data (well within the bounds of statistical experimental error). Plotting the distribution of each of the fitted parameter values shows that there is a limited degree of variability in some parameters between parameter sets (Fig. 2*C*). Fig. 2*D* and Fig. S2 show that the predicted relative changes between the WT and *dao1-1* match those observed for six key metabolites (see Table S1, set 2 for parameter values). Fig. 2 *E* and *F* shows that the rates of conjugation via GH3 increase more than 400-fold (to IAA-Asp) and more than 200-fold (to IAA-Glu) in *dao1-1* compared with in the WT, consistently across parameter sets.

Dynamic Regulation of *AtDAO1* and *GH3* by Auxin Allows a Context-Dependent Homeostatic Response to Changes in Auxin. As expected for important components of the auxin homeostasis machinery, *AtDAO1* and *GH3* genes are auxin inducible (11, 16). Affymetrix-based transcriptomic analysis of auxin-treated root tips revealed that *GH3.3* mRNA is induced very rapidly (peaking at 2 h), whereas *AtDAO1* mRNA is induced more slowly (peaking at the final 4-h time point). qRT-PCR–based transcriptomic analysis also showed that *GH3.3* is up-regulated 2.7-fold in *dao1-1* (Fig. 2*A*) and around 200-fold in WT seedlings exposed to IAA (Fig. 3*A* and Fig. S3*B*). In contrast, IAA-treated WT seedlings show at most a 75% increase in *AtDAO1* expression (Fig. 3*A* and Fig. S3*A*). We conclude that *AtDAO1* and *GH3.3* are up-regulated by auxin over different timescales and concentration ranges and with different fold changes in response.

To investigate the effect of these nonlinear feedbacks on auxin homeostasis, we incorporate them into an extended model (Fig. 3*B*), in which the expression of both *AtDAO1* and *GH3* increases as the concentration of IAA increases. To model these nonlinearities, we use Hill functions (Eqs. **2b** and **2c**), where the threshold parameters k_d and k_g determine the level of IAA at which gene expression reaches half-maximum, and the Hill coefficients n_d and n_g determine the sharpness of the transition from low to high expression. In the case of *AtDAO1*, we see at most a doubling of the mRNA level from basal expression under IAA treatment, with no sharp switch in expression observed (Fig. 3*A* and Fig. S3*A*), which suggests a half-maximum threshold similar to the basal IAA

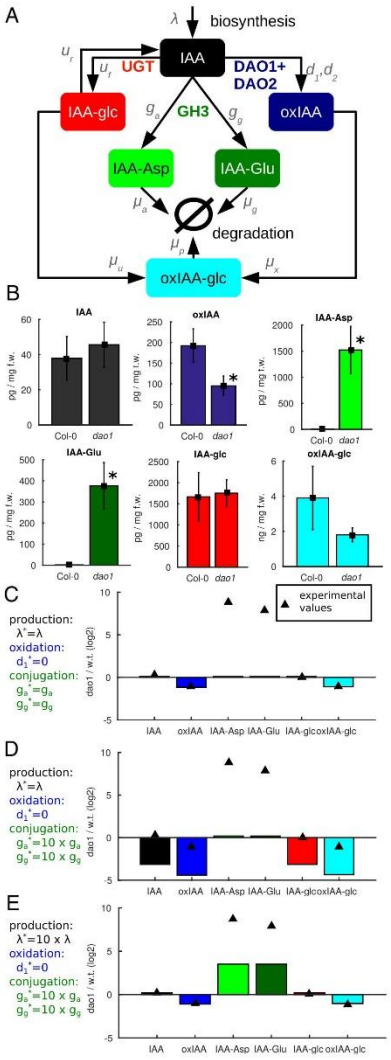

Fig. 1. A metabolic model suggests that the *dao1-1* mutant may have altered rates of metabolism other than IAA oxidation. (*A*) The principal degradation pathways in *Arabidopsis* include irreversible conjugation by GH3s and oxidation by DAO1/2. (*B*) In the *dao1-1* KO, oxidized IAA (oxIAA) levels are halved and conjugated forms, IAA-Asp and IAA-Glu, are increased by more than 438- and 240-fold, respectively, whereas the level of IAA is increased by only 20%. *Statistically significant differences from Col-0 ($P <$ 0.05; Student's *t* test). (*C* and *D*) Mathematical modeling predicts that a decrease in oxidation rate alone is not sufficient to account for the increase in conjugation products and IAA homeostasis in *dao1-1* and that increasing GH3 conjugation rates does not lead to a better qualitative match. (*E*) Increasing both IAA biosynthesis and GH3 conjugation rates in the *dao1-1* simulation can qualitatively match metabolomic data. f.w., Fresh weight; oxIAA-glc, 2-oxoindole-3-acetic acid glucose; w.t., Col-0 WT.

concentration. Hence, we fix $k_d = 1$ and the Hill coefficient $n_d = 1$ and fit the remaining model parameters to the steady-state metabolic WT and *dao1-1* data. The fitted nonlinear model shows good agreement with the data (Figs. S4 and S5) and shows that a small increase in IAA biosynthesis rate (36%) can result in a much larger (>100-fold) increase in the level of IAA-Asp and IAA-Glu conjugates (see Table S1, set 3 for parameter values).

Fig. 3*C* uses the estimated and fitted parameters to compare the contribution of the GH3 and AtDAO1 pathways with IAA degradation. Although the contribution of AtDAO1 increases slightly over the range shown and is still active even at low levels of IAA, conjugation rates are much lower at and below basal levels ($IAA \leq 1$) but rapidly increase as IAA increases, so that for high levels of IAA ($IAA \geq 2$), the conjugation pathway is dominant.

Fig. 3 *D–F* shows the temporal response of the model after changing the $[IAA]$ input rate, λ, from the basal steady-state value ($\lambda = 1$). To compare the relative importance of the AtDAO1 and GH3 degradation pathways as well as the "full" model with both up-regulated by IAA, we also show three alternate versions: one where only *AtDAO1* is induced by auxin, one where only *GH3* is induced by auxin, and one where neither response is induced. With the full model, there is a clearly homeostatic response with a transient peak, after which the steady-state level of IAA is much lower than the steady-state level without any *AtDAO1*/*GH3* induction. For a large change in IAA input (Fig. 3*D*), this homeostasis is much more rapid and pronounced than for a relatively small change in IAA input (Fig. 3*E*). This difference in homeostatic responses is caused by variations in the magnitude and speed of *AtDAO1* and *GH3* responses to increased IAA as can be inferred from the simulations where the inducibility of one or the other is switched off. In the absence of *GH3* induction, homeostasis is greatly reduced for a 10-fold increase in IAA input (Fig. 3*D*), whereas for a 2-fold reduction, the homeostatic response is largely unchanged from the full model (Fig. 3*F*). Conversely, in the absence of *AtDAO1* regulation, the homeostatic effect is only slightly reduced for a 10-fold IAA increase, whereas it is undetectable for a 2-fold reduction in IAA input. For a twofold increase in IAA input, both the AtDAO1 and GH3 pathways contribute to IAA homeostasis (Fig. 3*E*).

Mathematical modeling of these feedbacks on auxin degradation suggests that AtDAO1 is more effective for auxin homeostasis at lower auxin concentrations, whereas GH3s are much more important at high auxin levels. The difference between the GH3 and AtDAO1 degradation pathways is illustrated further in Fig. 3*G*, which shows the IAA steady state for a range of values of the auxin input rate λ for each of the model variants described above. Here, $IAA = 1$ corresponds to typical physiological levels. Around this level and below, the AtDAO1 degradation pathway is more active, but above this level, the GH3 pathway becomes more active and eventually, is much more important than *AtDAO1* in removing large quantities of excess IAA.

Multicellular Root Modeling Predicts Auxin Accumulation in Epidermal Tissues. We developed a spatial model for auxin transport and metabolism, combining our compartmental ODE model for IAA metabolism and IAA-dependent induction of *AtDAO1* and *GH3* (described above) with the multicellular model for IAA transport described in ref. 17. The multicellular model is based on actual root cell geometries and auxin influx and efflux carrier subcellular localizations. The IAA concentration is defined in each cell

together with terms for the rates of carrier-dependent transport between cells.

Following ref. 17, we prescribed PIN, AUX, and LAX auxin efflux and influx carrier distributions in our virtual root tissues, with the PIN carriers polarized according to reports in the literature and our own observations using anti-PIN antibodies. The model also incorporated a weak background efflux to account for low levels of nonpolar PIN and the presence of other transporters, such as ABCB. We specified small auxin production rates within every cell and higher auxin production in the quiescent centre and columella initials. The model also captured auxin diffusion through the apoplast, as measured in ref. 18. We treated auxin concentrations as uniform within each cell because of the small size of cells in this region and relatively rapid auxin diffusion within the cytoplasm compared with within the apoplast (18–20). The small cells near the root tip are in contrast with the larger cells farther from the root tip, where subcellular variations in auxin have previously been considered (21, 22).

The resulting model can be described by a system of ODEs for the auxin concentrations within each cell and each segment of apoplast. Details and model parameter values are in *SI Text* and ref. 17. As done previously, we included a flux of auxin from the shoot by prescribing a nonzero auxin concentration within the stele cells at the boundary of the modeled tissue. In the epidermal, cortical, and endodermal cells, we assume that the auxin concentrations have reached their far-field asymptotic values, hence setting them equal to those in neighboring (rootward) cells of the same type. This assumption implies an appropriate shootward flux of auxin through the outer tissue layers (19). Starting from an initial condition in which all remaining concentrations equal zero, we simulated the ODEs until the concentrations and fluxes reached a steady state.

Embedding our homeostasis model into a multicellular context allows us to predict the effect of the *dao1-1* mutant on IAA levels and distribution in root tissues compared with the WT. Simulations using our combined transport and homeostasis model predict that the WT IAA distribution (Fig. 4*A*) is in good agreement with spatial patterns inferred from the DII-VENUS fluorescent auxin signaling sensor (17). Although the spatial pattern in the *dao1-1* mutant is similar to the WT, the total concentration of IAA was predicted to increase by 26%, consistent with the metabolite data (Fig. 1*B*). Very interestingly, the simulated increase in auxin is predicted to be spatially inhomogeneous, with auxin concentrations in outer root tissues increased >40% (Fig. 4*B*). The predicted increase in IAA in the *dao1-1* mutant outer root tissues is consistent with the observed extraelongated root hair phenotype, which is known to be auxin dependent (23).

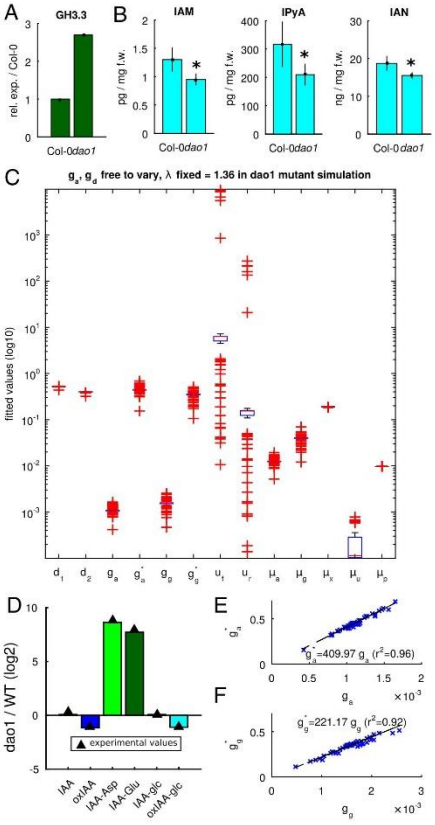

Fig. 2. Experimental evidence and model optimization support the hypothesis that, in addition to reduced oxidation, both IAA biosynthesis and conjugation are increased in *dao1-1*. (*A*) Expression of the conjugating enzyme *GH3.3* is elevated in *dao1-1*. (*B*) Levels of the IAA precursors IAM, IPyA, and IAN are all significantly reduced in dao1-1. *Statistically significant differences from Col-0 ($P < 0.05$; Student's *t* test). (*C*) Box plot showing the first and third quartiles (bottoms and tops of blue boxes), medians (red lines), and lowest and highest data points within 1.5× the interquartile range (black whiskers) plus outliers (red + symbols) of 100 fitted parameter sets. With IAA biosynthesis and conjugation rates free to vary in *dao1-1*, a wide range of parameter sets can fit the quantitative data. (*D*) Representative fit between model and data (*dao1-1* relative to WT simulation). (*E* and *F*) Conjugation rates in *dao1-1* (g_a^* and g_g^*) are predicted to be more than 200-fold larger than in WT (g_a and g_g) consistently across 100 parameter sets. f.w., Fresh weight; oxIAA-glc, 2-oxoindole-3-acetic acid glucose.

Discussion

Our systems-based study has revealed that auxin homeostasis is controlled by highly redundant regulatory mechanisms involving auxin oxidation, conjugation, and synthesis pathways. These auxin homeostasis regulatory mechanisms are also highly nonlinear, involving multiple feedback loops that control the expression of AtDAO1 IAA oxidase and GH3 IAA conjugation enzymes. These regulatory mechanisms also operate across a range of spatial and temporal scales and auxin concentrations. For example, *AtDAO1* and *GH3* exhibit contrasting slow and rapid temporal expression dynamics, respectively. These differences in timing of *AtDAO1* and *GH3* induction by auxin are likely to be functionally very important. The slow auxin induction of *AtDAO1* ensures that perturbations in this signal can still cause a desired developmental response, while helping the cell maintain an optimal level of auxin. *GH3*, however, is only induced when auxin is high and therefore, may be expressed rapidly to remove excess auxin as quickly as possible. The triggering of the GH3 degradation pathway at high levels of auxin is possibly a stress response to excess auxin levels and likely in effect during many laboratory experiments when large amounts of exogenous auxin are applied. However, Kramer and Ackelsberg (24) recently suggested that the GH3 conjugation pathway may be important at sites of high auxin accumulation during normal growth, such as lateral root primordia or within the shoot apical meristem.

Despite these myriad auxin homeostasis mechanisms operating in plants, our multicellular model predicted that disrupting just the IAA

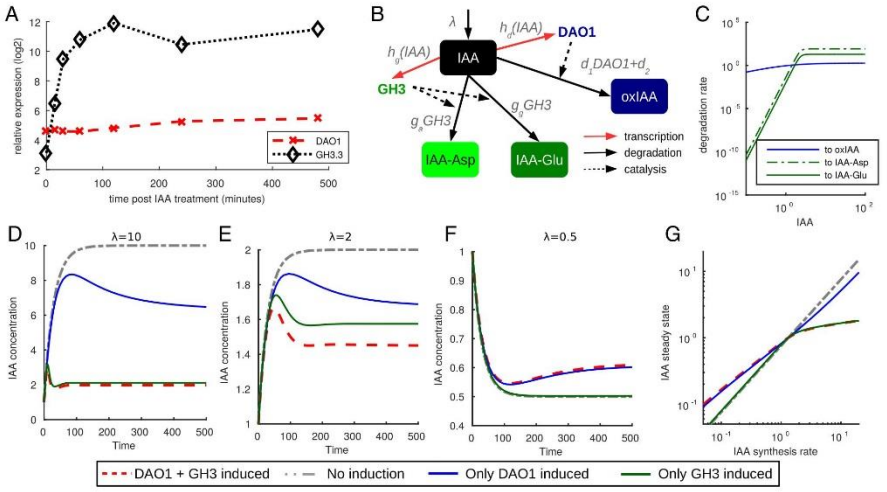

Fig. 3. *AtDAO1* transcriptional regulation by IAA provides sensitivity at low auxin concentrations, whereas *GH3* regulation contributes to homeostasis at high auxin concentrations. (*A*) Affymetrix data showing *AtDAO1* and *GH3.3* transcript abundance in microdissected root tips at time points after IAA treatment. (*B–G*) Mathematical modeling of these feedbacks on auxin degradation suggests that AtDAO1 is more effective in auxin homoeostasis at lower auxin concentrations, whereas GH3s contribute much more at high levels of auxin. (*B*) Submodel for IAA metabolism indicating the IAA-dependent transcription of *AtDAO1* and *GH3*. (*C*) Effective AtDAO1- and GH3-dependent IAA degradation rates at steady state for fixed levels of IAA input. (*D* and *E*) Temporal response to 10- and 2-fold increases in IAA input with different combinations of modeled regulation. *GH3* regulation is dominant. In each case, the model is shown with both *AtDAO1* and *GH3* inducible by auxin, only *AtDAO1* inducible, and only *GH3* inducible. (*F*) Temporal response to a twofold decrease in IAA input with different combinations of modeled regulation. *AtDAO1* regulation is dominant. (*G*) The steady-state patterns seen in *D–F* are found across a wide range of IAA input rates.

oxidase *AtDAO1* is still able to perturb auxin levels in selected root tissues. These changes in auxin levels included elevated concentration in the *dao1-1* mutant epidermis (Fig. 4*B*), the tissue from which root hairs originate and elongate in an auxin-dependent manner.

Datta et al. (25) have recently shown that root hair length is directly proportional to the abundance of a basic helix-loop-helix transcription factor RSL4, which has expression that is auxin inducible. Hence, we would predict (based on our multicellular model simulations) that RSL4 and root hair length would increase in proportion to the >40% increase in auxin levels in the *dao1-1* mutant epidermis. Consistent with our model predictions, Porco et al. (11) report similar increases in *RSL4* mRNA abundance and root hair length in the *dao1-1* mutant epidermis experimentally. Hence, we reason that auxin levels may also be perturbed in other *dao1-1* mutant tissues and/or stages of development, helping to explain why, despite the highly redundant organization of auxin homeostasis, *dao1-1* exhibits a number of subtle auxin-related mutant phenotypes in root, shoot, and floral tissues (11, 12).

Materials and Methods

Plant Material and Growth Conditions. *A. thaliana* Columbia-0 (Col-0) was used as the WT in all experiments. All transfer DNA insertion mutants were obtained from the Nottingham *Arabidopsis* Stock Centre. WT and mutant plants were grown as described in ref. 11.

RNA Isolation and Analysis. Sterilized seeds were plated on one-half Murashige and Skoog media, stratified at 4 °C for 24 h to synchronize germination, and then transferred to a controlled growth chamber; 7-d-old seedlings on plates were then transferred to Murashige and Skoog media containing 1 μM IAA for varying lengths of time. RNA was extracted from root tips and used for microarray analysis with the Affymetrix ATH1 array.

IAA Metabolite Profiling. *A. thaliana* WT Col-0 and the *dao1-1* mutant were grown under long-day conditions for 7 or 10 d. Whole seedlings or dissected tissues were collected in five replicates (20 mg tissue per sample). Sample purification and quantification of IAA metabolites were performed as described in ref. 26.

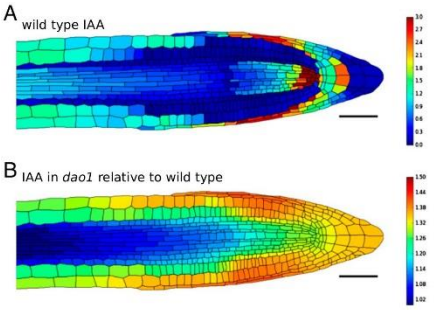

Fig. 4. Multicellular simulation showing auxin accumulation in outer tissues of the root apex in *dao1-1* relative to the WT. (*A*) Predicted IAA in the WT simulation relative to the fixed reference value of IAA = 1 in the stele at the shootward end of the tissue as defined in the boundary conditions. (*B*) In *dao1-1*, auxin is up to 40% higher in the epidermis, which is consistent with increased RSL4 expression, causing the increased root hair phenotype seen in the *dao1-1* mutant (11). (Scale bar: 50 μm.)

Mathematical Models and Parameter Estimation. Here, we summarize our mathematical models of the auxin homeostasis network. Full details of all models, definitions of model variables and parameters, and parameter estimation are in *SI Text*.

IAA Metabolism Model. The simplest model of the pathway shown in Fig. 1*A* has a constant rate of IAA biosynthesis (λ) and linear rates of degradation and conversion from one form of auxin to another:

$$\frac{d[IAA]}{dt} = \lambda - \left(u_f + g_a + g_g + d_1 + d_2\right)[IAA] + u_r[IAA-glc], \quad [1a]$$

$$\frac{d[oxIAA]}{dt} = (d_1 + d_2)[IAA] - \mu_x[oxIAA], \quad [1b]$$

$$\frac{d[IAA-Asp]}{dt} = g_a[IAA] - \mu_a[IAA-Asp], \quad [1c]$$

$$\frac{d[IAA-Glu]}{dt} = g_g[IAA] - \mu_g[IAA-Glu], \quad [1d]$$

$$\frac{d[IAA-glc]}{dt} = u_f[IAA] - (u_r + \mu_u)[IAA-glc], \quad [1e]$$

and

$$\frac{d[oxIAAglc]}{dt} = \mu_x[oxIAA] + \mu_u[IAA-glc] - \mu_p[oxIAA-glc]. \quad [1f]$$

Inducible *AtDAO1-GH3* Model. We extend Eqs. **1a–1f** by assuming that the rate of conversion of IAA to oxIAA (d_1) is proportional to the level of a new variable $[D]$ representing AtDAO1 and that the rates of conjugation of IAA to IAA-Asp (g_a) and IAA-Glu (g_g) are proportional to the level of another new variable $[G]$ representing GH3s. $[D]$ and $[G]$ are assumed to be produced in response to $[IAA]$, represented by Hill functions, and decay linearly, so that

$$g_a = \dot{g}_a[G],\ g_g = \dot{g}_g[G],\ d_1 = \dot{d}_1[D], \quad [2a]$$

$$\frac{d[D]}{dt} = \eta_d\left(\frac{[IAA]^{n_d}}{k_d^{n_d} + [IAA]^{n_d}} - [D]\right), \quad [2b]$$

and

$$\frac{d[G]}{dt} = \eta_g\left(\frac{[IAA]^{n_g}}{k_g^{n_g} + [IAA]^{n_g}} - [G]\right). \quad [2c]$$

Multicellular Model. The multicellular model is described in *SI Text*.

ACKNOWLEDGMENTS. N.M., L.R.B., T.H., M.H.W., U.V., J.R.K., M.J.B., and M.R.O. acknowledge support from the Biological and Biotechnology Science Research Council Responsive Mode Awards to the Centre for Plant Integrative Biology. N.M., M.J.B., and M.R.O. acknowledge European Research Council Futureroots funding. L.R.B. acknowledges funding from the Leverhulme Trust. A.R. and M.J.B. also acknowledge support from the Saudi Arabian Ministry of Higher Education.

1. Vanneste S, Friml J (2009) Auxin: A trigger for change in plant development. *Cell* 136(6):1005–1016.
2. Ludwig-Müller J (2011) Auxin conjugates: Their role for plant development and in the evolution of land plants. *J Exp Bot* 62(6):1757–1773.
3. Staswick PE, et al. (2005) Characterization of an Arabidopsis enzyme family that conjugates amino acids to indole-3-acetic acid. *Plant Cell* 17(2):616–627.
4. Östin A, Kowalyczk M, Bhalerao RP, Sandberg G (1998) Metabolism of indole-3-acetic acid in *Arabidopsis*. *Plant Physiol* 118(1):285–296.
5. Kai K, Horita J, Wakasa K, Miyagawa H (2007) Three oxidative metabolites of indole-3-acetic acid from *Arabidopsis thaliana*. *Phytochemistry* 68(12):1651–1663.
6. Pencik A, et al. (2013) Regulation of auxin homeostasis and gradients in *Arabidopsis* roots through the formation of the indole-3-acetic acid catabolite 2-oxindole-3-acetic acid. *Plant Cell* 25(10):3858–3870.
7. Jackson RG, et al. (2001) Identification and biochemical characterization of an *Arabidopsis* indole-3-acetic acid glucosyltransferase. *J Biol Chem* 276(6):4350–4356.
8. Peer WA, Cheng Y, Murphy AS (2013) Evidence of oxidative attenuation of auxin signalling. *J Exp Bot* 64(9):2629–2639.
9. Tanaka K, et al. (2014) UGT74D1 catalyzes the glucosylation of 2-oxindole-3-acetic acid in the auxin metabolic pathway in *Arabidopsis*. *Plant Cell Physiol* 55(1):218–228.
10. Voß U, et al. (2015) The circadian clock rephases during lateral root organ initiation in *Arabidopsis thaliana*. *Nat Commun* 6:7641.
11. Porco S, et al. (2016) Dioxygenase-encoding *AtDAO1* gene controls IAA oxidation and homeostasis in *Arabidopsis*. *Proc Natl Acad Sci USA*, 10.1073/pnas.1604375113.
12. Zhang J, et al. (2016) DAO1 catalyzes temporal and tissue-specific oxidative inactivation of auxin in *Arabidopsis thaliana*. *Proc Natl Acad Sci USA*, 10.1073/pnas.1604769113.
13. Butler ED, Gallagher TF (2000) Characterization of auxin-induced ARRO-1 expression in the primary root of *Malus domestica*. *J Exp Bot* 51(351):1765–1766.
14. Zhao Z, et al. (2013) A role for a dioxygenase in auxin metabolism and reproductive development in rice. *Dev Cell* 27(1):113–122.
15. Thomas SG, Phillips AL, Hedden P (1999) Molecular cloning and functional expression of gibberellin 2- oxidases, multifunctional enzymes involved in gibberellin deactivation. *Proc Natl Acad Sci USA* 96(8):4698–4703.
16. Park JE, et al. (2007) GH3-mediated auxin homeostasis links growth regulation with stress adaptation response in Arabidopsis. *J Biol Chem* 282(13):10036–10046.
17. Band LR, et al. (2014) Systems analysis of auxin transport in the *Arabidopsis* root apex. *Plant Cell* 26(3):862–875.
18. Kramer EM, Frazer NL, Baskin TI (2007) Measurement of diffusion within the cell wall in living roots of *Arabidopsis thaliana*. *J Exp Bot* 58(11):3005–3015.
19. Band LR, King JR (2012) Multiscale modelling of auxin transport in the plant-root elongation zone. *J Math Biol* 65(4):743–785.
20. Swarup R, et al. (2005) Root gravitropism requires lateral root cap and epidermal cells for transport and response to a mobile auxin signal. *Nat Cell Biol* 7(11):1057–1065.
21. Laskowski M, et al. (2008) Root system architecture from coupling cell shape to auxin transport. *PLoS Biol* 6(12):e307.
22. Payne RJH, Grierson CS (2009) A theoretical model for ROP localisation by auxin in *Arabidopsis* root hair cells. *PLoS One* 4(12):e8337.
23. Pitts RJ, Cernac A, Estelle M (1998) Auxin and ethylene promote root hair elongation in *Arabidopsis*. *Plant J* 16(5):553–560.
24. Kramer EM, Ackelsberg EM (2015) Auxin metabolism rates and implications for plant development. *Front Plant Sci* 6:150.
25. Datta S, Prescott H, Dolan L (2015) Intensity of a pulse of RSL4 transcription factor synthesis determines Arabidopsis root hair cell size. *Nat Plants* 1:15138.
26. Novák O, et al. (2012) Tissue-specific profiling of the *Arabidopsis thaliana* auxin metabolome. *Plant J* 72(3):523–536.
27. Ljung K (2013) Auxin metabolism and homeostasis during plant development. *Development* 140(5):943–950.
28. Pradal C, Dufour-Kowalski S, Boudon F, Fournier C, Godin C (2008) OpenAlea: A visual programming and component-based software platform for plant modelling. *Funct Plant Biol* 35(10):751–760.

Supporting Information

Mellor et al. 10.1073/pnas.1604458113

SI Text

1. Linear ODE Model of IAA Degradation. To investigate whether the conceptual model of the main IAA degradation pathways summarized in Fig. 1*A* is consistent with the metabolite data given in Fig. 1*B*, a simple linear ODE model was formulated as described below in *SI Text*, *1.1. Model reactions* and *SI Text*, *1.2. Model equations*. The model simulates the biosynthesis of IAA and its subsequent conversion to IAA-glc via UGT, IAA-Asp and IAA-Glu via *GH3*, and oxIAA via *AtDAO1/2*. IAA-glc and oxIAA can both be conjugated further to form 2-oxoindole-3-acetic acid glucose (oxIAA-glc), and oxIAA-glc and the conjugates IAA-Asp and IAA-Glu are then degraded at fixed rates (to prevent accumulation of these products in the model system).

1.1. Model reactions. In the following, the empty set notation is used to denote a fixed pool of molecules from and into which model variables can be synthesized and degraded, respectively. We assume that all substrates, such as the amino acids Asp and Glu, are available in excess, so that this pool is neither depleted nor increased. A review of the IAA metabolic pathways modeled here is in ref. 27.

We initially consider the input of IAA to the system to be at some fixed rate λ:

$$\emptyset \xrightarrow{\lambda} \mathrm{IAA}.$$

This IAA synthesis step is considered in more detail, taking into account quantitative IAA precursor data, in *SI Text*, *2. IAA Precursors*.

The oxidative pathway is modeled by the conversion of IAA to oxIAA by the combined action of *AtDAO1* and *AtDAO2* with respective rate constants d_1 and d_2, the subsequent conversion of oxIAA to oxIAA-glc with rate μ_x, and finally, the degradation of oxIAA-glc with rate μ_p:

$$\mathrm{IAA} \xrightarrow{d_1+d_2} \mathrm{oxIAA} \xrightarrow{\mu_x} \mathrm{oxIAA-glc} \xrightarrow{\mu_p} \emptyset.$$

GH3-mediated conjugation is modeled by two pathways: one that models the conjugation of IAA with aspartic acid with rate g_a to produce IAA-Asp and another that models the conjugation of IAA with glutamate with rate g_g to produce IAA-Glu:

$$\mathrm{IAA} \xrightarrow{g_a} \mathrm{IAA-Asp} \xrightarrow{\mu_a} \emptyset, \quad \mathrm{IAA} \xrightarrow{g_g} \mathrm{IAA-Glu} \xrightarrow{\mu_g} \emptyset,$$

where μ_a and μ_g are the respective degradation rates of IAA-Asp and IAA-Glu.

Finally, the conversion of IAA to IAA-glc via UGT is modeled with rate constant u_f, with the reverse reaction also included with rate u_r. IAA-glc can also be converted to oxIAA-glc with rate μ_u, which as previously stated, degrades with rate μ_p:

$$\mathrm{IAA} \underset{u_r}{\overset{u_f}{\rightleftharpoons}} \mathrm{IAA-glc} \xrightarrow{\mu_u} \mathrm{oxIAA-glc} \xrightarrow{\mu_p} \emptyset.$$

1.2. Model equations. Using the law of mass action, we cast the set of the reactions described in *SI Text*, *1.1. Model reactions* as a set of ODEs for six variables:

$$\frac{d[IAA]}{dt} = \lambda - \left(u_f + g_a + g_g + d_1 + d_2\right)[IAA] + u_r[IAA - glc], \quad \textbf{[S1a]}$$

$$\frac{d[oxIAA]}{dt} = (d_1 + d_2)[IAA] - \mu_x[oxIAA], \quad \textbf{[S1b]}$$

$$\frac{d[IAA - Asp]}{dt} = g_a[IAA] - \mu_a[IAA - Asp], \quad \textbf{[S1c]}$$

$$\frac{d[IAA - Glu]}{dt} = g_g[IAA] - \mu_g[IAA - Glu], \quad \textbf{[S1d]}$$

$$\frac{d[IAA - glc]}{dt} = u_f[IAA] - \mu_u[IAA - glc] - u_r[IAA - glc], \quad \textbf{[S1e]}$$

and

$$\frac{d[oxIAA - glc]}{dt} = \mu_x[oxIAA] + \mu_u[IAA - glc] - \mu_p[oxIAA - glc]. \quad \textbf{[S1f]}$$

Time is dimensionless, scaled by the dimensional biosynthesis rate (λ_w), and divided by the IAA concentration in the WT ($[IAA]_w$), so that for the WT, $\lambda = 1$. All other model species are nondimensionalized by scaling with $[IAA]_w$.

1.3. dao1-1 Mutant simulations. We use the * superscript notation to indicate the mutant value when parameter values may differ from their WT values in the *dao1-1* simulations. For example, the WT rate of *AtDAO1*-mediated oxidation is denoted d_1, whereas the value in the *dao1-1* mutant is denoted d_1^*.

The simplest way to model the *dao1-1* KO mutant is to set $d_1^* = 0$ in Eqs. **S1a–S1f**. However, if setting $d_1^* = 0$ is the only difference between WT and mutant simulations, it is not possible to get good agreement between the model steady states and the metabolic data (Fig. 1*C* and Fig. S1) when running the parameter fitting algorithm (*SI Text*, *3. Parameter Fitting*). The best fit parameter set is given in Table S1, set 1 and used as the base parameter set for additional modifications of parameter values in the *dao1-1* simulations (Fig. 1 *D* and *E*).

Based on this fitting of the initial model and with support from additional experimental data (Fig. 2 *A* and *B*) in subsequent parameter fitting exercises, we may also allow the IAA synthesis rate (λ^*) and the conjugation rates (g_a^* and g_g^*) to vary from their WT values in the *dao1-1* mutant simulations. Fig. 1*D* uses the parameters in Table S1, set 1, except $g_a^* = 10g_a$ and $g_g^* = 10g_g$, whereas in Fig. 1*E*, $g_a^* = 10g_a$, $g_g^* = 10g_g$, and $\lambda^* = 10\lambda$.

2. IAA Precursors. To fix the IAA synthesis rate in *dao1-1* (λ^*), we assume that IAA precursors have constant production rates (which do not vary between the WT and *dao1-1*) and that each precursor is converted to IAA at a rate that is different in *dao1-1* compared with the WT.

If we denote the pool of IAA precursors $[IAA_p]_w$ in the WT and $[IAA_p]_m$ in *dao1-1* and assume that they are governed by the following:

$$\frac{d[IAA_p]_w}{dt} = \delta - \lambda[IAA_p]_w$$

and

$$\frac{d[IAA_p]_m}{dt} = \delta - \lambda^*[IAA_p]_m,$$

where δ is the constant synthesis rate, and λ and λ^* are the respective conversion rates to $[IAA]$. Then, at steady state, we can rearrange to obtain

$$\frac{\lambda^*}{\lambda} = \frac{[IAA_p]_m}{[IAA_p]_w}.$$

It follows that λ^* is inversely proportional to the corresponding drop in auxin precursor concentrations (0.74 averaged across IAM, IPyA, and IAN from the whole-seedling metabolite data shown in Fig. 1), giving $\lambda^* = 1.36$ (because $\lambda = 1$).

3. Parameter Fitting. During the parameter fitting and all other single-compartment simulations, the systems of ODEs were solved from zero initial conditions in Matlab using the function ode15s. To simulate WT plants, the models were run with one parameter set to steady state, and the same model was run with another parameter set to represent the *dao1-1* mutant. The steady-state values were then compared with the data.

For the parameter estimation problems described below, we used the genetic algorithm (function ga) followed by local minimum search (function fmincon) from the Matlab Optimization toolbox to minimize the error between the data and model simulations. The objective function to be minimized was

$$f = \sum_{i \in X} \left(\frac{M_i^{wt} - D_i^{wt}}{\sigma_i^{wt}} \right)^2 + \sum_{i \in X} \left(\frac{M_i^{dao1} - D_i^{dao1}}{\sigma_i^{dao1}} \right)^2, \qquad \textbf{[S2]}$$

where M represents model steady-state values, and D represents data points with associated error σ. The superscript *wt* denotes the WT (Col-0), whereas *dao*1 denotes the *dao*1-1 KO model variant and mutant plants. X is the set of metabolites *IAA*, *oxIAA*, $IAA-Asp$, $IAA-Glu$, $IAA-glc$, and $oxIAA-glc$, the data for which are normalized relative to the WT IAA measurement, consistent with the nondimensional models. Unless stated, all parameters were identical in the WT and *dao1-1* simulations, save the mutant value for the *AtDAO1* oxidation rate $d_1^* = 0$, and constrained between 10^{-4} and 10^4. In all cases, the WT IAA production rate (λ) was fixed at 1.

The results of the parameter fitting in the simplest case, where only $d_1^* = 0$ differs from the WT in the *dao1-1* simulation, are shown in Fig. 1 and Fig. S1, and the parameters are given in Table S1, set 1.

In Fig. 2, the linear model (Eqs. **S1a–S1f**) was fitted against the data, with g_a^* and g_g^* free to vary within the default constraints, whereas λ^* was fixed at 1.36 (*SI Text*, *2. IAA Precursors*). The representative parameter set used to produce Fig. 2*D* and Fig. S2 is given in Table S1, set 2.

4. Inducible *AtDAO/GH3* Model.

4.1. Model formulation. The model is as the initial model (Eqs. **S1a–S1f**), except that the rate of conversion of IAA to oxIAA is proportional to the level of a new variable $[D]$ representing the level of *AtDAO1*, and the rates of conjugation of IAA to IAA-Asp and IAA-Glu are proportional to the level of another new variable $[G]$ representing the level of *GH3*, so that

$$g_a = \hat{g}_a[G], \qquad \textbf{[S3a]}$$

$$g_g = \hat{g}_g[G], \qquad \textbf{[S3b]}$$

and

$$d_1 = \hat{d}_1[D], \qquad \textbf{[S3c]}$$

where $\hat{g}_a$, $\hat{g}_g$, and $\hat{d}_1$ are new parameters.

$[D]$ and $[G]$ are themselves produced at rates nonlinearly dependent on the level of $[IAA]$ represented by Hill functions, so that

$$\frac{d[D]}{dt} = \eta_d \left(\frac{[IAA]^{n_d}}{k_d^{n_d} + [IAA]^{n_d}} - [D] \right) \qquad \textbf{[S3d]}$$

and

$$\frac{d[G]}{dt} = \eta_g \left(\frac{[IAA]^{n_g}}{k_g^{n_g} + [IAA]^{n_g}} - [G] \right). \qquad \textbf{[S3e]}$$

4.2. Parameter fitting. The inducible model was also fitted to the same metabolic data using the same algorithm as the linear model (*SI Text*, *3. Parameter Fitting*). The only parameter that differed from the WT in *dao1-1* was λ^*, which was again fixed at 1.36; n_g and k_g were found using the parameter fitting but constrained $1 \le n_g \le 9$ and $10^{-4} \le k_g \le 10$. This upper bound on k_g was selected to ensure that the response of *GH3* occurs within approximate physiological bounds of the level of IAA. The parameters n_d, k_d, η_d, and η_g do not directly affect the fit with the metabolic data, and they were instead separately estimated based on the available *GH3* and *AtDAO1* mRNA expression data and fixed during the parameter fitting algorithm. We fit the remaining model parameters to the steady-state metabolic WT and *dao1-1* data. Because we see, at most, a doubling of the mRNA level from basal expression under IAA treatment, with no sharp switch in expression observed (Fig. S3*A*), we fix both the Hill coefficient (n_d) and the binding threshold (k_d) =1; η_d and η_g affect the respective timescales over which *AtDAO1* and *GH3* can change. We estimate that gene expression will evolve over a slower timescale than biosynthesis, with *AtDAO1* changing more slowly than *GH3*, and therefore, we set $\eta_d = 0.005$ and $\eta_g = 0.01$.

The representative fitted parameter set used to produce Fig. 3 *C–G* and Figs. S4 and S5 is given in Table S1, set 3 and used as the basis for parameterization of the multicellular model.

4.3. Model variants. For each of the model variants described below, the model was run to steady state (using the parameters in Table S1, set 3) with $\lambda = 1$; then, using these results as the initial conditions for a new set of simulations for $\lambda \in \{0.5, 2.0, 10.0\}$, the time courses shown in Fig. 3 *D–F* were plotted. The steady state of each model variant is also plotted for $0.05 \le \lambda \le 20$ in Fig. 3*G*.

4.3.1. Only* AtDAO1 *induced. The induction of *GH3* is switched off by setting

$$\frac{d[G]}{dt} = 0,$$

with the initial condition that $[G]$ is equal to its steady-state value in Eq. **S3e** when $[IAA] = 1$, i.e.,

$$[G] = \frac{1^{n_g}}{k_g^{n_g} + 1^{n_g}}.$$

4.3.2. Only* GH3 *induced. Similarly, we switch off the induction of *AtDAO1* by setting

$$\frac{d[D]}{dt} = 0, \quad [D] = \frac{1^{n_d}}{k_d^{n_d} + 1^{n_d}}.$$

4.3.3. No induction. Both inducible pathways are switched off by setting

$$\frac{d[D]}{dt} = 0, \quad [D] = \frac{1^{n_d}}{k_d^{n_d} + 1^{n_d}}, \quad \frac{d[G]}{dt} = 0, \quad [G] = \frac{1^{n_g}}{k_g^{n_g} + 1^{n_g}}.$$

5. Multicellular Model. The multicellular model is based on that in ref. 17, in which auxin transport is embedded in a realistic root cell

geometry, using a vertex-based data structure from the OpenAlea modeling framework (28), with experimentally observed locations for the PIN, AUX, and LAX auxin efflux and influx carriers. To incorporate the *AtDAO1/GH3* homeostasis model, we replace the linear production and degradation of IAA in ref. 17 with the production and nonlinear degradation defined in Eqs. **S1a** and **S3a–S3c**, so that, in general terms, for every cell i,

$$\frac{d[IAA]_i}{dt} = \alpha\ \text{metabolism}_i + \text{transport}_i, \qquad \textbf{[S4]}$$

where $\alpha = 0.001$ (as in ref. 17) is a constant of proportionality to ensure that the relative contribution of metabolism and transport remains similar in the two models. All remaining model variables are simulated in every cell as in the inducible model.

The metabolism terms are identical to the right-hand side of Eq. **S1a**, with the IAA-inducible versions of g_a, g_g, and d_1 as defined in Eqs. **S3a–S3c**. Parameter values are as estimated by the fitting algorithm as defined in Table S1, set 3, with two exceptions. To maximize the number of cells in which the IAA homeostasis model works at basal levels of IAA in the same way as described in the single-compartment models (i.e., relatively low *GH3* conjugation and intermediate levels of *AtDAO1* oxidation), we set the thresholds in the Hill functions for $[G]$ and $[D]$ 5× higher, so that $k_d = 5.0$ and $k_g = 11.6135$; $\lambda = 1$ (WT) and $\lambda^* = 1.36$ (*dao1-1* mutant) in all cells except in the quiescent center and columella initials, where $\lambda = 10$ and $\lambda^* = 13.6$, again reflecting the cell type-specific differences modeled in ref. 17.

The transport terms, parameter values, initial conditions, and efflux/influx carrier positions are identical to those defined in ref. 17. In summary, movement of IAA (denoted *[Auxin]* in ref. 17) is simulated between every cell and its neighboring apoplastic compartments and between every apoplastic compartment and neighboring apoplastic compartments (via quasisteady-state concentrations of IAA at the vertices between apoplastic compartments) using the following model:

$$\frac{d[IAA]_i}{dt} = \alpha\ \text{metabolism}_i + \frac{1}{A_i}\sum_{j\in C_i}\sum_{k=1}^{N_{ij}} S_{ijk}J_{ijk} \qquad \textbf{[S5a]}$$

and

$$\frac{d[IAA_a]_{ijk}}{dt} = \frac{1}{\delta}\left(J_{ijk} + J_{jik}\right) + \frac{1}{S_{ijk}}\sum_{m\in V_{ijk}} J_{ijkl}, \qquad \textbf{[S5b]}$$

where $[IAA]_i$ and A_i denote the IAA concentration and area of cell i, respectively, and $[IAA_a]_{ijk}$ and S_{ijk} are the IAA concentration and segment length of the kth apoplastic compartment between cells i and j, respectively.

C_i is the set of neighboring cells to cell i, N_{ij} is the number of apoplastic compartments between cells i and j, and V_{ijk} is the pair of vertices adjacent to apoplastic compartment ijk; δ is a parameter defining the apoplast width.

Finally, J_{ijk} is the flux from apoplast compartment ijk into cell i, and J_{ijkl} is the flux into apoplastic compartment ijk from one of two neighboring vertices $l \in V_{ijk}$. Both J_{ijk} and J_{ijkl} are defined as in ref. 17.

For the boundary conditions, as done previously, we included a flux of auxin from the shoot by prescribing a nonzero auxin concentration within the stele cells at the shootward boundary of the modeled tissue (17). In the epidermal, cortical, and endodermal cells, we assume that the auxin concentrations have reached their far-field asymptotic values, hence setting them equal to those in neighboring (rootward) cells of the same type. This boundary condition is slightly different from that in ref. 17, which sets the boundary cells to have zero auxin concentration, and implies an appropriate shootward flux of auxin through the outer tissue layers (19)—moreover, we have checked that this modification makes no significant difference to the model predictions.

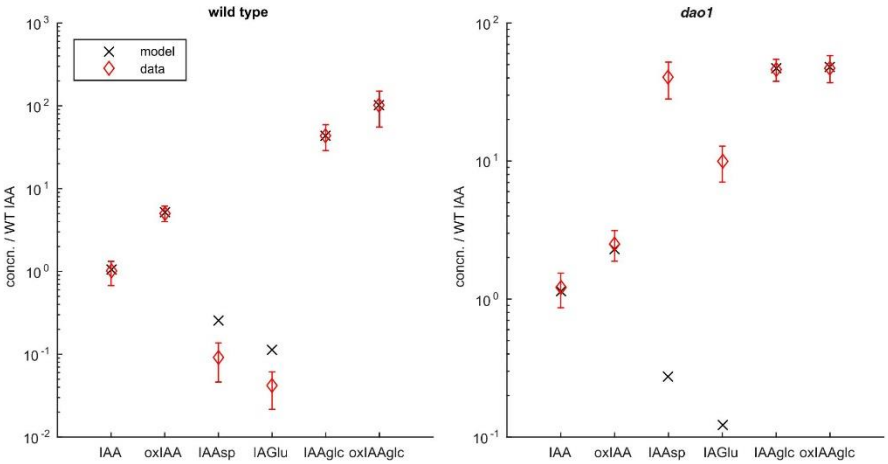

Fig. S1. Best fit between simple *dao1-1* KO model and metabolic data using Eqs. **S1a–S1f** and parameter values from Table S1, set 1.

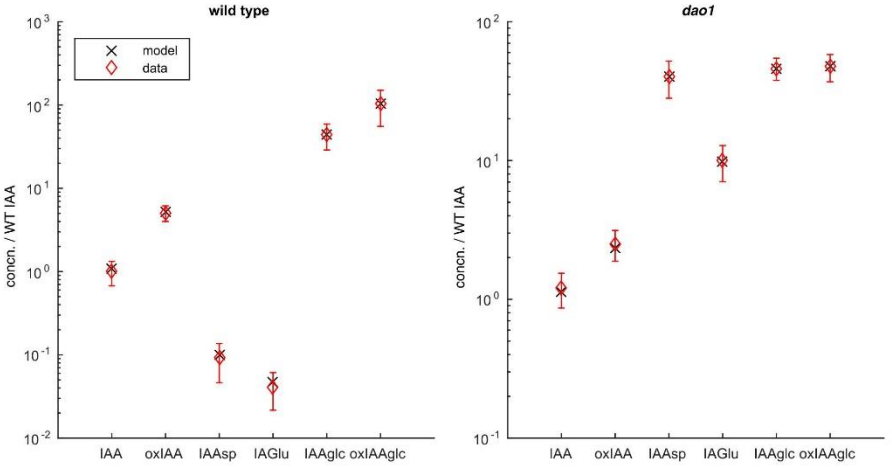

Fig. S2. Representative fit between *dao1-1* simulation (with $d_i^* = 0$, $\lambda^* = 1.36$, and g_a^* and g_g^* free to vary) and metabolic data using Eqs. **S1a–S1f** and parameter values from Table S1, set 2.

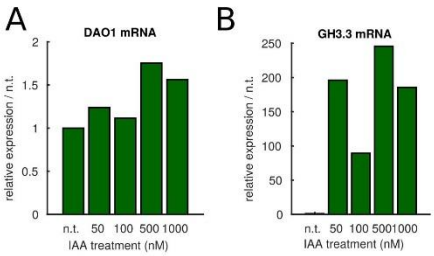

Fig. S3. qRT-PCR IAA dose–response data showing (*A*) *AtDAO1* and (*B*) *GH3.3* mRNA expression levels increasing with IAA; 7-d-old seedlings were treated with the stated IAA concentrations for 4 h. n.t., not treated.

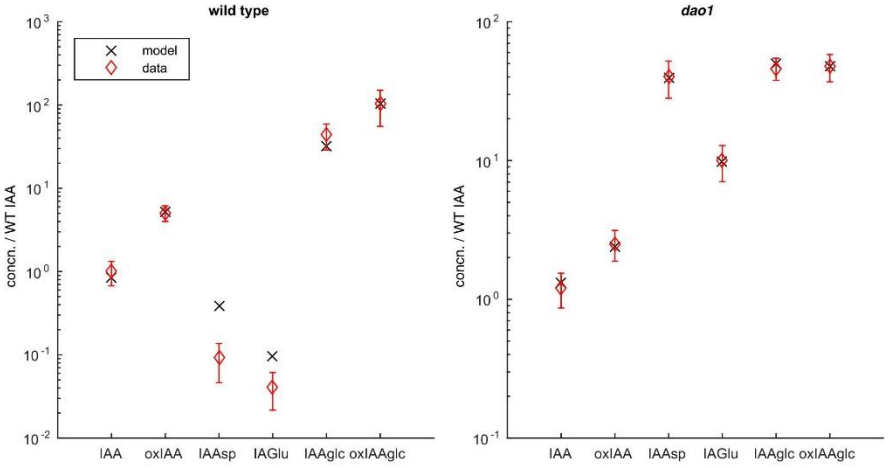

Fig. S4. Representative fit between model with inducible *AtDAO1* and *GH3* and metabolic data, showing absolute concentrations of auxin and its metabolites using Eqs. **S3a–S3e** and parameter values from Table S1, set 3.

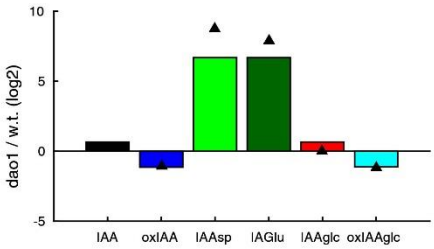

Fig. S5. Representative fit between model with inducible *AtDAO1* and *GH3* and metabolic data, showing auxin and metabolite concentrations in *dao1-1* relative to WT using Eqs. **S3a–S3e** and parameter values from Table S1, set 3.

Table S1. Dynamic regulation of *AtDAO1* and *GH3* modulates auxin homeostasis

Parameter	Set 1: *dao1-1* only differs in rate of IAA oxidation	Set 2: *dao1-1* differs in rates of IAA oxidation, biosynthesis, and conjugation	Set 3: *dao1-1* only differs in rate of IAA oxidation, but *AtDAO1* and *GH3* are auxin-inducible
λ	1	1	1
λ^*	1	1.36	1.36
d_1	0.0155	0.5224	—
d_1^*	0	0	—
g_a	0.3324	0.0012	—
g_a^*	0.3324	0.4382	—
g_g	0.6399	0.0018	—
g_g^*	0.6399	0.3594	—
u_f	0.131	1.7864	515.7453
u_r	0.0042	0.0428	13.5992
μ_a	1.4581	0.0123	0.0185
μ_g	3.0129	0.0407	0.0174
μ_u	0.0001	0.0006	0.0002
d_2	0.0159	0.3856	0.3379
μ_p	0.0563	0.0012	0.0097
μ_x	0.0059	0.1860	0.1893
$\tilde{d}_1$	—	—	1.8471
$\tilde{d}_1^*$	—	—	0
$\tilde{g}_a$	—	—	83.5023
$\tilde{g}_a^*$	—	—	83.5023
$\tilde{g}_g$	—	—	19.5837
$\tilde{g}_g^*$	—	—	19.5837
n_d	—	—	1
k_d	—	—	1
η_d	—	—	0.005
n_g	—	—	9.0
k_g	—	—	2.3227
η_g	—	—	0.01

Representative fitted parameter sets for the various models for auxin homeostasis. Set 1: simple *AtDAO1* KO model ($d_1^* = 0$ in *dao1-1* simulation) using Eqs. **S1a**–**S1f**. Parameters with superscript * are for the *dao1-1* case. Here, we assume $g_a = g_a^*$, $g_g = g_g^*$, and $\lambda = \lambda^*$. Set 2: fitted parameter set using Eqs. **S1a**–**S1f** for *dao1-1* simulation with $d_1^* = 0$, $\lambda^* = 1.36$, and g_a^* and g_g^* free to vary within the default constraints. Set 3: Representative fitted parameter set for model with inducible *AtDAO1* and *GH3* used to produce Fig. 3 and as the basis for the parameterization of the multicellular model. Parameter constraints are in *SI Text*.

INVESTIGATION OF THE ROLE OF LATERAL ROOT KINASES (*LRK1* AND *LRK2*) DURING LATERAL ROOT INITIATION AND DEVELOPMENT

4.1 ABSTRACT

During the past decade, our understanding of the molecular mechanisms controlling lateral root initiation and development has advanced rapidly using the model plant *Arabidopsis*. The plant hormone auxin triggers oscillatory gene expression and is a key regulator of lateral root (LR) primordia formation. Auxin induce the transcription factor *GATA23*. LATERAL ROOT KINASE 1 and 2 (*LRK1*; AT2G15300 and *LRK2*; AT4G34220) are co-expressed with *GATA23*. In order to identify and characterise the role of these two genes, loss-of function mutant lines were isolated and lateral root phenotypic defects detected. Transcriptional and translational fusion lines for *LRK1* and *LRK2* were generated, revealing spatiotemporal expression in endodermal root cells overlaying new lateral root primordia.

4.2 INTRODUCTION

4.2.1 THE HIDDEN PART OF THE PLANT

Plant roots are important for anchoring the plant via the provision of mechanical support from the root mass embedded in the soil, plus additionally enable the plant to acquire the essential nutrients and water (Beeckman et al., 2001, De Smet et al., 2007). In *Arabidopsis,* the origin of lateral roots (LR) occurs along the primary root axis in a specific zone termed the distal meristem, close to the root apical meristem in left-right patterning (Malamy and Benfey, 1997, De Rybel et al., 2010). An auxin-based oscillatory mechanism strongly controls LR initiation (LRI) steps, LRP development and LR emergence. Auxin regulates the initiation of the new organ (LR), via the SCF^{TIRI} pathway (see Fig. 1-8). Leaf-derived auxin is also required for LRP emergence as removing the shoot inhibits development beyond LRP initiation during early *Arabidopsis* seedling

development (Goh et al., 2012, Voss et al., 2015). Lateral root formation is composed of 8 stages. LR initiate from founder cells at the xylem pole in the pericycle layer (XPP) of the main root. Several rounds of anticlinal divisions give rise to stage I. Additional rounds of periclinal and tangential cell divisions give rise to stage II to VIII LRP. (Fig. 4-1 shows LR initiation zones) (Goh et al., 2012, Tian et al., 2014b, Vermeer and Geldner, 2015).

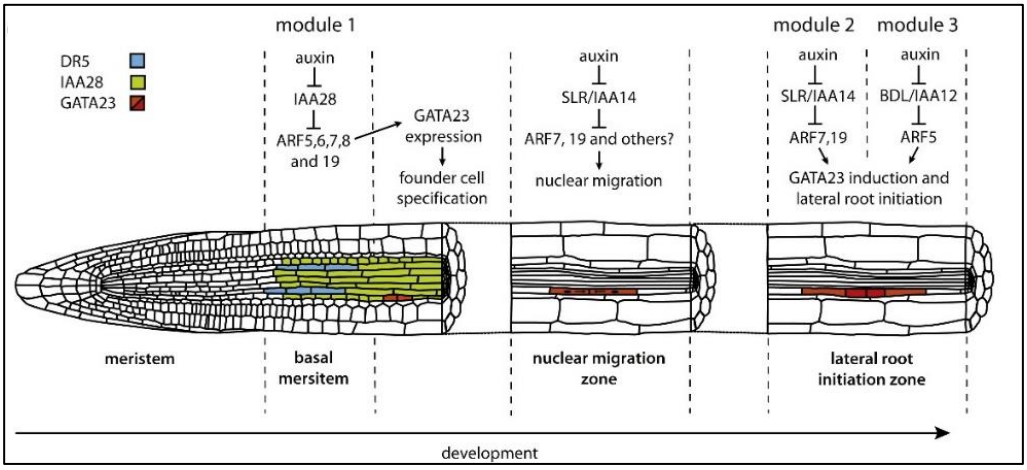

Figure 4-1: The molecular mechanism for auxin and several regulatory genes that have function in regulating lateral root initiation and emergence. (This figure is reproduced from De Rybel et al. (2010)).

Numerous genetic studies to investigate the molecular mechanism for LR initiation, development and emergence have been performed with the model plant *Arabidopsis* (reviewed in Lavenus et al. (2013)). A number of genes have been described to contribute to the regulation of LR development and emergence including GATA TRANSCRIPTION FACTOR 23 (*GATA23*), SOLITARY ROOT (*SLR/IAA14*), LATERAL ORGAN BOUNDARIES domain (*LBDs*), AUXIN RESPONSE FACTORS *ARF7* and *ARF19* (Okushima et al., 2005, Ditengou et al., 2008). In a previous study, LR development was synchronized to perform transcriptome profiling. The microarray data set revealed a spike of

expression of the transcription factor *GATA23* (AT5G26930), which is one of the first regulators that controls LR founder cell specification (De Rybel et al., 2010). Two genes are co-expressed with *GATA23* during LR development: *AT2G15300* and *AT4G34220*. This chapter describes the expression characterisation of these two putative novel regulators of lateral root development.

4.2.2 *AT2G15300* AND *AT4G34220*: ENCODE PUTATIVE LEUCINE-RICH REPEAT KINASE-LIKE PROTEINS

AT2G15300 and *AT4G34220* (*LRK1* and *LRK2* respectively) are members of the receptor-like protein kinase family (RLK). RLKs are considered to be one of the major families of putative receptor-encoding genes in the *Arabidopsis thaliana* genome. The family can be divided into 44 subfamilies and its members are localized on the plasma membrane. Indeed, *A. thaliana* has over 600 *RLK* genes, which feature transmembrane regions and cytoplasmic protein kinase domains (Shiu and Bleecker, 2001, ten Hove et al., 2011, Tanaka et al., 2012). The group of genes featuring leucine-rich repeats (LRR) is the largest class of RLKs, and has around 235 members (13 subfamilies) containing extracellular leucine-rich domains repeated sequence 24 amino acids long. Functional analysis revealed that LRR RLKs are key regulators of plant growth behaviour, plus responses to pathogens and to physiological, hormonal and environmental signals (Shiu and Bleecker, 2003, Morillo and Tax, 2006, Marshall et al., 2012).

LRK1 and *LRK2* belong to the LRRIII subfamily. They are predicted to have functions including protein serine/threonine kinase activity and ATP binding. In

addition, they are involved in protein amino acid phosphorylation and the transmembrane receptor protein tyrosine kinase signalling pathway.

4.3 MATERIALS AND METHODS

4.3.1 *ARABIDOPSIS THALIANA* MUTANT LINES

All seeds of T-DNA insertion mutant lines (Table 4-1) were from Columbia (*Col-0*) background and were obtained from Nottingham *Arabidopsis* stock centre (NASC). The locations of the T-DNA insertion sites for each mutant line were determined from the TAIR website.

Table 4-1: *Arabidopsis thaliana* Knock-out (KO) lines.

Gene ID	Mutants	NASC ID	CODE	INSERT POSITION
AT2G15300 (*LRK1*)	*lrk1-1*	N597787	SALK_097787	Exon 2
AT4G34220 (*LRK2*)	*lrk2-1*	N654837	SAIL_112336C	Exon 1
LRK1/LRK2	*lrk1-2/lrk2-2*	N2102741	GK_2702	*lrk1-2*: Exon 2 *lrk2-2*: Exon 1

4.3.2 PLANT MATERIALS AND GROWTH CONDITIONS

Seeds were surface sterilised with 70% (v/v) ethanol for 1 min, followed by 5% (v/v) hypochloric acid for 5 min. Then 0.1% (v/v) triton was used to wash the seeds three times (30-60 seconds). Finally, the seeds were washed twice with sterile ddH_2O. Sterile seeds were grown vertically on plastic square Petri dishes on half MS medium (pH 5.8), Plates were stored at 4^0Cbefore being transferred

to grow under controlled conditions (see section 2.2 for further details of growth conditions).

4.3.3 GENOMIC DNA EXTRACTION FOR GENOTYPING

Two cotyledons per plant were homogenised in DNA extraction buffer to extract the genomic DNA (see the DNA extraction protocol described in section 2.3.1 for extraction details). Two Polymerase Chain Reaction (PCR) assays were performed in order to identify homozygous lines for each gene (see section 2.3.3 for the PCR conditions). Forward and reverse primers LP and RP (gene specific primers) were used as well as the T-DNA left border primer (LB). For designing genotyping primers, the SIGnAL website was used (Table 4-2).

Table 4-2: Gene specific primer sequences of T-DNA insertion lines.

T-DNA insertion mutant line			Forward Primer	Reverse Primer
LRK1-1	*lrk1-1* (SALK_097787)		TCGTCACCCAAATCTCGTTAG	CATGGGTTTGTAGGCTTTGAG
LRK2-1	*lrk2-1* (SALK_112336C)		CAATCTCTCTGGTGATTTGCC	CTCTCGAATTCCTTGGGTTTC
LRK1-2/LRK2-2	GK_2702	*lrk1-2*	ACTCAACTAGTGACAGTGGATGGA	TGTCATTTGAATTGTTGTTCGTTT
		lrk2-2	AACACACCAGACATGTTCAGAGTC	AGTACAGCTCCAATAAACCCTTTG

4.3.4 RNA EXTRACTION, cDNA SYNTHESIS AND REVERSE TRANSCRIPTASE POLYMERASE CHAIN REACTION

RNA was extracted from the whole root system of 7 day old seedlings using Trizol Reagent (Invitrogen). The extraction was cleaned up using RNase Mini Kit protocol (Qiagensection 2.4.1). RNA (1 µg) was used to prepare cDNA samples according to the Superscript II Reverse Transcriptase protocol (Invitrogen, section 2.4.2). Reverse Transcriptase-Polymerase Chain Reaction

(RT-PCR) analysis used 100 ng μl^{-1} cDNA, and the sequences of the forward and reverse primers used are given in Table 4-3.

Table 4-3: RT-PCR specific primer sequences**.**

Line	Forward Primer	Reverse Primer
AT2G15300 (*LRK1*)	CGATCGAGATTTGGTTCG	GGTCGCTTTTGAGGCAAG
AT4G34220 (*LRK2*)	GCGGAAGAGAATGGCCGG	CCCTAACCTAAAGCACGC

A LightCycler® 480 system (Roche, USA) with the fluorescent dye SYBR® Green Master Mixes (Bioline) was used according to the manufacturer's instructions. The Universal Probe Library Assay Design Centre was used for the design of specific primer pairs (Table 4-4). All data were normalized to AT1G04850 and analysed with Microsoft Excel 2010 (Microsoft Corporation, Redmond, USA).

Table 4-4: QRT-PCR specific primer sequences.

Line	Forward Primer	Reverse Primer
AT2G15300 (*LRK1*)	CGCATGCTTGAAGTTAGGC	ATAGACGGTCGCTTTTGAGG
AT4G34220 (*LRK2*)	TTTCCGATTATGTTCCCAATG	GAGCTTGAGCTTGCCTTAGTG

4.3.5 ROOT PHENOTYPING ANALYSIS: PRIMARY ROOT LENGTH, LATERAL ROOT NUMBER AND LATERAL ROOT DENSITY

Twenty seeds were grown vertically on half MS under controlled conditions for 10 days. Primary root length, lateral root number and lateral root density were analysed for individual seedlings according to methods described previously

(sections 2.5.1 & 2.5.2) whereby the roots were photographed then measurements were made and analysed using Fiji software.

4.3.6 ROOT GRAVITY RESPONSE ANALYSIS

Six day old seedlings were grown and placed in a controlled growth chamber (12 h / 12 h light / dark photoperiod) then turned by 90^0. The primary root angle for individual seedling was measured after 8 h the data was analysed using Fiji software (section 2.5.3).

4.3.7 TRANSCRIPTIONAL AND TRANSLATIONAL FUSION LINES OF *AT2G15300* AND *AT4G34220*

4.3.7.1 AMPLIFICATION OF GENES OF INTEREST

Gateway-compatible vectors were used to generate transcriptional and translational fusions lines for *LRK1* and *LRK2*. PCR amplification was carried out using Q5 High-Fidelity DNA polymerase to amplify the genes of interest. Genomic DNA from *Col-0* was used as a DNA template and amplified using forward (FP) and reverse primers (RP).PCR reagents and reactions plus primer sequences are shown in Tables 4-5 – 4-7.

Table 4-5: PCR reaction (the reagents and volumes in 20 µl) to amplify the gene of interest.

REAGENTS	VOLUME (µl)
Phusion Buffer	10
10 mM dNTPs	1
Forward primer; FP (10µM)	0.5
Reverse primer; RP (10µM)	0.5
Genomic DNA	2
Q5- High-Fidelity DNA Polymerase	0.5
ddH_2O	x
Total volume	50

Table 4-6: PCR cycling for DNA fragments amplification.

Step	Temperature °C	Time	No. Cycle
Initial Denaturation	98	0:30	1
Denaturation	98	0:10	35
Annealing	58	0:30	
Extension	72	1/2:00 *	
Final Extension	72	7:00	1
	4	∞	

*dependent on the product size (30 sec per 500bp product).

Table 4-7: PCR primer sequences to amplify the gene of interest.

Line	Construct	Forward Primers	Reverse Primers
AT2G15300 (*LRK1*)	pLRK1::GFP	GAAGGATGGGAAGAGATCGG	GGTTCGAGTTCTTAGGTTTTC
	LRK1:GFP	GAAGGATGGGAAGAGATCGG	AACAAACATTTTCTCTAGCACTTGC
AT4G34220 (*LRK2*)	pLRK2::GFP	GATGACATTATCTTTTATGGGGTA	GGTCTTTCAGTTCTTGGTTTC
	LRK:GFP	GATGACATTATCTTTTATGGGGTA	AACTAAAACACAAATTTTCTCCAA

All PCR products (50 µl) were run on agarose gel (1%) to check the product sizes. A clean and sharp scalpel was used to cut the gel around the single discrete band of isolated PCR product, and then each piece of gel was put into a pre-weighed Eppendorf tube and stored at -20 °C.

4.3.7.2 EXTRACTION AND PURIFICATION OF DNA FRAGMENTS FROM THE GEL

Thermo Scientific GeneJET Gel Extraction Kit (#K0691; #K0692) was used to purify DNA fragments from gel slices according to manufacturer's instructions..

4.3.7.3 INTRODUCTION OF DNA FRAGMENT TO pENTR™-D-TOPO® ENTRY VECTOR

Four µl of fresh, purified PCR products were cloned into pENTR™-D-TOPO® entry vector (Invitrogen). PCR product was added to 1 µl of salt solution and 1 µl of TOPO® vector. The mixture was incubated at room temperature for 5 min then chilled on ice.

4.3.7.4 TRANSFORMATION OF ONE SHOT® COMPETENT *ESCHERICHIA COLI*

Five µl of pENTR mixture was added to 50 µl of DH5-α (One Shot® Competent *Escherichia coli*) then mixed gently. The tubes were incubated on ice for 30 min, and then transferred to a hot plate (42 °C) to heat-shock the cells for 20-30 s and then immediately transferred to ice to chill for 2 min. Liquid LB media (950 µl) was added to each tube, and then incubated at 37 °C for 1 h. The tubes were centrifuged (1 min at 13,000 rpm) and 600 µl of the supernatant was discarded.

The remaining solution were plated onto LB media containing a selective antibiotic (0.5% Kanamycin), and incubated overnight at 37 °C. Approximately 10 surviving colonies were selected and analysed in a PCR assay using specific primers for the gene of interest. Colonies which were shown to be positive for the gene of interest were cultured overnight at 37 °C in liquid LB media containing 0.5% Kanamycin.

4.3.7.5 PLASMID PURIFICATION

For the purification of plasmids, a Thermo-Scientific (GeneJET Plasmid miniprep kit #K0502, #K0503) was used according to the manufacturer's instructions.

4.3.7.6 LR REACTION

After amplifying the correct sites (by performing digestion with restriction enzymes), the orientations were verified (using cutting enzymes) and the correct construct sequences of each recombinant vector were confirmed (by https://ecom.mwgdna.com/register/index.tcl). Following this, an LR reaction was performed to introduce the sequence of interest into the destination vector (the binary pGWB4 vector, Nakagawa et al., 2007). For this work the destination vectors had a recombination reaction between *attl* and *attr* sites. In a 1.5 ml microcentrifuge tube, about 50-150 ng of the entry clone (3 µl plasmid DNA) was added to 150 ng μl^{-1} of the destination vector (1 µl) with 4 µl of TE buffer (pH 8.0). Then 2 µl of LR Clonase^{TM} II enzyme mix was added to the reaction. The mixture was incubated at 25 °C for 1 h. To terminate the reaction, 1 µl of

the Proteinase K solution was added and the samples incubated at 37 °C for 10 min. One µl from each LR reaction was transformed into 50 µl of One Shot® Competent *E. coli*, and then the positive constructs were purified by using GeneJET Plasmid miniprep kit (#K0502, #K0503).

4.3.7.7 TRANSFORMATION OF AGROBACTERIUM TUMEFACIENS

Plasmid DNA (1 µl; miniprep product) was transformed into 50 µl of *Agrobacterium tumefaciens* competent cells (C58 strain) by electroporation in 1.5 mL electroshock tubes. The *A. tumefaciens* mixture was added to 1 ml of LB medium and incubated at 28 °C for 2 h. Solid LB medium containing selective antibiotics was used to screen for colonies positive for the construct of interest. In order to confirm the construct was correctly amplified, PCR assays were performed. Selective colonies were grown overnight at 28 °C in 5 µl of liquid LB medium which contained antibiotics. The pre-culture (1 ml) was inoculated into 200 ml of LB liquid medium with the antibiotics, and incubated at the same temperature for an additional 24 h. The cells were centrifuged at 5000 rpm for 15 – 30 min. Cells were then re-suspended in 400 ml of infiltration solution (5% sucrose, 0.02% Silwet, up to 400 ml by ddH_2O).

4.3.7.8 TRANSFORMATION OF *ARABIDOPSIS*

The *Agrobacterium tumefaciens* suspensions were transferred to floral organs of *Arabidopsis thaliana* (ecotype, *Col-0*) by floral dipping method (Zhang et al., 2006). The transformants were screened on half MS medium (Sigma) containing

a selective antibiotic (0.5% Kanamycin) for the plasmid. And the antibiotic resistant plants were transferred to soil. Seeds from T3 100% antibiotic resistance plants were used as homozygous plants for the transgene.

4.4 RESULTS

A transcriptomic data-set was generated by Dr. Ute Voβ (2015). 3 days old *Col-0* seedlings were turned 90̊ to stimulate the initiation of lateral root primordia. Different LR stages were determined every 3 h (from 6 h to 54 h) (Fig. 4-2). The LR transcriptomic dataset identified several novel differentially expressed genes. Two kinases genes were selected which were co-expressed with *GATA23* (the transcription factor that controls the specification of pericycle cells to become lateral root founder cell) during LRP development (Fig. 4-3): *LATERAL ROOT KINASE 1 and 2* (*LRK1 & LRK2)*, two closely related LRR kinase. Single and double mutants of *lrk1 and lrk2* have been isolated and analysed for LR phenotypes.

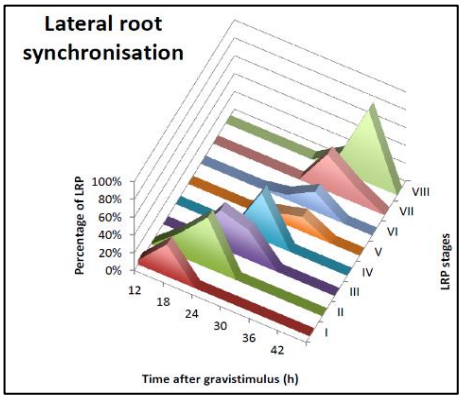

Figure 4-2: Lateral root development was synchronized using the gravistimulation for transcriptomic profiling (This figure is reproduced fromVoss et al. (2015)).

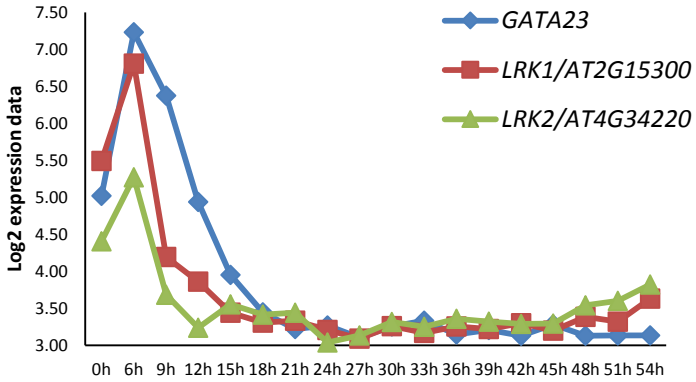

Figure 4-3: Log_2 expression data of *GATA23*; *LRK1*: AT2G15300 and *LRK2*: AT4G34220 (This figure is shows the transcriptomic data from Voss et al. (2015)).

4.4.1 GENOTYPIC ANALYSIS OF T-DNA INSERTION LINES

Genomic DNA was extracted from two cotyledons from plants of different variations of mutant alleles and also from WT (Columbia *Col-0*). To test the presence of T-DNA insertions in the gene of interest, T-DNA lines were genotyped by using PCR with three primers: forward and reverse gene specific primers (LP & RP), and the left T-DNA border primer (LB) with RP.

For *AT2G15300* (*LRK1*) and *AT4G34220* (*LRK2*) one allele for each gene (*lrk1-1:* SALK_097787 and *lrk2-1:* SALK_112336C) were genotyped, as well as a double mutant line (*lrk1-2/lrk2-2: gk*_2702) to identify homozygous plants. The PCR products showed bands in assays using the RP + LB primers, whereas in assays using the genomic primers (LP + RP) there were no bands in all mutant seedlings yet bands were present in the WT (Columbia, *Col-0*) (Figs. 4-4- 4-7).As such, it was concluded that all lines were homozygous.

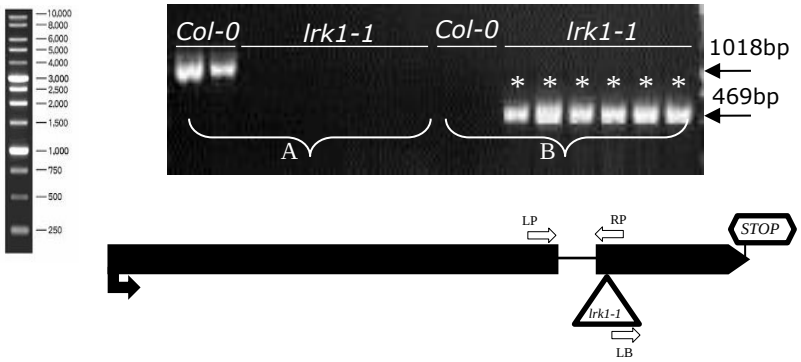

Figure 4-4: Genotypic PCR analysis for *lrk1-1* (SALK_097787), using: A) two genomic primers (LP + RP: forward and reverse primers) Product size = 1018bp; and B) RP + left T-DNA border primer (LB) Product size= 469bp. WT: wild type (Columbia) and 6 SALK_097787 lines seedlings. (1kB DNA ladder; *: Homozygous plants).

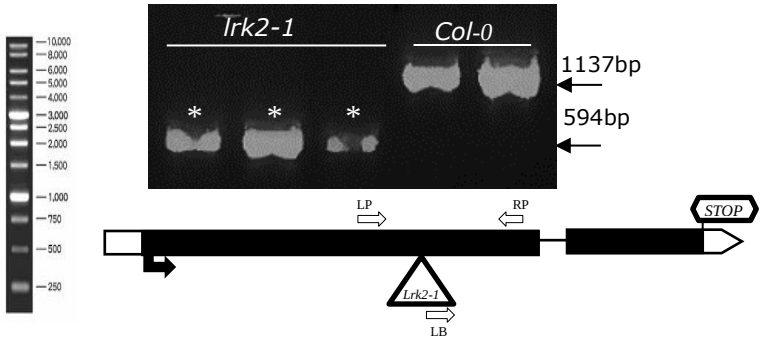

Figure 4-5: Genotyping PCR analysis for *lrk2-1* (SALK_112336C) using two genomic primers (LP + RP: left and right primers) Product size = 1137bp; and left T-DNA border primer (LB) Product size= 594bp. WT: wild type (Columbia) and 3 SALK__112336C lines seedlings. (1kB DNA ladder; *: Homozygous plants).

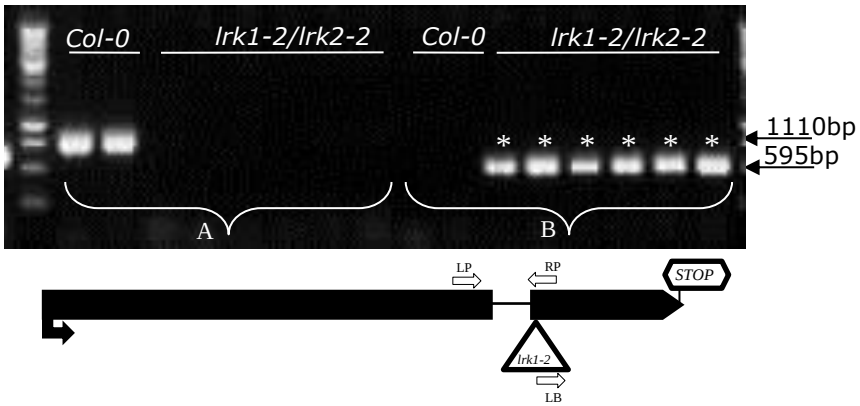

Figure 4-6: Genotyping PCR analysis for *lrk1-2/lrk2-2* (gk_2702) using: A) two genomic primers of *LRK1* (LP + RP: forward and reverse primers) Product size = 1110bp; and B) RP + left T-DNA border primer (LB) Product size= 595bp. WT: wild type (Columbia) and 6 individual seedlings. (1kB DNA ladder; *: Homozygous plants).

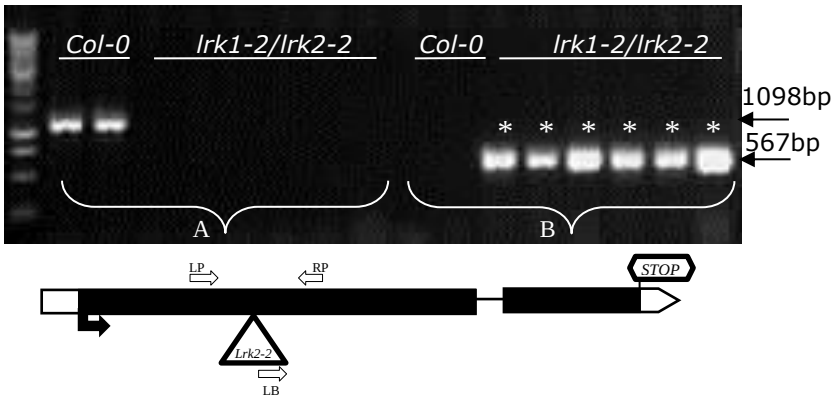

Figure 4-7: Genotyping PCR analysis for *lrk1-2/lrk2-2* (gk_2702) using: A) two genomic primers of *LRK2* (LP + RP forward and reverse primers) Product size = 1098bp, and B) RP + left T-DNA border primer (LB) Product size= 567bp. WT: wild type (Columbia) and 6 individual seedlings. (1kB DNA ladder; *: Homozygous plants).

4.4.2 RT-PCR AND qRT-PCR

RNA was extracted from the roots of different mutant lines of AT2G15300, AT4G34220 and the double mutant line, followed by generating cDNA samples by using the Superscript II protocol. RT-PCR was performed using forward (FP) and reverse (RP) primers to confirm that the gene of interest was not expressed in the T-DNA insertion lines, alongside housekeeping primer (At1G04850) (Fig. 4-8 A] to test the quality of cDNA and the RT-PCR.

There was no gene expression in the T-DNA insertion lines of AT2G15300 (*lrk1-1)* and the double mutant line (*lrk1-2/lrk2-2*) when using FP and RP *LRK1* cDNA primers, however there was expression in the AT4G34220 (*lrk2-1)* line and *lrk1-2/lrk2-2*, when using *LRK2* cDNA primers (Fig. 4-8B and 4-8C) which indicates that *lrk2-1* and *lrk1-2/lrk2-2* lines are not complete knock-out lines for *LRK2*.

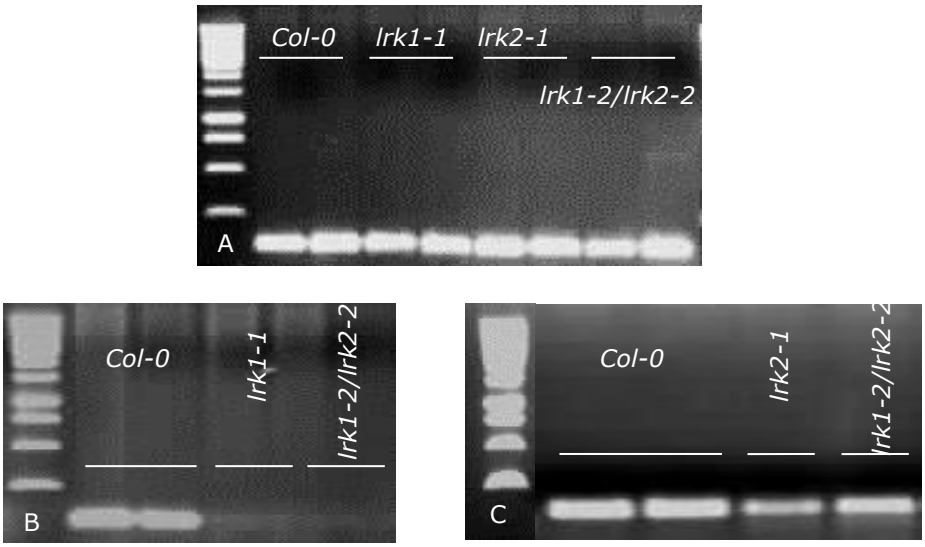

Figure 4-8: RT-PCR expression analysis of the different knockout lines of AT2G15300, AT4G34220 and the double mutant line, in comparison to WT (*Col-0*). A) Expression of a house-keeping gene using house-keeping primers (product size ~ 200bp). B) Expression analysis of AT2G15300, *lrk1-1* (SALK_097787) and *lrk1-2/lrk2-2* (gk_2702) using forward and reverse *LRK1* cDNA specific primers (Product size = 162 bp). C) Expression analysis of AT4G34220, *lrk2-1* (SALK_112336C) and *lrk1-2/lrk2-2* (gk_2702) using forward and reverse *LRK2* cDNA specific primers. (Product size = 104 bp).

In addition, the gene expression level was analysed by qRT-PCR with forward and reverse qRT-PCR primers to quantify expression of the gene of interest in all mutant lines in comparison to the expression in the WT. The results revealed that there is no *LRK1* expression in *lrk1-1* (SALK_097787) and *lrk1-2/lrk2-2* (gk_2702). However, there was expression of *LRK2* in *lrk2-1* (SALK_112336C); moreover, the double mutant line showed overexpression of *LRK2,* with an increase in expression of approximately 8 fold (Fig. 4-9), (Figs. 4-10 and 4-11 give details of the RT-PCR and qRT-PCR primers).

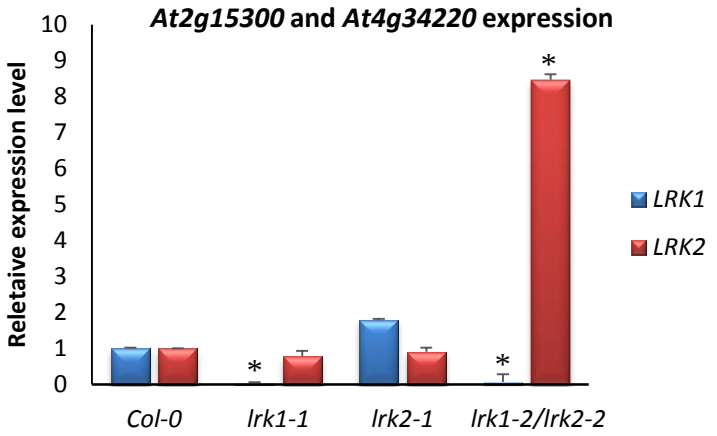

Figure 4-9: qRT-PCR expression quantification for *AT2G15300* and *AT4G34220* of *lrk1-1* (SALK_097787), *lrk2-1* (SALK_112336C) and the double mutant *lrk1-2/lrk2-2* (gk_2702) lines, normalized to WT (*Col-0*). * denotes significant difference compared to WT ($P < 0.05$).

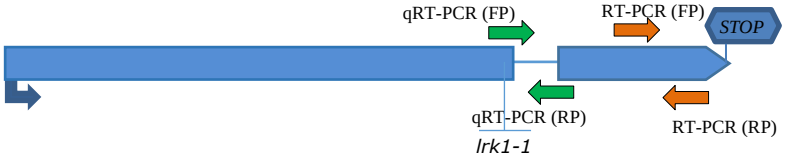

Figure 4-10: Map of *AT2G15300* indicating the T-DNA insertion line position of *lrk1-1* (SALK_097787) with RT-PCR (forward: FP + reverse: RP) and qRT-PCR (forward: FP + reverse: RP) primers.

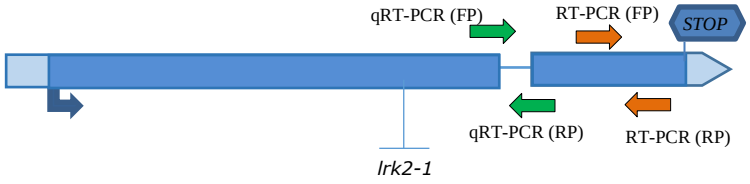

Figure 4-11: Map of *AT4G34220* indicating the T-DNA insertion line position of *lrk2-1* (SALK_112336C) with RT-PCR (forward: FP + reverse: RP) and qRT-PCR (forward: FP + reverse: RP) primers.

4.4.3 PHENOTYPIC ANALYSIS

Root phenotyping analyses were performed for all knock out lines of these two genes (*AT2G15300*, *AT4G34220*) including the double mutant line *lrk1/lrk2*, in order to identify the function of these genes during root growth and development.

4.4.3.1 PRIMARY ROOT LENGTH AND LATERAL ROOT NUMBER

The primary root length for 10 day old seedlings was measured, and the LR number was counted to determine the LR density for each T-DNA insertion line for comparison to the WT. The results showed that LR density in *lrk1-1* was significantly higher than *Col-0*, as was this also true for the double mutant line *lrk1-2/lrk2-2*. On the other hand, there was no significant difference in LR density in *lrk2-1* compared with *Col-0* (Figs. 4-12 - 4-14).

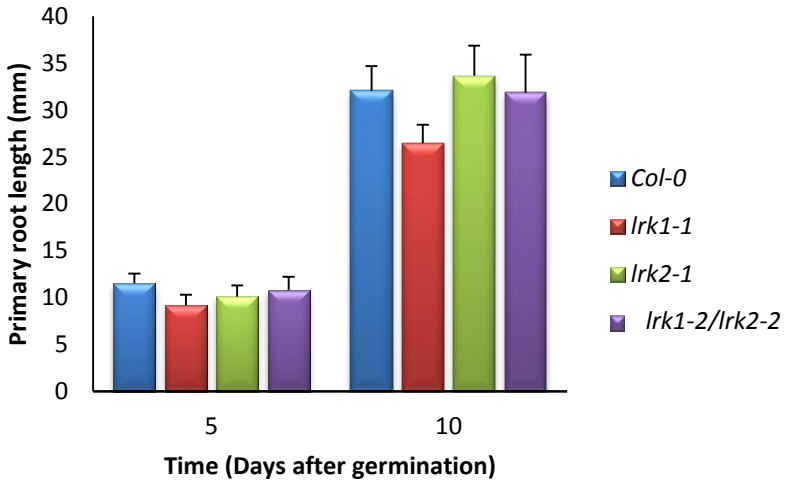

Figure 4-12: The primary root length of 5 and 10 day old seedlings for AT2G15300 *lrk1-1* (SALK_097787), AT4G34220 *lrk2-1* (SALK_112336C) and the double mutant *lrk1-2/lrk2-2* (gk_2702), in compared to WT (*Col-0*).

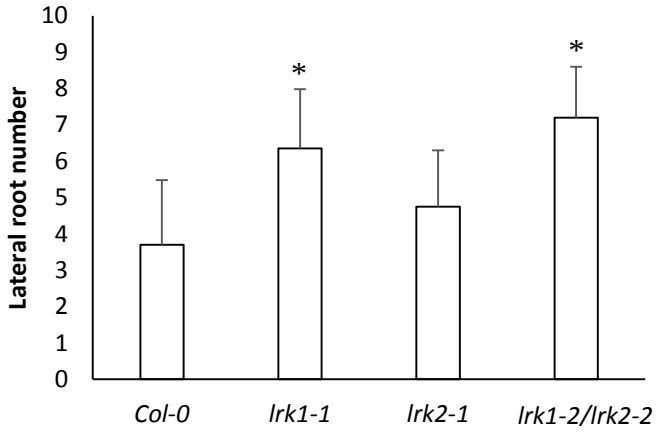

Figure 4-13: The lateral root number of 10 day old seedlings for AT2G15300 *lrk1-1* (SALK_097787), AT4G34220 *lrk2-1* (SALK_112336C) and the double mutant *lrk1-2/lrk2-2* (gk_2702), in comparison to WT (*Col-0*). * denotes significant difference compared to WT ($P < 0.05$).

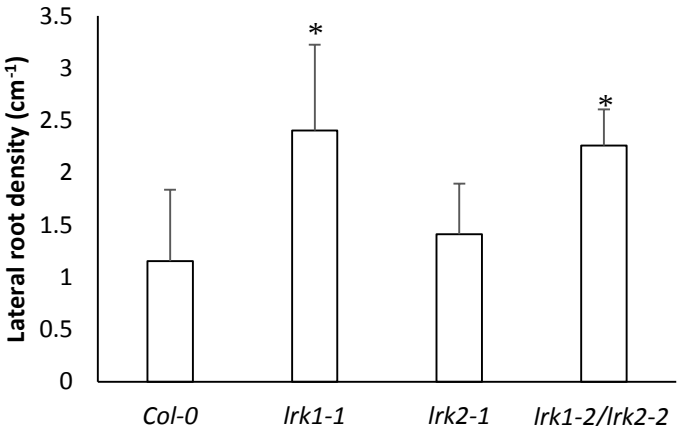

Figure 4-14: Lateral root density (cm^{-1}) of 10 day old seedlings for AT2G15300 *lrk1-1* (SALK_097787), AT4G34220 *lrk2-1* (SALK_112336C) and the double mutant *lrk1-2/lrk2-2* (gk_2702), in comparison to WT (*Col-0*). * denotes significant difference compared to WT ($P < 0.05$).

4.4.3.2 GRAVITROPISUM ASSAY

In order to investigate a gravity response phenotype, the root angle of gravistimulated 6 day old seedlings were measured for 8 h and analysed by Fiji software. The results indicate that there were no significant changes between all

knockout alleles of *LRK1*, *LRK2* and *LRK1/LRK2* compared with the WT (Fig. 4-15).

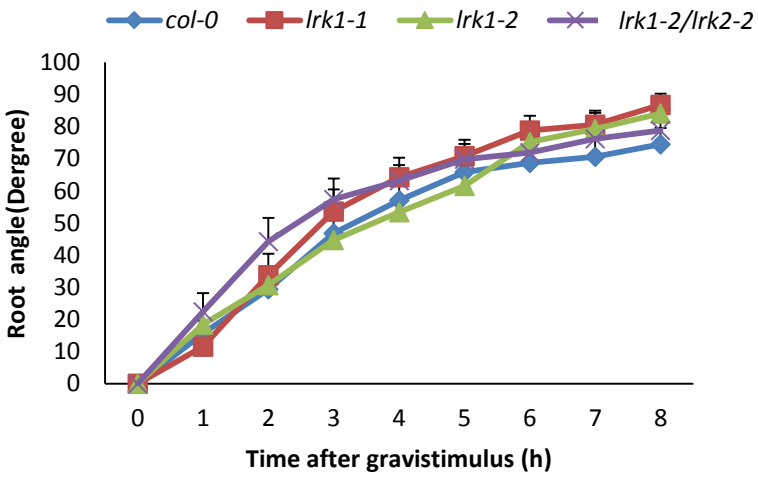

Figure 4-15: Responses of gravistimulated roots of 6 day old seedlings after turning through 90° for AT2G15300 *lrk1-1* (SALK_097787), AT4G34220 *lrk2-1* (SALK_112336C) and the double mutant *lrk1-2/lrk2-2* (gk_2702), in comparison to WT (*Col-0*).

4.4.4 TRANSCRIPTIONAL AND TRANSLATIONAL FUSION LINES

For *LRK1* and *LRK2* transcriptional fusion constructs DNA fragments of 1973bp and 1821bp were amplified upstream of the start codon of *LRK1* and *LRK2* respectively, (the promoter region without the start codon). Whereas, for translational fusion constructs, DNA fragments of 4351bp and 4220bp were isolated which contained the promoter regions and gene sequences without the stop codon. Homozygous lines of the third generation of the transgenic *Arabidopsis* plants of *AT2G15300* and *AT4G34220* were analysed by confocal microscopy for translational and transcriptional fusion expression, so as to detect the GFP localisation associated with the inserted DNA constructs. This revealed

GFP expression within the cytosol of the endodermis tissue of the primary root in the differentiation zone (Figs. 4-16 – 4-19).

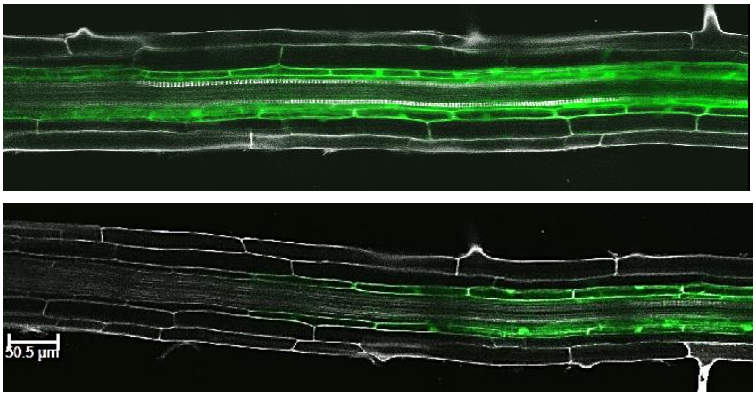

Figure 4-16: Expression pattern of GFP in the transgenic plants of *AT2G15300* (*LRK1*). *pLRK1*::GFP of 5 day old seedlings of *A. thaliana* root tip. GFP expression is present in the endodermis tissues beginning where the vascular tissue differentiating zone.

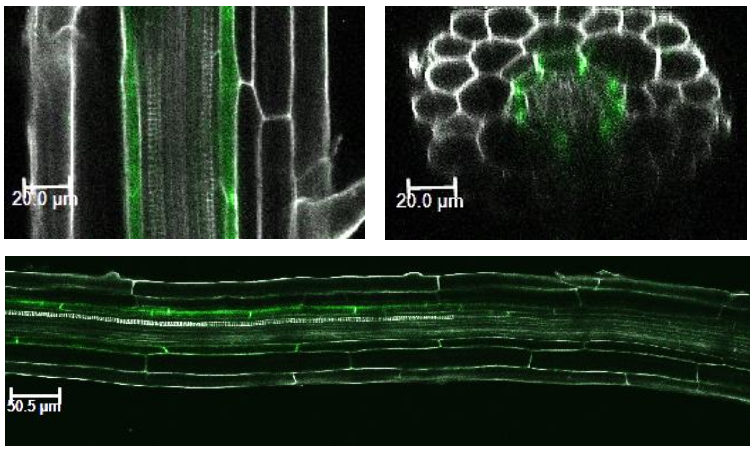

Figure 4-17: *AT2G15300* (*LRK1*) localization in the cytosol. Expression pattern of GFP in the transgenic plants of *pLRK1*::*LRK1*:GFP of 5 day old seedlings of *A. thaliana* root tip. GFP expression is present in the cytosol of the endodermis tissues beginning where the vascular tissue differentiating zone.

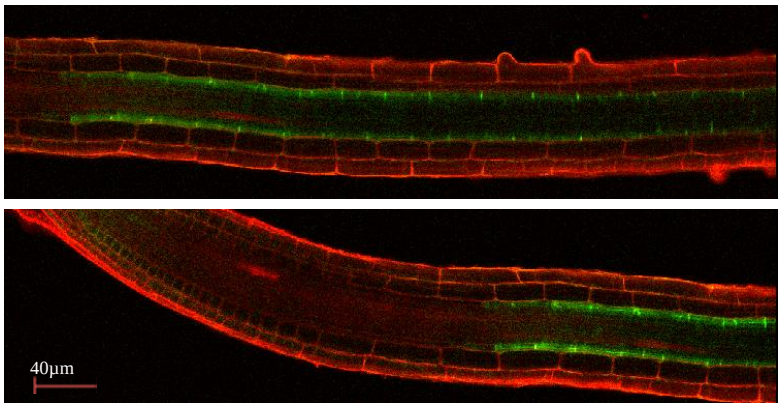

Figure 4-18: Expression pattern of GFP in the transgenic plants of *AT4G34220* (*LRK2*). *pLRK2*::GFP of 5 day old seedlings of *A. thaliana* root tip. GFP expression is present in the endodermis tissues beginning where the vascular tissue differentiating zone.

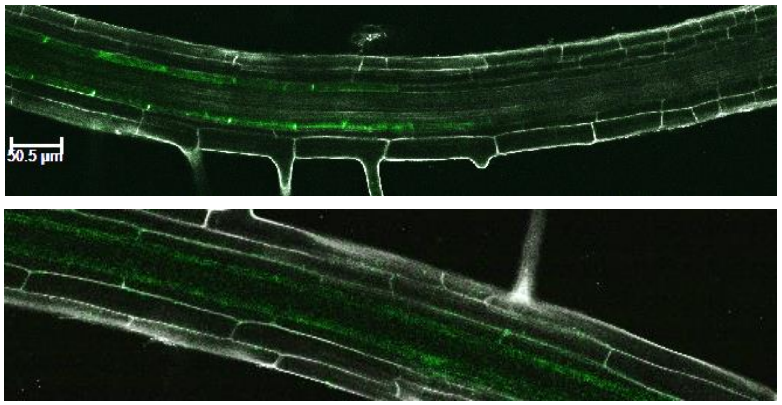

Figure 4-19: *AT4G34220* (*LRK2*) localization in the cytosol. Expression pattern of GFP in the transgenic plants of *pLRK2*::*LRK2*:GFP of 5 day old seedlings of *A. thaliana* root tip. GFP expression is present in the cytosol of the endodermis tissues beginning where the vascular tissue differentiating zone.

To provide independent validation for my results, figure 4-20 (ten Hove et al., 2011) presented the expression pattern of *LRK1* and *LRK2* in the Birnbaum root tissue-specific expression data set (Birnbaum et al., 2003). The results indicate that these two genes are expressed in the endodermis of the meristem tissues of *Arabidopsis* root.

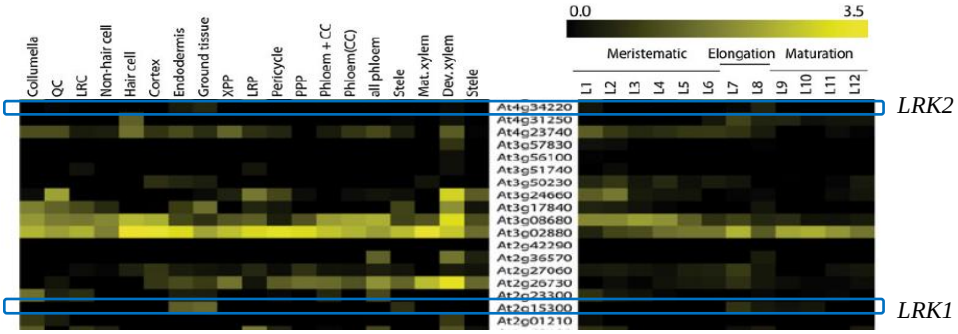

Figure 4-20: *LRK1* (AT2G15300) and *LRK2* (AT4G34220) genes expression patterns in different tissues of Arabidopsis roots ten Hove et al. (2011)).

4.5 DISCUSSION

The plant hormone auxin controls LR initiation, development and emergence via the Aux/IAA28 signalling pathway (Kiss et al., 2002, De Rybel et al., 2010, Goh et al., 2012). Many studies have been performed to identify the molecular components underlying LR development (Lavenus et al., 2013, De Rybel et al., 2010). Micro-array data sets have helped identify many novel candidates genes that might function during LR development (Lavenus et al., 2015).

A meta-analysis of a lateral root-related transcriptomic dataset of gravistimulated root across time point revealed several differentially expressed genes such as *GATA23* (Voss et al., 2015). The transcription factor *GATA23* plays a critical role during early LR initiation; controlling the pericycle founder cell specification. *GATA23* is expressed in XPP cells before the first asymmetric division that initiates LRs occurs (Behringer and Schwechheimer, 2015).

Two kinases *LRK1* (AT2G15300) and *LRK2* (AT4G34220) were co-expressed with *GATA23*. In order to determine the possible functions of these two genes in LR initiation, bioinformatics and molecular biological techniques were used.

LRK1 and *LRK2* contain leucine-rich repeats (LRRs) and belong to the largest group in the receptor-like protein kinase family (RLKs). LRRs are considered to play a major role in controlling plant responses to the environmental, physiological and hormonal signals (Gomez-Gomez and Boller, 2000, Gomez-Gomez et al., 2001). Knock-out lines in *LRK1* and *LRK2* revealed an increase in lateral root number.

Transgenic lines expressing GFP-tagged transcriptional and translational fusion lines for both genes revealed that they are expressed in root endodermal tissues overlying new lateral root primordia. This spatial expression patterns suggests these kinases may control lateral root development indirectly. Endodermal cells have been discriped to play an important role during lateral root initiation via controlling the volume of underlying pericycle lateral roots founder cells (Vermeer et al., 2014). Plasmodesmata are likely to play role controlling volume exchanges between the pericycle founder cells and overlying endodermal cells. Reseptor kinases are known to localise to plasmodesmata (Vermeer et al., 2014). Hence, *LRK1* and *LRK2* may function to control lateral root numbers via controlling plasmodesmata opening. However,By conducting many experiments using transcriptional and translational fusion plants we can identify the expression pattern and functional localization of these two kinases.

As the lateral root founder cells divide in the pericycle layer, they have to emergence throughout several overlying root tissues layers (endodermis, cortex and epidermis) to reach the primary root surface. The endodermis layer plays a crucial role in lateral root primordia's growth and emergence (Swarup et al., 2008). Recently (Lucas et al., 2013) described how the mechanical forces in this layer and other outer layers affects the initiation, differentiation and the development of lateral roots. For example, the endodermis contains the casparian strip composed of lignin, that is required to be broken by the new primordia to emerge. Hence, *LRK1* and *LRK2* may play roles in Casparian strip development. Therefore, further characterization of *LRK1* and *LRK2* is required to reveal

whether they function as part of the pathway reported by Vermeer et al. (2014) and Lucas et al. (2013).

Gene translation products (RNA and proteins) helps in understanding the gene function in the plant cells. Investigating the subcellular protein functions of both genes (*LRK1* and *LRK2*) could help provide a clearer idea of the role of these two kinases in regulating lateral root initiation and emergence.

INVESTIGATING THE FUNCTION OF *MO25* IN REGULATING PLANT GRAVITROPIC RESPONSE

5.1 ABSTRACT

Environmental signals limit plant development and productivity. Gravity significantly affects plant growth and development. Plants respond to gravity by orienting the root towards gravity, while the shoots redirect in the opposite direction. Many studies have shown the role of the plant hormone auxin in root gravitropism. Two genes, *AT2G25900* (*TF*: a putative transcription factor) and *AT5G47540* (*MO25*: putative mo25-like protein) have been predicted to have a function in regulating root gravitropism. In this chapter several mutants for each gene have been identified, characterized and phenotyped to determine their functions. Unexpectedly, both of these genes have no function during the plant response to gravity. Surprisingly, one of the *Mo25* alleles displayed a strong defect in lateral root development. Backcrossing results show that there is another mutation in the background of this line which may be responsible for this phenotype.

5.2 INTRODUCTION

5.2.1 GRAVITY RESPONSE IN ROOT

Plant development under natural growth conditions is subjected to several environmental factors, for instance gravity, light intensity, temperature, water and nutrient availability. Plants have the ability to alter their architecture and reproduction depending on the surrounding environmental changes during the plant life cycle. This adaption helps the plant to survive and grow under different growth conditions (Kiss et al., 2002, Band et al., 2012, Guyomarc'h et al., 2012, Baldwin et al., 2013, Sato et al., 2014).

The gravity vector is one of the primary environmental signals that occur in both shoots and roots. It directs the shoot growth upward (negative gravitropism) to

the opposite direction of gravity (to provide a suitable position for plant's leaves for more efficient gas exchange and photosynthesis). On the other hand, it leads the root to orient immediately downward (positive gravitropism) into the same direction as gravity (in order to anchor the plant in the soil to the substrate and increase the surface area for water and mineral ion uptake) even in dark conditions (Swarup and Bennett, 2009, Baldwin et al., 2013, Sato et al., 2014). Primary roots extend vertically downward in response to gravity, whereas the lateral roots emerge and grow out first horizontally then in varied direction in response to the availability of soil water, oxygen and nutrients that are required for plant growth and development (Chen et al., 1999, Kiss et al., 2002, Swarup et al., 2005, Dubrovsky et al., 2011, Baldwin et al., 2013). According to Kiss et al. (2002) lateral roots start responding to gravity when they reach about 10 mm in length.

In 1880, the Darwins noticed and described plant movement tropisms, and that plant hormones had a major influence on these reactions (Feldman, 1985, Moulia and Fournier, 2009, Baluška et al., 2010). In the following decades, scientists have tried to explain the mechanism of how plants respond to gravity, as well as the different plant hormones which are involved in regulating these responses. In the 20th century with the development of molecular biological tools and analyses this understanding of gravitropism became more detailed (Baldwin et al., 2013, Sato et al., 2014).

The reorientation of the root growth according to a gravitational stimulus occurs within several hours (Guyomarc'h et al., 2012). In higher plants, the root

gravitropism pathway is believed to be divided into three sequential phases: (i) gravity perception, (ii) gravitropic signal transduction and (iii) gravitropic response (Hou et al., 2004, Swarup et al., 2005, Swarup and Bennett, 2009, Swarup and Peret, 2012, Meroz and Bastien, 2014).

5.2.1.1 GRAVITY PERCEPTION

The primary root tip of *Arabidopsis thaliana* has a root cap to protect the root during its expansion through the soil. The centre of the primary root cap is composed of columella cells. These cells are considered to be the first receptor of gravity because they contain sedimenting statoliths (starch-bodies; amyloplasts) that have the ability of sedimentation in response to the gravity stimulus to the lower side of the cells in under five minutes (see Fig. 5-1 and 5-2). Therefore, within columella cells, statolith bodies are the rapid gravity-sensing component (Chen et al., 1999, Hou et al., 2004, Morita, 2010, Band et al., 2012, Hashiguchi et al., 2013, Sato et al., 2014).

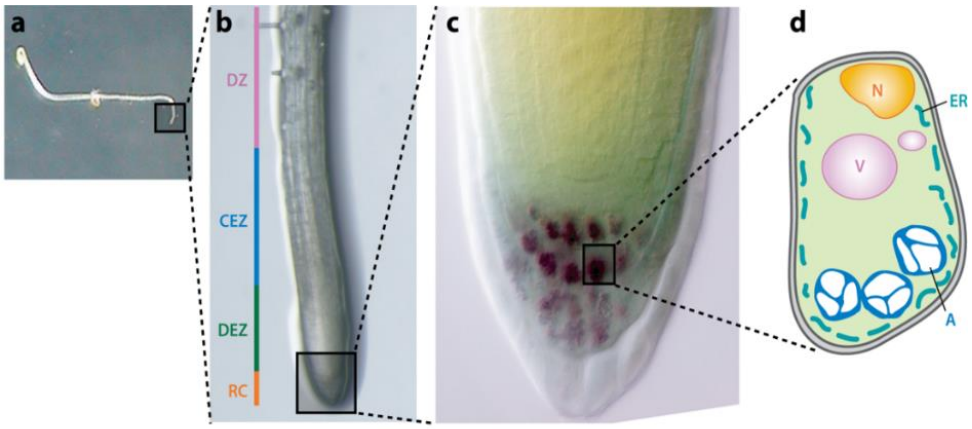

Figure 5-1: 3 day-day-old *Arabidopsis thaliana* root structure. a) Gravistimulated seedling. b) Root dissection zones; root cap (RC), distal elongation zone (DEZ), central elongation zone (CEZ) and differentiation zone (DZ). c) Stained root tip (with iodine-potassium iodide) showing the statoliths bodies in columella cells. d) Columella cell structure (A. starch bodies, ER endoplasmic reticulum, V. vacuole and N. the nucleus. (This figure is reproduced from Morita (2010)).

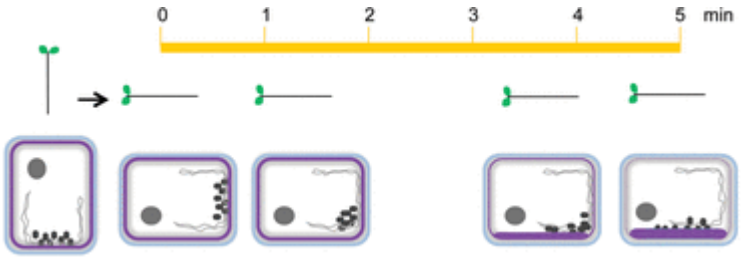

Figure 5-2: Statoliths bodies have the ability to reposition on the lower side of collumella cells in the gravistimulated root tip within 5 minutes. (This figure is reproduced from Sato et al. (2014)).

5.2.1.2 GRAVITROPIC SIGNAL TRANSDUCTION

The most critical part of the root in gravitropic signal tranduction is the elongation zone (which is the region of the root above the meristem zone, where the cells reach its maximum elongation size) where the gravitropic bending occurs. Under gravistimulation, the statolith bodies re-localize to the bottom side of columella cells and this generates a signal from the columella cells to the

elongation zone cells, which is believed to be the plant hormone auxin. The difference in intercellular auxin concentrations between the two sides of a gravistimulated root can be visualised using auxin response reporter DR5 or auxin sensor DII (Swarup et al., 2005, Rahman et al., 2010, Band et al., 2012, Baldwin et al., 2013, Hijazi, 2013).

Auxin, along with other hormones such as ethylene, cytokinin and abscisic acid, confers gravitropic signals; and most genetic evidence identifies a strong role for auxin in the gravity response (Swarup and Peret, 2012, Pernisova et al., 2016). In ideal vertical growth conditions, the auxin gradient in the root tip is distributed equally between the two sides of the root (upper and lower sides). Auxin is transported through the plant cells (shootward or rootward) by influx carrier complexes, such as *AUX1* and *LAX* (AUXIN INSENSITIVE 1 and Like AUX1) and efflux facilitators, such as the PIN (PIN-FORMED) family of proteins, in a process known as the polar transport mechanism (Swarup et al., 2005, Kleine-Vehn et al., 2010, Morita, 2010, Demeulenaere and Beeckman, 2014).

The auxin efflux carriers PIN1 and PIN4 regulate auxin transport through the phloem to columella cells. Another member from the PIN gene family (*PIN3*) has the ability to rapidly re-localize (within 2 minutes) in gravistimulated roots from the basal side of columella cells to the lower face of the cells by mechanism which is yet to be elucidated. *PIN3* and *PIN7* relocalization within the plasma membrane of columella cells generates lateral auxin gradients in the root cap cells, followed by redirection of auxin towards the epidermal cells in the

elongation zone (in the upper side of gravistimulated roots) by *AUX1* and *PIN2* (Hou et al., 2004, Rahman et al., 2010, Sato et al., 2014).

5.2.1.3 GRAVITROPIC RESPONSE

As a consequence of the lateral auxin gradient, auxin is differentiated between the opposite sides of the epidermal cells in the elongation zone of a gravistimulated root. Auxin becomes highly concentrated in the epidermal cells in the lower side of the root (about 10 to 20 fold more than the upper side), resulting in inhibition of cell expansion. However, due to the normal auxin level in the epidermal cells in the upper side, the cells elongate normally on the upper edge. This differentiation in cellular auxin gradients and cell expansion leads to root curvature in response to gravity, whereby roots curve downward in the same direction as gravity (Swarup and Bennett, 2009, Leyser, 2010, Pernisova et al., 2016).

At the molecular level, the genetic studies in *A. thaliana* have shown numerous auxin inducible genes such as *ARFs* and *Aux/IAAs* are highly expressed within 15 min after a gravitational stimulus. Indeed, the auxin responsive factors *ARF7* and *ARF19* are considered to be the transcriptional activators of several downstream auxin response genes (at the upper and lower sides of the root) which control the re-orientation of the root in response to gravity vector (Okushima et al., 2005, Okushima et al., 2007).

5.2.2 IDENTIFICATION OF REGULATORY GENE FOR PLANT GROWTH RESPONSES BY MICROARRAY TRANSCRIPTOME ANALYSIS

According to Okushima et al. (2005), microarray data of auxin treated samples (5 µM IAA) of *arf7*, *arf19* and *arf7 arf19* mutants revealed from 22,800 genes that 271 genes are auxin regulated genes (203 auxin-induced and 68 auxin-repressed genes, with a threshold of an approximately twofold change in expression for both groups). Additionally, by micro-dissecting the five zones of the primary root of *arf7 arf19* double mutants and WT (of 7 days old seedlings). 790 differentially expressed genes were identified from the elongation zone (see Fig. 1-2) (Holman et al., 2010). Further, by overlapping these two transcriptome data sets, 195 differentially expressed genes regulated by auxin and *ARF7 ARF19* were identified (Hijazi, 2013).

A gravitropism-dependent transcriptomic dataset was generated to identify differentially expressed genes during root gravitropism. For this zone 1 and zone 2 (root tip and elongation zone) of gravistimulated roots were dissected at specific time points (0, 15, 30, 60, 120 and 480 min), revealing 566 differentially expressed genes (Sato, 2013). Prior to my involvement in this project, bioinformatics analyses, phenotypical and molecular characterisation have been performed to identify mutant lines displaying defects in their gravitropic response. g(Sato, 2013, Hijazi, 2013). Based on this, two genes were confirmed to be differentially expressed in the *Arabidopsis* root in response to gravity, and found to be especially important in the lateral root cap and/or epidermis cells

(*AT2G25900* and *AT5G47540*) (Hijazi, 2013). Here, AT2G25900 was chosen to investigate its function in root gravitropism.

5.2.2.1 AT2G25900 (CYSTEINE- CYSTEINE- CYSTEINE-HISTAMINE TANDEM ZINC FINGER PROTEIN) OR CYS3HIS ZINC FINGER TRANSCRIPTION FACTOR

One gravity-response gene product, known as either A. THALIANA TANDEM ZINC FINGER PROTEIN 1, ATTZF1, ATCTH, or Cys3His transcription factor (TF), has been shown to possess a Zinc ion binding domain at C3H23. It is located in the cytoplasm and nucleus of cells, and has functions in DNA and RNA binding. It also has sequence-specific DNA binding transcription factor activity (Wang et al., 2008a, Peng et al., 2012, Yuan et al., 2015).

Bioinformatic analysis has revealed that ATTZF1 is one of 68 members of the CCCH gene family in *Arabidopsis*, which is subdivided into 11 subfamilies (see Fig.5-3) (Chai et al., 2012, Wang et al., 2008a). The subfamily of this gene is a unique family in higher plants. Most genes in this subfamily have roles in biotic and abiotic stress tolerance, such as salt, drought and cold stress (Sun et al., 2007, Zhang et al., 2013, Liu et al., 2014). Some of these family members are also involved in secondary wall biosynthesis regulation (Ko et al., 2009). Furthermore, 34 CCCH zinc finger (Znf) genes identified in *Medicago truncatula* were found to have roles in plant developmental and adaptive processes (Zhang et al., 2013). In *Populus trichocarpa*, 91 members of CCCH family have been characterised, 12 of which were shown to have an active

function in xylem differentiation and adaptation to drought conditions (Chai et al., 2012). *AT2G25900* is expressed in roots, leaves and siliques (Wang et al., 2008b), with unknown function in plants (Pomeranz et al., 2010).

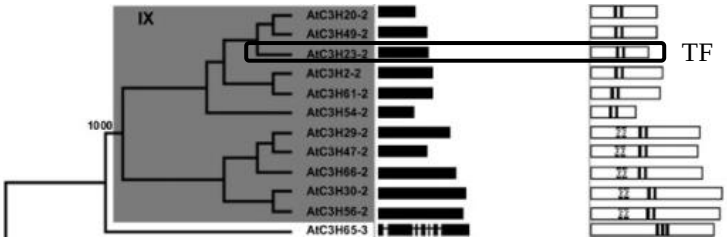

Figure 5-3: Analytical view of the AT2G25900 (TF) subfamily of CCCH zinc-finger family. AT2G25900 contains two CCCH motifs with 35464.6 Da (This figure is reproduced from Wang et al. (2008a)).

According to Hijazi (2013) *AT2G25900* was up regulated by IAA. The knock out lines of this gene showed a defect in gravitropic responses compared to Columbia.

5.2.2.2 *AT5G47540*: PUTATIVE MO25-LIKE PROTEIN

AT5G47540 is a member of the Mo25 superfamily. The majority of studies of this family have been done in yeast (*Schizosaccharomyces pombe*) (Kanai et al., 2005, Hijazi, 2013), and have identified that most of these genes have functions in growth polarization, cytokinesis, including some which are putative calcium binding proteins. Mo25 is protein that is present in all eukaryotes. It was identified in mouse embryogenesis during the cleavage stage. In budding yeast, a Mo25 homologue participates in cell separation and polar growth plus it has an essential role during cell division (anaphase stage, Pmo25 localized at the

mitotic spindle pole bodies) along with other genes such as *Orb6* and *Nak1* (Kanai et al., 2005, Mendoza et al., 2005, Hijazi, 2013) Hijazi (2013) has predicted this gene to have a function during gravity responses in *Arabidopsis thaliana* roots.

This chapter focuses on the function characterisation of these two genes (*AT2G25900* and *AT5G47540*) by using a reverse genetic approach. The aim was to enrich our understanding of the molecular mechanism by which the genes regulate the plant growth and development according to gravity. Firstly, several knock-out lines were identified for each gene. Gravity bending assays were then performed to detect the possible role of these two genes during plant responses to gravity.

5.3 MATERIALS AND METHODS

5.3.1 *ARABIDOPSIS THALIANA* MUTANTS LINES

Arabidopsis thaliana ecotype Columbia (*Col-0*) and all T-DNA insertion mutants (Knock-out; KO) lines (Table 5-1) were ordered from Nottingham *Arabidopsis* stock centre (NASC). To determine the exact position of each T-DNA insert among the full gene sequence, the TAIR website (https://www.arabidopsis.org/ was used.

Table 5-1: *Arabidopsis thaliana* T-DNA insertion lines**.**

Gene ID	Mutants	NASC ID	CODE	INSERT POSITION
AT2G25900 (*TF*) Transcription Factor	*tf_112*	N612158	SALK_112158	Exon 1
	tf_980	N639980	SALK_139980	Exon 1
	tf_14	N643721	SALK_143721	Exon 1
	gk_8	N731217	GK-788F09.01 [SET]	Exon 1
AT5G47540 (*Mo25*) Mo25 like protein	*mo25-1*	N500304	SALK_000304	Intron 2
	mo25-2	N576387	SALK_076387	Exon 5
	mo25-3	N821637	SAIL_513_B05	Intron 5
	mo25-4	N844951	SAIL_1227_H04	Intron 7
	mo25-5	N660463	SALK_066597	Exon 3

5.3.2 STERILIZATION, GERMINATION AND GROWTH CONDITIONS

In a sterile laminar flow hood, seeds from each line were surface sterilised with 70% Ethanol then 5% (v/v) hypochlorric acid for 5 min, followed by three washes with 0.1% (v/v) triton (30-60 sec.). Then the seeds were washed twice by sterile ddH_2O. Sterile seeds were plated on square plates containing half MS medium (Sigma). For germination synchronisation, the plates were stored at 4^0C for 24h. All plates then were transferred to a controlled growth room until the seeds became ready for analysis (see section 2.2 for more growth conditions details).

5.3.3 GENOTYPIC ANALYSIS

Genomic DNA was extracted from two cotyledons (according to the DNA extraction protocol described in section 2.3.1). To test the presence or absence of each T-DNA insertion in the mutant lines, two Polymerase Chain Reaction (PCR) assays were performed (see section 2.3.3 for the PCR conditions): one using gene specific primers (forward and reverse primers: LP and RP), and the other using the gene specific reverse primer (RP) with the T-DNA LB primer. The SIGnAL website (http://signal.salk.edu/tdnaprimers.2.html) was used to design the genotyping primers (Table 5-2).

Table 5-2: Gene specific primer sequences for T-DNA insertion lines.

T-DNA insertion mutant line		Forward Primer	Reverse Primer
AT2G25900 (TF)	*tf_112* (SALK_112158)	TCGGATGTTACGACTTTGACT	TCCAATCATGAGATCGACCTC
	tf_980 (SALK_139980)	TTTCCTCATCGACGCAATAAG	TTGAAAAGAGTTTTGAAATTTTATGG
	tf_14 (SALK_143721)	CGATCCATATCCCTCAATGG	GCTAGTTCCGTCTTTACACG
	gk_8 (GK-788F09.01)	CTTGCATACATCTCCGCTCTC	TGTCATCATCTGCAGATTTGC
AT5G47540 (Mo25)	*mo25-1* (SALK_000304)	CTACCTCTTTGCCTGACCTCC	CGGCAACAGTAGACTTATGCC
	mo25-2 (SALK_076387)	AGGTTCCAAAACAAAACTCGC	GTTGGTTCAAGCAAGATCTCG
	mo25-3 (SAIL_513_B05)	AAGCCAACATTGATCTCATGG	CCAACAATCTCAGAAGCTTGC
	mo25-4 (SAIL_1227_H04)	AGGTTCCAAAACAAAACTCGC	GTTGGTTCAAGCAAGATCTCG
	mo25-5 (SALK_066597)	GCCTACCTTAATAGCTTGCCG	AATTAAGCCGGAATATCCGTG

5.3.4 RNA EXTRACTION, cDNA SYNTHESIS, REVERSE TRNANSCRIPTASE-POLYMERASE CHAIN REACTION AND QUANTITATIVE REVERSE TRANSCRIPTASE-POLYMERASE CHAIN REACTION

RNA samples were extracted from the whole root of 7 day old seedlings. By using Trizol Reagent (Invitrogen), the extraction was carried out according to the RNase Mini Kit protocol (Qiagen) (section 2.4.1). RNA (1 µg) was used to synthesize cDNA with the Superscript II Reverse Transcriptase protocol (Invitrogen; section 2.4.2). A reverse transcriptase-polymerase chain reaction (RT-PCR) reaction was performed in order to determine the nature of gene expression (Table 5-3 shows the RT-PCR specific primers sequences).

Table 5-3: RT-PCR specific primer sequences.

Line	Forward Primer	Reverse Primer
AT2G25900 (TF)	AACCGGCCACATCCAACGAT	GGAGAAGTAGCTAATCCTGAG
AT5G47540 (Mo25)	TCGATCTACCTCTTTGCC	AAAGTAGCAGCAGCATCG

A LightCycler® 480 system (Roche, USA) with the fluorescent dye SYBR® Green Master Mix (Bioline) was used to measure the level of gene expression in all T-DNA insertion mutant lines via quantitative reverse transcriptase-polymerase chain reaction (qRT-PCR). All data were analysed with Microsoft Excel 2010 (Microsoft Corporation, Redmond, USA). In addition, the Universal Probe Library Assay Design Centre was used for specific primer pair design. Table 5-4 shows the specific primer sequences which were used in qRT-PCR analysis.

Table 5-4: qRT-PCR specific primer sequences.

Line	Forward Primer	Reverse Primer
AT2G25900 (TF)	GAGATGATAATGAGAGAATTTGAGAGC	CCAAAATAAAAACAAGAAAATAACGAA
AT5G47540 (Mo25)	AAGCATTCCATGTCTTTAAGGTA	TCAGCCAACAATCTCAGAAGC

5.3.5 PLANT PHENOTYPIC ANALYSIS

In order to identify any root growth and development phenotype, 20 seeds were germinated on sterile square Petri dishes on half MS (pH 5.8) and incubated under controlled conditions for 10 days (see section 2.2 for growth condition details). The length of the primary root for the individual seedlings was measured and analysed by Fiji software. The number of all emerged lateral roots was counted using a binocular microscope. Lastly, the lateral root density was calculated for each line.

The root clearing protocol described in section 2.6.2 was used to clarify all roots. Roots were loaded in 50% of glycerol on glass microscope slides. The total

number of the different stages of the lateral root primordia was counted by using Leica Light Microsystems.

5.3.6 GRAVITISTIMULATION ASSAY

Seedlings were grown vertically on Petri dishes in controlled environment chamber with a 12 h photoperiod. Six day old seedlings were gravistimulated by a rotation of 90^0; subsequently the angle of the primary root was measured every 60 minutes for 8 h. Images of the gravity stimulated roots were taken by an automated image acquisition system (Wells et al., 2012) and were analysed using Fiji software.

5.3.7 MERISTEM TISSUE SIZE

Propidium iodide (5 μg ml^{-1} H_2O) (Sigma) was used to stain the cell walls of root tissues. Images of the meristem tissue were taken by laser scanning confocal microscope (Leica SP5, Leica Microsystems). Their sizes were measured using Fiji software.

5.4 RESULTS

A previous study which has generated by Hijazi, (2013) identified two candidate genes to have functions in the regulation of root responses to gravity: *AT2G25900* (Cys3His zinc finger transcription factor) and *AT5G47540* (Mo25-like protein). In order to investigate the possible contribution of these two genes in the gravity response, genotyping analysis was carried out to select T-DNA insertion lines for each gene.

5.4.1 GENOTYPIC ANALYSIS OF T-DNA INSERTION LINES

T-DNA lines were genotyped to test for the presence of the T-DNA insertion in the open reading frame of the gene in interest. For Polymerase Chain Reaction (PCR), three different primers were used: forward and reverse gene specific primers (LP and RP), and the left T-DNA border primer (LB). From two cotyledons genomic DNA was extracted from knock out lines and from the wildtype (WT, Columbia *Col-0*).

Genotyping analysis for the different mutant alleles of AT2G25900 *tf_112* (SALK_112158), *tf_14* (SALK_143721) and *gk_8* (GK-788F09.1) showed that all plants were homozygous for the T-DNA insertion. The PCR products showed bands on agarose gel under UV light in all seedlings following amplification using RP + LB primers, whereas, when the genomic primers (LP + RP) where used there were no products in all homozygous mutant seedlings compared with WT (Columbia, *Col-0*) (Fig.5-4, 5-5 and 5-6).

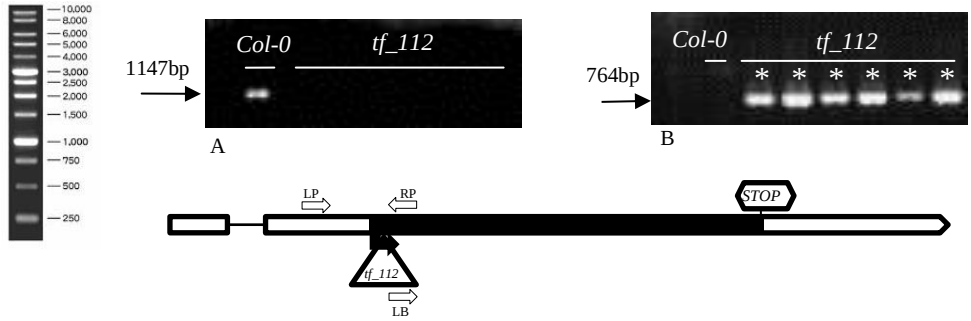

Figure 5-4: Genotyping analysis by PCR for *tf_112* (SALK_112158), using A) two genomic primers (LP + RP: forward and reverse primers) Product size = 1147bp, and B) RP + left T-DNA border primer (LB) Product size= 764bp. WT: wild type (Columbia) and 6 SALK__112158 line seedlings. (1kB DNA ladder; *: Homozygous plants).

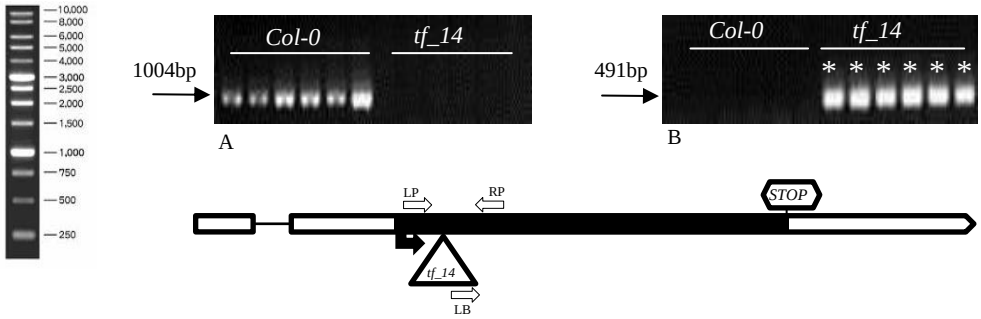

Figure 5-5: Genotyping analysis by PCR for *tf_14* (SALK_143721), using A) two genomic primers (LP + RP: forward and reverse primers) Product size = 1004bp, and B) RP + left T-DNA border primer (LB) Product size= 491bp. WT: wild type (Columbia) and 6 SALK_143721 line seedlings. (1kB DNA ladder; *: Homozygous plants).

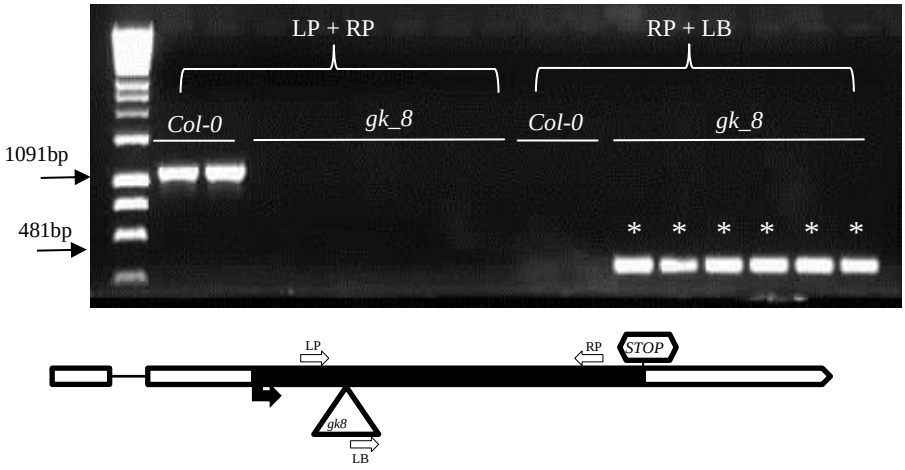

Figure 5-6: Genotyping analysis by PCR for *gk_8* (GK-788F09.1), using two genomic primers (LP + RP: forward and reverse primers) Product size = 1091bp, and RP + left T-DNA border primer (LB) Product size= 481bp. WT: wild type (Columbia) and 6 GABI-Kat_788F09.1 line seedlings. (1kB DNA ladde; *: Homozygous plants).

PCR genotyping of *tf_980* (SALK_139980) revealed that some plants were homozygous for the T-DNA insertion (1, 3 and 6) whereas, others were wild type (2, 4 and 5) (Fig. 5-7).

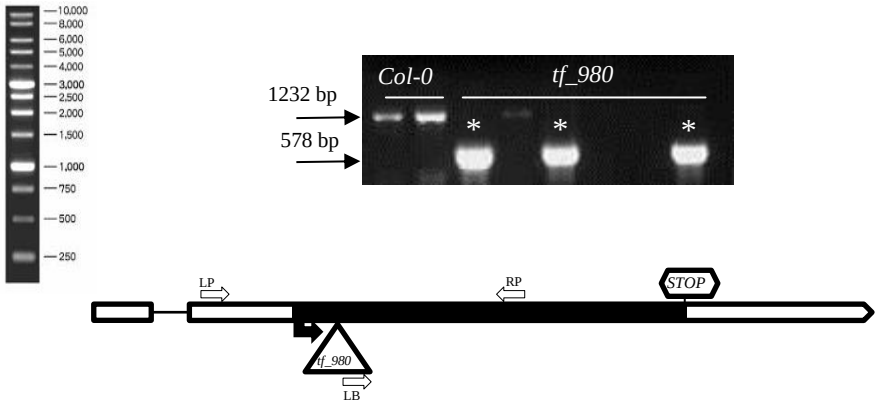

Figure 5-7: Genotyping analysis by PCR for *tf_980* (SALK_139980), using two genomic primers (LP + RP: forward and reverse primers) Product size = 1232bp, and RP + left T-DNA border primer (LB) Product size= 578bp. WT: wild type (Columbia) and 6 SALK__139980 line seedlings. (1kB DNA ladder; *: Homozygous plants).

Genotyping analysis for AT5G47540 *mo25-1* (SALK_000304), *mo25-2* (SALK_076387), *mo25-3* (SAIL_513_B05), *mo25-4* (SAIL_1227_H04) and *mo25-5* (SALK_066597), showed that all of the knock out lines were homozygous for the T-DNA insertion (Fig. 5-8 to 5-12 respectively).

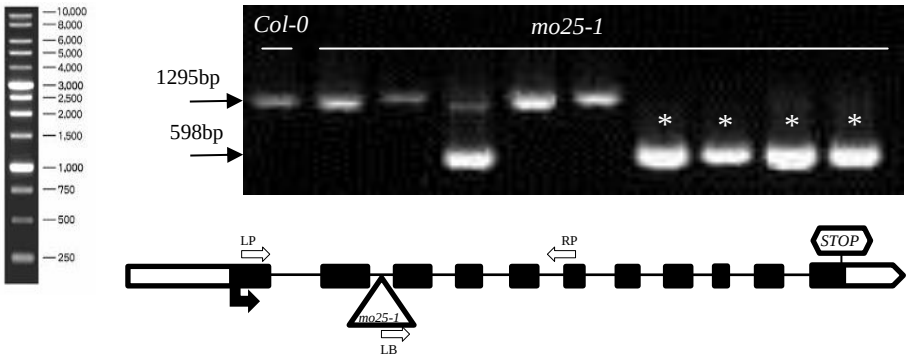

Figure 5-8: Genotyping analysis by PCR for *mo25-1* (SALK_000304), using two genomic primers (LP + RP: forward and reverse primers) Product size = 1295bp, and RP + left T-DNA border primer (LB) Product size= 598bp. WT: wild type (Columbia) and 9 SALK_000304 line seedlings. (1kB DNA ladder; *: Homozygous plants).

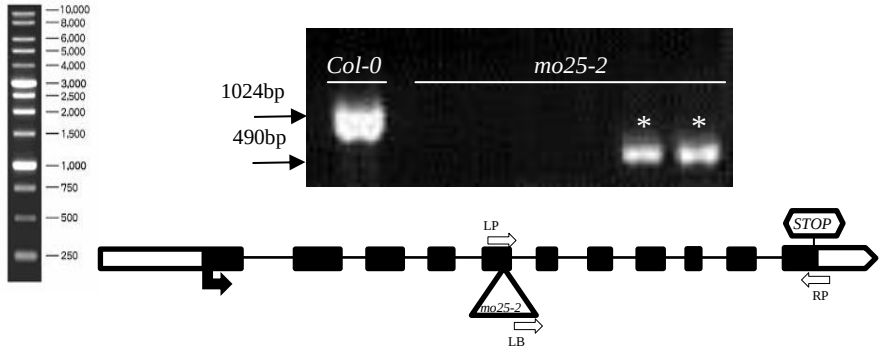

Figure 5-9: Genotyping analysis by PCR for *mo25-2* (SALK_076387), using two genomic primers (LP + RP: forward and reverse primers) Product size = 1024bp, and RP + left T-DNA border primer (LB) Product size= 490bp. WT: wild type (Columbia) and 6 SALK_076387 line seedlings. (1kB DNA ladder; *: Homozygous plants).

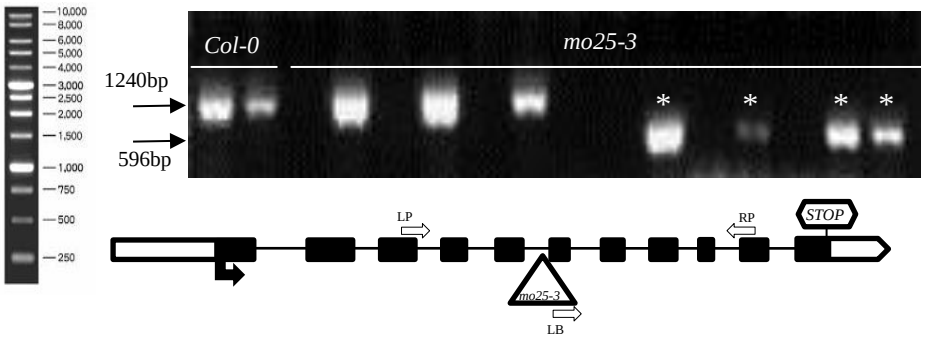

Figure 5-10: Genotyping analysis by PCR for *mo25-3* (SAIL_513_B05), using two genomic primers (LP + RP: forward and reverse primers) Product size = 1240bp, and RP + left T-DNA border primer (LB) Product size= 596bp. WT: wild type (Columbia) and 14 SAIL_513_B05 line seedlings. (1kB DNA ladder; *: Homozygous plants).

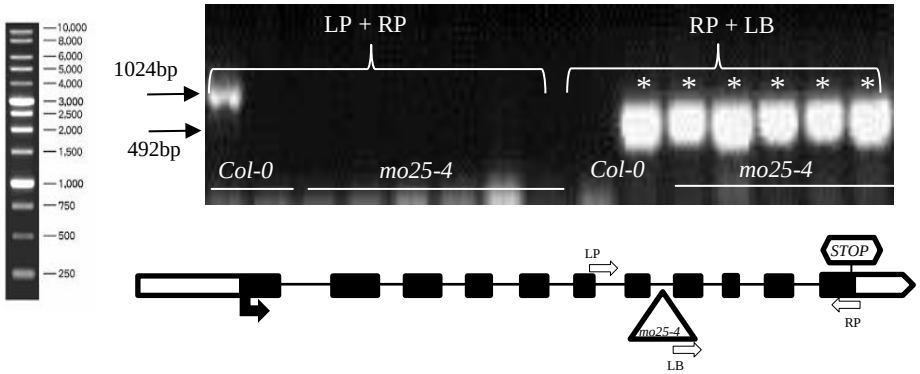

Figure 5-11: Genotyping analysis by PCR for *mo25-4* (SAIL_1227_H04), using two genomic primers (LP + RP: forward and reverse primers) Product size = 1024bp, and RP + left T-DNA border primer (LB) Product size= 492bp. WT: wild type (Columbia) and 6 SAIL_1227_H04 line seedlings. (1kB DNA ladder; *: Homozygous plants).

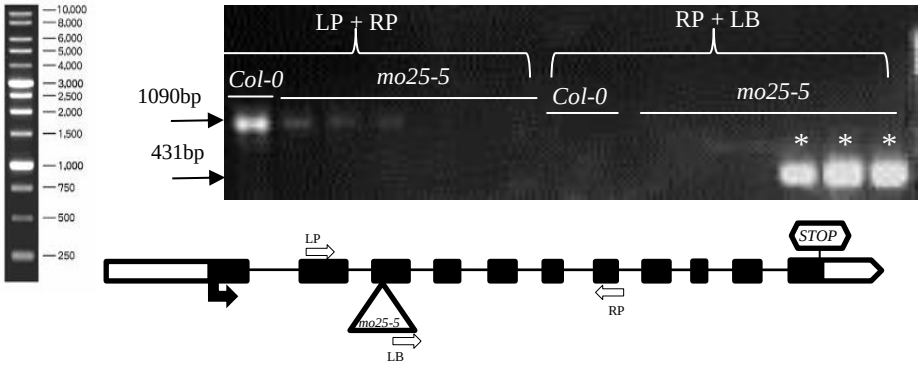

Figure 5-12: Genotyping analysis by PCR for *mo25-5* (SALK_066597), using two genomic primers (LP + RP: forward and reverse primers) Product size = 1090bp, and RP + left T-DNA border primer (LB) Product size= 431bp. WT: wild type (Columbia) and 6 SALK_066597 line seedlings. (1kB DNA ladder; *: Homozygous plants).

5.4.2 RT-PCR

In order to confirm that the gene of interest was not expressed in the genotyped T-DNA insertion lines of all different alleles of AT2G25900 and AT5G47540, RNA was extracted from plant roots. Complementary DNA (cDNA) was generated from those RNA samples. RT-PCR was performed using forward (FP) and reverse (RP) primers (Fig. 5-13 B, C and 5-14 B), and house-keeping primers (Fig. 5-13 A and 5-14 A).

The results showed that there was no gene expression in two alleles of AT2G25900 *tf_112* (SALK_112158) and *tf_14* (SALK_143721) (Fig. 5-13.B). However, AT2G25900 was still expressed in *tf_980* (SALK_139980) and *gk_8* (GK-788F09.1) (Fig. 5-13.C). This means that *tf_980* (SALK_139980) and *gk_8* (GK-788F09.1) of AT2G25900 are not full knock-out lines.

There was no gene expression in all T-DNA insertion lines of AT5G47540 when using FP and RP primers (Fig. 5-14.B), leading to the conclusion that all insertion lines for AT5G47540 are knock outs.

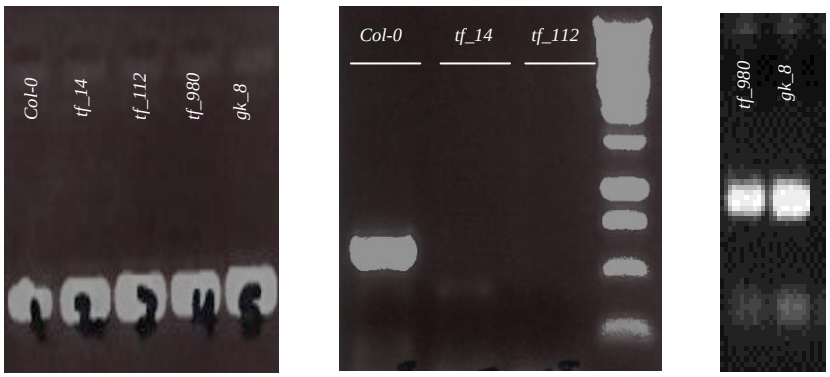

Figure 5-13: RT-PCR expression analysis of the different mutants of AT2G25900 compared with WT (*Col-0*). A) Expression of a house-keeping gene using house-keeping primers (product size ~ 200bp). B) Expression analysis of AT2G25900 *tf_112* (SALK_112158) and *tf_14* (SALK_143721). C) The expression analysis of AT2G25900 (*gk_8* (GK-788F09.1) and *tf_980* (SALK_139980) using forward and reversed cDNA specific primers (Product size= 614 bp).

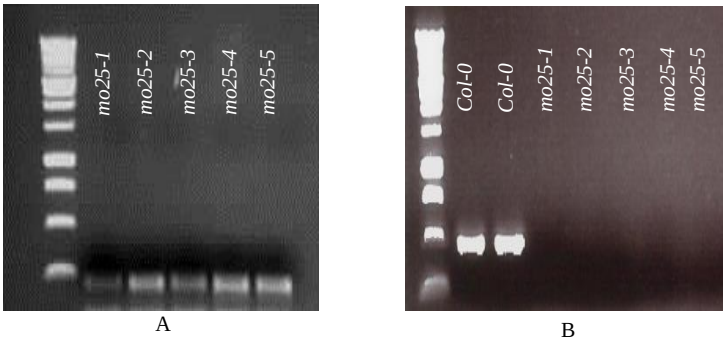

Figure 5-14: RT-PCR expression analysis of the different mutants of AT5G47540 compared with WT (*Col-0*). A) Expression of a house-keeping gene using house-keeping primers (product size ~ 200bp). B) Expression analysis of AT5G47540 *mo25-1* (SALK_000304), *mo25-2* (SALK_076387), *mo25-3* (SAIL_513_B05), *mo25-4* (SAIL_1227_H04) and *mo25-5* (SALK_066597) using forward and reversed cDNA specific primers. (Product size= 440 bp).

For a more precise quantification of gene expression and to confirm there was no expression in all T-DNA insertions lines, qRT-PCR was performed. By using cDNA samples with forward and reverse primers (Fig. 5-15 and 5-17), all different mutant alleles of AT2G25900 and AT5G47540 were analysed and normalized against the WT (*Col-0*).

The obtained data were compatible with previous RT-PCR results. The gene expression was reduced in the two alleles of AT2G25900 *tf_112* (SALK_112158) and *tf_14* (SALK_143721). In contrast, there was an over expression in *gk_8* (GK-788F09.1) line, and the same expression of WT line in *tf_980* (SALK_139980) line (Fig. 5-16).

AT5G47540 data indicated that all alleles were full knock-outs (*mo25-1*, *mo25-2* and *mo25-3*). However, *mo25-4* (SAIL_1227_H04) and *mo25-5* (SALK_066597) analysis showed only a significant reduction in the gene expression compared with WT (Columbia; *Col-0*) (Fig. 5-18).

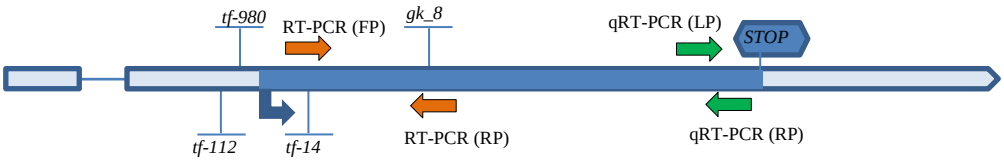

Figure 5-15: The map of *AT2G25900* indicating the four different T-DNA insertion positions *tf_112* (SALK_112158), *tf_14* (SALK_143721), *gk_8* (GK-788F09.1) and *tf_980* (SALK_139980), with RT-PCR (forward; FP + reverse; RP) and QRT-PCR (forward; FP + reverse; RP) primers.

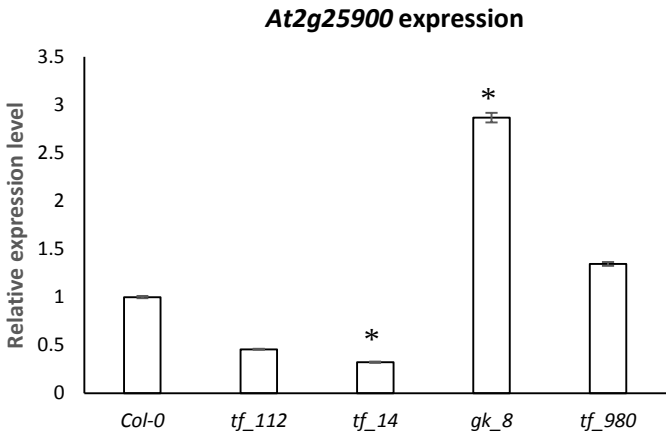

Figure 5-16: qRT-PCR expression quantification for *AT2G25900* of *tf_112* (SALK_112158), *tf_14* (SALK_143721), *gk_8* (GK-788F09.1) and *tf_980* (SALK_139980), normalized to WT (*Col-0*). * denotes significant difference compared to WT ($P < 0.05$).

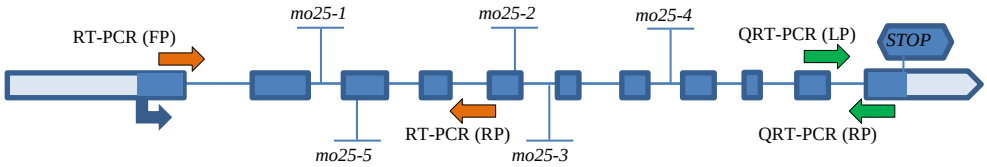

Figure 5-17: The map of *AT5G47540* indicating the different T-DNA insertion positions of *mo25-1* (SALK_000304), *mo25-2* (SALK_076387) and *mo25-3* (SAIL_513_B05), *mo25-4* (SAIL_1227_H04) and *mo25-5* (SALK_066597), with RT-PCR (forward; FP + reverse; RP) and qRT-PCR (forward; FP + reverse; RP) primers.

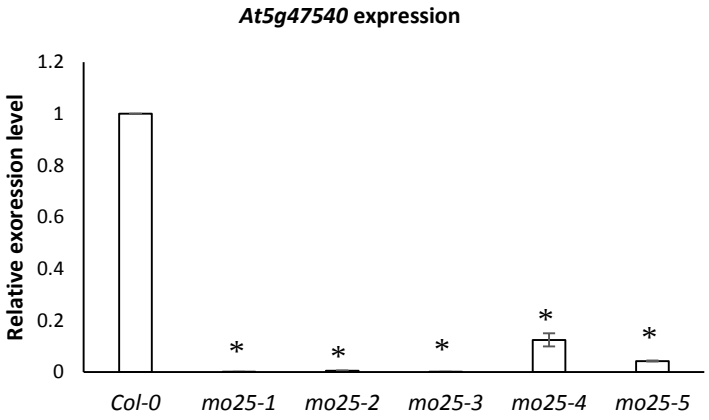

Figure 5-18: qRT-PCR expression quantification for *AT5G47540* of *mo25-1* (SALK_000304), *mo25-2* (SALK_076387), *mo25-3* (SAIL_513_B05), *mo25-4* (SAIL_1227_H04) and *mo25-5* (SALK_066597), normalized to WT (*Col-0*). * denotes significant difference compared to WT ($P < 0.05$).

5.4.3 PHENOTYPIC ANALYSIS

In order to investigate the function of these two genes (*AT2G25900* and *AT5G47540*) in gravistimulated roots, phenotyping analyses were carried out for all knock out lines.

5.4.3.1 PRIMARY ROOT GRAVITROPISM

To determine the roles of AT2G25900 and AT5G47540 in the primary root response to gravity, homozygous seedlings were grown on half MS plant growth media under 12 h photoperiod. 6 days old seedlings were turned 90° and the angle of the primary root was measured over 8 h during dark conditions to avoid phototropism (Fig. 5-19), for all different mutants of AT2G25900 and AT5G47540.

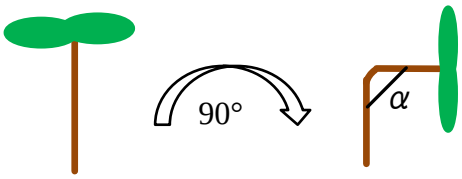

Figure 5-19: 6 day old homozygous seedlings were turned 90°, and then the primary root angle (α) in response to gravity was measured.

The figures show that there was no significant difference between all of the AT2G25900 alleles compared with WT (Columbia; *Col-0*) in response to gravity after 8 h in dark conditions (Fig. 5-20).

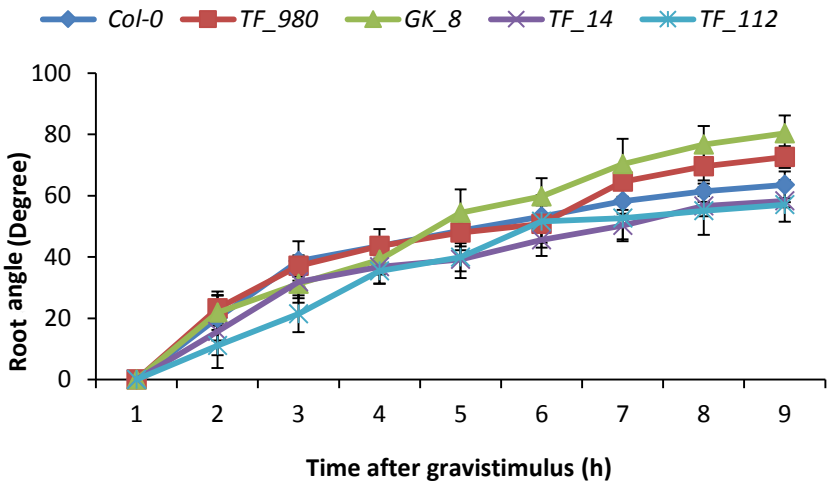

Figure 5-20: The response of the gravistimulated root of the 6 day old seedlings after turning 90° for AT2G25900 *tf_112* (SALK_112158), *tf_14* (SALK_143721), *gk_8* (GK-788F09.1) and *tf_980* (SALK_139980), Compared with WT (*Col-0*).

The response to gravity of four different alleles of AT5G47540 *mo25-1* (SALK_000304), *mo25-3* (SAIL_513_B05), *mo25-4* (SAIL_1227_H04) and *mo25-5* (SALK_066597) were similar to WT. However, *mo25-2* (SALK_076387) showed a slower response to gravity. It reached 45° after 8 h, whereas, Col-0 reached 70° (Fig. 5-21).

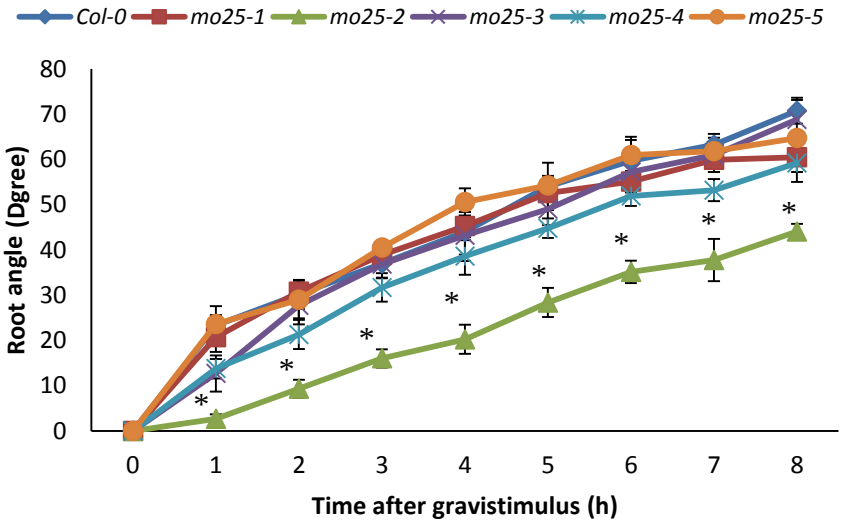

Figure 5-21: The response of the primary root to gravity after seedlings turned 90° for 8 hours. For AT5G47540 *mo25-1* (SALK_000304), *mo25-2* (SALK_076387), *mo25-3* (SAIL_513_B05), *mo25-4* (SAIL_1227_H04) and *mo25-5* (SALK_066597), compared with WT (*Col-0*) * denotes a significant difference from WT ($P < 0.05$).

5.4.3.2 PRIMARY ROOT LENGTH

The primary root growth depends on the activity of the root apical meristem and can affect the response of the root to gravity. To determine this, primary root length was measured for 3, 5 and 7 days, for all different mutants of AT2G25900, and for 10 day old seedlings for AT5G47540.

There was no difference in the primary root growth in all different alleles of AT2G25900 *tf_112* (SALK_112158), *gk_8* (GK-788F09.1) and *tf_980* (SALK_139980). However, the total primary root length of *tf_14* (SALK_143721) 7 day old seedlings was significantly shorter than other alleles (Fig. 5-22).

The primary root lengths of 10 day old seedlings of the different T-DNA insertions of AT5G47540 *mo25-1* (SALK_000304), *mo25-3* (SAIL_513_B05), *mo25-4* (SAIL_1227_H04) and *mo25-5* (SALK_066597), were similar to WT. On the other hand, *mo25-2* (SALK_076387) showed a significant reduction in growth compared with Columbia (WT) (Fig. 5-23).

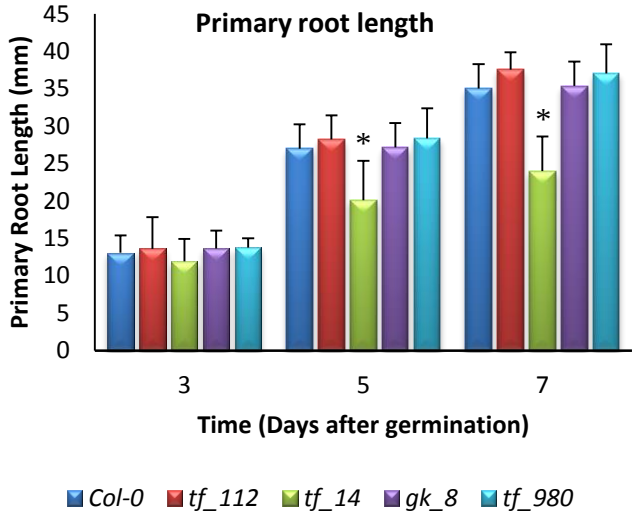

Figure 5-22: The primary root length after 3, 5 and 7 days, for AT2G25900 *tf_112* (SALK_112158), *tf_14* (SALK_143721), *gk_8* (GK-788F09.1) and *tf_980* (SALK_139980)), compared with WT (*Col-0*). * denotes a significant difference from WT ($P < 0.05$).

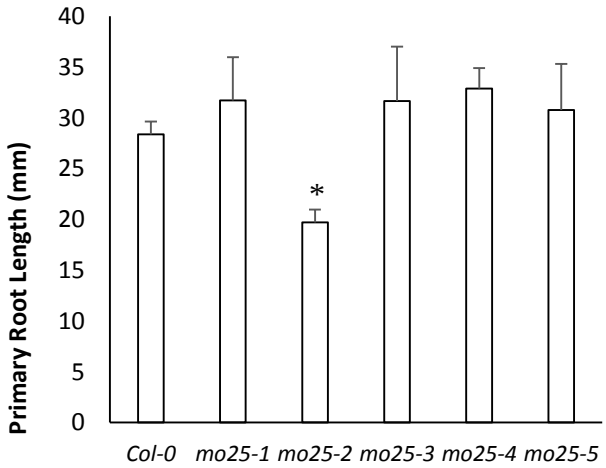

Figure 5-23: The primary root length of 10 day old seedlings, For AT5G47540 *mo25-1* (SALK_000304), *mo25-2* (SALK_076387), *mo25-3* (SAIL_513_B05), *mo25-4* (SAIL_1227_H04) and *mo25-5* (SALK_066597), compared with WT (*Col-0*). * denotes a significant difference from WT ($P < 0.05$).

5.4.3.3 MERISTEM SIZE

According to RT-PCR and qRT-PCR results, the two T-DNA insertion lines of AT2G25900 (*tf_14* (SALK_143721) and *gk_8* (GK-788F09.1) had a reduction in expression and over expression, respectively, compared with WT. As a means of phenotyping analysis, the number (Fig 5-24) and length (Fig. 5-25) of the meristem cells in the root tip of *tf_14* (SALK_143721) and *gk_8* (GK-788F09.1) were counted using confocal microscope, then analysed by Fiji software (Fig. 5-26). The results revealed no significant differences between the two alleles compared with *Col-0* in either cell number or length.

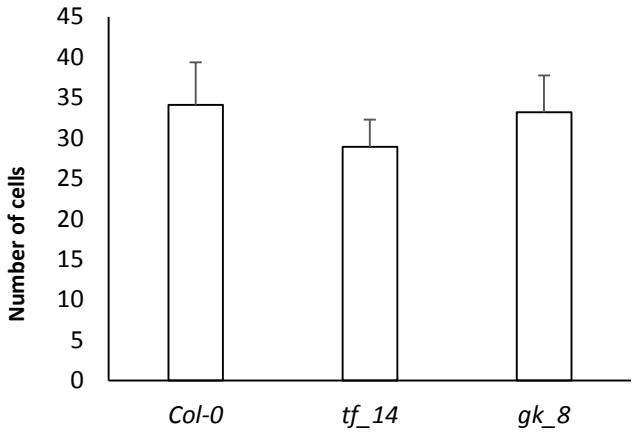

Figure 5-24: The number of the meristem cells of AT2G25900 *tf_14* (SALK_143721) and *gk_8* (GK-788F09.1), compared with WT (*Col-0*).

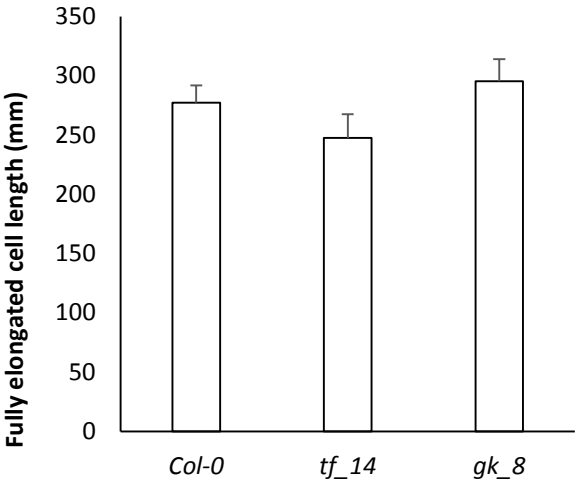

Figure 5-25: The meristem tissue cell length of AT2G25900 *tf_14* (SALK_143721) and *gk_8* (GK-788F09.1), compared with WT (*Col-0*).

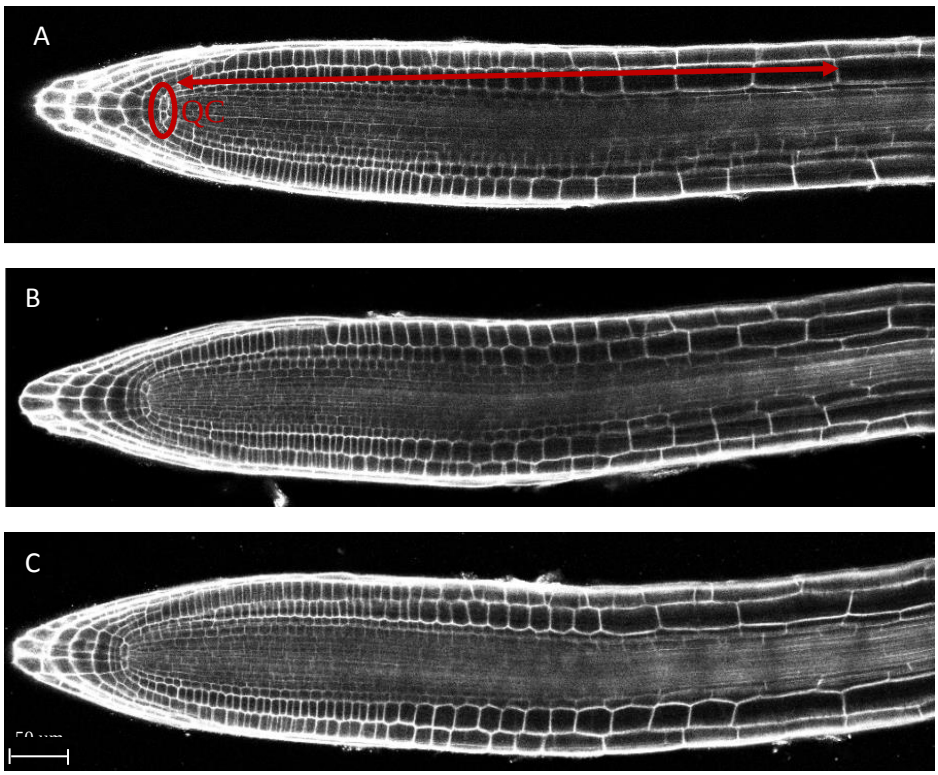

Figure 5-26: Confocal image of the root tip cross sections of of AT2G25900 mutants and wildtype: A) *tf_14* (SALK_143721) and B) *gk_8* (GK-788F09.1), compared with WT (C, *Col-0*). The number of cortical cells were counted from the QC to the beginning of the elongation zone were the cortex cells start to elongate.

5.4.3.4 LATERAL ROOT NUMBER

The total number of emerged lateral root of ten day old seedlings of the T-DNA insertion line of AT5G47540 *mo25-2* (SALK_076387) was counted. It showed a strong phenotype in lateral root development. Only 0 - 2 lateral roots emerged in 10 day old seedlings (Fig. 5-27 B), while 15 – 17 lateral roots emerged in 10 day old seedlings of WT (Fig. 5-27 A). The number of lateral roots were also counted for the 10 day old seedlings of AT5G47540 *mo25-1* (SALK_000304), *mo25-2* (SALK_076387), *mo25-3* (SAIL_513_B05), *mo25-4* (SAIL_1227_H04) and *mo25-5* (SALK_066597), and compared to Columbia *Col-0*. The data showed extreme reductions in the lateral root number (Fig. 5-28) and lateral root density (Fig. 5-29) in only *mo25-2* mutants.

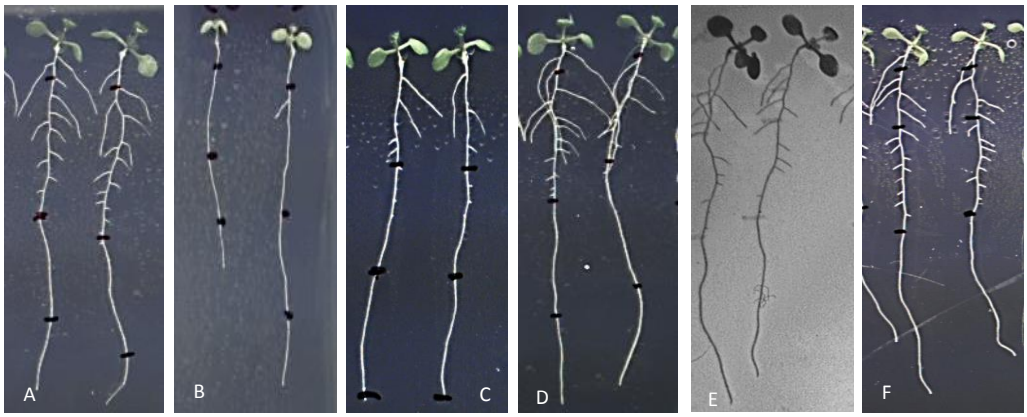

Figure 5-27: 10 day old seedlings of AT5G47540 mutants. A) WT (*Col-0*), B) *mo25-2* (SALK_076387), C) *mo25-3* (SAIL_513_B05), D) *mo25-4* (SAIL_1227_H04) and E) *mo25-5* (SALK_066597) and F) *mo25-1* (SALK_000304). The black marks used to follow seedlings growth.

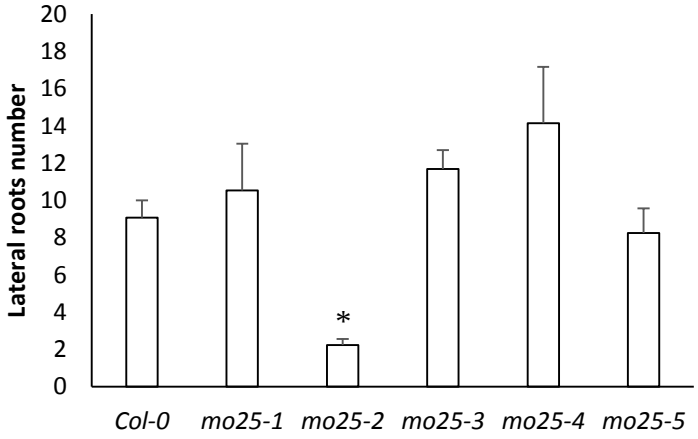

Figure 5-28: The lateral root number of 10 day old seedlings for AT5G47540 mutants. *mo25-1* (SALK_000304), *mo25-2* (SALK_076387), *mo25-3* (SAIL_513_B05), *mo25-4* (SAIL_1227_H04) and *mo25-5* (SALK_066597) compared with WT (*Col-0*). * denotes significant difference from WT ($P < 0.05$).

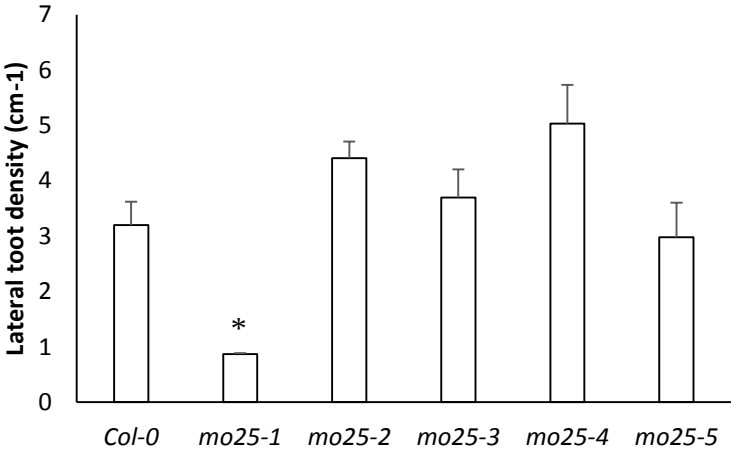

Figure 5-29: The lateral root density (cm^{-1}) of 10 day old seedlings, for AT5G47540 *mo25-1* (SALK_000304), *mo25-2* (SALK_076387), *mo25-3* (SAIL_513_B05), *mo25-4* (SAIL_1227_H04) and *mo25-5* (SALK_066597), compared with WT (*Col-0*). * denotes significant difference from WT ($P < 0.05$).

5.4.3.5 LATERAL ROOT NUMBER AND PRIMORDIUM DENSITY

In order to measure the differential lateral root development and the primordium density between *mo25-2* (SALK_076387) and *Col-0* (WT), 10 day old seedlings were cleared by gradiant concentrations of ethanol then loaded on slides. The numbers of roots at each of the 8 stages of lateral root development were counted under a Leica light microscope. The results showed a significant difference in lateral root density (Fig. 5-30) and the primordium density (Fig. 5-31).

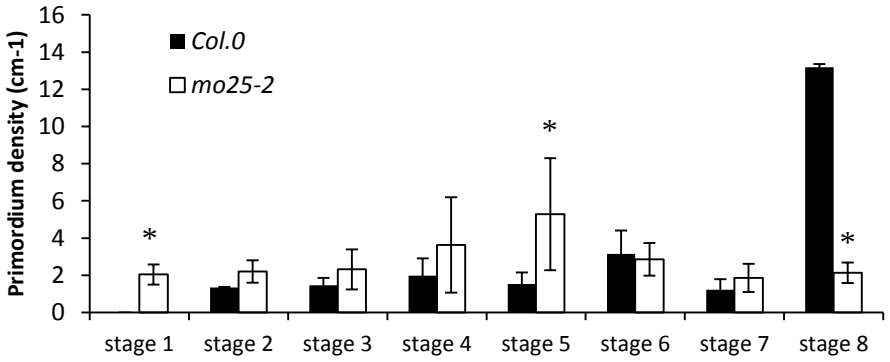

Figure 5-30: The density of different stages of the primordium for AT5G47540 *mo25-2* (SALK_076387), compared with WT (*Col-0*). * denotes significant difference from WT ($P < 0.05$).

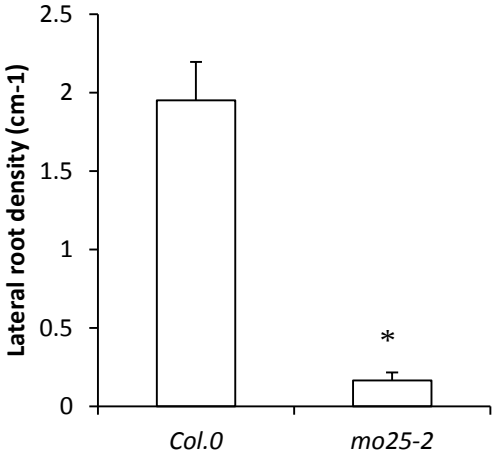

Figure 5-31: Total lateral root density of AT5G47540 *mo25-2* (SALK_076387), compared with WT (*Col-0*) * denotes significant difference from WT ($P < 0.05$).

5.4.3.6 BACKCROSSING OF *mo25-2*

Genotyping and phenotyping analysis of the five different T-DNA insertion lines of AT5G47540 showed that *mo25-2* had a strong phenotype in the primary root response to gravity and in the lateral root number. Conversely, the others did not show the same phenotype, despite that all of them were full knock out for *Mo25* as shown by QRT-PCR. Therefore *Col-0* and *mo25-2* were crossed to confirm the gene responsible for the strong phenotype.

Genotyping analysis of the first generation (F1) revealed that all seedlings were heterozygous for *mo25-2* (Fig. 5-32). None of the F1 seedlings displayed the previously described phenotype which means the mutation was not dominant. However, genotyping and phenotyping analysis of the F2 generation showed a segregation of the phenotype and genotype. 23.5% of 276 seedlings had fewer than 4 lateral roots. 7% of this group of 23.5% were homozygous for *Mo25*, whereas, 2.5% of them were WT for *Mo25* (Fig. 5-33).

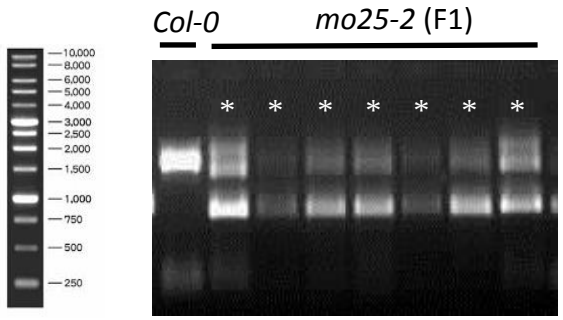

Figure 5-32: The F1 generation of *Col-0* X *mo25-2* (SALK_076387). By using genotyping primers (LP + RP (Product size = 1024bp) + LB (Product size= 490bp), all seedlings were generated to be heterozygous lines (1kB DNA ladder; *: Hetrozygous plants).

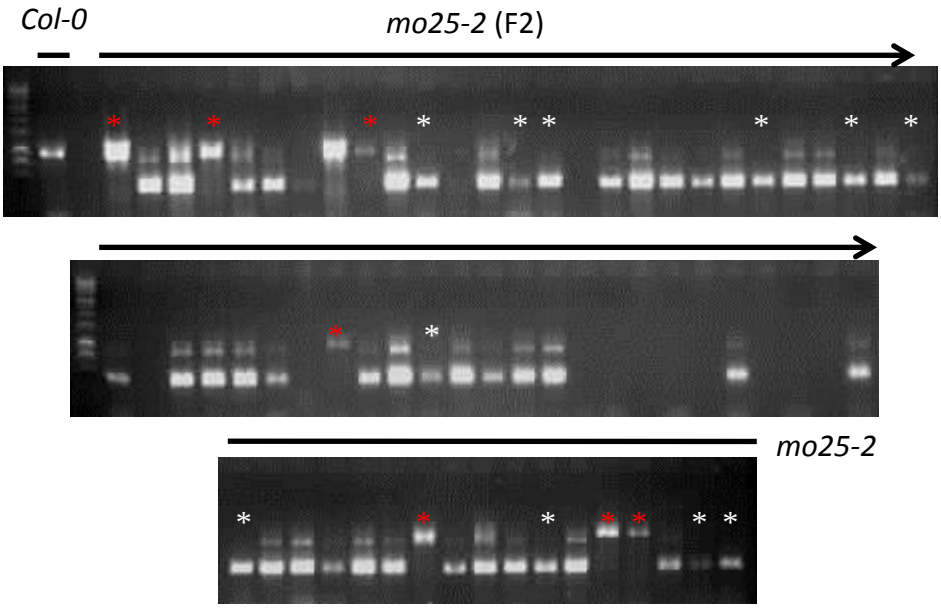

Figure 5-33: The F2 generation of *Col-0* X *mo25-2* (SALK_076387). By using genotyping primers (LP + RP (Product size = 1024bp) + LB (Product size= 490bp), 7% of the seedlings (with strong phenotype) were homozygous lines for *Mo25*(*), and 2.5% of the seedlings (with strong phenotype) were WT for *Mo25* (*).

5.5 DISCUSSION

Environmental signals can affect plant growth and development. Plants have the ability to develop efficient response systems to adapt their growth under the variety of surrounding biotic and abiotic stresses (Jackson and Overpeck, 2000, Yang et al., 2009, Hoson and Wakabayashi, 2015). Gravity is a unique, stable and reliable environmental vector that affects the direction of plant growth. In particular, gravity regulates and controls the growth of the primary root, and the overall root system architecture and expansion (Swarup et al., 2005, Baldwin et al., 2013, Bizzarri et al., 2014). In order to understand and characterise the different gravitropism pathways, a wealth of molecular and physiological experiments have been conducted .

In vascular plants, the response to gravity is divided into three stages: gravity perception (statolithes bodies in columella cells), gravitropic signal transduction (auxin transport) and gravitropic response (the root bending which occurs in the elongation zone) (Swarup and Bennett, 2009, Band et al., 2012, Swarup and Peret, 2012).The plant hormone auxin control the gravitropic growth response. For instance, the accumulation of auxin in the lower side of the elongation zone cells (Brunoud et al., 2012, Band et al., 2012) results in differential cell expansion which leads to bending of the root toward the direction of gravity. On top of this, auxin gradiant regulates the expression of downstream genes that control root gravitropism.

By following a reverse genetic approach, two candidate genes in *Arabidopsis* were reported by (Hijazi, 2013) to have functions during the plant response to gravity: *AT2G25900* (*TF*: a putative transcription factor) and *AT5G47540* (*Mo25:* putative Mo25-like protein). To examine this hypothesis, T-DNA insertions lines were selected for each gene to determine their functions. However, contrary to the earlier study (Hijazi, 2013), the results of genotyping and phenotyping additional alleles revealed that there was no significant change in root bending in response to gravity in all knock-out lines obtained.

Interestingly, one of the T-DNA lines of *Mo25* (*mo25-2*, SALK_076387) showed a strong phenotype in the lateral root number compared to WT (*Columbia*, *Col-0*). 10 day-old-seedlings had 0 to 2 emerged lateral roots, whereas in WT seedlings of the same age, 15 to 17 emerged lateral roots were observed. RT-PCR revealed that this and all other T-DNA lines of mo25 were full knock-outs, despite that only one of them showed a phenotype distinct from WT. Therefore, it can be assumed that there is another T-DNA insertion in the *mo25-2* line, and that this unknown T-DNA insertion might be responsible for the strong phenotype, or it act alongside *mo25-2* to produce this phenomenon.

To determine the unknown T-DNA insertion, backcrossing was carried out using Col-0 as a background. In the F1 generation, all seedlings had no phenotype which means that the mutation was not dominant. In the F2 generation, after phenotyping and genotyping the seedlings, the results showed that the *mo25* genotype and the lateral root phenotype did not co-segregate, indicating it was

likely that there was another mutation that might have been responsible for the phenotype.

In order to distinguish the position and the type of the additional mutation, Kanamycin primers (forward and reverse pairs, respectively: 5'-GAAGGCGATAGAAGGCGA-3' and 5'-CCAAATAATCTGCACCGG-3') had been designed and tested to identify if there is any additional T-DNA insertion in this line, in parallel with growing seeds on Kanamycin plates. The results showed that there was not an additional full T-DNA insertion in this line.

Although the phenotyping results clearly show that *mo25-2* has an interesting phenotype, the cause of this phenotype remains unresolved. The mutation in *Mo25* is not responsible for the appearance of these seedlings. This suggests that the genomic DNA of the subsequent generation of the both lines (*mo25-2* and Mo25-WT) needs to be sequenced to determine the molecular basis of this phenotype. Thermal asymmetric interlaced polymerase chain reaction (TAIL-PCR) is an important technique that can be used to determined unknown flanked insertion sites by known DNA sequence in Arabidopsis (Liu and Chen, 2007, Singer and Burke, 2003). Moreover, Southern blot is another molecular method to detect a specific DNA sequence in a complex mixture of DNA samples by probe hybridization (Brown, 2001).

SUMMARY AND CONCLUSION

6.1 SUMMARY

Variations in climate, such as temperature, drought, salinity, rainfall, light intensity, carbon emission, plus other factors, have an enormous impact on every aspect of the life of plants. Plants have the ability to adapt their growth and development in response to environmental conditions by modifying shoot or root systems (Kazan, 2013).

Plants modify their lateral root architecture according to the availability of water and nutrients (Zhao et al., 2014, Bao et al., 2014). However, the molecular mechanisms controlling such adaptive responses are not currently clear. In this thesis, I describe two kinase genes (*AT2G15300; LRK1* and *AT4G3422; LRK2*) that control lateral root initiation and development. Transcriptional and translational GFP fusion lines for these kinases genes reveal their expression patterns in the root endodermis around the initiation site of the new lateral root. This suggests that *LRK1* and *LRK2* expression patterns may control lateral root development indirectly. Since lateral roots originate from pericycle cells.

Indeed, endodermal cells accomodate the volume increase of the pericycle lateral root founder cells during its specification. The volume exchange between cells is regulated partly by the opening and closing of the plasmodesmata (Vermeer and Geldner, 2015). *LRK1* and *LRK2* are expressed in a puncture pattern in endodermal cells, suggesting they may be localized to plasmodesmata.

The root endodermis also contains the Casparian strip which consists of lignin, which needs to be broken during lateral root emergence. The auxin influx carrier

LAX3 was determined to function in regulating the expression of several cell-wall remodelling enzymes (CWR) in cortical and endodermal cells during the development of lateral root primordia (Swarup et al., 2008). Crossing *lrk1* and *lrk2* lines with *lax3* and other CWR mutants lines may help in investigating the actual role of these two kinases during the lateral root emergence process.

Preliminary phenotypic assays observed that environmental conditions significantly affect the phenotype of knock-out lines for these two kinases. By applying different abiotic stresses to the mutant lines of these genes may help increase our understanding of the functions of the kinase genes during LR development. For instance, water availability influences root branching and lateral root position by a mechanism known by hydroatterning (Bao et al., 2014). The lack of water also can affect cell osmolarity and volume (Madhusudhan et al., 1995). Therefore, growing plants under different drought conditions may enrich our understanding of the molecular basis of these kinases in controlling lateral root development. In addition, isolating and characterising new alleles in both two kinases genes (*LRK1* and *LRK2*) can provide more information to validate the role of these kinases in regulating lateral root initiation and emergence.

Plants can also adjust their physiological processes in response to the environment. For instance they can increase or decrease the rate of photosynthesis and metabolic processes under abiotic stresses. In many instances, environmental signals critically influence hormone response and

molecular pathways to modify plant growth and development (Pauli et al., 2012, Bellard et al., 2012, Reusch, 2014, Trenberth et al., 2014).

The plant hormone auxin, along with other hormones like cytokinin, gibberellins, ethylene and abscisic acid, represent important regulators of plant growth and adaptation. Auxin (indole-3-acetic acid, IAA) is considered to be the key controller of almost every aspect of plant growth and development (Miransari and Smith, 2014, Colebrook et al., 2014). Like all important signals, it is important to maintain a suitable auxin level in plant cells. This is performed using homeostatic mechanisms controlling auxin synthesis, transport, conjugation and degradation pathways (Ljung, 2013, Mellor et al., 2016).

Most studies on this phytohormone have focused on the genetic mechanisms which regulate auxin synthesis and transport. As a result of the preoccupation of the field with these aspects of auxin biology, auxin oxidation and conjugation pathways have been understudied (Porco et al., 2016).

Very recently, two genes encoding *DIOXYGENASE FOR AUXIN OXIDATION* 1 and 2 (*AT1G14130* and *AT1G14120* (*AtDAO1* and *AtDAO2*)) were identified to function in catalysing the oxidation of IAA to oxIAA in the model plant *Arabidopsis thaliana* (Porco et al., 2016, Mellor et al., 2016). Using reverse genetic approaches, one of these two genes (*AT1G14130* (*AtDAO1*) was studied in this thesis in order to determine any phenotypic changes in the loss-of function lines. This revealed that *dao1* knock-out lines (*dao1-1* and *dao1-3*) exhibited longer root hairs (~80%) compared with wild type. The abundance of the auxin inducible basic helix-loop-helix transcription factor RSL4 in the *dao1* loss of

function lines was significantly higher in agreement with multicellular model simulation (Mellor et al., 2016).

Metabolic profiling data showed that the knock-out line (*dao1-1*) had a significant reduction in the oxidation of IAA. In contrast, it has extremely high concentrations of IAA conjugates IAA-Asp and IAA-Glu (Fig. 1-10), amino acid conjugates controlled by Gretchen Hagen3s (*GH3*). Moreover, *GH3.3* expression level was higher in *dao1-1* compared with the wildtype (Porco et al., 2016). The mRNA expresstion levels of *DAO1* and *GH3.3* increased in response to auxin concentration over different timescales (Mellor et al., 2016). Crossing *dao1-1* and *gh3.3* mutant lines (in progress) may help increase our knowledge of the homeostasis mechanisms in IAA conjugation pathways and reveal a stronger root phenotype.

In addition, generating lines using auxin response markers such as DR5 and an auxin biosensor (DII-Venus) could reveal the auxin levels in different root tissues (Brunoud et al., 2012). Furthermore, crossing *dao1-1* with CYCB1:1:GFP (reporters were expressed in the dividing pericycle cells) and WAVE131:YFP (yellow fluorescent protein (YFP) plasma membrane marker) would help in biological experiments seeking to determine the rate of cell division and cell expansion in loss of function as well as overexpressing lines (Marhavý et al., 2016).

Using more advanced molecular tools such as Clustered regularly interspaced short palindromic repeats (CRISPR-Cas9) to knock-out both *AtDAO1* and *AtDAO2* genes and RNA interference (artificial microRNA) to silence *AtDAO1*

and *AtDAO2* may provide more information about the importance of these two genes in the IAA oxidation pathway (Zhang et al., 2016), taking into consideration the difference in regulation of both genes.

6.1 CONCLUSIONS

To conclude, by using a reverse genetic approach, this study revealed that the following genes have functions during plant growth and development:

- Dioxygenase for auxin oxidation 1 (*AtDAO1; AT1G14130),* a novel gene which regulates auxin degradation in *Arabidopsis thaliana.*
- Putative leucine-rich repeat protein kinase-like proteins (*LRK1: AT2G15300* and *LRK2: AT4G3422*) that function during lateral root initiation and/or development.

These results provide information that may also present an important opportunity to increase our knowledge of auxin degradation and conjugation pathways, lateral root initation and development which may be of benefit for the improvement of other plants technology, productivity and in the conservation of crop genetics researches.

REFERENCES

REFERENCES

. Available: http://www.arabidopsis.org/portals/education/aboutarabidopsis.jsp [Accessed].

2000. *Analysis of the genome sequence of the flowering plant Arabidopsis thaliana* [Online]. Macmillian Magazines Ltd. Available: http://dx.doi.org/10.1038/35048692 [Accessed 6814 408].

2016. *"TAIR - Home Page". Arabidopsis.org.* [Online]. Available: Web. 22 Sept. 2016. [Accessed].

ABEL, S. & THEOLOGIS, A. 2010. Odyssey of auxin. *Cold Spring Harb Perspect Biol,* 2**,** a004572.

ATKINSON, J. A., RASMUSSEN, A., TRAINI, R., VOSS, U., STURROCK, C., MOONEY, S. J., WELLS, D. M. & BENNETT, M. J. 2014. Branching out in roots: uncovering form, function, and regulation. *Plant Physiol,* 166**,** 538-50.

AUBRY-HIVET, D., NZIENGUI, H., RAPP, K., OLIVEIRA, O., PAPONOV, I. A., LI, Y., HAUSLAGE, J., VAGT, N., BRAUN, M., DITENGOU, F. A., DOVZHENKO, A. & PALME, K. 2014. Analysis of gene expression during parabolic flights reveals distinct early gravity responses in Arabidopsis roots. *Plant Biol (Stuttg),* 16 Suppl 1**,** 129-41.

BALDWIN, K. L., STROHM, A. K. & MASSON, P. H. 2013. Gravity sensing and signal transduction in vascular plant primary roots. *Am J Bot,* 100**,** 126-42.

BALUŠKA, F., MANCUSO, S., VOLKMANN, D. & BARLOW, P. W. 2010. Root apex transition zone: a signalling–response nexus in the root. *Trends in Plant Science,* 15**,** 402-408.

BAND, L. R., WELLS, D. M., FOZARD, J. A., GHETIU, T., FRENCH, A. P., POUND, M. P., WILSON, M. H., YU, L., LI, W., HIJAZI, H. I., OH, J., PEARCE, S. P., PEREZ-AMADOR, M. A., YUN, J., KRAMER, E., ALONSO, J. M., GODIN, C., VERNOUX, T., HODGMAN, T. C., PRIDMORE, T. P., SWARUP, R., KING, J. R. & BENNETT, M. J. 2014. Systems analysis of auxin transport in the Arabidopsis root apex. *Plant Cell,* 26**,** 862-75.

BAND, L. R., WELLS, D. M., LARRIEU, A., SUN, J., MIDDLETON, A. M., FRENCH, A. P., BRUNOUD, G., SATO, E. M., WILSON, M. H., PERET, B., OLIVA, M., SWARUP, R., SAIRANEN, I., PARRY, G., LJUNG, K., BEECKMAN, T., GARIBALDI, J. M., ESTELLE, M., OWEN, M. R., VISSENBERG, K., HODGMAN, T. C., PRIDMORE, T. P., KING, J. R., VERNOUX, T. & BENNETT, M. J. 2012. Root

gravitropism is regulated by a transient lateral auxin gradient controlled by a tipping-point mechanism. *Proc Natl Acad Sci U S A,* 109**,** 4668-73.

BAO, Y., AGGARWAL, P., ROBBINS, N. E., 2ND, STURROCK, C. J., THOMPSON, M. C., TAN, H. Q., THAM, C., DUAN, L., RODRIGUEZ, P. L., VERNOUX, T., MOONEY, S. J., BENNETT, M. J. & DINNENY, J. R. 2014. Plant roots use a patterning mechanism to position lateral root branches toward available water. *Proc Natl Acad Sci U S A,* 111**,** 9319-24.

BARBEZ, E., KUBES, M., ROLCIK, J., BEZIAT, C., PENCIK, A., WANG, B., ROSQUETE, M. R., ZHU, J., DOBREV, P. I., LEE, Y., ZAZIMALOVA, E., PETRASEK, J., GEISLER, M., FRIML, J. & KLEINE-VEHN, J. 2012. A novel putative auxin carrier family regulates intracellular auxin homeostasis in plants. *Nature,* 485**,** 119-22.

BAREJA, B. G. 2011. The Plant Root System Distinguished from the Shoot, Its Functions.

BARI, R. & JONES, J. D. 2009. Role of plant hormones in plant defence responses. *Plant Mol Biol,* 69**,** 473-88.

BEECKMAN, T., BURSSENS, S. & INZÉ, D. 2001. The peri-cell-cycle in Arabidopsis. *Journal of Experimental Botany,* 52**,** 403-411.

BEHRINGER, C. & SCHWECHHEIMER, C. 2015. B-GATA transcription factors - insights into their structure, regulation, and role in plant development. *Front Plant Sci,* 6**,** 90.

BELLARD, C., BERTELSMEIER, C., LEADLEY, P., THUILLER, W. & COURCHAMP, F. 2012. Impacts of climate change on the future of biodiversity. *Ecol Lett,* 15**,** 365-77.

BENGOUGH, A. G., LOADES, K. & MCKENZIE, B. M. 2016. Root hairs aid soil penetration by anchoring the root surface to pore walls. *Journal of Experimental Botany*.

BENNETT, M. J., MARCHANT, A., GREEN, H. G., MAY, S. T., WARD, S. P., MILLNER, P. A., WALKER, A. R., SCHULZ, B. & FELDMANN, K. A. 1996. Arabidopsis AUX1 gene: a permease-like regulator of root gravitropism. *Science,* 273**,** 948-50.

BENT, A. F. 2000. Arabidopsis in Planta Transformation. Uses, Mechanisms, and Prospects for Transformation of Other Species. *Plant Physiology,* 124**,** 1540-1547.

BEVAN, M. & WALSH, S. 2006. *4 The Arabidopsis Genome: A Foundation for Plant Research.*

BHALERAO, R. P., EKLOF, J., LJUNG, K., MARCHANT, A., BENNETT, M. & SANDBERG, G. 2002. Shoot-derived auxin is essential for early lateral root emergence in Arabidopsis seedlings. *Plant J,* 29**,** 325-32.

BIRNBAUM, K., SHASHA, D. E., WANG, J. Y., JUNG, J. W., LAMBERT, G. M., GALBRAITH, D. W. & BENFEY, P. N. 2003. A gene expression map of the Arabidopsis root. *Science,* 302**,** 1956-60.

BIZZARRI, M., CUCINA, A., PALOMBO, A. & MASIELLO, M. G. 2014. Gravity sensing by cells: mechanisms and theoretical grounds. *Rendiconti Lincei,* 25**,** 29-38.

BLANCAFLOR, E. B. 2013. Regulation of plant gravity sensing and signaling by the actin cytoskeleton. *Am J Bot,* 100**,** 143-52.

BORTESI, L. & FISCHER, R. 2015. The CRISPR/Cas9 system for plant genome editing and beyond. *Biotechnology Advances,* 33**,** 41-52.

BROWN, T. 2001. Southern blotting. *Curr Protoc Immunol,* Chapter 10**,** Unit 10.6A.

BRUNOUD, G., WELLS, D. M., OLIVA, M., LARRIEU, A., MIRABET, V., BURROW, A. H., BEECKMAN, T., KEPINSKI, S., TRAAS, J., BENNETT, M. J. & VERNOUX, T. 2012. A novel sensor to map auxin response and distribution at high spatio-temporal resolution. *Nature,* 482**,** 103-6.

BUTLER, E. D. & GALLAGHER, T. F. 2000. Characterization of auxin-induced ARRO-1 expression in the primary root of Malus domestica. *J Exp Bot,* 51**,** 1765-6.

CAMEHL, I., SHERAMETI, I., VENUS, Y., BETHKE, G., VARMA, A., LEE, J. & OELMULLER, R. 2010. Ethylene signalling and ethylene-targeted transcription factors are required to balance beneficial and nonbeneficial traits in the symbiosis between the endophytic fungus Piriformospora indica and Arabidopsis thaliana. *New Phytol,* 185**,** 1062-73.

CARNEIRO, J. M. T., MADRID, K. C., MACIEL, B. C. M. & ARRUDA, M. A. Z. 2015. Arabidopsis thaliana and omics approaches: a review. *Journal of Integrated OMICS,* 5.

CHAI, G., HU, R., ZHANG, D., QI, G., ZUO, R., CAO, Y., CHEN, P., KONG, Y. & ZHOU, G. 2012. Comprehensive analysis of CCCH zinc finger family in poplar (Populus trichocarpa). *BMC Genomics,* 13.

CHEN, R., ROSEN, E. & MASSON, P. H. 1999. Gravitropism in Higher Plants. *Plant Physiology,* 120**,** 343-350.

CHOI, J., CHOI, D., LEE, S., RYU, C. M. & HWANG, I. 2011. Cytokinins and plant immunity: old foes or new friends? *Trends Plant Sci,* 16**,** 388-94.

COLEBROOK, E. H., THOMAS, S. G., PHILLIPS, A. L. & HEDDEN, P. 2014. The role of gibberellin signalling in plant responses to abiotic stress. *The Journal of Experimental Biology*, 217**,** 67-75.

DAHLKE, R. I., LUETHEN, H. & STEFFENS, B. 2010. ABP1. *Plant Signaling & Behavior,* 5**,** 1-3.

DAL BOSCO, C., DOVZHENKO, A., LIU, X., WOERNER, N., RENSCH, T., EISMANN, M., EIMER, S., HEGERMANN, J., PAPONOV, I. A., RUPERTI, B., HEBERLE-BORS, E., TOURAEV, A., COHEN, J. D. & PALME, K. 2012. The endoplasmic reticulum localized PIN8 is a pollen-specific auxin carrier involved in intracellular auxin homeostasis. *Plant J,* 71**,** 860-70.

DATTA, S., KIM, C. M., PERNAS, M., PIRES, N. D., PROUST, H., TAM, T., VIJAYAKUMAR, P. & DOLAN, L. 2011. Root hairs: development, growth and evolution at the plant-soil interface. *Plant and Soil,* 346**,** 1-14.

DE RYBEL, B., VASSILEVA, V., PARIZOT, B., DEMEULENAERE, M., GRUNEWALD, W., AUDENAERT, D., VAN CAMPENHOUT, J., OVERVOORDE, P., JANSEN, L., VANNESTE, S., MOLLER, B., WILSON, M., HOLMAN, T., VAN ISTERDAEL, G., BRUNOUD, G., VUYLSTEKE, M., VERNOUX, T., DE VEYLDER, L., INZE, D., WEIJERS, D., BENNETT, M. J. & BEECKMAN, T. 2010. A novel aux/IAA28 signaling cascade activates GATA23-dependent specification of lateral root founder cell identity. *Curr Biol,* 20**,** 1697-706.

DE SMET, I. 2012. Lateral root initiation: one step at a time. *New Phytologist,* 193**,** 867-873.

DE SMET, I., LAU, S., MAYER, U. & JÜRGENS, G. 2010. Embryogenesis – the humble beginnings of plant life. *The Plant Journal,* 61**,** 959-970.

DE SMET, I., TETSUMURA, T., DE RYBEL, B., FREI DIT FREY, N., LAPLAZE, L., CASIMIRO, I., SWARUP, R., NAUDTS, M., VANNESTE, S., AUDENAERT, D., INZE, D., BENNETT, M. J. & BEECKMAN, T. 2007. Auxin-dependent regulation of lateral root positioning in the basal meristem of Arabidopsis. *Development,* 134**,** 681-90.

DEMEULENAERE, M. J. F. & BEECKMAN, T. 2014. The Interplay Between Auxin and the Cell Cycle During Plant Development. *In:*

ZAŽÍMALOVÁ, E., PETRÁŠEK, J. & BENKOVÁ, E. (eds.) *Auxin and Its Role in Plant Development.* Vienna: Springer Vienna.

DING, Z., WANG, B., MORENO, I., DUPLAKOVA, N., SIMON, S., CARRARO, N., REEMMER, J., PENCIK, A., CHEN, X., TEJOS, R., SKUPA, P., POLLMANN, S., MRAVEC, J., PETRASEK, J., ZAZIMALOVA, E., HONYS, D., ROLCIK, J., MURPHY, A., ORELLANA, A., GEISLER, M. & FRIML, J. 2012. ER-localized auxin transporter PIN8 regulates auxin homeostasis and male gametophyte development in Arabidopsis. *Nat Commun,* 3**,** 941.

DITENGOU, F. A., TEALE, W. D., KOCHERSPERGER, P., FLITTNER, K. A., KNEUPER, I., VAN DER GRAAFF, E., NZIENGUI, H., PINOSA, F., LI, X., NITSCHKE, R., LAUX, T. & PALME, K. 2008. Mechanical induction of lateral root initiation in Arabidopsis thaliana. *Proc Natl Acad Sci U S A,* 105**,** 18818-23.

DOLAN, L., JANMAAT, K., WILLEMSEN, V., LINSTEAD, P., POETHIG, S., ROBERTS, K. & SCHERES, B. 1993. Cellular organisation of the Arabidopsis thaliana root. *Development,* 119**,** 71-84.

DUBROVSKY, J. G. & FORDE, B. G. 2012. Quantitative analysis of lateral root development: pitfalls and how to avoid them. *Plant Cell,* 24**,** 4-14.

DUBROVSKY, J. G., GAMBETTA, G. A., HERNANDEZ-BARRERA, A., SHISHKOVA, S. & GONZALEZ, I. 2006. Lateral root initiation in Arabidopsis: developmental window, spatial patterning, density and predictability. *Ann Bot,* 97**,** 903-15.

DUBROVSKY, J. G., NAPSUCIALY-MENDIVIL, S., DUCLERCQ, J., CHENG, Y., SHISHKOVA, S., IVANCHENKO, M. G., FRIML, J., MURPHY, A. S. & BENKOVA, E. 2011. Auxin minimum defines a developmental window for lateral root initiation. *New Phytol,* 191**,** 970-83.

DUBROVSKY, J. G., SOUKUP, A., NAPSUCIALY-MENDIVIL, S., JEKNIĆ, Z. & IVANCHENKO, M. G. 2009. The lateral root initiation index: an integrative measure of primordium formation. *Annals of Botany*.

ELDA, Y., CYTRYN, E., MELLER HAREL, Y., LEW, B. & GRABER, E. R. 2012. *The biochar effect: plant resistance to biotic stresses*.

FELDMAN, L. J. 1985. Root gravitropism. *Physiologia Plantarum,* 65**,** 341-344.

FINKELSTEIN, R. 2013. Abscisic Acid Synthesis and Response. *Arabidopsis Book,* 11.

FRANKLIN, K. A., LEE, S. H., PATEL, D., KUMAR, S. V., SPARTZ, A. K., GU, C., YE, S., YU, P., BREEN, G., COHEN, J. D., WIGGE, P. A. & GRAY, W. M. 2011. PHYTOCHROME-INTERACTING FACTOR 4 (PIF4) regulates auxin biosynthesis at high temperature. *Proceedings of the National Academy of Sciences,* 108**,** 20231-20235.

FRIML, J., VIETEN, A., SAUER, M., WEIJERS, D., SCHWARZ, H., HAMANN, T., OFFRINGA, R. & JURGENS, G. 2003. Efflux-dependent auxin gradients establish the apical-basal axis of Arabidopsis. *Nature,* 426**,** 147-53.

GAO, X. H., XIAO, S. L., YAO, Q. F., WANG, Y. J. & FU, X. D. 2011. An updated GA signaling 'relief of repression' regulatory model. *Mol Plant,* 4**,** 601-6.

GEISLER, M., WANG, B. & ZHU, J. 2014. Auxin transport during root gravitropism: transporters and techniques. *Plant Biol (Stuttg),* 16 Suppl 1**,** 50-7.

GIFFORD, M. L., DEAN, A., GUTIERREZ, R. A., CORUZZI, G. M. & BIRNBAUM, K. D. 2008. Cell-specific nitrogen responses mediate developmental plasticity. *Proceedings of the National Academy of Sciences,* 105**,** 803-808.

GOH, T., KASAHARA, H., MIMURA, T., KAMIYA, Y. & FUKAKI, H. 2012. Multiple AUX/IAA-ARF modules regulate lateral root formation: the role of Arabidopsis SHY2/IAA3-mediated auxin signalling. *Philos Trans R Soc Lond B Biol Sci,* 367**,** 1461-8.

GOMEZ-GOMEZ, L., BAUER, Z. & BOLLER, T. 2001. Both the extracellular leucine-rich repeat domain and the kinase activity of FSL2 are required for flagellin binding and signaling in Arabidopsis. *Plant Cell,* 13**,** 1155-63.

GOMEZ-GOMEZ, L. & BOLLER, T. 2000. FLS2: an LRR receptor-like kinase involved in the perception of the bacterial elicitor flagellin in Arabidopsis. *Mol Cell,* 5**,** 1003-11.

GRIERSON, C., NIELSEN, E., KETELAARC, T. & SCHIEFELBEIN, J. 2014. Root hairs. *Arabidopsis Book,* 12**,** e0172.

GUYOMARC'H, S., LERAN, S., AUZON-CAPE, M., PERRINE-WALKER, F., LUCAS, M. & LAPLAZE, L. 2012. Early development and gravitropic response of lateral roots in Arabidopsis thaliana. *Philos Trans R Soc Lond B Biol Sci,* 367**,** 1509-16.

HA, S., VANKOVA, R., YAMAGUCHI-SHINOZAKI, K., SHINOZAKI, K. & TRAN, L. S. 2012. Cytokinins: metabolism and function in plant adaptation to environmental stresses. *Trends Plant Sci,* 17**,** 172-9.

HABETS, M. E. & OFFRINGA, R. 2014. PIN-driven polar auxin transport in plant developmental plasticity: a key target for environmental and endogenous signals. *New Phytol,* 203**,** 362-77.

HASHIGUCHI, T., SAKAKIBARA, Y., HARA, Y., SHIMOHIRA, T., KUROGI, K., AKASHI, R., LIU, M. C. & SUIKO, M. 2013. Identification and characterization of a novel kaempferol sulfotransferase from Arabidopsis thaliana. *Biochem Biophys Res Commun,* 434**,** 829-35.

HAVENS, K. A., GUSEMAN, J. M., JANG, S. S., PIERRE-JEROME, E., BOLTEN, N., KLAVINS, E. & NEMHAUSER, J. L. 2012. A synthetic approach reveals extensive tunability of auxin signaling. *Plant Physiol,* 160**,** 135-42.

HERRANZ, R. & MEDINA, F. J. 2014. Cell proliferation and plant development under novel altered gravity environments. *Plant Biol (Stuttg),* 16 Suppl 1**,** 23-30.

HIJAZI, H. 2013. *MOLECULAR CHARACTERISATION OF ROOT GRAVITROPISM IN Arabidopsis thaliana.* PhD, the university of Nottingham.

HOLMAN, T. J., WILSON, M. H., KENOBI, K., DRYDEN, I. L., HODGMAN, T. C., WOOD, A. T. & HOLDSWORTH, M. J. 2010. Statistical evaluation of transcriptomic data generated using the Affymetrix one-cycle, two-cycle and IVT-Express RNA labelling protocols with the Arabidopsis ATH1 microarray. *Plant Methods,* 6**,** 9.

HOSON, T. & WAKABAYASHI, K. 2015. Role of the plant cell wall in gravity resistance. *Phytochemistry,* 112**,** 84-90.

HOU, G., KRAMER, V. L., WANG, Y. S., CHEN, R., PERBAL, G., GILROY, S. & BLANCAFLOR, E. B. 2004. The promotion of gravitropism in Arabidopsis roots upon actin disruption is coupled with the extended alkalinization of the columella cytoplasm and a persistent lateral auxin gradient. *Plant J,* 39**,** 113-25.

IQBAL, RAHAT NAZAR, M. IQBAL R. KHAN, AND, A. M. & KHAN, N. A. 2011. Role of gibberellins in regulation of source–

sink relations under optimal and limiting

environmental conditions. *CURRENT SCIENCE,* 100**,** 10.

JACKSON, S. T. & OVERPECK, J. T. 2000. Responses of plant populations and communities to environmental changes of the late Quaternary. *Paleobiology,* 26**,** 194-220.

JAILLAIS, Y. & CHORY, J. 2010. Unraveling the paradoxes of plant hormone signaling integration. *Nat Struct Mol Biol,* 17**,** 642-5.

JANSEN, L., RYBEL, B. D., VASSILEVA, V. & BEECKMAN, T. 2009. *Root Development,* Springer Berlin Heidelberg.

JONES, M. A., RAYMOND, M. J. & SMIRNOFF, N. 2006. Analysis of the root-hair morphogenesis transcriptome reveals the molecular identity of six genes with roles in root-hair development in Arabidopsis. *The Plant Journal,* 45**,** 83-100.

KANAI, M., KUME, K., MIYAHARA, K., SAKAI, K., NAKAMURA, K., LEONHARD, K., WILEY, D. J., VERDE, F., TODA, T. & HIRATA, D. 2005. Fission yeast MO25 protein is localized at SPB and septum and is essential for cell morphogenesis. *EMBO J,* 24**,** 3012-25.

KANEDA, M., SCHUETZ, M., LIN, B., CHANIS, C., HAMBERGER, B., WESTERN, T., EHLTING, J. & SAMUELS, A. 2011. ABC transporters coordinately expressed during lignification of Arabidopsis stems include a set of ABCBs associated with auxin transport. *J Exp Bot,* 62**,** 2063-77.

KANNO, Y., JIKUMARU, Y., HANADA, A., NAMBARA, E., ABRAMS, S. R., KAMIYA, Y. & SEO, M. 2010. Comprehensive hormone profiling in developing Arabidopsis seeds: examination of the site of ABA biosynthesis, ABA transport and hormone interactions. *Plant Cell Physiol,* 51**,** 1988-2001.

KAZAN, K. 2013. Auxin and the integration of environmental signals into plant root development. *Annals of Botany*.

KEYES, S. D., DALY, K. R., GOSTLING, N. J., JONES, D. L., TALBOYS, P., PINZER, B. R., BOARDMAN, R., SINCLAIR, I., MARCHANT, A. & ROOSE, T. 2013. High resolution synchrotron imaging of wheat root hairs growing in soil and image based modelling of phosphate uptake. *New Phytol,* 198**,** 1023-9.

KHRAIWESH, B., ZHU, J. K. & ZHU, J. 2012. Role of miRNAs and siRNAs in biotic and abiotic stress responses of plants. *Biochim Biophys Acta,* 1819**,** 137-48.

KISS, J. Z., MILLER, K. M., OGDEN, L. A. & ROTH, K. K. 2002. Phototropism and Gravitropism in Lateral Roots of Arabidopsis. *Plant and Cell Physiology,* 43**,** 35-43.

KLEINE-VEHN, J., DING, Z., JONES, A. R., TASAKA, M., MORITA, M. T. & FRIML, J. 2010. Gravity-induced PIN transcytosis for polarization of auxin fluxes in gravity-sensing root cells. *Proceedings of the National Academy of Sciences,* 107**,** 22344-22349.

KO, J. H., KIM, W. C. & HAN, K. H. 2009. Ectopic expression of MYB46 identifies transcriptional regulatory genes involved in secondary wall biosynthesis in Arabidopsis. *Plant J,* 60**,** 649-65.

KOMAKI, M. K., OKADA, K., NISHINO, E. & SHIMURA, Y. 1988. Isolation and characterization of novel mutants of Arabidopsis thaliana defective in flower development. *Development,* 104**,** 195-203.

KOORNNEEF, M. & MEINKE, D. 2010. The development of Arabidopsis as a model plant. *Plant J,* 61**,** 909-21.

KORASICK, D. A., ENDERS, T. A. & STRADER, L. C. 2013. Auxin biosynthesis and storage forms. *Journal of Experimental Botany*.

KRAMER, U. 2015. Planting molecular functions in an ecological context with Arabidopsis thaliana. *Elife,* 4.

LARRIEU, A. P. 2011. *Dissection of the auxin response pathway using functional and chemical genetics approaches.* PhD, The university of Nottingham.

LAVENUS, J., GOH, T., GUYOMARC'H, S., HILL, K., LUCAS, M., VOß, U., KENOBI, K., WILSON, M. H., FARCOT, E., HAGEN, G., GUILFOYLE, T. J., FUKAKI, H., LAPLAZE, L. & BENNETT, M. J. 2015. Inference of the Arabidopsis Lateral Root Gene Regulatory Network Suggests a Bifurcation Mechanism That Defines Primordia Flanking and Central Zones. *The Plant Cell*.

LAVENUS, J., GOH, T., ROBERTS, I., GUYOMARC'H, S., LUCAS, M., DE SMET, I., FUKAKI, H., BEECKMAN, T., BENNETT, M. & LAPLAZE, L. 2013. Lateral root development in Arabidopsis: fifty shades of auxin. *Trends Plant Sci,* 18**,** 450-8.

LEE, O. R. & CHO, M. 2014. Trafficking of ABCB-type Auxin Transporters. *In:* GEISLER, M. (ed.) *Plant ABC Transporters.* Cham: Springer International Publishing.

LEITNER, D., KLEPSCH, S., PTASHNYK, M., MARCHANT, A., KIRK, G. J., SCHNEPF, A. & ROOSE, T. 2010. A dynamic model of nutrient uptake by root hairs. *New Phytol,* 185**,** 792-802.

LEYSER, O. 2010. The Power of Auxin in Plants. *Plant Physiology,* 154**,** 501-505.

LI, D. X., CHEN, W. Q., XU, Z. H. & BAI, S. N. 2015. HISTONE DEACETYLASE6-Defective Mutants Show Increased Expression and Acetylation of ENHANCER OF TRIPTYCHON AND CAPRICE1 and GLABRA2 with Small But Significant Effects on Root Epidermis Cellular Pattern. *Plant Physiol,* 168**,** 1448-58.

LI, H., JOHNSON, P., STEPANOVA, A., ALONSO, J. M. & ECKER, J. R. 2004. Convergence of signaling of differential cell growth pathways in the control in Arabidopsis. *Developmental Cell,* 7**,** 193-204.

LIU, S., KHAN, M., LI, Y., ZHANG, J. & HU, C. 2014. Comprehensive analysis of CCCH-type zinc finger gene family in citrus (Clementine mandarin) by genome-wide characterization. *Mol Genet Genomics,* 289.

LIU, Y. G. & CHEN, Y. 2007. High-efficiency thermal asymmetric interlaced PCR for amplification of unknown flanking sequences. *Biotechniques,* 43**,** 649-50, 652, 654 passim.

LJUNG, K. 2013. Auxin metabolism and homeostasis during plant development. *Development,* 140**,** 943-50.

LUCAS, M., KENOBI, K., VON WANGENHEIM, D., VOBETA, U., SWARUP, K., DE SMET, I., VAN DAMME, D., LAWRENCE, T., PERET, B., MOSCARDI, E., BARBEAU, D., GODIN, C., SALT, D., GUYOMARC'H, S., STELZER, E. H., MAIZEL, A., LAPLAZE, L. & BENNETT, M. J. 2013. Lateral root morphogenesis is dependent on the mechanical properties of the overlaying tissues. *Proc Natl Acad Sci U S A,* 110**,** 5229-34.

LUDWIG-MULLER, J. 2011. Auxin conjugates: their role for plant development and in the evolution of land plants. *J Exp Bot,* 62**,** 1757-73.

MADHUSUDHAN, R., RAMACHANDRA RAO, S. & RAVISHANKAR, G. A. 1995. Osmolarity as a measure of growth of plant cells in suspension cultures. *Enzyme and Microbial Technology,* 17**,** 989-991.

MALAMY, J. E. & BENFEY, P. N. 1997. Organization and cell differentiation in lateral roots of Arabidopsis thaliana. *Development,* 124**,** 33-44.

MANO, Y. & NEMOTO, K. 2012. The pathway of auxin biosynthesis in plants. *J Exp Bot,* 63**,** 2853-72.

MARCHANT, A., BHALERAO, R., CASIMIRO, I., EKLÖF, J., CASERO, P. J., BENNETT, M. & SANDBERG, G. 2002. AUX1 Promotes Lateral Root Formation by Facilitating Indole-3-Acetic Acid Distribution between Sink and Source Tissues in the Arabidopsis Seedling. *The Plant Cell,* 14**,** 589-597.

MARHAVÝ, P., MONTESINOS, J. C., ABUZEINEH, A., VAN DAMME, D., VERMEER, J. E. M., DUCLERCQ, J., RAKUSOVÁ, H., NOVÁKOVÁ, P., FRIML, J., GELDNER, N. & BENKOVÁ, E. 2016. Targeted cell elimination reveals an auxin-guided biphasic mode of lateral root initiation. *Genes & Development,* 30**,** 471-483.

MARSHALL, A., AALEN, R. B., AUDENAERT, D., BEECKMAN, T., BROADLEY, M. R., BUTENKO, M. A., CANO-DELGADO, A. I., DE VRIES, S., DRESSELHAUS, T., FELIX, G., GRAHAM, N. S., FOULKES, J., GRANIER, C., GREB, T., GROSSNIKLAUS, U., HAMMOND, J. P., HEIDSTRA, R., HODGMAN, C., HOTHORN, M., INZE, D., OSTERGAARD, L., RUSSINOVA, E., SIMON, R., SKIRYCZ, A., STAHL, Y., ZIPFEL, C. & DE SMET, I. 2012. Tackling drought stress: receptor-like kinases present new approaches. *Plant Cell,* 24**,** 2262-78.

MASHIGUCHI, K., TANAKA, K., SAKAI, T., SUGAWARA, S., KAWAIDE, H., NATSUME, M., HANADA, A., YAENO, T., SHIRASU, K., YAO, H., MCSTEEN, P., ZHAO, Y., HAYASHI, K.-I., KAMIYA, Y. & KASAHARA, H. 2011. The main auxin biosynthesis pathway in Arabidopsis. *Proceedings of the National Academy of Sciences,* 108**,** 18512-18517.

MEINKE, D. W., CHERRY, J. M., DEAN, C., ROUNSLEY, S. D. & KOORNNEEF, M. 1998. Arabidopsis thaliana: a model plant for genome analysis. *Science,* 282**,** 662, 679-82.

MELLOR, N., BAND, L. R., PĚNČÍK, A., NOVÁK, O., RASHED, A., HOLMAN, T., WILSON, M. H., VOß, U., BISHOPP, A., KING, J. R., LJUNG, K., BENNETT, M. J. & OWEN, M. R. 2016. Dynamic regulation of auxin oxidase and conjugating enzymes AtDAO1 and GH3 modulates auxin homeostasis. *Proceedings of the National Academy of Sciences*.

MENDOZA, M., REDEMANN, S. & BRUNNER, D. 2005. The fission yeast MO25 protein functions in polar growth and cell separation. *Eur J Cell Biol,* 84**,** 915-26.

MEROZ, Y. & BASTIEN, R. 2014. Stochastic processes in gravitropism. *Front Plant Sci,* 5.

MIRANSARI, M. & SMITH, D. L. 2014. Plant hormones and seed germination. *Environmental and Experimental Botany,* 99**,** 110-121.

MORENO-RISUENO, M. A. & BENFEY, P. N. 2011. Time-based patterning in development: The role of oscillating gene expression. *Transcription,* 2**,** 124-129.

MORENO-RISUENO, M. A., VAN NORMAN, J. M., MORENO, A., ZHANG, J., AHNERT, S. E. & BENFEY, P. N. 2010. Oscillating gene expression determines competence for periodic Arabidopsis root branching. *Science,* 329**,** 1306-11.

MORILLO, S. A. & TAX, F. E. 2006. Functional analysis of receptor-like kinases in monocots and dicots. *Curr Opin Plant Biol,* 9**,** 460-9.

MORITA, M. T. 2010. Directional gravity sensing in gravitropism. *Annu Rev Plant Biol,* 61**,** 705-20.

MOULIA, B. & FOURNIER, M. 2009. The power and control of gravitropic movements in plants: a biomechanical and systems biology view. *J Exp Bot,* 60**,** 461-86.

NAKASHIMA, K., TAKASAKI, H., MIZOI, J., SHINOZAKI, K. & YAMAGUCHI-SHINOZAKI, K. 2012. NAC transcription factors in plant abiotic stress responses. *Biochim Biophys Acta,* 1819**,** 97-103.

NANAO, M. H., VINOS-POYO, T., BRUNOUD, G., THÉVENON, E., MAZZOLENI, M., MAST, D., LAINÉ, S., WANG, S., HAGEN, G., LI, H., GUILFOYLE, T. J., PARCY, F., VERNOUX, T. & DUMAS, R. 2014. Structural basis for oligomerization of auxin transcriptional regulators. *Nature Communications,* 5**,** 3617.

NGARA, R. & NDIMBA, B. K. 2014. Model plant systems in salinity and drought stress proteomics studies: a perspective on Arabidopsis and Sorghum. *Plant Biol (Stuttg),* 16**,** 1029-32.

NISHIYAMA, R., WATANABE, Y., FUJITA, Y., LE, D. T., KOJIMA, M., WERNER, T., VANKOVA, R., YAMAGUCHI-SHINOZAKI, K., SHINOZAKI, K., KAKIMOTO, T., SAKAKIBARA, H., SCHMULLING, T. & TRAN, L. S. 2011. Analysis of cytokinin mutants and regulation of cytokinin metabolic genes reveals important regulatory roles of cytokinins in drought, salt and abscisic acid responses, and abscisic acid biosynthesis. *Plant Cell,* 23**,** 2169-83.

NIU, Y., FIGUEROA, P. & BROWSE, J. 2011. Characterization of JAZ-interacting bHLH transcription factors that regulate jasmonate responses in Arabidopsis. *J Exp Bot,* 62**,** 2143-54.

OKUSHIMA, Y., FUKAKI, H., ONODA, M., THEOLOGIS, A. & TASAKA, M. 2007. ARF7 and ARF19 regulate lateral root formation via direct activation of LBD/ASL genes in Arabidopsis. *Plant Cell,* 19**,** 118-30.

OKUSHIMA, Y., OVERVOORDE, P. J., ARIMA, K., ALONSO, J. M., CHAN, A., CHANG, C., ECKER, J. R., HUGHES, B., LUI, A., NGUYEN, D., ONODERA, C., QUACH, H., SMITH, A., YU, G. & THEOLOGIS, A.

2005. Functional genomic analysis of the AUXIN RESPONSE FACTOR gene family members in Arabidopsis thaliana: unique and overlapping functions of ARF7 and ARF19. *Plant Cell,* 17**,** 444-63.

ORMAN-LIGEZA, B., PARIZOT, B., GANTET, P. P., BEECKMAN, T., BENNETT, M. J. & DRAYE, X. 2013. Post-embryonic root organogenesis in cereals: branching out from model plants. *Trends in Plant Science,* 18**,** 459-467.

OVERVOORDE, P., FUKAKI, H. & BEECKMAN, T. 2010. Auxin control of root development. *Cold Spring Harb Perspect Biol,* 2**,** a001537.

PACIOREK, T. & FRIML, J. 2006. Auxin signaling. *Journal of Cell Science,* 119**,** 1199-1202.

PAGE, D. R. & GROSSNIKLAUS, U. 2002. The art and design of genetic screens: Arabidopsis thaliana. *Nat Rev Genet,* 3**,** 124-36.

PAULI, H., GOTTFRIED, M., DULLINGER, S., ABDALADZE, O., AKHALKATSI, M., BENITO ALONSO, J. L., COLDEA, G., DICK, J., ERSCHBAMER, B., FERNANDEZ CALZADO, R., GHOSN, D., HOLTEN, J. I., KANKA, R., KAZAKIS, G., KOLLAR, J., LARSSON, P., MOISEEV, P., MOISEEV, D., MOLAU, U., MOLERO MESA, J., NAGY, L., PELINO, G., PUSCAS, M., ROSSI, G., STANISCI, A., SYVERHUSET, A. O., THEURILLAT, J. P., TOMASELLI, M., UNTERLUGGAUER, P., VILLAR, L., VITTOZ, P. & GRABHERR, G. 2012. Recent plant diversity changes on Europe's mountain summits. *Science,* 336**,** 353-5.

PELEG, Z. & BLUMWALD, E. 2011. Hormone balance and abiotic stress tolerance in crop plants. *Curr Opin Plant Biol,* 14**,** 290-5.

PĚNČÍK, A., SIMONOVIK, B., PETERSSON, S. V., HENYKOVÁ, E., SIMON, S., GREENHAM, K., ZHANG, Y., KOWALCZYK, M., ESTELLE, M., ZAŽÍMALOVÁ, E., NOVÁK, O., SANDBERG, G. & LJUNG, K. 2013. Regulation of Auxin Homeostasis and Gradients in Arabidopsis Roots through the Formation of the Indole-3-Acetic Acid Catabolite 2-Oxindole-3-Acetic Acid. *Plant Cell,* 25**,** 3858-70.

PENG, X., ZHAO, Y., CAO, J., ZHANG, W., JIANG, H., LI, X., MA, Q., ZHU, S. & CHENG, B. 2012. CCCH-type zinc finger family in maize: genome-wide identification, classification and expression profiling under abscisic acid and drought treatments. *PLoS One,* 7**,** e40120.

PERET, B., LARRIEU, A. & BENNETT, M. J. 2009. Lateral root emergence: a difficult birth. *J Exp Bot,* 60**,** 3637-43.

PERET, B., SWARUP, K., FERGUSON, A., SETH, M., YANG, Y., DHONDT, S., JAMES, N., CASIMIRO, I., PERRY, P., SYED, A., YANG, H., REEMMER, J., VENISON, E., HOWELLS, C., PEREZ-AMADOR, M. A., YUN, J., ALONSO, J., BEEMSTER, G. T., LAPLAZE, L., MURPHY, A., BENNETT, M. J., NIELSEN, E. & SWARUP, R. 2012. AUX/LAX genes encode a family of auxin influx transporters that perform distinct functions during Arabidopsis development. *Plant Cell,* 24**,** 2874-85.

PERNISOVA, M., PRAT, T., GRONES, P., HARUSTIAKOVA, D., MATONOHOVA, M., SPICHAL, L., NODZYNSKI, T., FRIML, J. & HEJATKO, J. 2016. Cytokinins influence root gravitropism via differential regulation of auxin transporter expression and localization in Arabidopsis. *New Phytol*.

PITAKSARINGKARN, W., MATSUOKA, K., ASAHINA, M., MIURA, K., SAGE-ONO, K., ONO, M., YOKOYAMA, R., NISHITANI, K., ISHII, T., IWAI, H. & SATOH, S. 2014. XTH20 and XTH19 regulated by ANAC071 under auxin flow are involved in cell proliferation in incised Arabidopsis inflorescence stems. *Plant J,* 80**,** 604-14.

POMERANZ, M. C., HAH, C., LIN, P. C., KANG, S. G., FINER, J. J., BLACKSHEAR, P. J. & JANG, J. C. 2010. The Arabidopsis tandem zinc finger protein AtTZF1 traffics between the nucleus and cytoplasmic foci and binds both DNA and RNA. *Plant Physiol,* 152**,** 151-65.

PORCO, S., PĚNČÍK, A., RASHED, A., VOß, U., CASANOVA-SÁEZ, R., BISHOPP, A., GOLEBIOWSKA, A., BHOSALE, R., SWARUP, R., SWARUP, K., PEŇÁKOVÁ, P., NOVÁK, O., STASWICK, P., HEDDEN, P., PHILLIPS, A. L., VISSENBERG, K., BENNETT, M. J. & LJUNG, K. 2016. Dioxygenase-encoding AtDAO1 gene controls IAA oxidation and homeostasis in Arabidopsis. *Proceedings of the National Academy of Sciences*.

PORRI, A., TORTI, S., ROMERA-BRANCHAT, M. & COUPLAND, G. 2012. Spatially distinct regulatory roles for gibberellins in the promotion of flowering of Arabidopsis under long photoperiods. *Development,* 139**,** 2198-209.

RAHMAN, A., TAKAHASHI, M., SHIBASAKI, K., WU, S., INABA, T., TSURUMI, S. & BASKIN, T. I. 2010. Gravitropism of Arabidopsis thaliana roots requires the polarization of PIN2 toward the root tip in meristematic cortical cells. *Plant Cell,* 22**,** 1762-76.

REUSCH, T. B. H. 2014. Climate change in the oceans: evolutionary versus phenotypically plastic responses of marine animals and plants. *Evol Appl,* 7**,** 104-22.

SAINI, S., SHARMA, I. & PATI, P. K. 2015. Versatile roles of brassinosteroid in plants in the context of its homoeostasis, signaling and crosstalks. *Front Plant Sci,* 6.

SALAZAR-HENAO, J. E., VÉLEZ-BERMÚDEZ, I. C. & SCHMIDT, W. 2016. The regulation and plasticity of root hair patterning and morphogenesis. *Development,* 143**,** 1848-1858.

SATO, E. M. 2013. *Molecular characterization of the auxin response during root gravitropism.* PhD, the university of Nottingham.

SATO, E. M., HIJAZI, H., BENNETT, M. J., VISSENBERG, K. & SWARUP, R. 2014. New insights into root gravitropic signalling. *Journal of Experimental Botany*.

SCHERES, B. & LASKOWSKI, M. 2016. Root patterning: it takes two to tangle. *Journal of Experimental Botany,* 67**,** 1201-1203.

SHIU, S. H. & BLEECKER, A. B. 2001. Receptor-like kinases from Arabidopsis form a monophyletic gene family related to animal receptor kinases. *Proc Natl Acad Sci U S A,* 98**,** 10763-8.

SHIU, S. H. & BLEECKER, A. B. 2003. Expansion of the receptor-like kinase/Pelle gene family and receptor-like proteins in Arabidopsis. *Plant Physiol,* 132**,** 530-43.

SIMON, S., SKUPA, P., VIAENE, T., ZWIEWKA, M., TEJOS, R., KLIMA, P., CARNA, M., ROLCIK, J., DE RYCKE, R., MORENO, I., DOBREV, P. I., ORELLANA, A., ZAZIMALOVA, E. & FRIML, J. 2016. PIN6 auxin transporter at endoplasmic reticulum and plasma membrane mediates auxin homeostasis and organogenesis in Arabidopsis. *New Phytol,* 211**,** 65-74.

SINGER, T. & BURKE, E. 2003. High-throughput TAIL-PCR as a tool to identify DNA flanking insertions. *Methods Mol Biol,* 236**,** 241-72.

SIRICHANDRA, C., DAVANTURE, M., TURK, B. E., ZIVY, M., VALOT, B., LEUNG, J. & MERLOT, S. 2010. The Arabidopsis ABA-activated kinase OST1 phosphorylates the bZIP transcription factor ABF3 and creates a 14-3-3 binding site involved in its turnover. *PLoS One,* 5**,** e13935.

SMIT, M. E. & WEIJERS, D. 2015. The role of auxin signaling in early embryo pattern formation. *Current Opinion in Plant Biology,* 28**,** 99-105.

SUN, J., JIANG, H., XU, Y., LI, H., WU, X., XIE, Q. & LI, C. 2007. The CCCH-type zinc finger proteins AtSZF1 and AtSZF2 regulate salt stress responses in Arabidopsis. *Plant Cell Physiol,* 48.

SUN, P., TIAN, Q. Y., CHEN, J. & ZHANG, W. H. 2010. Aluminium-induced inhibition of root elongation in Arabidopsis is mediated by ethylene and auxin. *J Exp Bot,* 61**,** 347-56.

SWARUP, K., BENKOVA, E., SWARUP, R., CASIMIRO, I., PERET, B., YANG, Y., PARRY, G., NIELSEN, E., DE SMET, I., VANNESTE, S., LEVESQUE, M. P., CARRIER, D., JAMES, N., CALVO, V., LJUNG, K., KRAMER, E., ROBERTS, R., GRAHAM, N., MARILLONNET, S., PATEL, K., JONES, J. D., TAYLOR, C. G., SCHACHTMAN, D. P., MAY, S., SANDBERG, G., BENFEY, P., FRIML, J., KERR, I., BEECKMAN, T., LAPLAZE, L. & BENNETT, M. J. 2008. The auxin influx carrier LAX3 promotes lateral root emergence. *Nat Cell Biol,* 10**,** 946-54.

SWARUP, R. & BENNETT, M. J. 2009. Root Gravitropism. *Annual Plant Reviews Volume 37: Root Development.* Wiley-Blackwell.

SWARUP, R., FRIML, J., MARCHANT, A., LJUNG, K., SANDBERG, G., PALME, K. & BENNETT, M. 2001. Localization of the auxin permease AUX1 suggests two functionally distinct hormone transport pathways operate in the Arabidopsis root apex. *Genes Dev,* 15**,** 2648-53.

SWARUP, R., KRAMER, E. M., PERRY, P., KNOX, K., LEYSER, H. M., HASELOFF, J., BEEMSTER, G. T., BHALERAO, R. & BENNETT, M. J. 2005. Root gravitropism requires lateral root cap and epidermal cells for transport and response to a mobile auxin signal. *Nat Cell Biol,* 7**,** 1057-65.

SWARUP, R. & PERET, B. 2012. AUX/LAX family of auxin influx carriers-an overview. *Front Plant Sci,* 3**,** 225.

TANAKA, H., OSAKABE, Y., KATSURA, S., MIZUNO, S., MARUYAMA, K., KUSAKABE, K., MIZOI, J., SHINOZAKI, K. & YAMAGUCHI-SHINOZAKI, K. 2012. Abiotic stress-inducible receptor-like kinases negatively control ABA signaling in Arabidopsis. *Plant J,* 70**,** 599-613.

TEALE, W. D., PAPONOV, I. A. & PALME, K. 2006. Auxin in action: signalling, transport and the control of plant growth and development. *Nat Rev Mol Cell Biol,* 7**,** 847-859.

TEN HOVE, C. A., BOCHDANOVITS, Z., JANSWEIJER, V. M., KONING, F. G., BERKE, L., SANCHEZ-PEREZ, G. F., SCHERES, B. & HEIDSTRA, R. 2011. Probing the roles of LRR RLK genes in Arabidopsis thaliana roots using a custom T-DNA insertion set. *Plant Mol Biol,* 76**,** 69-83.

TIAN, H., DE SMET, I. & DING, Z. 2014a. Shaping a root system: regulating lateral versus primary root growth. *Trends Plant Sci,* 19**,** 426-31.

TIAN, H., JIA, Y., NIU, T., YU, Q. & DING, Z. 2014b. The key players of the primary root growth and development also function in lateral roots in Arabidopsis. *Plant Cell Rep,* 33**,** 745-53.

TRENBERTH, K. E., DAI, A., VAN DER SCHRIER, G., JONES, P. D., BARICHIVICH, J., BRIFFA, K. R. & SHEFFIELD, J. 2014. Global warming and changes in drought. *Nature Clim. Change,* 4**,** 17-22.

TROMAS, A., PAPONOV, I. & PERROT-RECHENMANN, C. 2010. AUXIN BINDING PROTEIN 1: functional and evolutionary aspects. *Trends Plant Sci,* 15**,** 436-46.

UBEDA-TOMAS, S., BEEMSTER, G. T. & BENNETT, M. J. 2012. Hormonal regulation of root growth: integrating local activities into global behaviour. *Trends Plant Sci,* 17**,** 326-31.

UEDA, J., SAKAMOTO-KANETAKE, M., TODA, Y., MIYAMOTO, K., UHEDA, E. & DAIMON, H. 2014. Auxin Polar Transport is Essential for the Early Growth Stage of Etiolated Maize (Zea mays L. cv. Honey Bantam) Seedlings. *Plant Production Science,* 17**,** 144-151.

VANNESTE, S. & FRIML, J. 2009. Auxin: a trigger for change in plant development. *Cell,* 136**,** 1005-16.

VERMEER, J. E. M. & GELDNER, N. 2015. Lateral root initiation in Arabidopsis thaliana: a force awakens. *F1000Prime Rep,* 7.

VERMEER, J. E. M., VON WANGENHEIM, D., BARBERON, M., LEE, Y., STELZER, E. H. K., MAIZEL, A. & GELDNER, N. 2014. A Spatial Accommodation by Neighboring Cells Is Required for Organ Initiation in Arabidopsis . *Science,* 343**,** 178-183.

VIAENE, T., DELWICHE, C. F., RENSING, S. A. & FRIML, J. 2013. Origin and evolution of PIN auxin transporters in the green lineage. *Trends in Plant Science,* 18**,** 5-10.

VOSS, U., WILSON, M. H., KENOBI, K., GOULD, P. D., ROBERTSON, F. C., PEER, W. A., LUCAS, M., SWARUP, K., CASIMIRO, I., HOLMAN, T. J., WELLS, D. M., PERET, B., GOH, T., FUKAKI, H., HODGMAN, T. C., LAPLAZE, L., HALLIDAY, K. J., LJUNG, K., MURPHY, A. S., HALL, A. J., WEBB, A. A. & BENNETT, M. J. 2015. The circadian clock rephases during lateral root organ initiation in Arabidopsis thaliana. *Nat Commun,* 6**,** 7641.

WANG, D., GUO, Y., WU, C., YANG, G., LI, Y. & ZHENG, C. 2008a. Genome-wide analysis of CCCH zinc finger family in Arabidopsis and rice. *BMC Genomics,* 9**,** 44.

WANG, L., XU, Y., ZHANG, C., MA, Q., JOO, S. H., KIM, S. K., XU, Z. & CHONG, K. 2008b. OsLIC, a novel CCCH-type zinc finger protein with transcription activation, mediates rice architecture via brassinosteroids signaling. *PloS one,* 3.

WANG, Y. H. & IRVING, H. R. 2011. Developing a model of plant hormone interactions. *Plant Signal Behav,* 6**,** 494-500.

WEBB, S. R. & HALL, J. C. 1995. Auxinic Herbicide-Resistant and -Susceptible Wild Mustard (Sinapis arvensis L.) Biotypes: Effect of Auxinic Herbicides on Seedling Growth and Auxin-Binding Activity. *Pesticide Biochemistry and Physiology,* 52**,** 137-148.

WELLS, D. M., FRENCH, A. P., NAEEM, A., ISHAQ, O., TRAINI, R., HIJAZI, H., BENNETT, M. J. & PRIDMORE, T. P. 2012. Recovering the dynamics of root growth and development using novel image acquisition and analysis methods. *Philosophical Transactions of the Royal Society B: Biological Sciences,* 367**,** 1517-1524.

WOODWARD, A. W. & BARTEL, B. 2005. Auxin: regulation, action, and interaction. *Ann Bot,* 95**,** 707-35.

YADAV, S. R., BISHOPP, A. & HELARIUTTA, Y. 2010. Plant development: early events in lateral root initiation. *Curr Biol,* 20**,** R843-5.

YANG, D. L., YANG, Y. & HE, Z. 2013. Roles of plant hormones and their interplay in rice immunity. *Mol Plant,* 6**,** 675-85.

YANG, J., KLOEPPER, J. W. & RYU, C. M. 2009. Rhizosphere bacteria help plants tolerate abiotic stress. *Trends Plant Sci,* 14**,** 1-4.

YI, K., MENAND, B., BELL, E. & DOLAN, L. 2010. A basic helix-loop-helix transcription factor controls cell growth and size in root hairs. *Nat Genet,* 42**,** 264-7.

YUAN, S., XU, B., ZHANG, J., XIE, Z., CHENG, Q., YANG, Z., CAI, Q. & HUANG, B. 2015. Comprehensive analysis of CCCH-type zinc finger family genes facilitates functional gene discovery and reflects recent allopolyploidization event in tetraploid switchgrass. *BMC Genomics,* 16**,** 1-16.

ZHANG, C., ZHANG, H., ZHAO, Y., JIANG, H., ZHU, S., CHENG, B. & XIANG, Y. 2013. Genome-wide analysis of the CCCH zinc finger gene family in Medicago truncatula. *Plant Cell Rep,* 32.

ZHANG, J., LIN, J. E., HARRIS, C., CAMPOS MASTROTTI PEREIRA, F., WU, F., BLAKESLEE, J. J. & PEER, W. A. 2016. DAO1 catalyzes temporal and tissue-specific oxidative inactivation of auxin in

Arabidopsis thaliana. *Proceedings of the National Academy of Sciences,* 113**,** 11010-11015.

ZHANG, M., YUAN, B. & LENG, P. 2009. The role of ABA in triggering ethylene biosynthesis and ripening of tomato fruit. *Journal of Experimental Botany,* 60**,** 1579-1588.

ZHANG, X., HENRIQUES, R., LIN, S. S., NIU, Q. W. & CHUA, N. H. 2006. Agrobacterium-mediated transformation of Arabidopsis thaliana using the floral dip method. *Nat Protoc,* 1**,** 641-6.

ZHAO, Y. 2010. Auxin biosynthesis and its role in plant development. *Annu Rev Plant Biol,* 61**,** 49-64.

ZHAO, Y., XING, L., WANG, X., HOU, Y.-J., GAO, J., WANG, P., DUAN, C.-G., ZHU, X. & ZHU, J.-K. 2014. The ABA Receptor PYL8 Promotes Lateral Root Growth by Enhancing MYB77-Dependent Transcription of Auxin-Responsive Genes. *Science signaling,* 7**,** ra53-ra53.

ZHAO, Z., ZHANG, Y., LIU, X., ZHANG, X., LIU, S., YU, X., REN, Y., ZHENG, X., ZHOU, K., JIANG, L., GUO, X., GAI, Y., WU, C., ZHAI, H., WANG, H. & WAN, J. 2013. A role for a dioxygenase in auxin metabolism and reproductive development in rice. *Dev Cell,* 27**,** 113-22.